VALIDATION REPORT – TIR and SWIR-TIR combined retrievals

Technical Note

ESA project METHANE+ led by SRON

Task 2, WP 2000, Deliverable 3 (D3) TIR

Change log

Version	Date	Status	Reason for change
1	08-Apr-2021	First release	New document
2	10-June-2022		Updated with results from RAL Methane+ V2 data and SWIR-TIR data
2.1	21-July-2022	Final version following ESA comments	Ch 2, p1 : Clarified version numbering. Ch2, p8: Clarified choice of parameters in CAMS/ACE merging. Fig 2.12, 2.14: Caption extended with comment on IASI artefact over Venezuela. Fig 2.22: Comment on land/sea differences added to caption. Ch 3.3.2: Duplicated text replaced by reference to Ch 2.3.2 Ch 4.3.2: Fixed wrong figure references.

Authors

RAL :

- Lucy Ventress
- Richard Siddans
- Brian Kerridge

LMD :

- Nicolas Meilhac
- Cyril Crevoisier

Table of Contents

1. Overview

This report describes the validation of thermal-ir (TIR) methane retrievals from Metop-B IASI measurements in 2018 and 2019. In this period, MetOp-B was the principal MetOp satellite[1] and TROPOMI on Sentinel-5 Precursor was observing methane concurrently in the SWIR. .

Validation of two TIR retrieval schemes is reported:

- The RAL scheme (Siddans, 2017, 2020) which uses optimal estimation to retrieve height-resolved information provided as column average and surface-450hPa (0-6km) and 450-175hPa (6-12km) layer average mixing ratios. Two versions of this scheme are validated:
  - Methane+ version 1 data: The basis for the inverse modelling tests carried out in the ESA Methane+ project.
  - Methane+ version 2 data, based on an updated algorithm developed during the course of the Methane+ project.
- The LMD scheme (Crevoisier, 2009a, 2009b, 2013) which uses a neural network approach to retrieve a mid-tropospheric layer average mixing ratio.

Validation of the version 1 TIR+SWIR retrieval (combining SRON SWIR and RAL Methane+ version 1 data) is also reported here.

Because the RAL and LMD schemes have different vertical sensitivities, it is not possible to compare them directly. This report presents independent comparisons of the two schemes with respect to common independent profile datasets (AirCore, Atom-4 and the CAMS GHG flux inversion v19r1). RAL results for column average are also compared with TCCON and with Sentinel-5P in preparation for joint use of TIR and SWIR data for surface flux inversion in this study.

[1] MetOp-A was continuing to observe from a drifting orbit and MetOp-C was newly launched.

2. Validation and comparisons of RAL TIR IASI Metop-B (Methane+ Version 1 data)

Comparisons have been carried out using IASI Metop-B data for 2018 and 2019 processed with the RAL retrieval scheme, described in detail in the RAL IASI Methane Retrieval ATBD and User Guide. This version of the scheme uses output from the RAL Infrared and Microwave Sounder (IMS) scheme (Siddans, 2020) to specify temperature profiles and surface spectral emissivity. This is version 2 of the RAL retrieval scheme (developed prior to the Methane+ project), however we emphasise that this was used to produce *Methane+ Version 1* data (following the version naming adopted within the project).

In this exercise we consider three quantities derived from the retrieved methane profile:

- Column average (dry-air) volume mixing ratio.
- Layer average volume mixing ratio from the surface to 421.7 hPa, referred to as "0-6km" sub-column.
- Layer average volume mixing ratio between 421.7 and 177.8 hPa, referred to as "6-12km" sub-column.

Methane profiles from CAMS flux inversions are used in the comparisons. Here we use data from the v19 methane flux inversion which uses only surface measurements. To overcome limitations in the representation of the stratosphere in this data, most comparisons are made to CAMS profiles which have been modified using the ACE-FTS version 4.1.2 methane climatology [RD-6]. These "CAMS+ACE" profiles are constructed as follows:

- The ACE-FTS v4 climatology contains solar occultation profiles averaged into bins of equivalent latitude (5 degrees) and pressure for each month from 2005 to 2020. However, ACE-FTS does not give complete sampling of all equivalent latitude bins in a single month and profiles do not extend far into the troposphere. The climatology is post-processed at RAL to obtain complete fields as follows:
    - Seasonal averages are formed by combining individual months in each year to give averages for (December-January-February (DJF), March-April-May (MAM), June-July-August (JJA), September-October-November (SON). December of the previous year is used to form DJF assigned to a given calendar year.
    - For each season/year, missing data in the troposphere is filled using a climatology of ECMWF tropopause pressure to identify which levels are 2km or more below the tropopause. The mean of valid data at these levels is used to fill all missing values at these levels.
    - Missing data above these levels are filled by linear interpolation of the valid values at each level (where necessary extrapolating to high latitudes at fixed value)

- An equivalent latitude profile is determined for each CAMS profile using ERA-5 potential vorticity data for the same location and time. This equivalent latitude profile is used (together with the date/time of the profile) to interpolate the post-processed seasonal/yearly ACE-FTS climatology. This gives a methane profile based on the ACE climatology, consistent with the stratospheric dynamics according to ERA-5.
- A combined CAMS and ACE methane profile $V_{CAMS+ACE}(p)$, is defined which uses CAMS in the troposphere and ACE in the stratosphere. The merging is carried out using the CAMS mixing ratio profile itself to determine the relative weight given to the two profiles (rather than explicitly identifying the tropopause):

$$V_{CAMS+ACE}(p) = w(p)V_{CAMS}(p) + \big(1 - w(p)\big)V_{ACE}(p)$$

- Where
  - $V_{CAMS}(p)$ is the CAMS mixing ratio profile (as function of pressure, p)
  - $V_{ACE}(p)$ is the equivalent latitude / time interpolated ACE profile
  - $w(p)$ is a weight from 0-1 which depends on the CAMS mixing ratio at the given level and the mean CAMS mixing ratio (in the same profile) at levels below ~6km, V_{TR}:
    - If $V_{CAMS}(p) \leq 0.8 * V_{TR}$, then $w(p)$=0
      (i.e. the ACE profile is assumed at these levels)
    - If $V_{CAMS}(p) \geq 0.95 * V_{TR}$, then $w(p)$=1
      (i.e. the CAMS profile is assumed at these levels)
    - If $0.85 * V_{TR} < V_{CAMS}(p) < 0.95 * V_{TR}$, then

$$w(p) = \frac{V_{CAMS}(p) - 0.8 * V_{TR}}{0.95 * V_{TR} - 0.8 * V_{TR}}$$

      I.e. at these levels, there is a linear interpolation (in CAMS vmr) between the two profiles. The values 0.8 and 0.95 in the equation are chosen empirically to give reasonable merging between CAMS and ACE in the region above the tropopause where methane starts to monotonically decrease with height, while using CAMS exclusively in the troposphere and ACE exclusively in the mid-to upper stratosphere.

2.1. Global model and satellite comparisons

IASI results are compared to the following global datasets:

- Profiles from the CAMS+ACE data as described above.
- SRON retrievals from the TROPOMI instrument onboard the Sentinel-5 Precursor (S5P). Version 18_17 data with qa_value=1 is used.

Global maps have been produced as follows:

- Methane column and layer averages (produced for individual IASI soundings) are averaged into monthly 2.5˚x2.5˚ latitude/longitude grid boxes.
- Only IASI data that pass the following quality control criteria are included:
  - Retrieved cloud fraction <0.2.
  - Solution cost <120.
  - Surface emissivity at 1232cm^{-1} is greater than 0.85. In practise this removes scenes over desert where there is a particularly strong spectral dependence of surface emissivity across the methane fit window, which is found to degrade the methane retrieval.
  - In plots shown here only descending node ("daytime") data are used.
  - When comparing to S5P, only IASI retrievals which have a co-located S5P retrieval (as described below) are used.

  Note that the methane retrieval is not carried out at all for IASI scenes which are flagged as cloudy by a simple brightness-temperature difference test where the 950cm^{-1} scene brightness temperature is colder than 240K (this automatically eliminates many scenes over Antarctica).
- CAMS+ACE fields for the same day are interpolated to the location of each accepted IASI retrieval. The corresponding column and layer average vmrs are computed from these profiles with and without applying averaging kernels to account for the vertical sensitivity of the retrieval.
- The monthly gridded data are combined into seasonal averages (DJF, MAM, JJA and SON). The seasonal means combine results from the relevant months in both 2018 and 2019[2].

Metop has a descending node equator crossing time of 09:30am, while S5P has an ascending node equator crossing time of 13:30. When comparing to S5P, we select co-located individual IASI and S5P observations as follows:

- For a given IASI scene (which passes IASI quality control as defined above), all S5P orbits starting within 0 to 8 hours of the IASI orbit start time are identified.
- From these orbits, the orbit whose satellite ground track is closest in distance to the IASI scene is identified.
- From this orbit, the closest S5P scene to the IASI scene is identified.
- If this S5P scene is within the 12km IASI field-of-view and the corresponding S5P retrieval has a qa_value of 1, then the match is accepted.

Comparisons to CAMS are illustrated in Figure 2-1 for the column average and in Figure 2-2 and Figure 2-3 for the 0-6km and 6-12km layers, respectively. These figures show the mean fields from IASI and CAMS, together with the difference IASI-CAMS. They also show the mean of the estimated standard deviation (ESD) on the individual IASI retrievals and the number of individual retrievals which contribute to the mean in each latitude/longitude bin. The ESD is estimated from the optimal estimation retrieval

[2] For co-locations with S5P, note that there is no S5P before 7 March 2018 – averages for DJF only include January and February 2019, combined with December 2018 and 2019..

as the combination of random measurement errors and smoothing error (i.e error associated with the prior contribution). The uncertainties on seasonal mean values would be expected to be much smaller than the mean ESD of individual retrievals. Purely random contributions would reduce with the square-root of the number of samples), however there is a systematic contribution to the smoothing error together with other sources of systematic error. These panels mainly serve to indicate how the retrieval sensitivity varies spatially (e.g. reflecting variations in surface temperature and surface-air temperature contrast).

Bottom panels in Figure 2-1 to Figure 2-3 show the difference between IASI and CAMS averaged as a function of view zenith angle. These indicate a tendency for stronger negative bias at high view zenith in the tropics.

Note that the number of samples varies considerably geographically. Particularly low numbers of samples are found over Antarctica (because retrievals are not carried out for very cold scenes), the Sahara (because of the imposed surface emissivity threshold and the retrieval often has high cost due to problems fitting the spectral dependence of surface emissivity). The number of retrievals is also reduced in particularly cloudy regions (e.g. Southern Ocean, South-East Asia in summer).

The IASI column average is compared to S5P in Figure 2-4. Coverage is mainly over land as S5P sampling over sea depends on the occurrence of sun-glint. The number of samples over land is also much reduced (as a consequence of the strict cloud-clearing and quality control applied to S5P, and the careful co-registration of individual IASI/S5P retrievals described above).

Some of the differences between IASI and S5P could be explained by known differences in their vertical sensitivity (as characterised by their averaging kernels). In particular, over persistent source regions (where methane mixing ratio is highest near the ground), it might be expected that S5P column averages would be larger than IASI (which is less sensitive to methane near the ground). In regions where methane is relatively high in the mid-upper troposphere (e.g. Asian monsoon or Amazon outflow over S Atlantic), IASI could give higher columns than S5P (due to vertical correlation in the prior constraint, there is a tendency for the IASI retrieval to extend information from the mid/upper-troposphere to lower altitudes). Here we attempt to adjust for this in comparisons to S5P by applying IASI averaging kernels to CAMS profiles used as a transfer standard. In particular, the 4th row of Figure 2-4 shows the difference between S5P and IASI column averages, accounting for the effect of the IASI averaging kernel, by computing “S5PxAK“ (S5P column adjusted for the IASI averaging kernel) as follows:

$$S5PxAK = S5P + CAMSxAK - CAMS$$

Where “S5P“ is the column average retrieved from S5P; “CAMS“ is the column average from CAMS; “CAMSxAK“ is the value by applying the IASI averaging kernel to the

CAMS profile. (Note that this approach can be extended to also compensate for the effect of the S5P averaging kernel, although doing so has been found to make very little difference in previous work.)

Figure 2-5 shows the time-series of monthly zonal mean methane column and layer averages as Hovmöller plots. The zonal means are obtained by averaging IASI and CAMS data in the manner described for the global maps (above) but using 10 degree latitude bins (and longitude bins spanning 180E to 180W). Figure 2-6 shows differences between IASI and CAMS as well as standard deviation in the mean difference of the individual retrievals. These show general patterns consistent with the maps of ESD in the maps (tendency for larger standard deviation towards high latitude winter), though values are generally smaller, especially for the 0-6km layer. This is consistent with the fact that ESD includes the smoothing error (which should not contribute to the standard deviation in difference between retrievals and model after averaging kernels are accounted for).

Figure 2-7 shows similar plots comparing co-located IASI and S5P column averages.

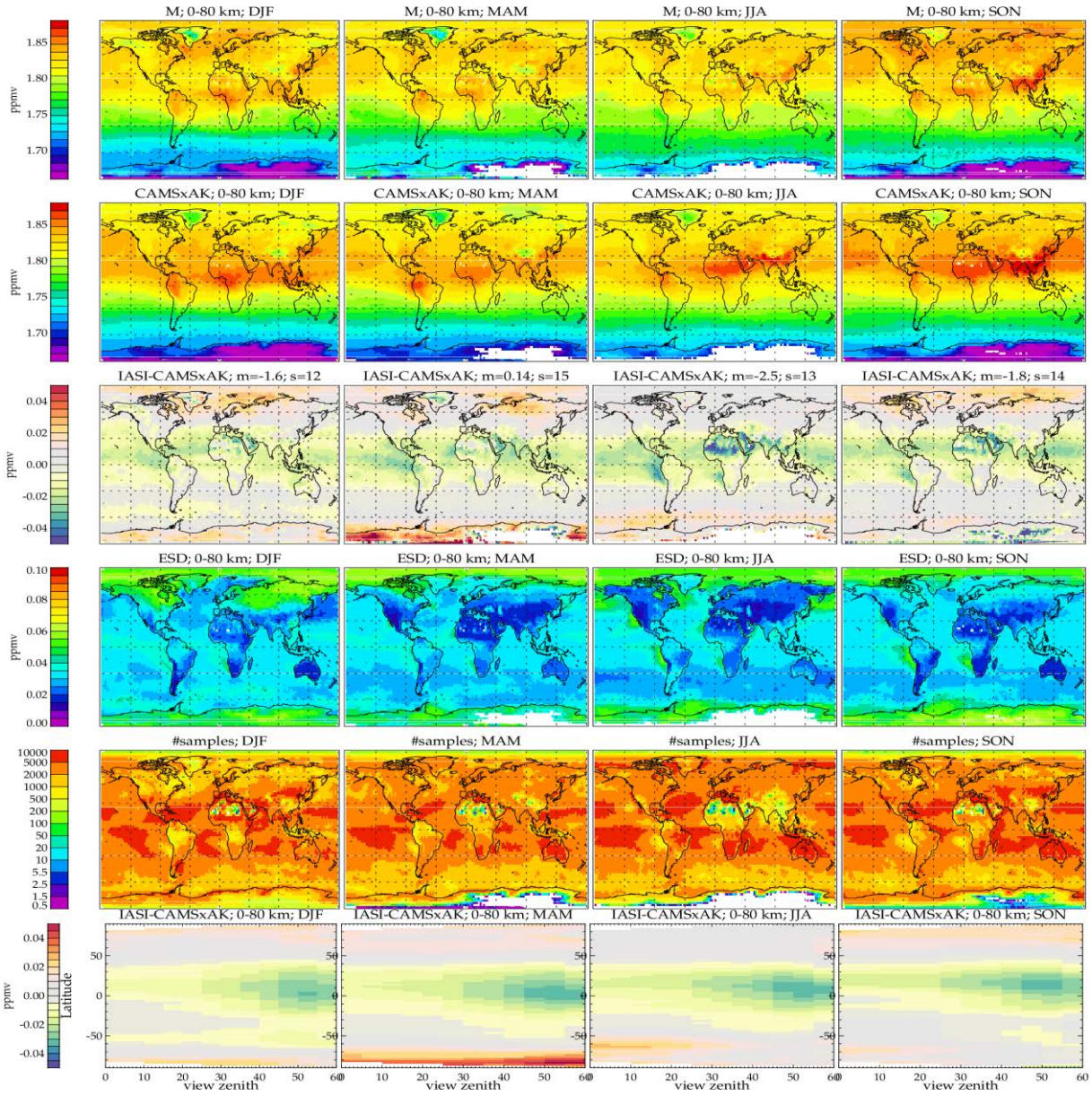

Figure 2-1 : RAL Methane+ version 1 TIR global daytime column average retrievals: columns show results for different seasons (2018 and 2019 combined). Rows from top-bottom show, respectively, results from IASI retrievals; CAMS with averaging kernels applied (CAMSxAK); the difference between IASI and CAMSxAK; the mean of the estimated standard deviation (ESD) on the IASI retrieval; the number of individual IASI retrievals in each of the 2.5x2.5 degree bins. Bottom panels show differences between IASI and CAMSxAK averaged as a function of view zenith angle and latitude.

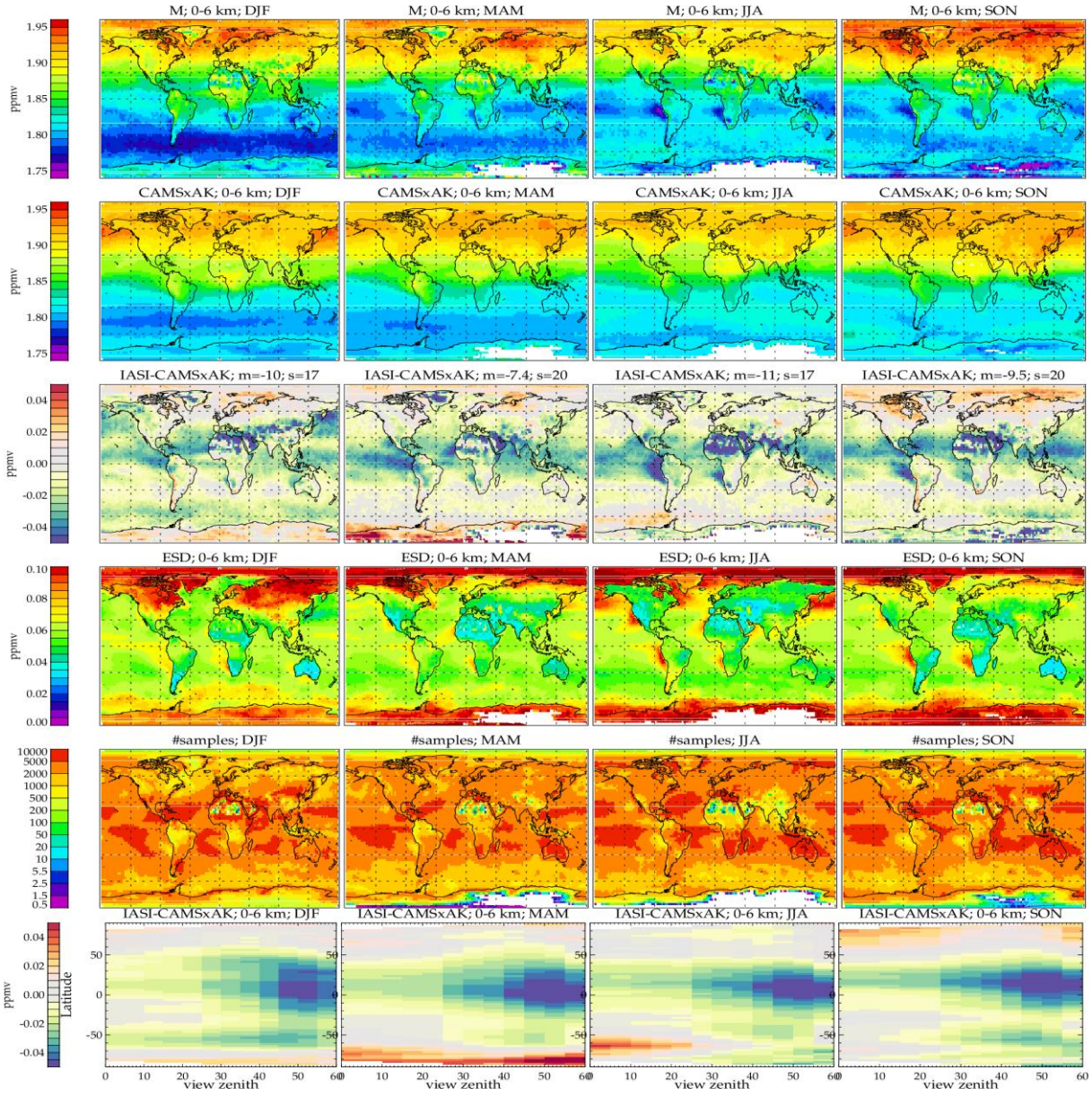

Figure 2-2 : RAL Methane+ version 1 TIR global daytime retrievals for the 0-6km layer average.

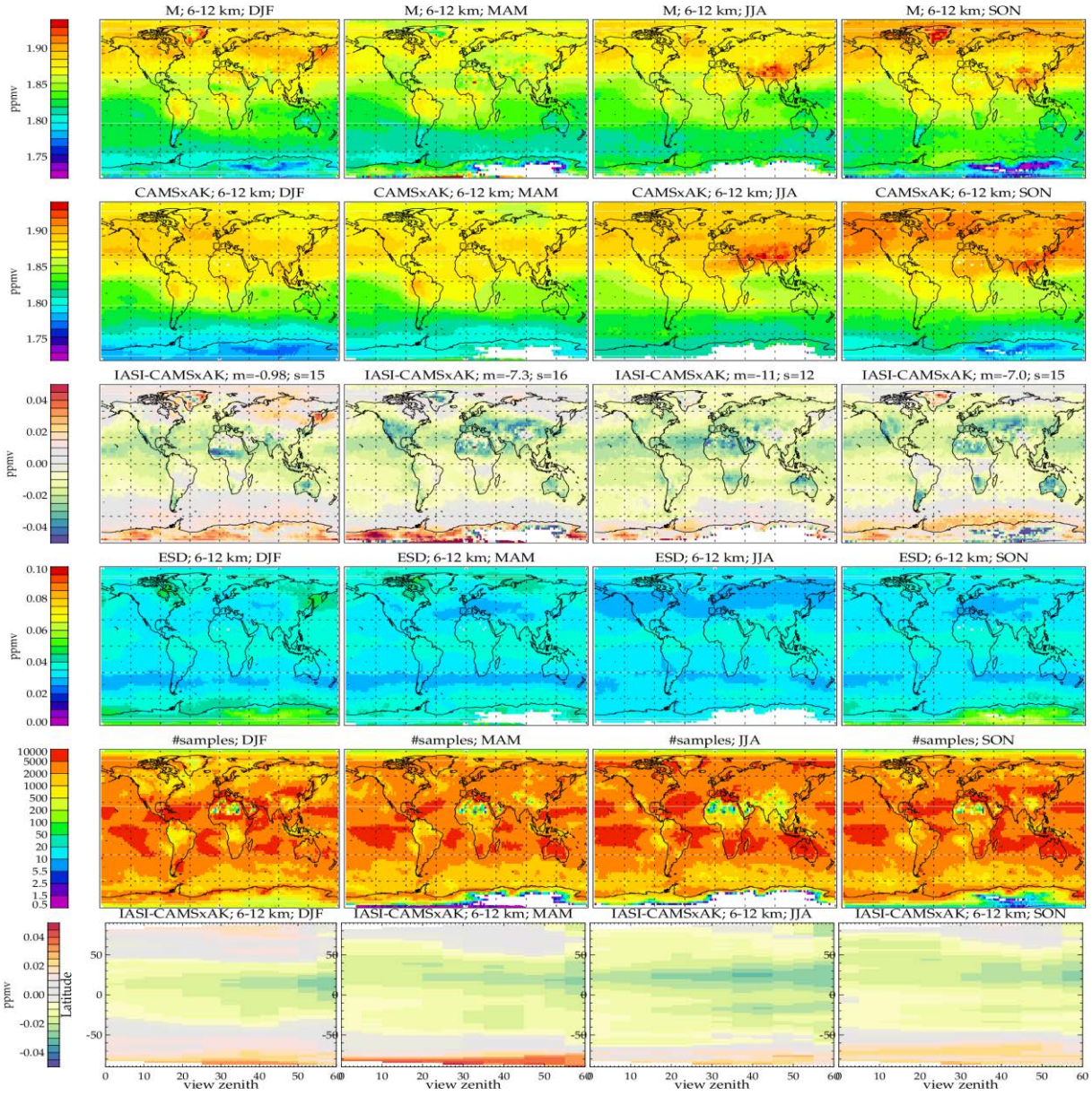

Figure 2-3 : RAL Methane+ version 1 TIR global daytime retrievals for the 6-12km layer average.

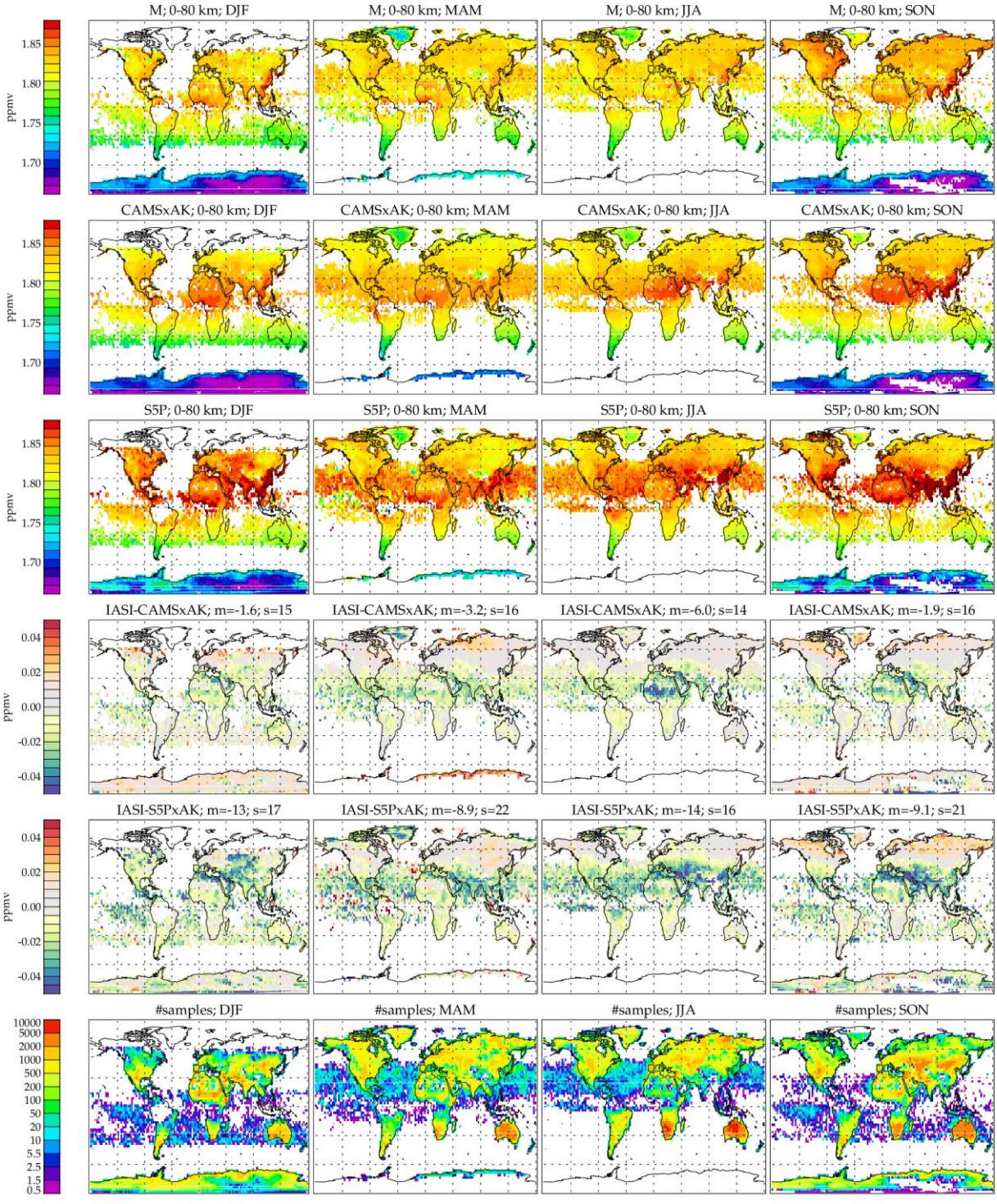

bin_iasich4_seasonal_fcov_dia_as5p3_amacc2_mcost120_cfr20_iv-1

Figure 2-4 : RAL Methane+ version 1 TIR global daytime column average retrievals co-located with S5P: Panels as previous figures except that the 2nd row shows S5P results, the 3rd row shows differences between IASI and S5P and the 4th row shows the difference between IASI and S5P after using CAMS to correct for the influence of the IASI averaging kernel.

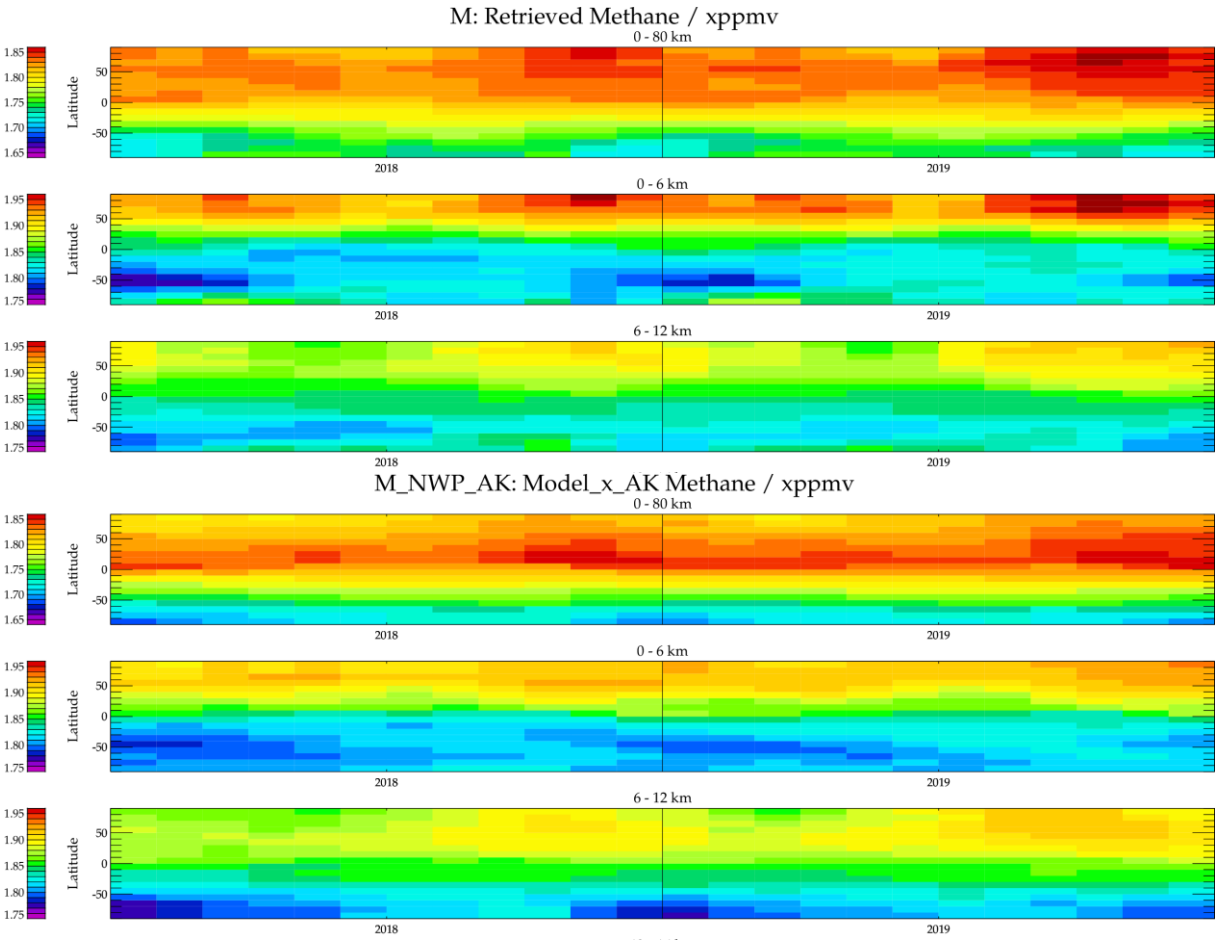

Figure 2-5 : RAL Methane+ version 1 TIR Hovmöller time-series for (a) IASI-B retrieved methane and (b) CAMS v19r1 methane flux inversion with IASI averaging kernels applied. Panels are shown for the column average (0-80km), 0-6km and 6-12km layer averages.

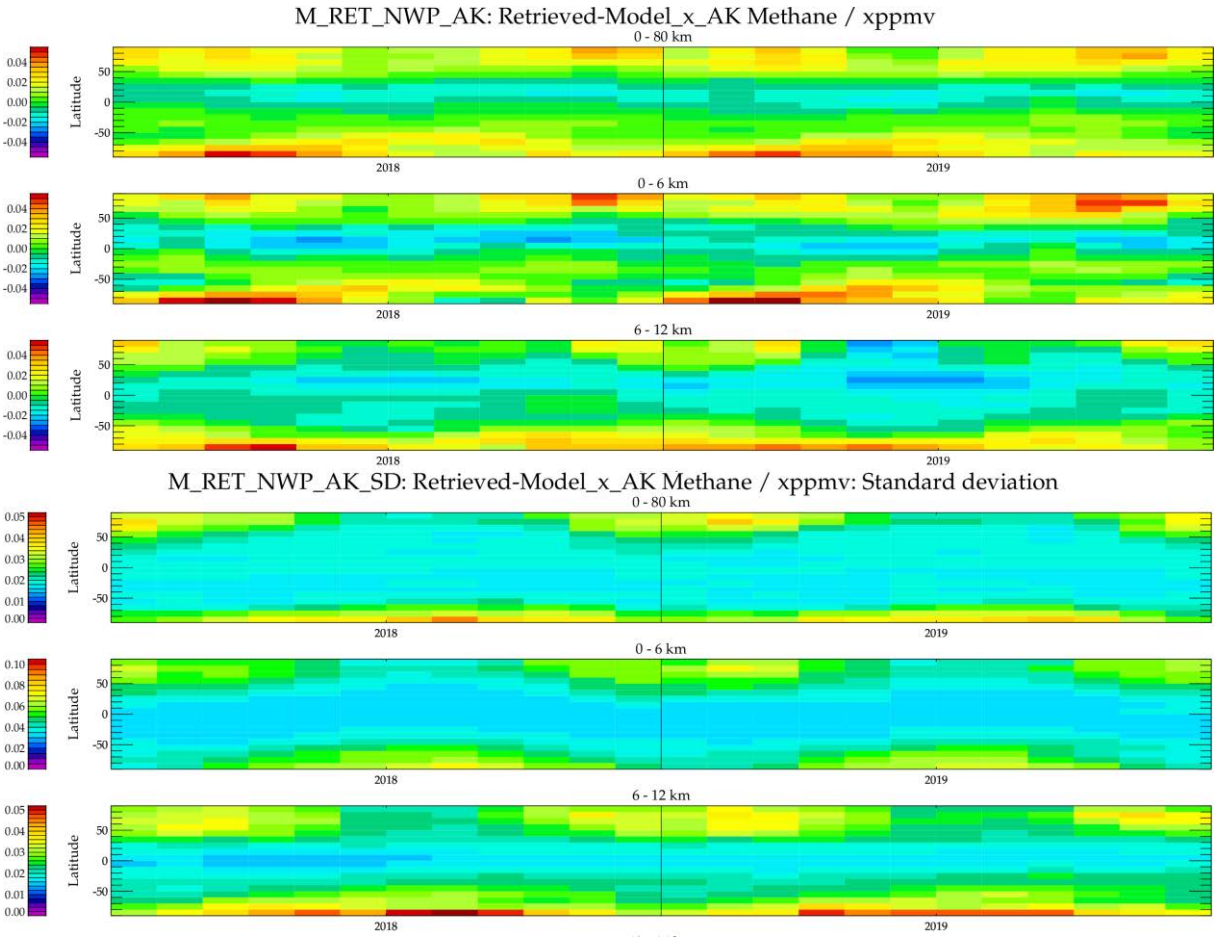

Figure 2-6 : RAL Methane+ version 1 TIR Hovmöller time-series for (a) the mean difference between IASI and CAMS and (b) the standard deviation in the mean difference. Panels are shown for the column average (0-80km), 0-6km and 6-12km layer averages.

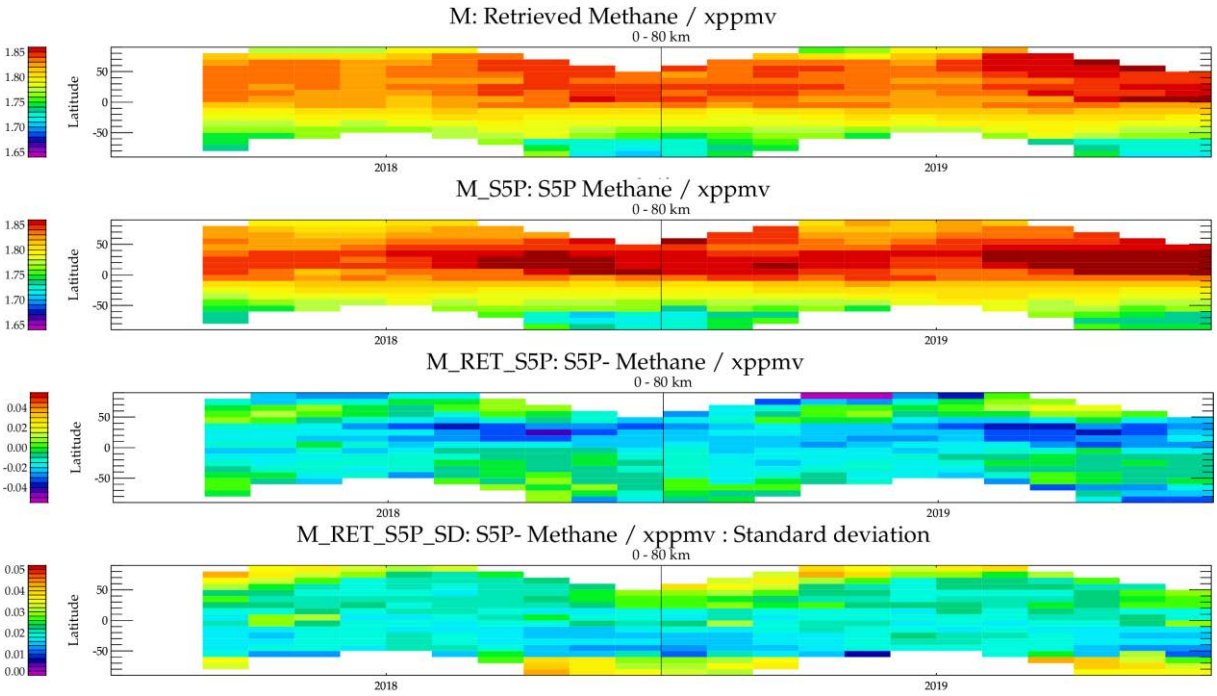

Figure 2-7 : RAL Methane+ version 1 TIR Hovmöller time-series for (a) IASI-B retrieved methane, (b) S5P retrieved methane, and (c) the difference between (a) and (b). Panels are shown for the column averages (0-80km).

2.2. Model and satellite comparisons over target regions

In this section maps of daytime IASI methane retrievals are presented focusing on regions of particular interest. These have been selected either because they are of scientific interest to this study or for the scientific/technical challenges which they present to retrieval. The locations of the five selected regions and the challenging features of the regions to be examined are given in Table 1 (taken from the Requirements Baseline Document).

Maps are constructed in the same manner as the global maps shown in the previous section, but using a 0.5 degree latitude, longitude grid restricted to the regions of interest.

Comparisons to CAMS are presented as maps (0.5x0.5 degree gridded seasonal averages) in Figure 2-8 to Figure 2-27. For each region (A-E as in the table), figures compare the IASI column averages to CAMS and S5P (in separate figures), and the 0-6km and 6-12km layer averages to CAMS. In panels which show the differences between the retrieval and CAMS or S5P, the panel title indicates the mean differences over the region (“m”) and standard deviation in the mean (“s”), considering each binned spatial sample in the mean. I.e. the standard deviation represents quasi-systematic differences in the seasonally averaged spatial distribution (at 0.5 degrees resolution), as opposed to differences in the individual retrievals contributing to the mean in each 0.5 degree box.

Figure 2-28 summarises the mean and standard deviations in the differences of IASI and CAMS for each region and layer. Figure 2-29 summarises the differences in total column with respect to S5P.

Table 1 The locations and reason for the selected target regions.

Target region	Where and when?	Relevance	Comments
Region A: India/China	70-120E; 10-35N Sept. 2018, 2019	Uplift of rice paddies emission by summer monsoon and outflow towards China and the Middle East, mixing local emissions, and long distance transport	Made consistent with corresponding science case for inverse modelling
Region B : Amazon Basin	45W – 100W; 15S-15N NH summer of 2018 and 2019	Cloudy region and strong CH4 gradient between land and sea	Made consistent with corresponding science case for inverse modelling
Region E: High northern latitude	60-90N	Specific thermodynamic condition, with few knowledge of CH4	Large region, covered by global analysis
Region C: Saharan Desert	5N-35N; 20W-40E May 2018-May 2019	Difficulty characterising surface emissivity of Saharan sand.	Made consistent with corresponding SWIR region
Region D: North Pacific Ocean (off the west coast of USA and Mexico)	20N-50N; 130W-100W May 2018-May 2019	TIR retrieval complication by temperature inversion over sea	Includes California from SWIR target regions

Time-series comparisons for the 2 years are shown as line plots in Figure 2-30 (column average vs CAMS), Figure 2-31 (0-6km layer average vs CAMS), Figure 2-32 (6-12km layer average vs CAMS) and Figure 2-33 (column average vs S5P). Each Figure contains separate panels showing averages over the following regions (including the methane+ focus regions):

- Tr+MdLat: All tropics and Mid-latitudes (60S to 60N).
- SHiLat: Southern high latitude (90S-60S).
- SMdLat: Southern mid-latitude (60S-30S).
- Trop: Tropics (30S-30N).
- NMdLat: Northern Mid-latitudes (30N-60N).
- NHiLat: Norther high-latitude (60N-90N). I.e. methane+ region E.
- IndChn: India/China. I.e. methane+ region A.

- Amzn: Amazon. I.e. methane+ region B.
- Sah: Sahara. I.e. methane+ region C.
- NAmCo: North America / Pacific coast. I.e. methane+ region D.
- Grnlnd: Greenland (part of region E).
- ArcOc: Arctic ocean. I.e. Northern high latitudes excluding land (part of region E).

The lines in each panel are as follows:

- Red: A priori value assumed by the IASI retrieval. Note the retrieval assumes a latitude dependent prior, which is fixed in time at values approximately appropriate for 2009 methane levels. It is therefore generally negatively biased in 2018/19. For some regions, a slight time dependence in the prior is evident, caused by seasonal changes in the latitude sampling of the regions by valid retrievals.
- Black: The IASI retrieval
- Green: CAMS value
- Blue: CAMS value accounting for the IASI averaging kernel
- Magenta: S5P value (in Figure 2-33 only)

Each of the panels contains a caption which summarises the agreement with IASI as follows:

- Mn: Mean difference (ppbv)
- SD: Standard deviation of the difference (ppbv). I.e. the standard deviation of the 24 monthly mean differences between IASI and each correlative data set
- Cx: The correlation coefficient for the 24 monthly mean values.

Figure 2-34 to Figure 2-37 summarise these statistics. In almost all regions the correlation, standard deviation and bias are much improved for retrieval vs CAMS compared to retrieval vs prior and there is also a small further improvement in retrieval vs CAMS when the averaging kernel is applied (as expected). Exceptions to this behaviour are seen for the 0-6km layer in the Southern High Latitude and Saharan regions.

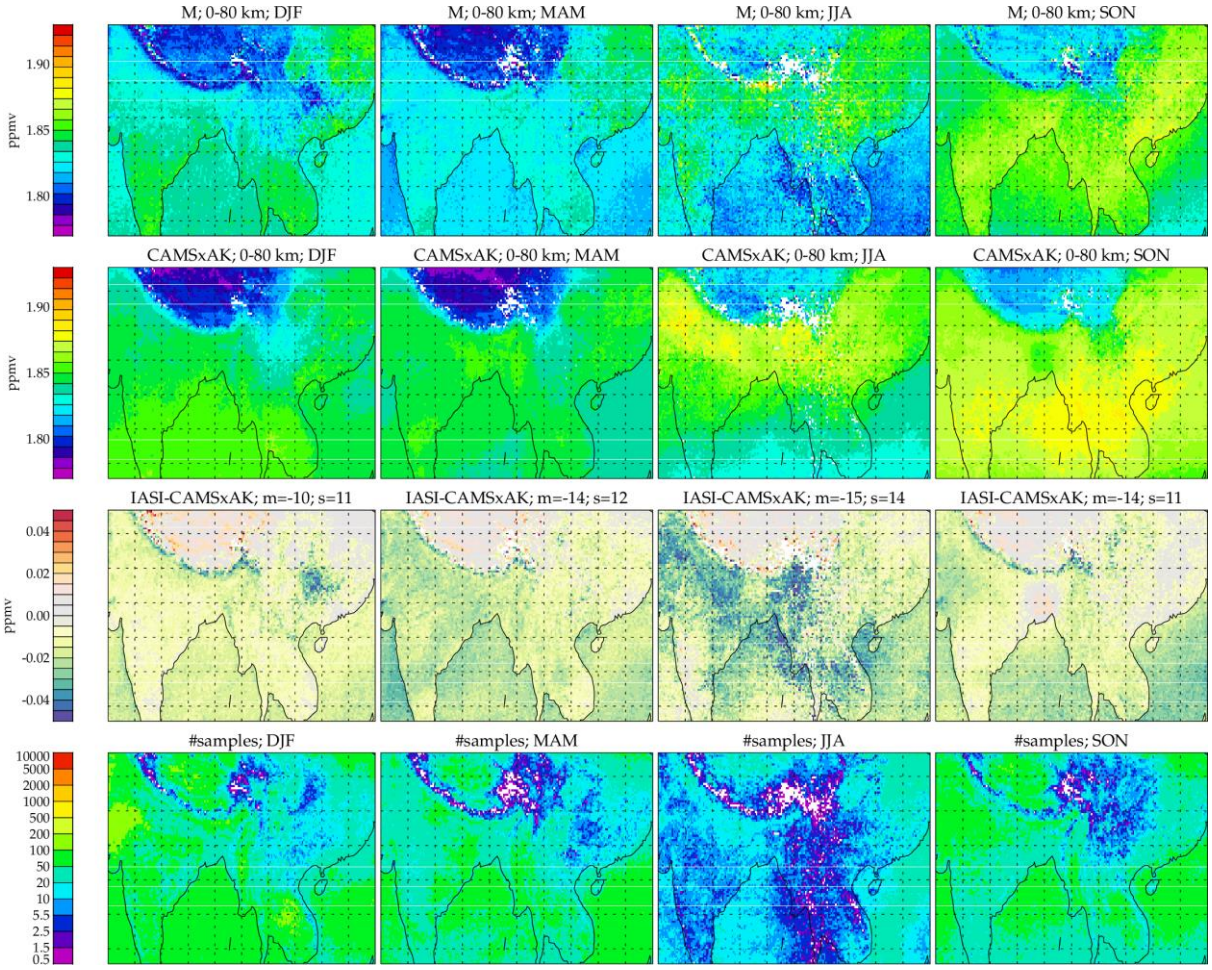

Figure 2-8 : RAL Methane+ version 1 TIR global daytime column average retrievals for region A: Each column of the figure shows results for a different season (2018 and 2019 combined). Rows from top-bottom show, respectively, results from IASI retrievals; CAMS with averaging kernels applied (CAMSxAK); the difference between IASI and CAMSxAK; the number of individual IASI retrievals in each of the 0.5x0.5 degree bins.

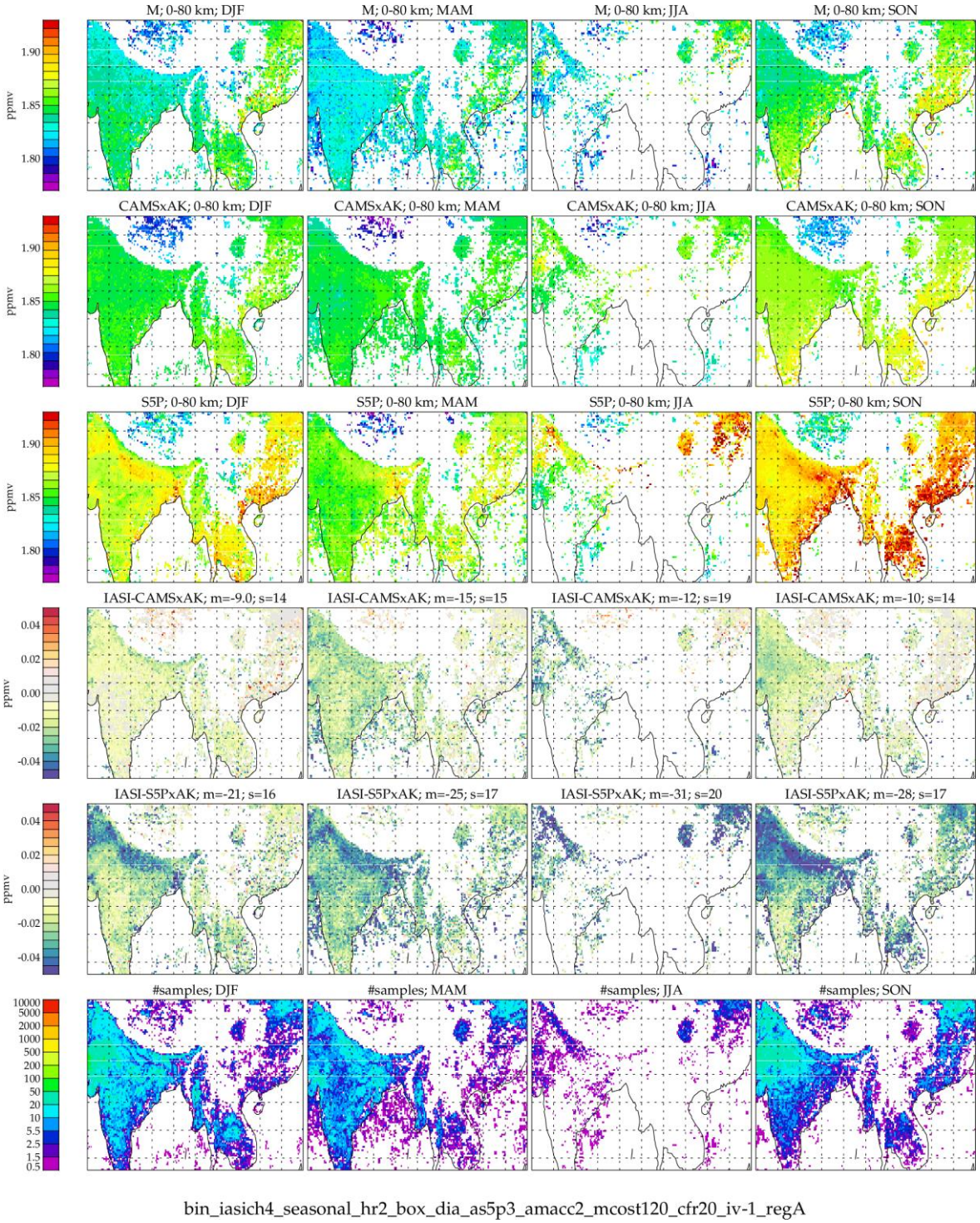

Figure 2-9 : RAL Methane+ version 1 TIR global daytime column average retrievals for region A, collocated with S5P: Each column of the figure shows results for a different season (2018 and 2019 combined). Panels from top-bottom show, respectively, results from IASI retrievals; CAMS; S5P retrievals; Difference between IASI and S5P; Difference between IASI and S5P accounting for the IASI averaging kernel using CAMS; the number of individual IASI retrievals in each of the 0.5x0.5 degree bins.

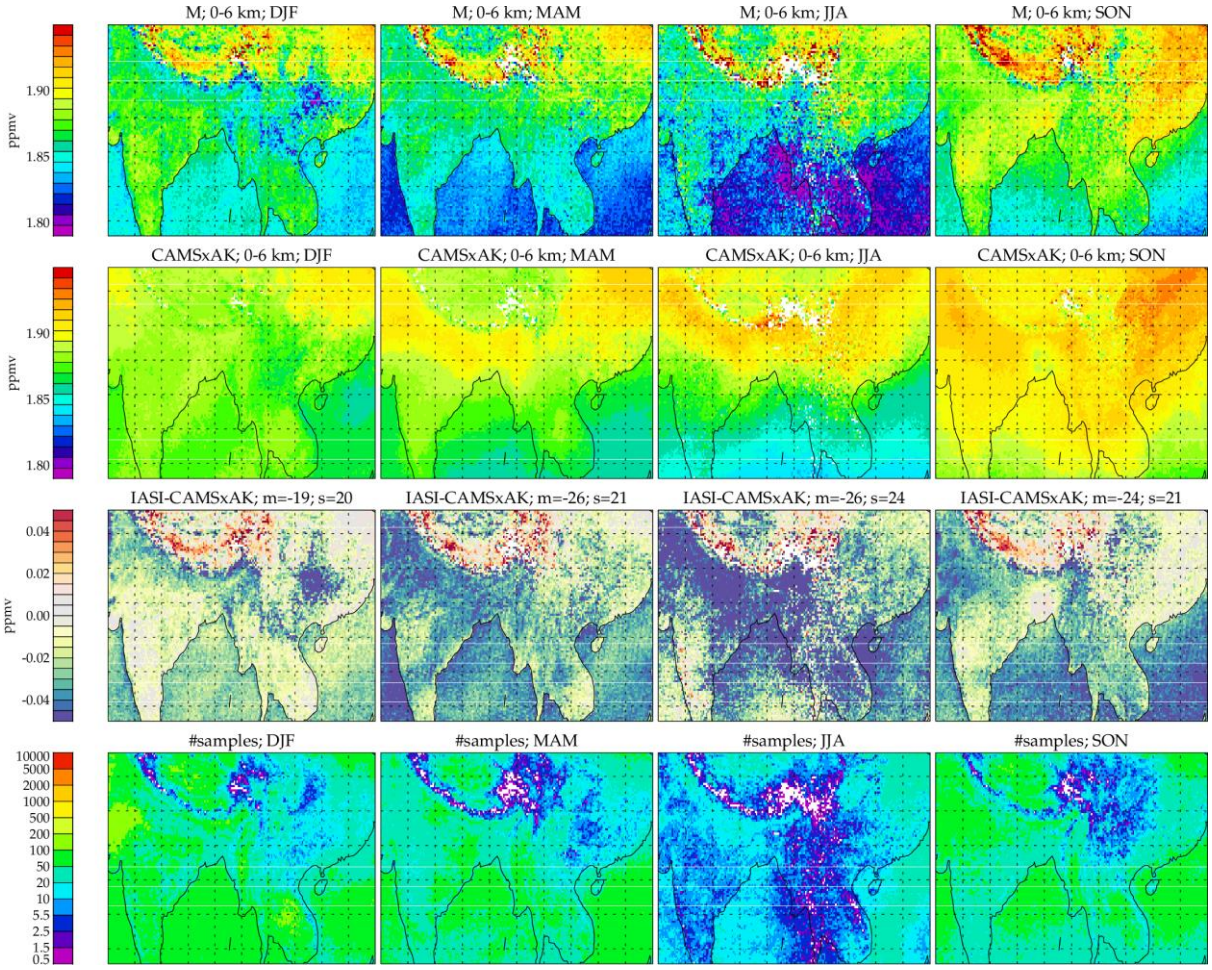

Figure 2-10 : RAL Methane+ version 1 TIR daytime 0-6km layer average retrievals over target region A.

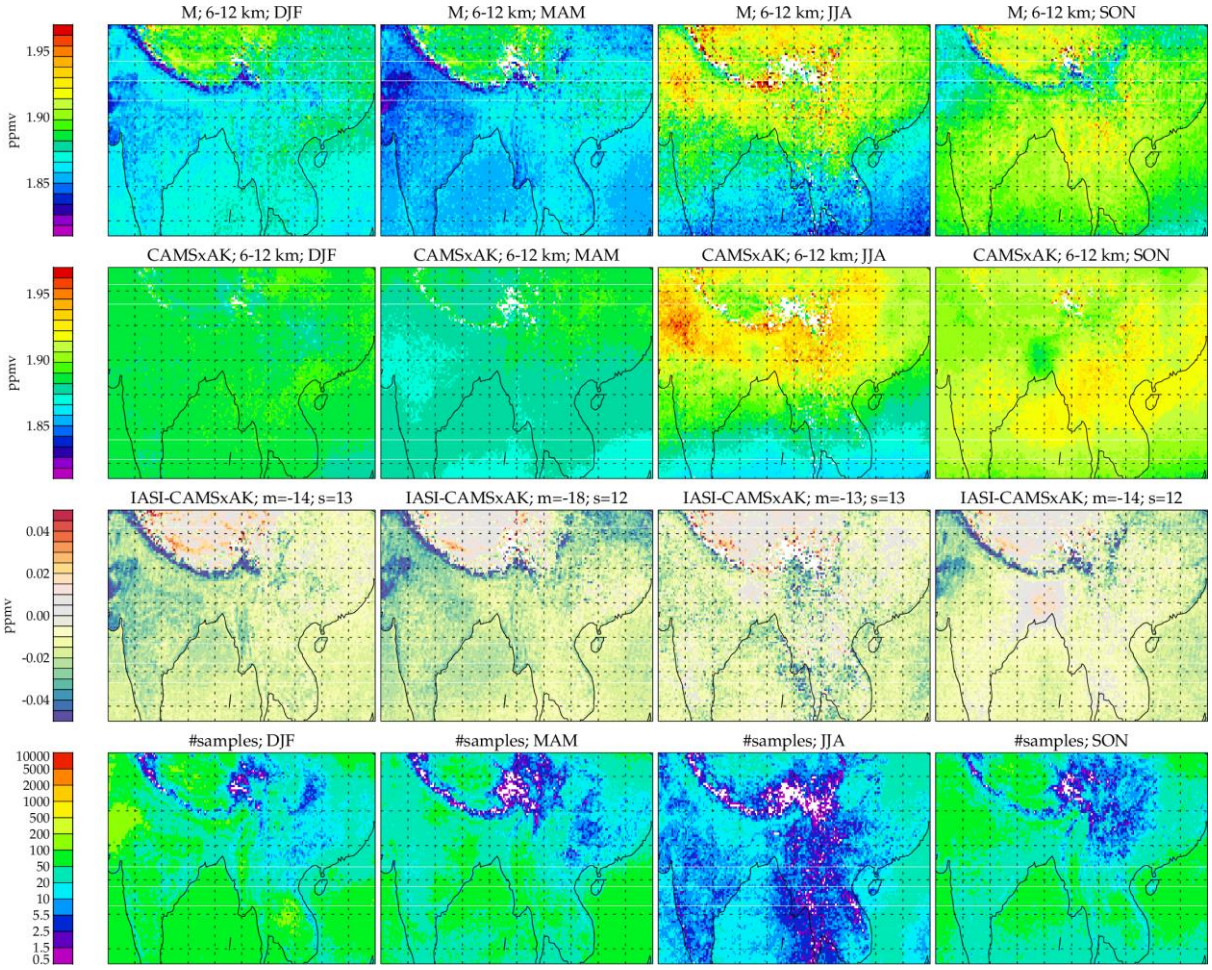

Figure 2-11 : RAL Methane+ version 1 TIR daytime 6-12km layer average retrievals over target region A.

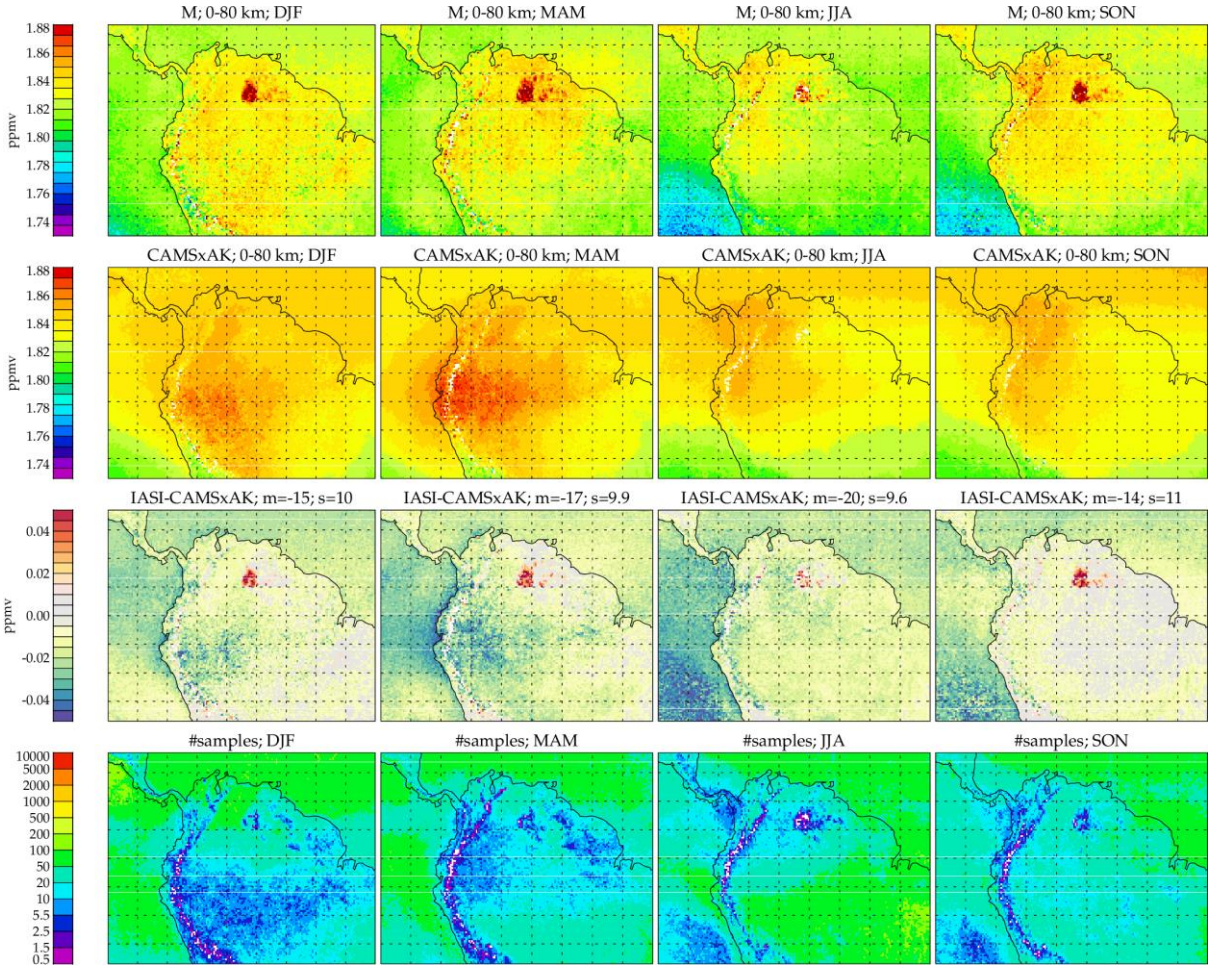

Figure 2-12 : RAL Methane+ version 1 TIR global daytime column average retrievals for region B: Each column of the figure shows results for a different season (2018 and 2019 combined). Rows from top-bottom show, respectively, results from IASI retrievals; CAMS with averaging kernels applied (CAMSxAK); the difference between IASI and CAMSxAK; the number of individual IASI retrievals in each of the 0.5x0.5 degree bins. Note that the positive anomaly scene in IASI over Venezuela is caused by errors in the surface altitude database used in producing the V1 data, and has been corrected in the V2 data (see discussion section 2.4 and corresponding figures in chapter 4).

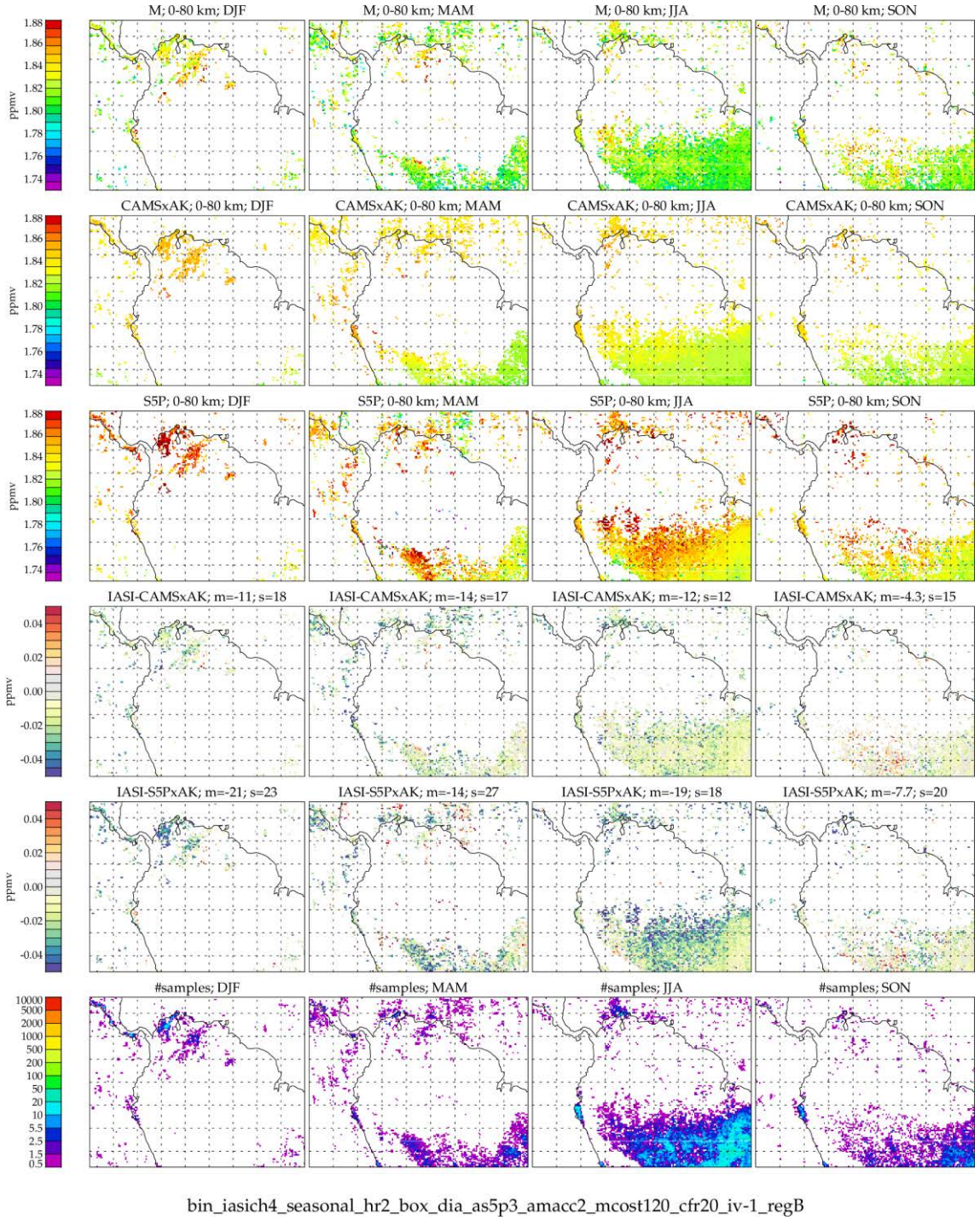

Figure 2-13 : RAL Methane+ version 1 TIR global daytime column average retrievals for region B, collocated with S5P: Each column of the figure shows results for a different season (2018 and 2019 combined). Panels from top-bottom show, respectively, results from IASI retrievals; CAMS; S5P retrievals; Difference between IASI and S5P; Difference between IASI and S5P accounting for the IASI averaging kernel using CAMS; the number of individual IASI retrievals in each of the 0.5x0.5 degree bins.

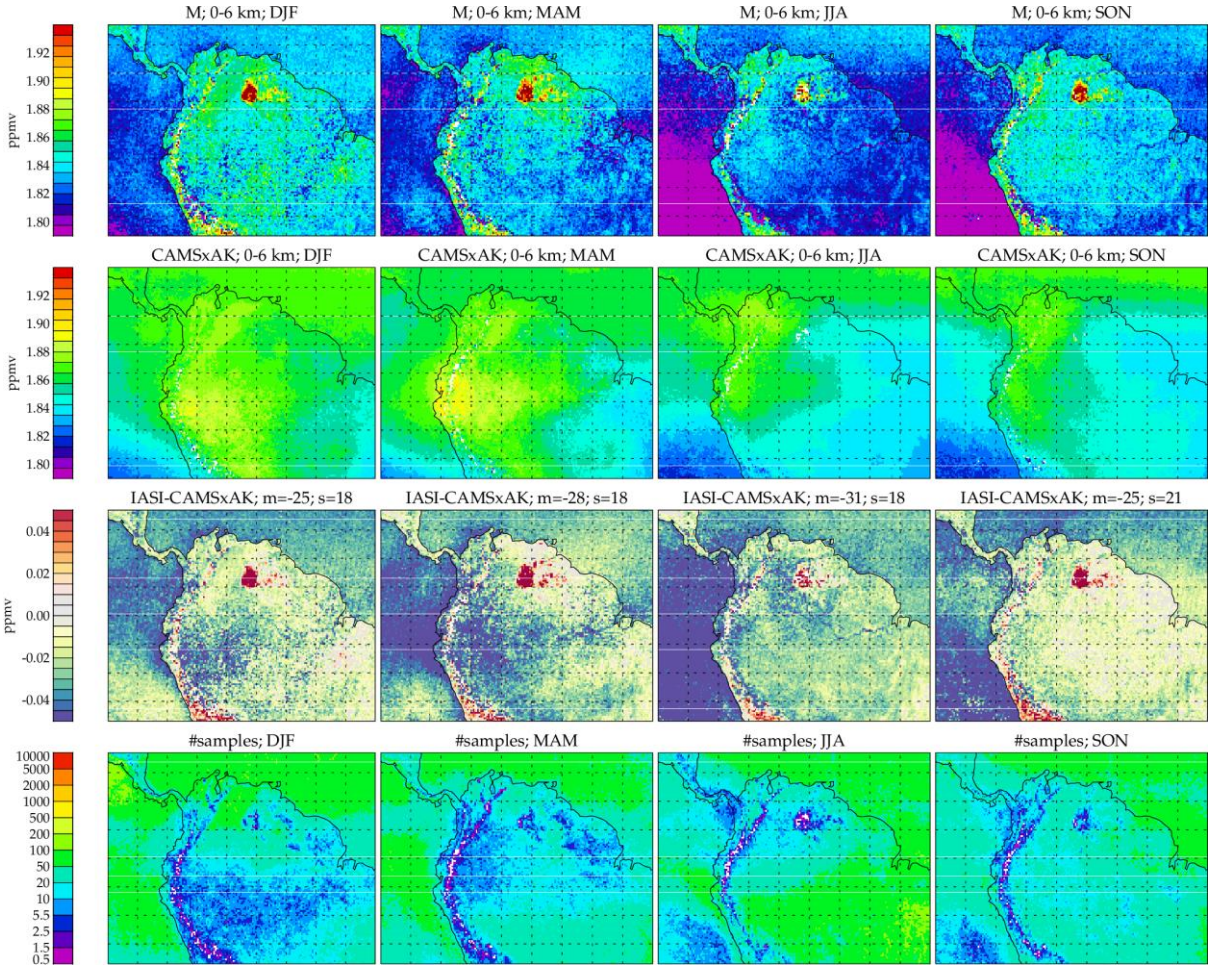

Figure 2-14 : RAL Methane+ version 1 TIR daytime 0-6km layer average retrievals over target region B. Note that the positive anomaly scene in IASI over Venezuela is caused by errors in the surface altitude database used in producing the V1 data, and has been corrected in the V2 data (see discussion section 2.4 and corresponding figures in chapter 4).

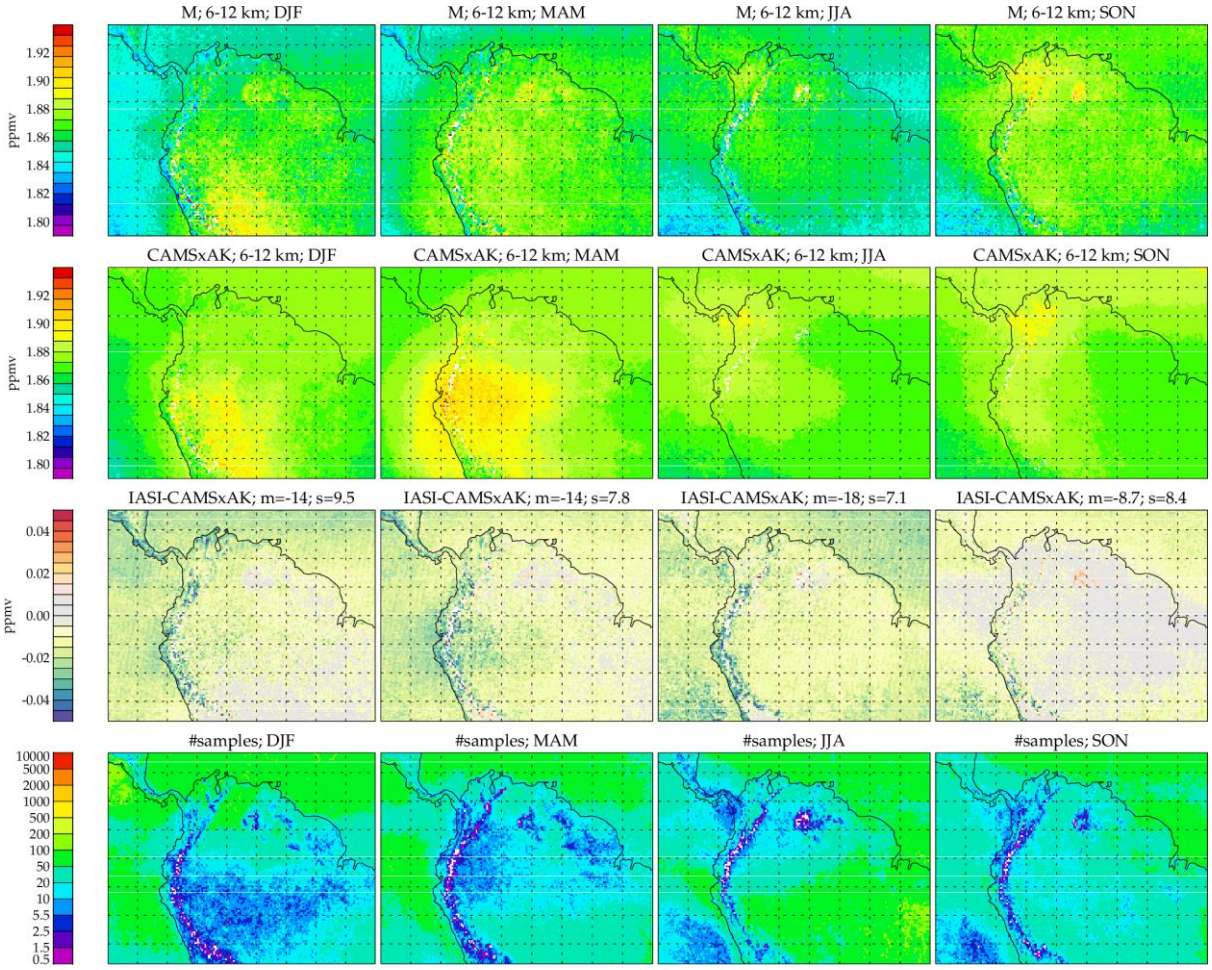

Figure 2-15 : RAL Methane+ version 1 TIR daytime 6-12km layer average retrievals over target region B.

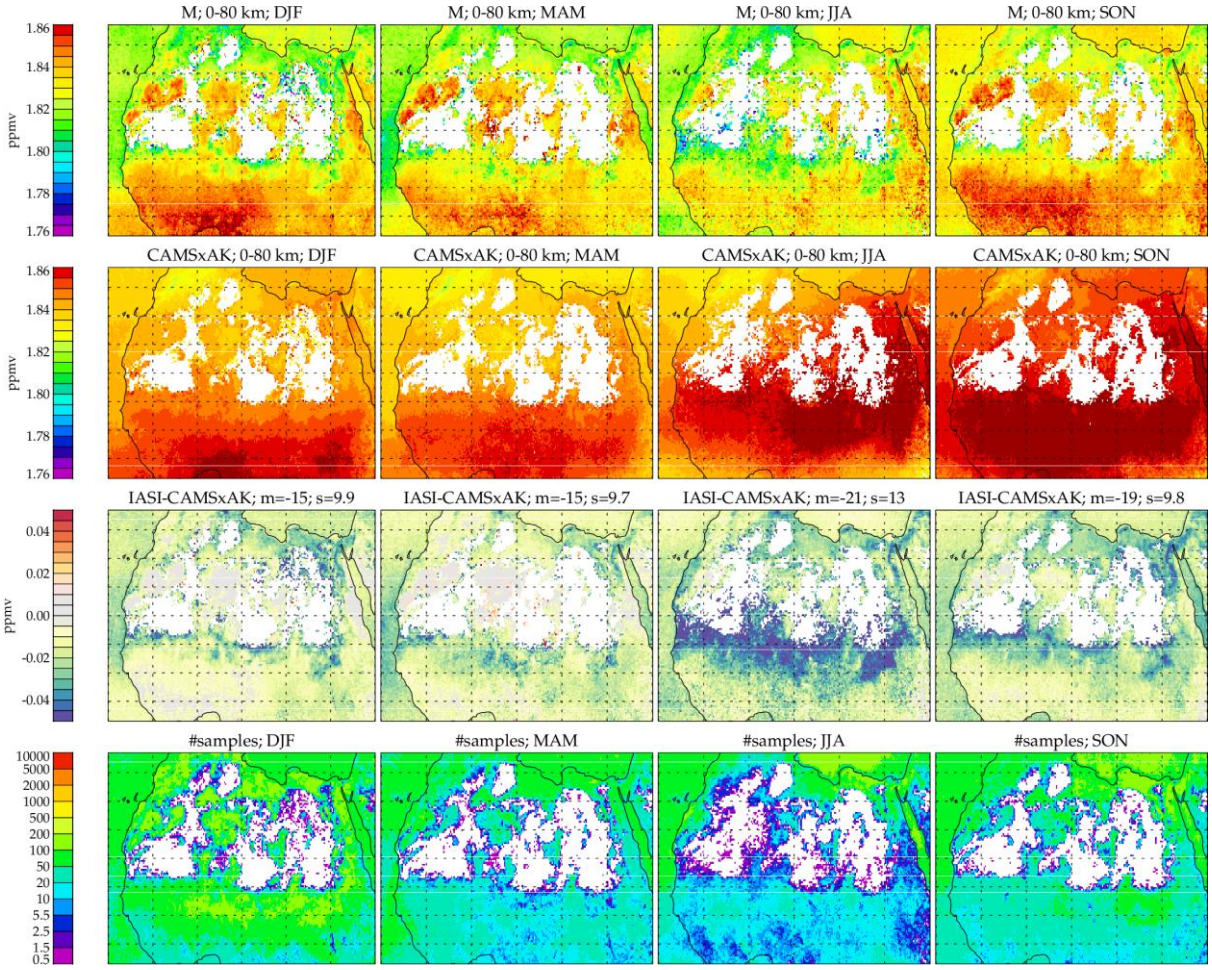

Figure 2-16 : RAL Methane+ version 1 TIR global daytime column average retrievals for region C: Each column of the figure shows results for a different season (2018 and 2019 combined). Rows from top-bottom show, respectively, results from IASI retrievals; CAMS with averaging kernels applied (CAMSxAK); the difference between IASI and CAMSxAK; the number of individual IASI retrievals in each of the 0.5x0.5 degree bins.

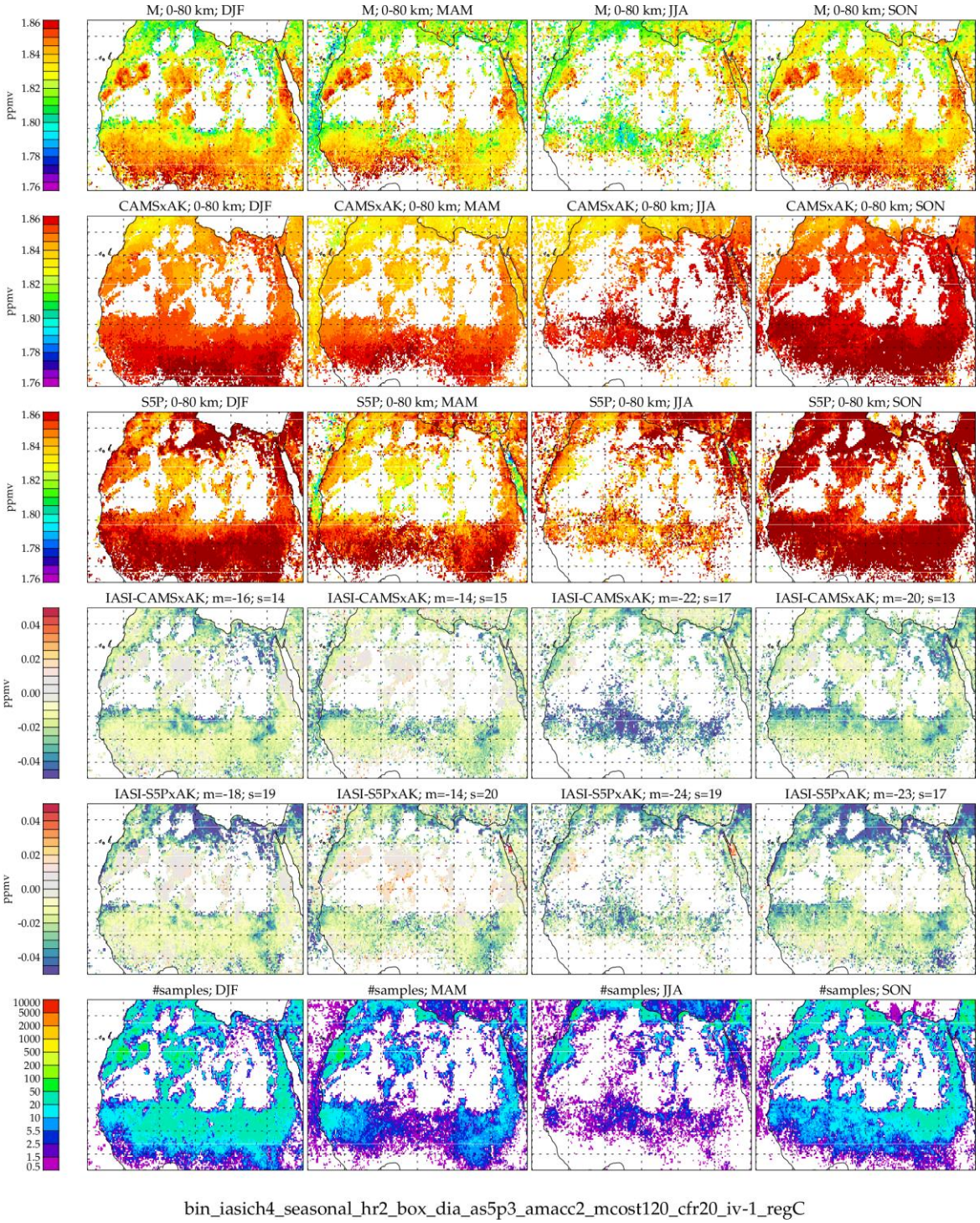

Figure 2-17 : RAL Methane+ version 1 TIR global daytime column average retrievals for region C, collocated with S5P: Each column of the figure shows results for a different season (2018 and 2019 combined). Panels from top-bottom show, respectively, results from IASI retrievals; CAMS; S5P retrievals; Difference between IASI and S5P; Difference between IASI and S5P accounting for the IASI averaging kernel using CAMS; the number of individual IASI retrievals in each of the 0.5x0.5 degree bins.

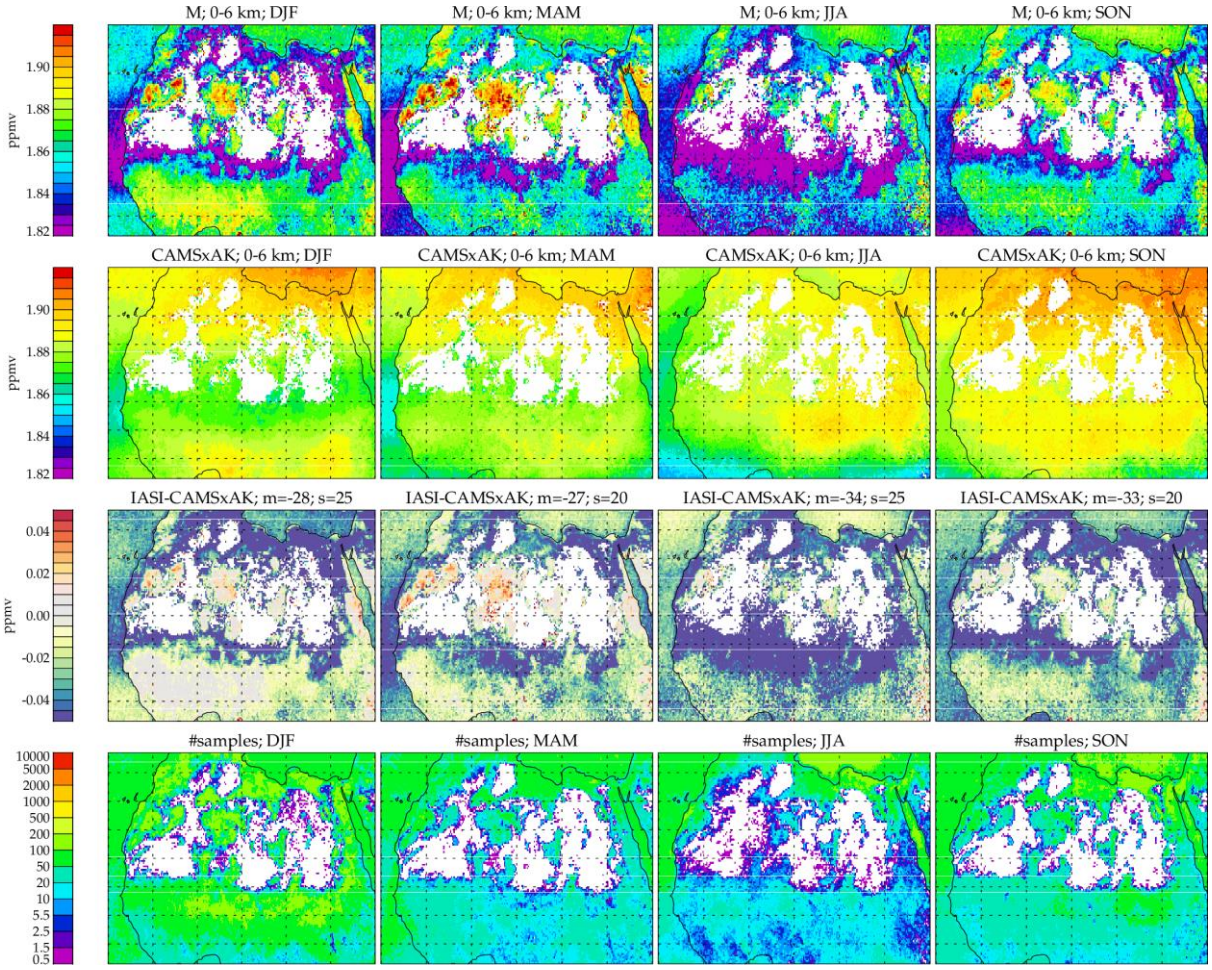

Figure 2-18 : RAL Methane+ version 1 TIR daytime 0-6km layer average retrievals over target region C.

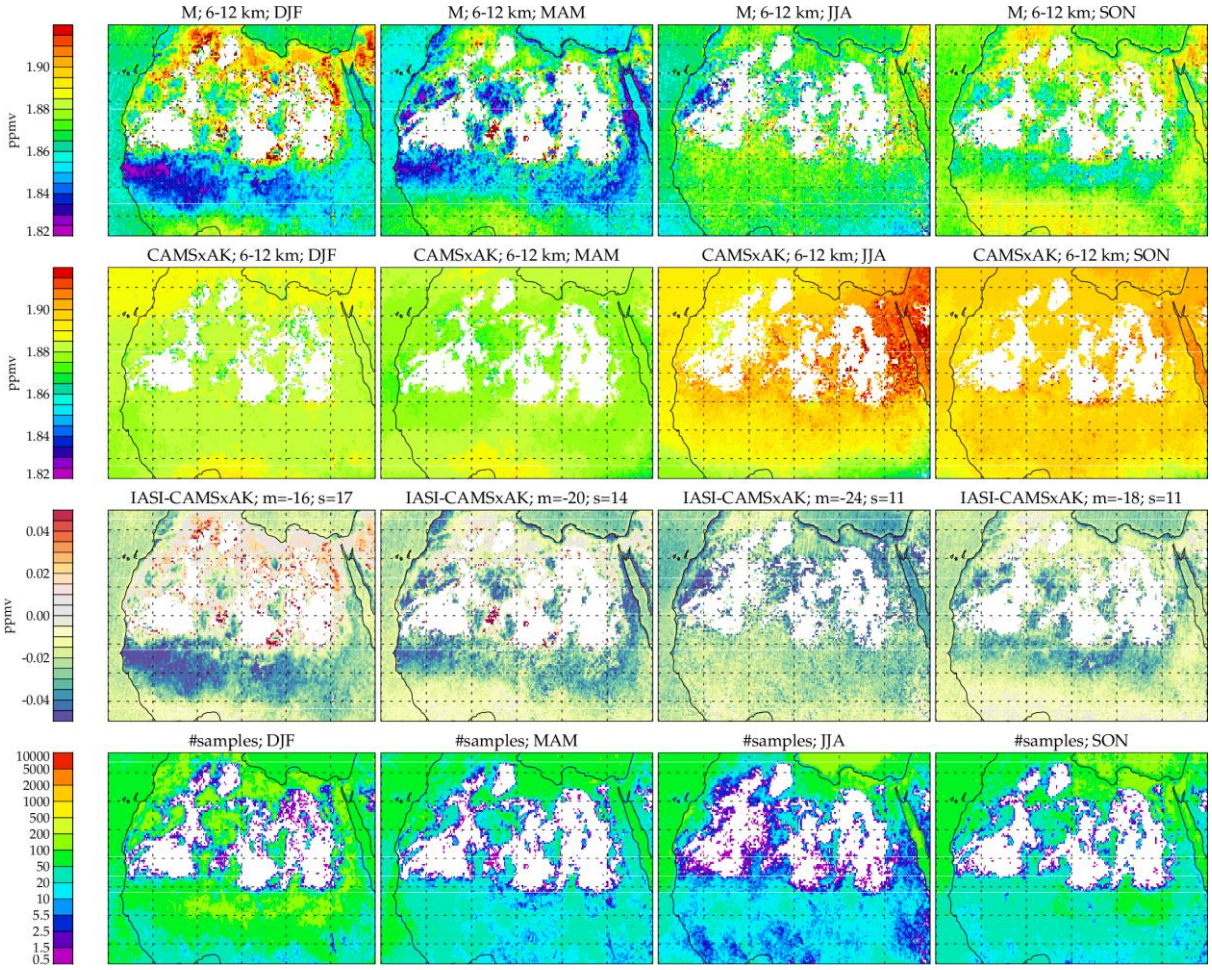

Figure 2-19 : RAL Methane+ version 1 TIR daytime 6-12km layer average retrievals over target region C.

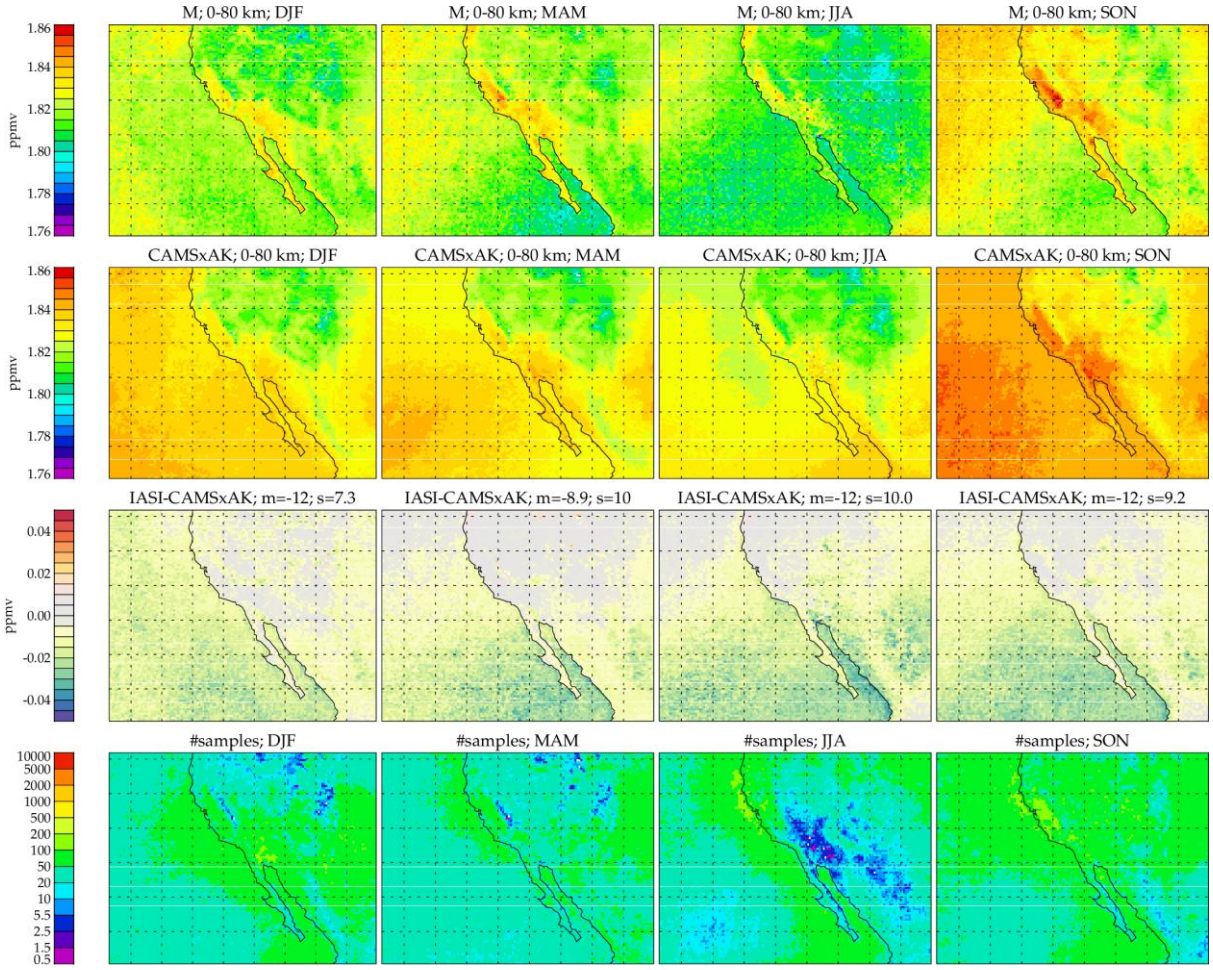

Figure 2-20 : RAL Methane+ version 1 TIR global daytime column average retrievals for region D: Each column of the figure shows results for a different season (2018 and 2019 combined). Rows from top-bottom show, respectively, results from IASI retrievals; CAMS with averaging kernels applied (CAMSxAK); the difference between IASI and CAMSxAK; the number of individual IASI retrievals in each of the 0.5x0.5 degree bins.

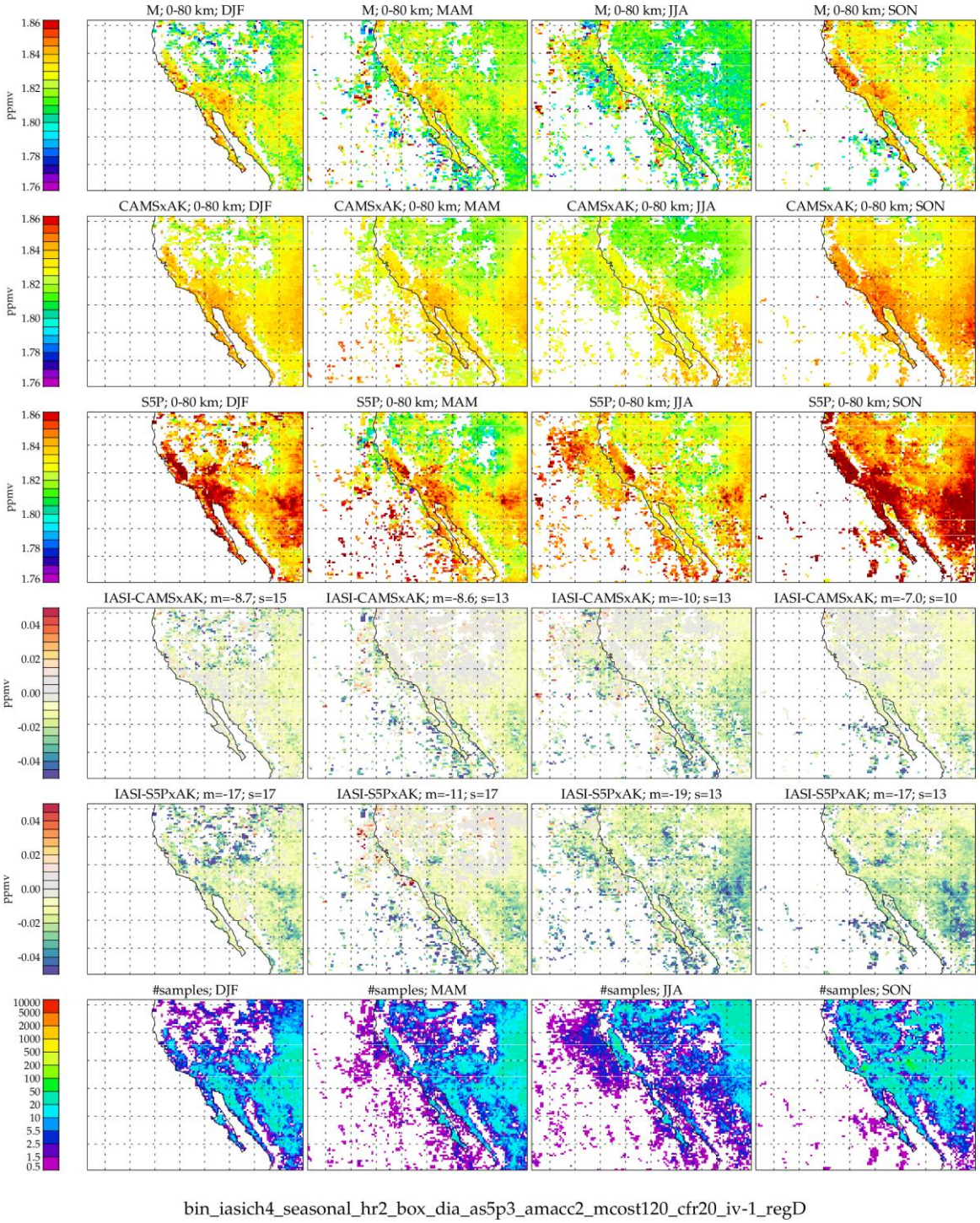

Figure 2-21 : RAL Methane+ version 1 TIR global daytime column average retrievals for region D, collocated with S5P: Each column of the figure shows results for a different season (2018 and 2019 combined). Panels from top-bottom show, respectively, results from IASI retrievals; CAMS; S5P retrievals; Difference between IASI and S5P; Difference between IASI and S5P accounting for the IASI averaging kernel using CAMS; the number of individual IASI retrievals in each of the 0.5x0.5 degree bins.

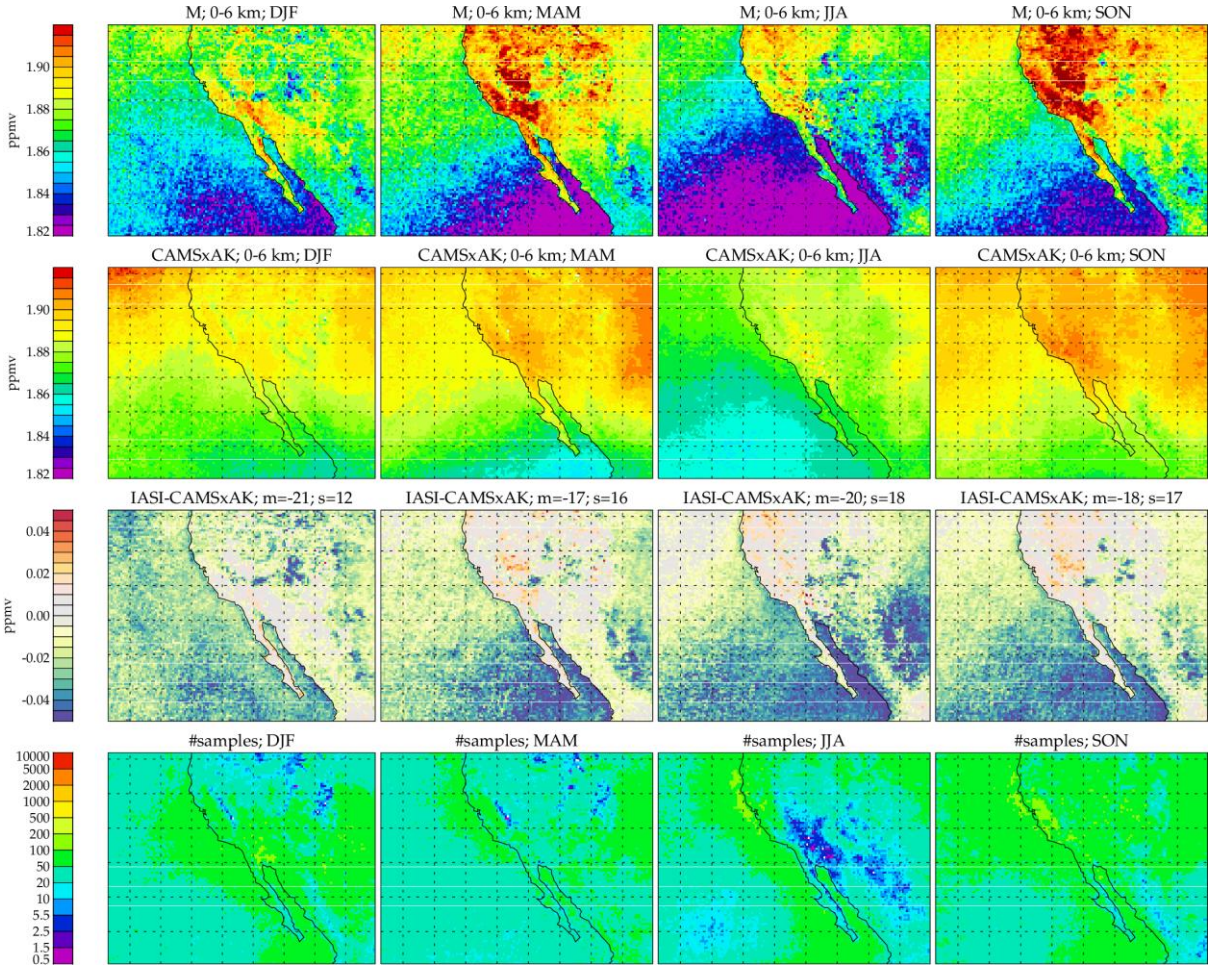

Figure 2-22 : RAL Methane+ version 1 TIR daytime 0-6km layer average retrievals over target region D. Note that this region is prone to land/sea related artefacts in the IASI retrieval related to outflow of relatively warm air from the continent over the sea, much higher total column water vapour over sea compared to the land, and the common occurrence of low altitude marine cloud. These lead to land/sea dependent differences between IASI and CAMS, which are to some extent mitigated in the candidate version 2 product described in chapter 4.

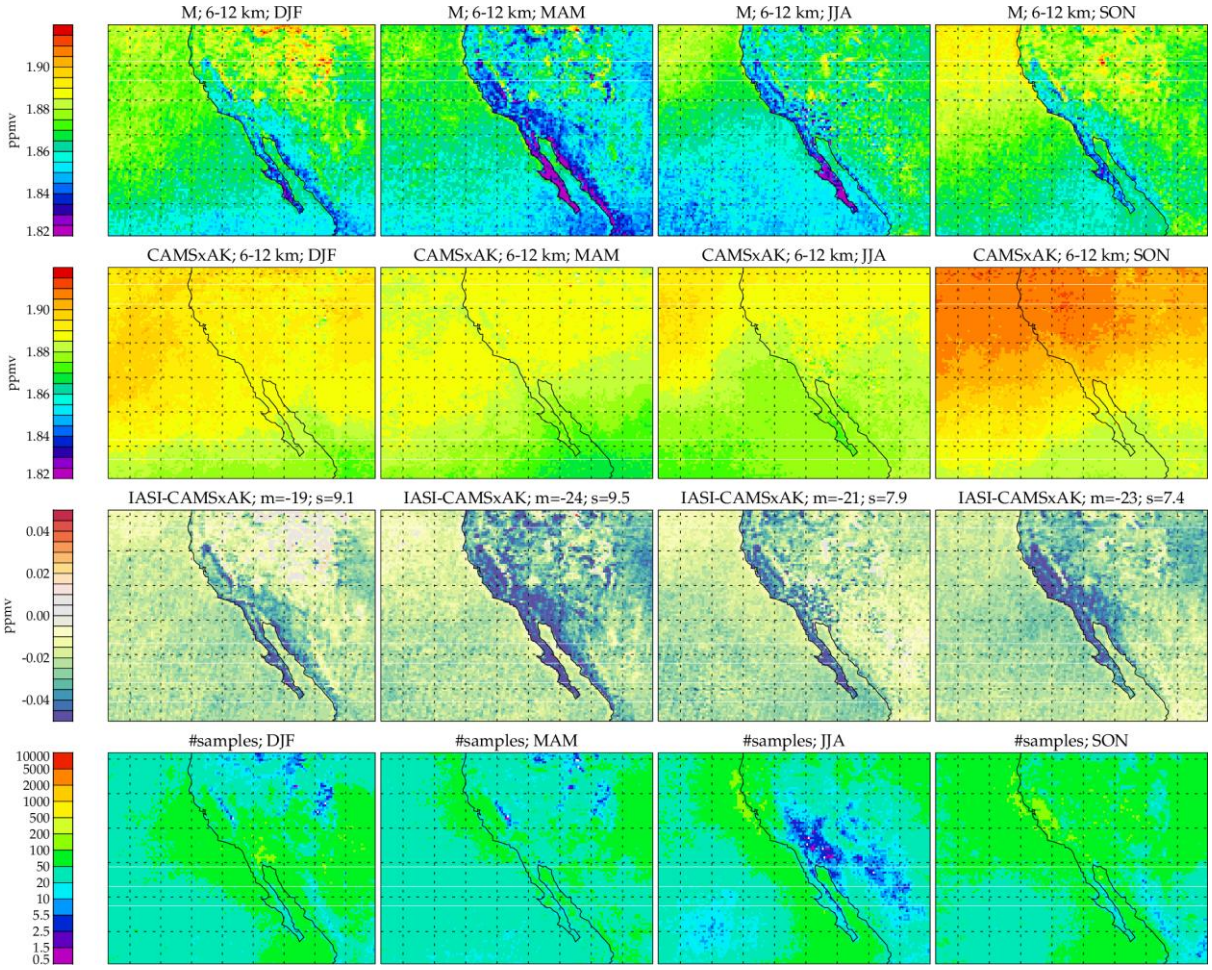

Figure 2-23 : RAL Methane+ version 1 TIR daytime 6-12km layer average retrievals over target region D.

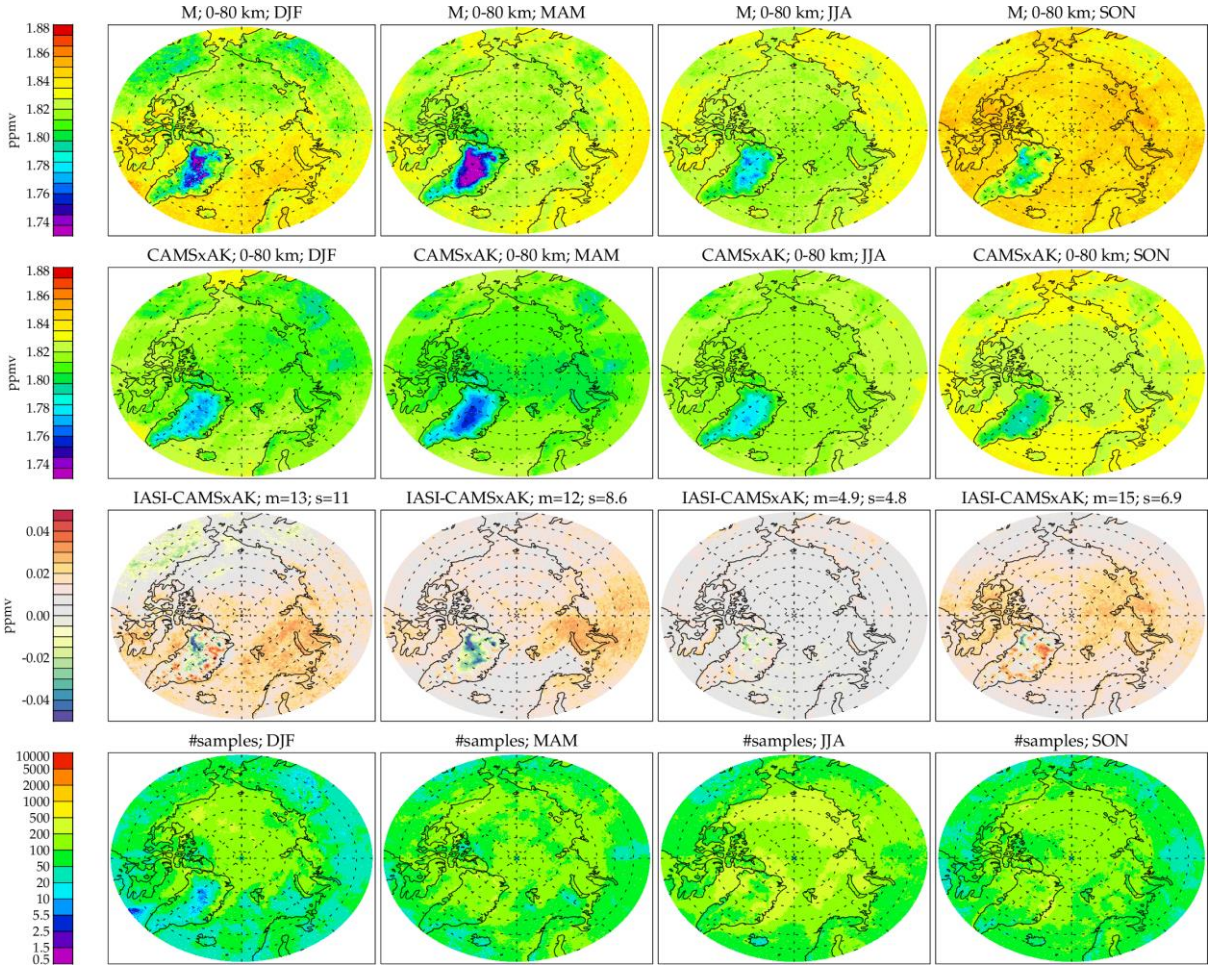

Figure 2-24 : RAL Methane+ version 1 TIR global daytime column average retrievals for region E: Each column of the figure shows results for a different season (2018 and 2019 combined). Rows from top-bottom show, respectively, results from IASI retrievals; CAMS with averaging kernels applied (CAMSxAK); the difference between IASI and CAMSxAK; the number of individual IASI retrievals in each of the 0.5x0.5 degree bins. In panels showing differences, the mean ("m") and standard deviation ("s") of the binned data are given, in ppbv, in the panel title.

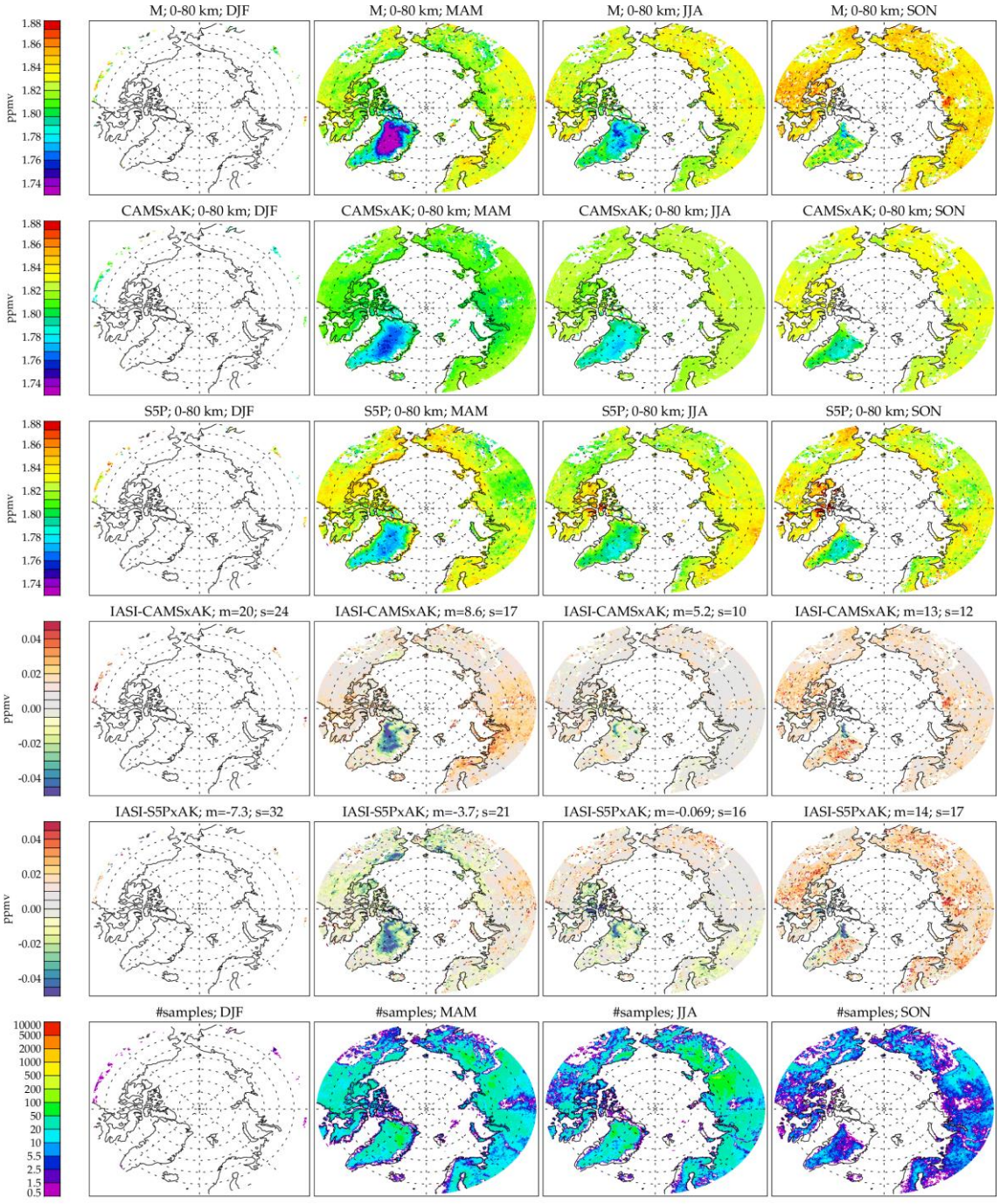

Figure 2-25 : RAL Methane+ version 1 TIR global daytime column average retrievals for region E, collocated with S5P: Each column of the figure shows results for a different season (2018 and 2019 combined). Panels from top-bottom show, respectively, results from IASI retrievals; CAMS; S5P retrievals; Difference between IASI and S5P; Difference between IASI and S5P accounting for the IASI averaging kernel using CAMS; the number of individual IASI retrievals in each of the 0.5x0.5 degree bins. In panels showing differences, the mean ("m") and standard deviation ("s") of the binned data are given, in ppbv, in the panel title.

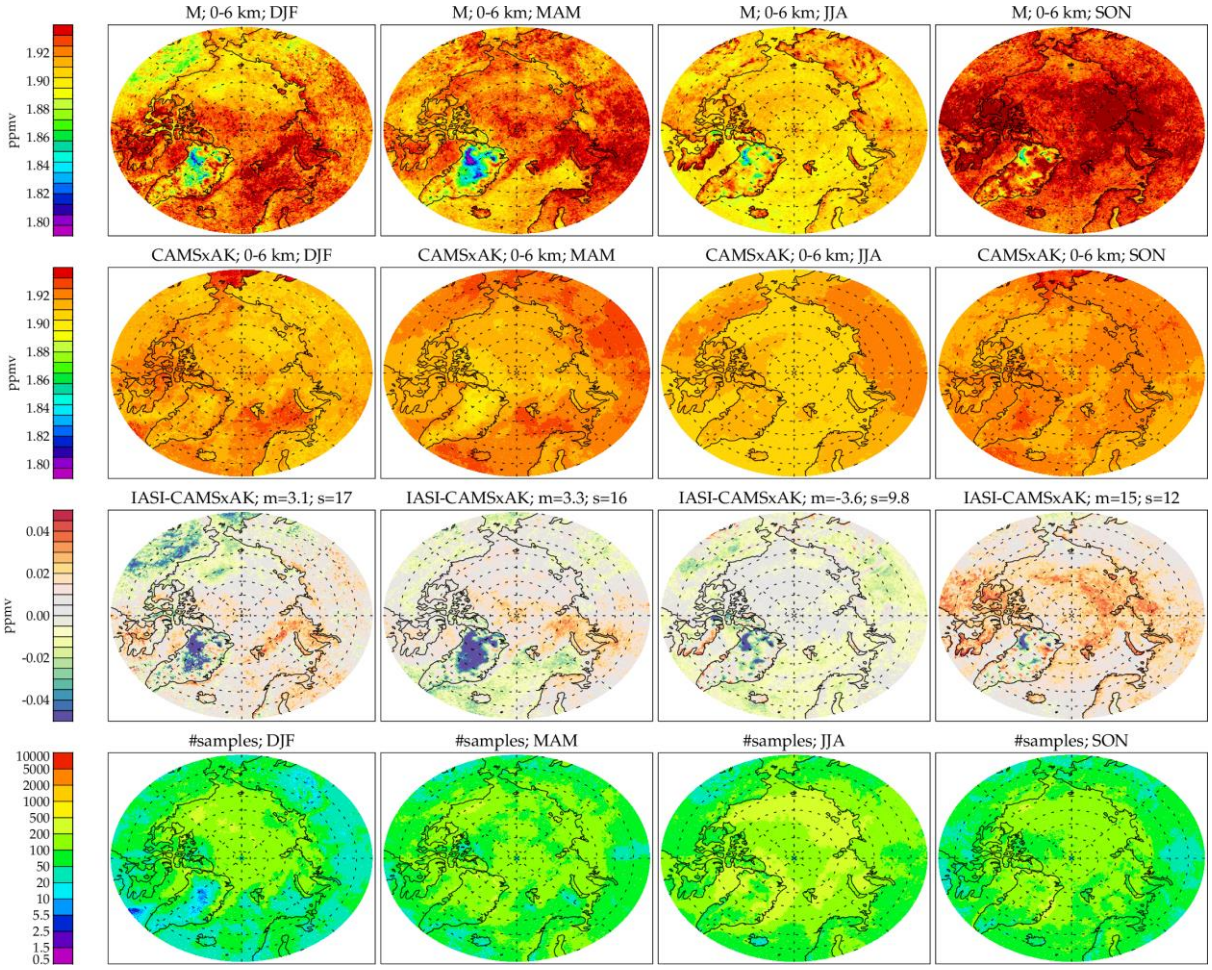

Figure 2-26 : RAL Methane+ version 1 TIR daytime 0-6km layer average retrievals over target region E.

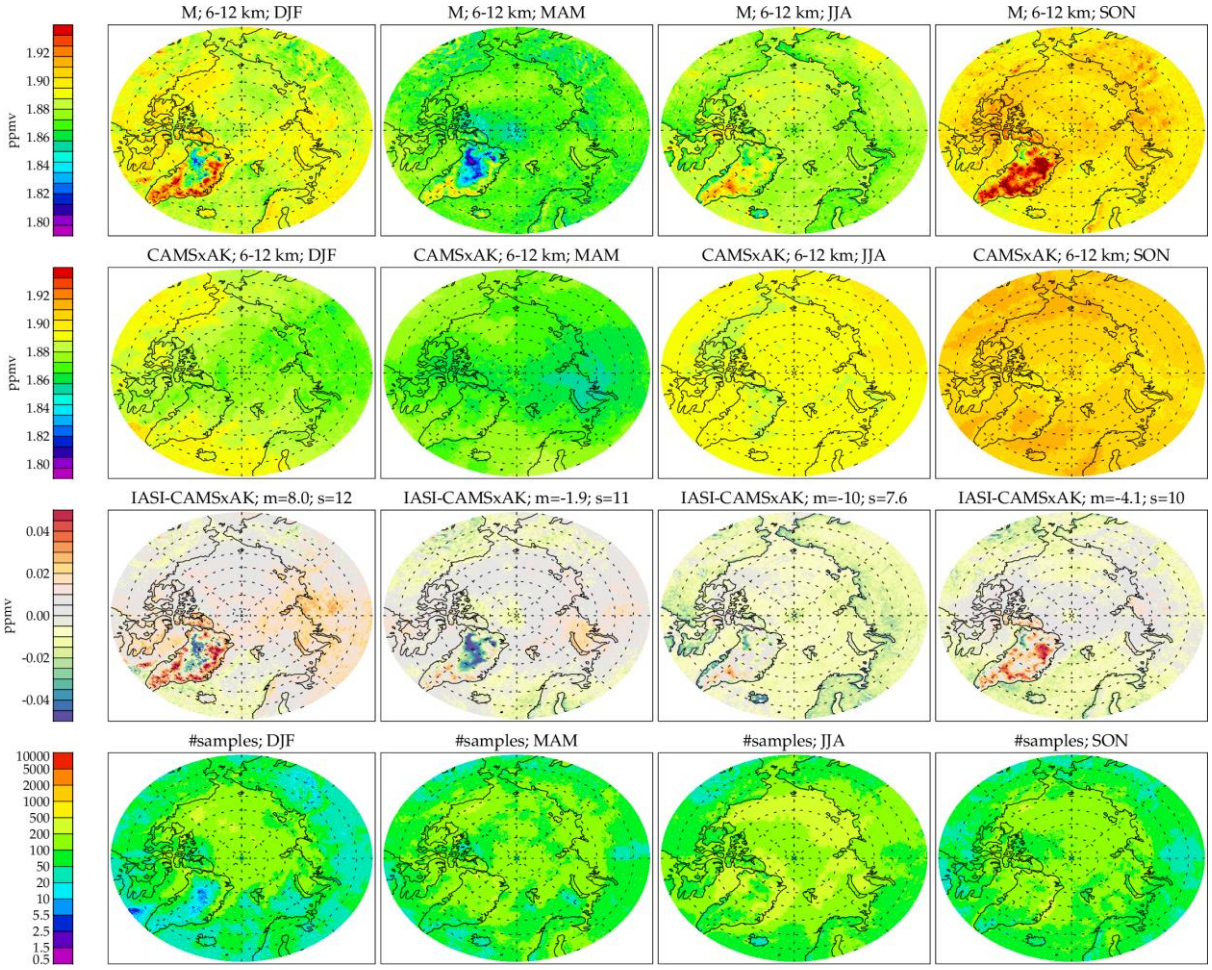

Figure 2-27 : RAL Methane+ version 1 TIR daytime 6-12km layer average retrievals over target region E.

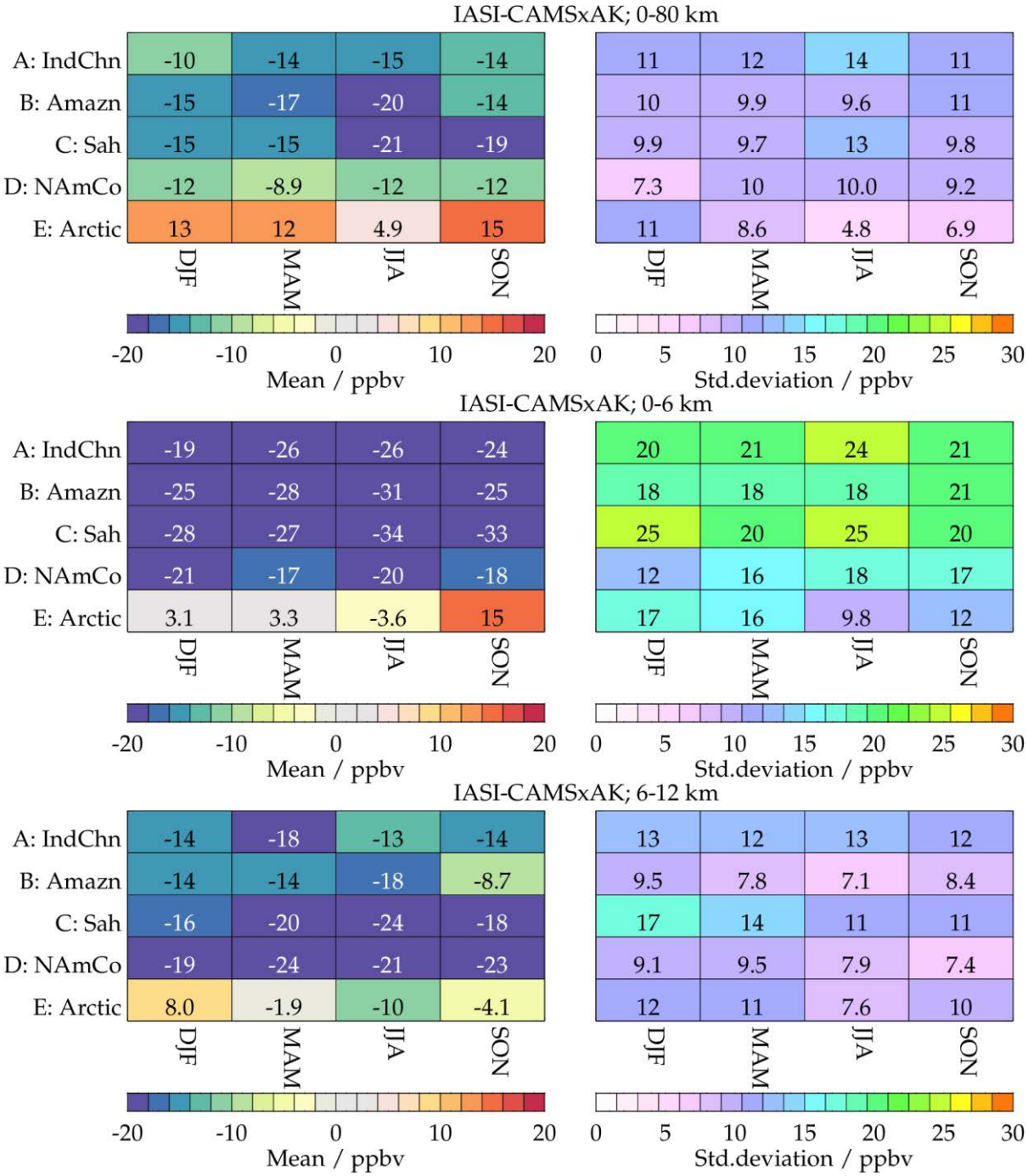

Figure 2-28 : Summary of seasonally averaged differences between RAL Methane+ version 1 TIR retrievals and CAMS for each region. Left-hand panel shows the mean difference in each region/season; Right-hand panel shows the standard deviation in the mean (considering the spatial variation of the difference for each of the 0.5x0.5 degree bins). Panels from top-bottom show results for total, 0-6 and 6-12km layer averages.

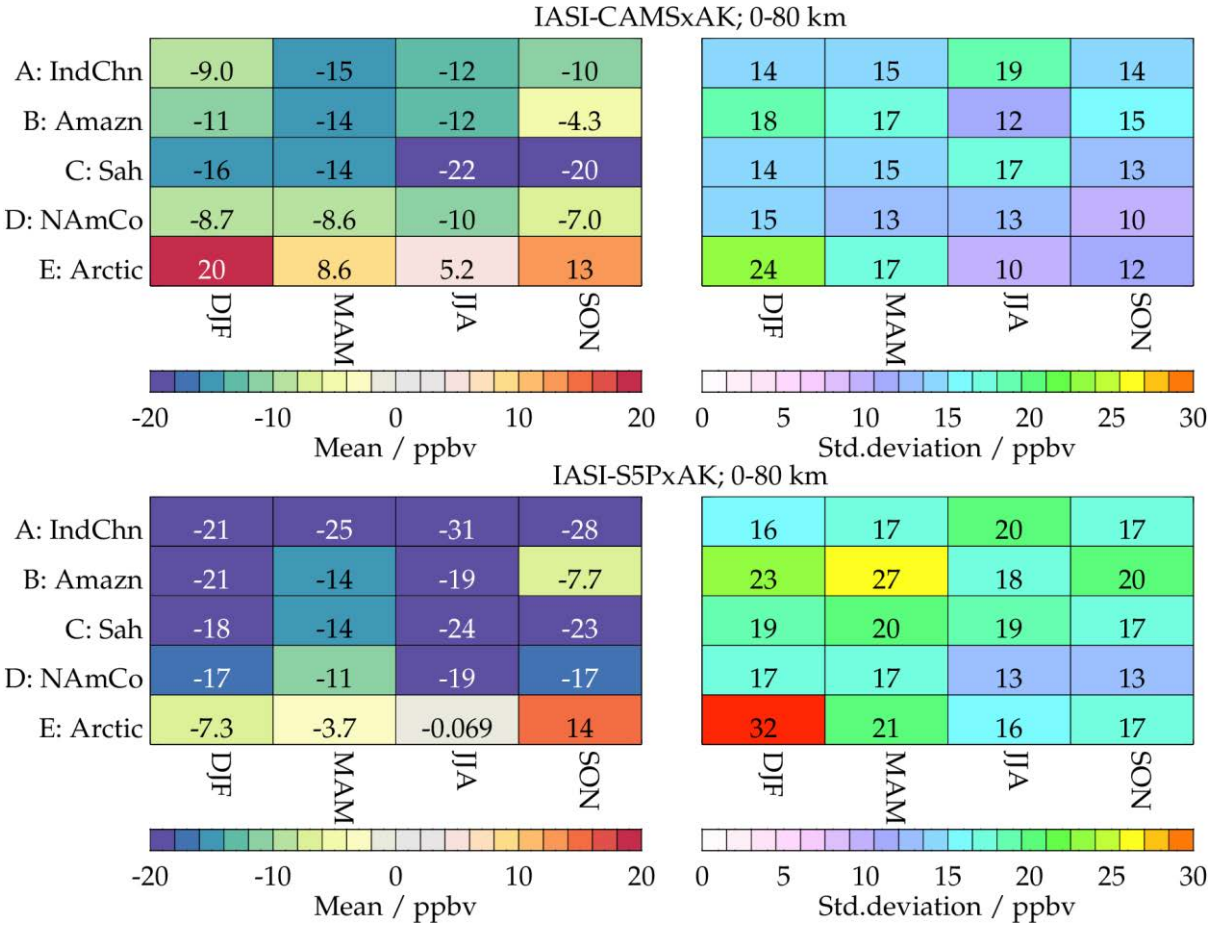

Figure 2-29 : Summary of seasonally averaged total column differences between RAL Methane+ version 1 TIR retrievals, CAMS and S5P for each region. Left-hand panel shows the mean difference in each region/season; Right-hand panel shows the standard deviation in the mean (considering the spatial variation of the mean difference for each of the 0.5x0.5 degree bins). Upper panels show the difference between IASI and CAMS (with averaging kernels); lower panels show the difference between IASI and S5P. Note that, in this figure, the comparisons to CAMS in upper panels are for the same sub-set of scenes for which there are S5P co-locations.

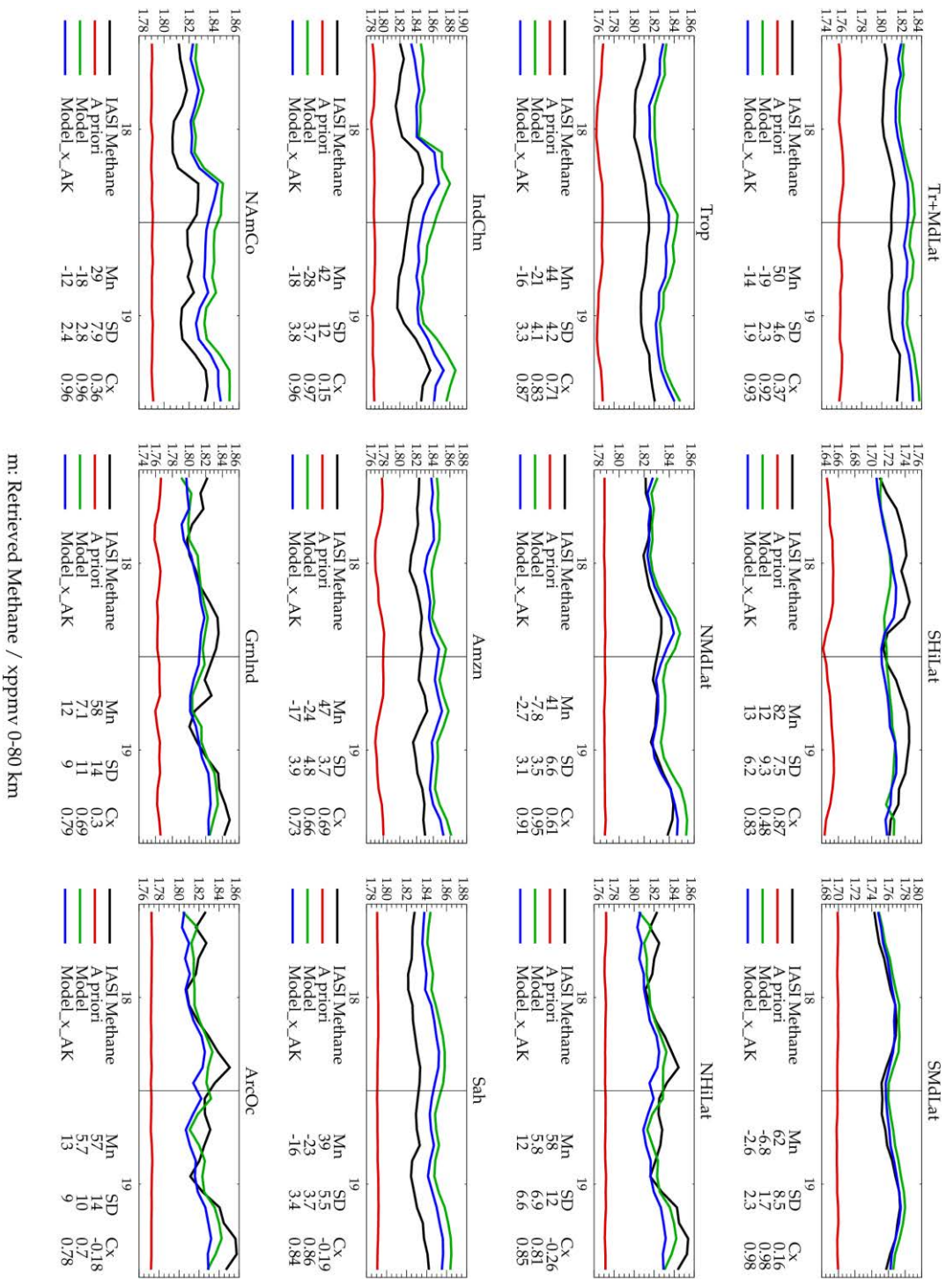

Figure 2-30 : Time series comparisons of RAL Methane+ version 1 TIR and CAMS column average methane for various regions. Each panel shows a different region as described in section 2.2. Statistics given in the legend under each panel give the mean difference (Mn); standard deviation of the monthly mean differences (SD); correlation between IASI and CAMS monthly mean values.

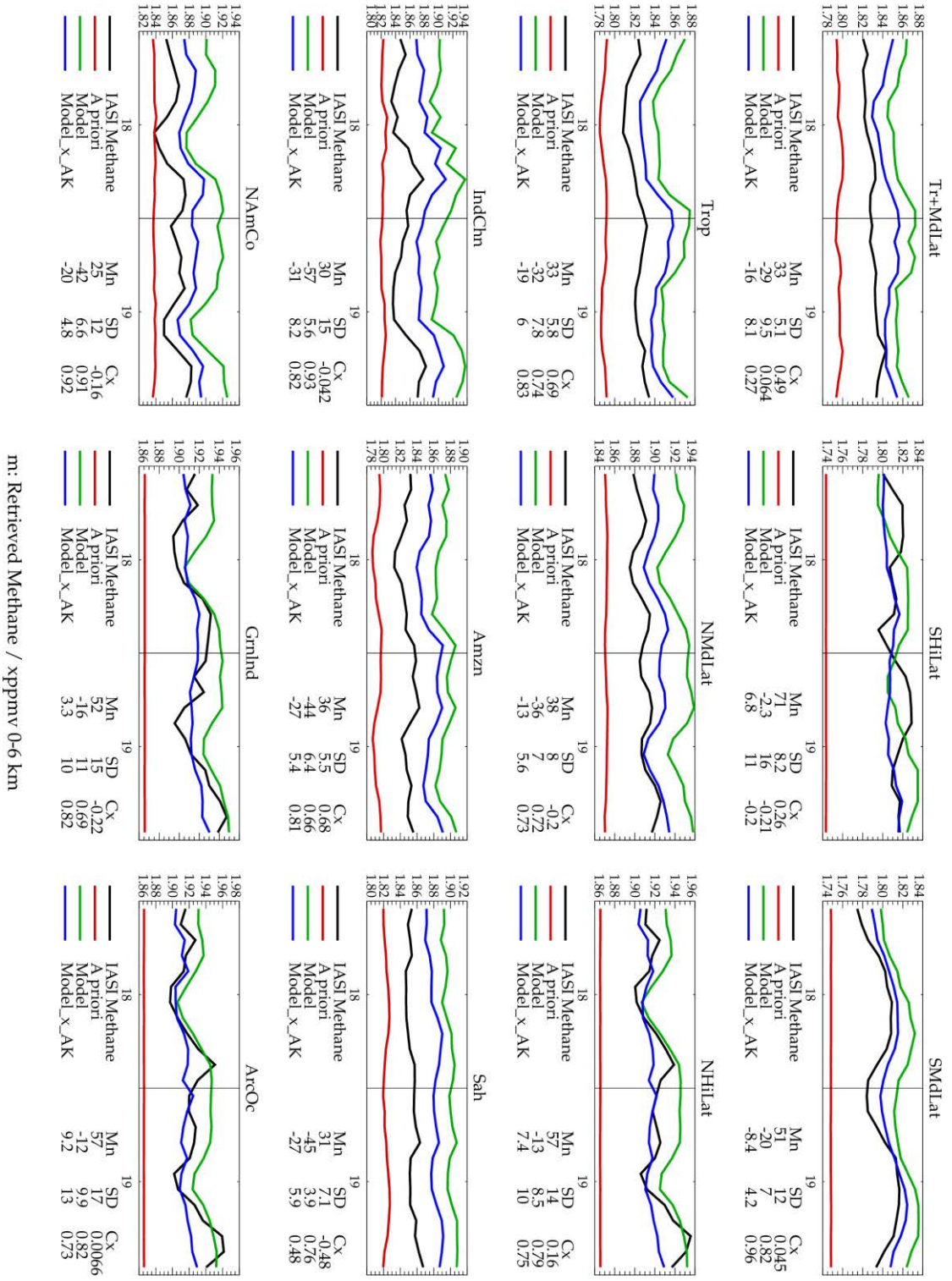

Figure 2-31 : Time series comparisons of RAL Methane+ version 1 TIR and CAMS 0-6km sub-column average methane for various regions. Each panel shows a different region as described in section 2.2. Statistics given in the legend under each panel give the mean difference (Mn); standard deviation of the monthly mean differences (SD); correlation between IASI and CAMS monthly mean values.

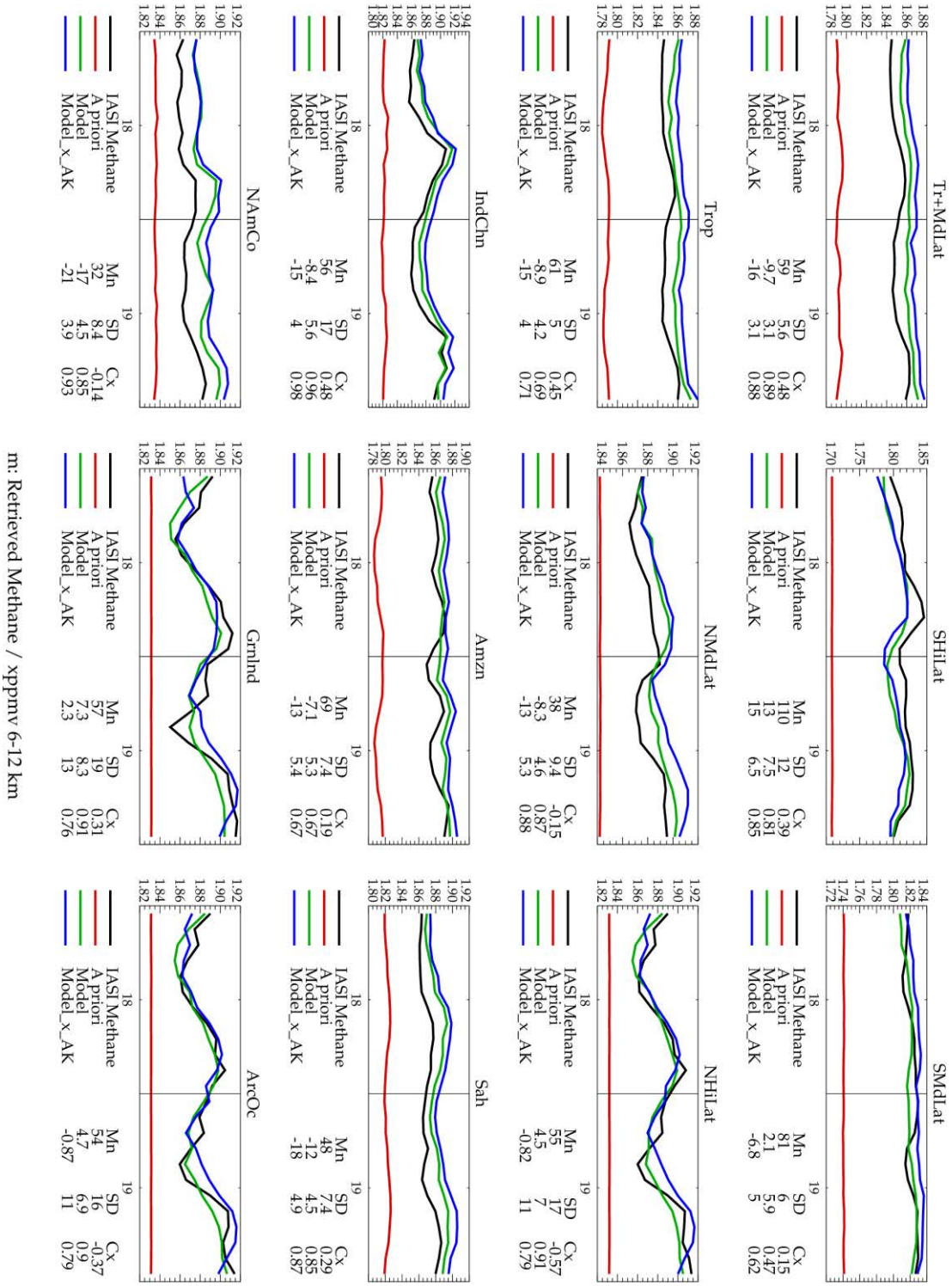

Figure 2-32 : Time series comparisons of RAL Methane+ version 1 TIR and CAMS 6-12km sub-column average methane for various regions. Each panel shows a different region as described in section 2.2. Statistics given in the legend under each panel give the mean difference (Mn); standard deviation of the monthly mean differences (SD); correlation between IASI and CAMS monthly mean values.

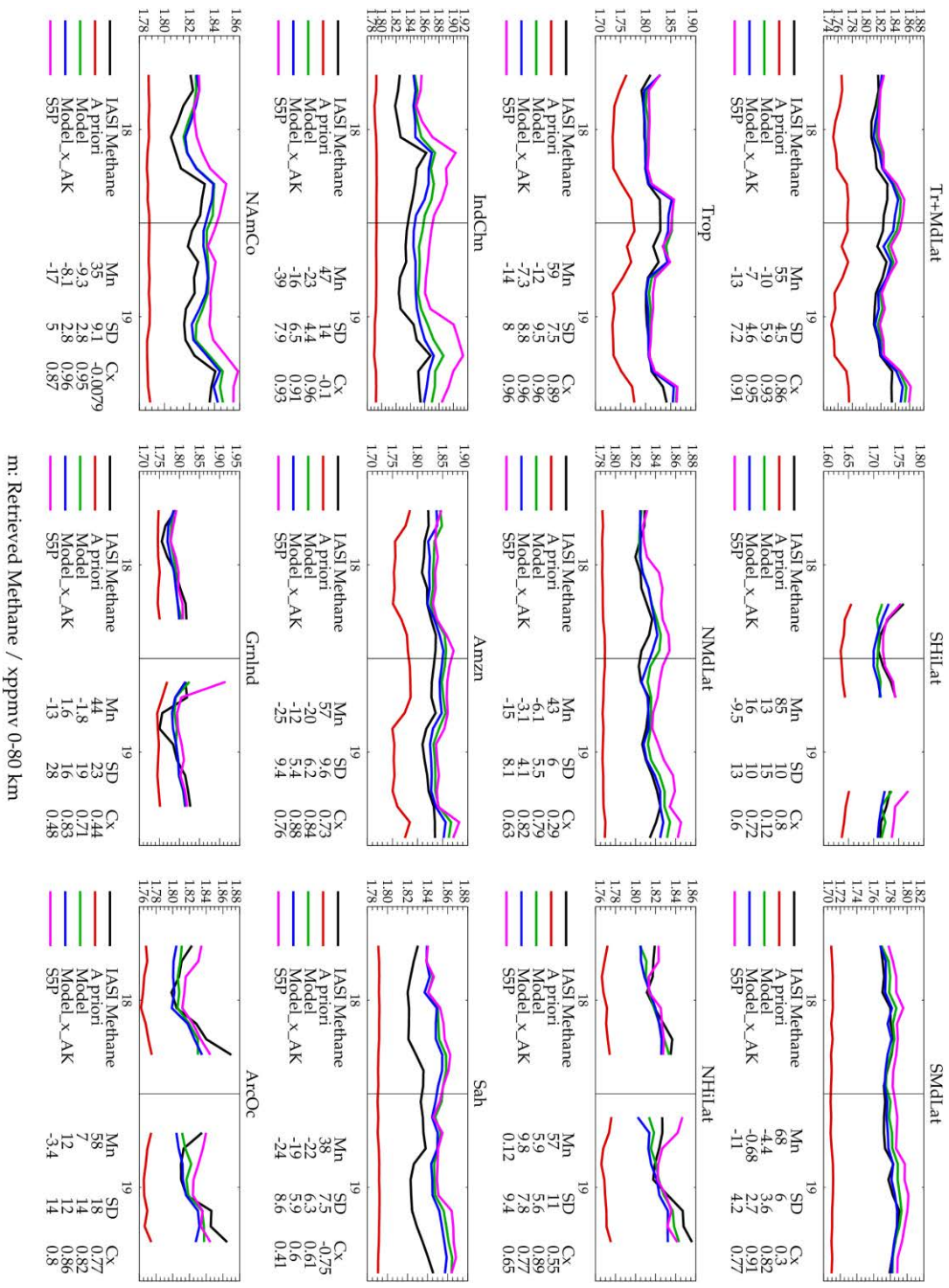

Figure 2-33 : Time series comparisons of RAL Methane+ version 1 TIR column average averaged methane to S5P (and CAMS sampled to S5P) for various regions. Each panel shows a different region as described in section 2.2. Statistics given in the legend under each panel give the mean difference from IASI (Mn); standard deviation of the monthly mean difference (SD); Correlation of the monthly mean values with IASI.

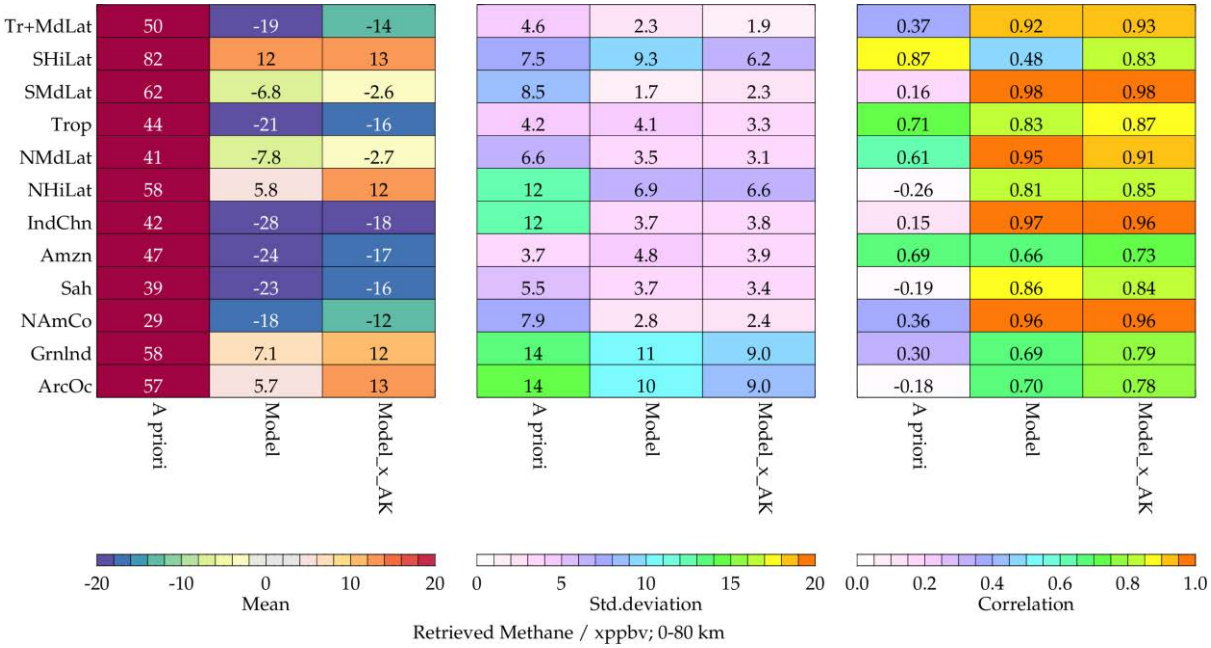

Figure 2-34 : Summary of statistics from monthly time-series comparisons of RAL Methane+ version 1 TIR and CAMS column average methane for various regions. Panels from left to right show the mean difference; standard deviation of the monthly mean differences; correlation between IASI and CAMS monthly mean values.

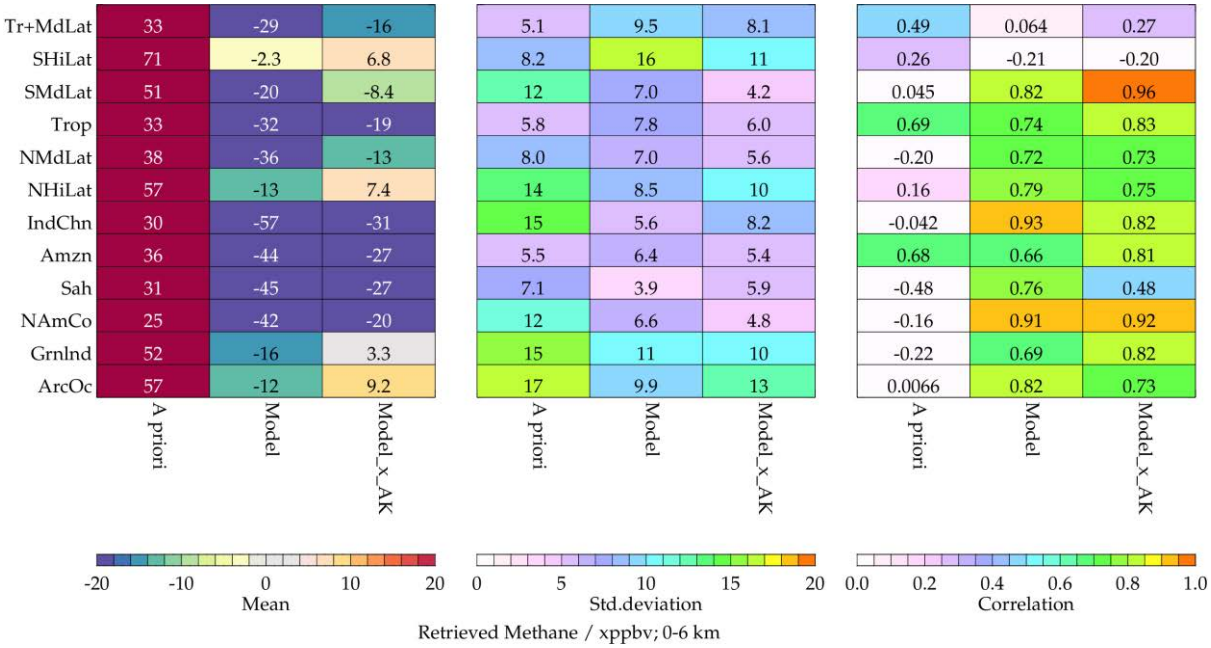

Figure 2-35 : Summary of statistics from monthly time-series comparisons of RAL Methane+ version 1 TIR and CAMS 0-6km sub-column average methane for various regions. Panels from left to right show the mean difference; standard deviation of the monthly mean differences; correlation between IASI and CAMS monthly mean values.

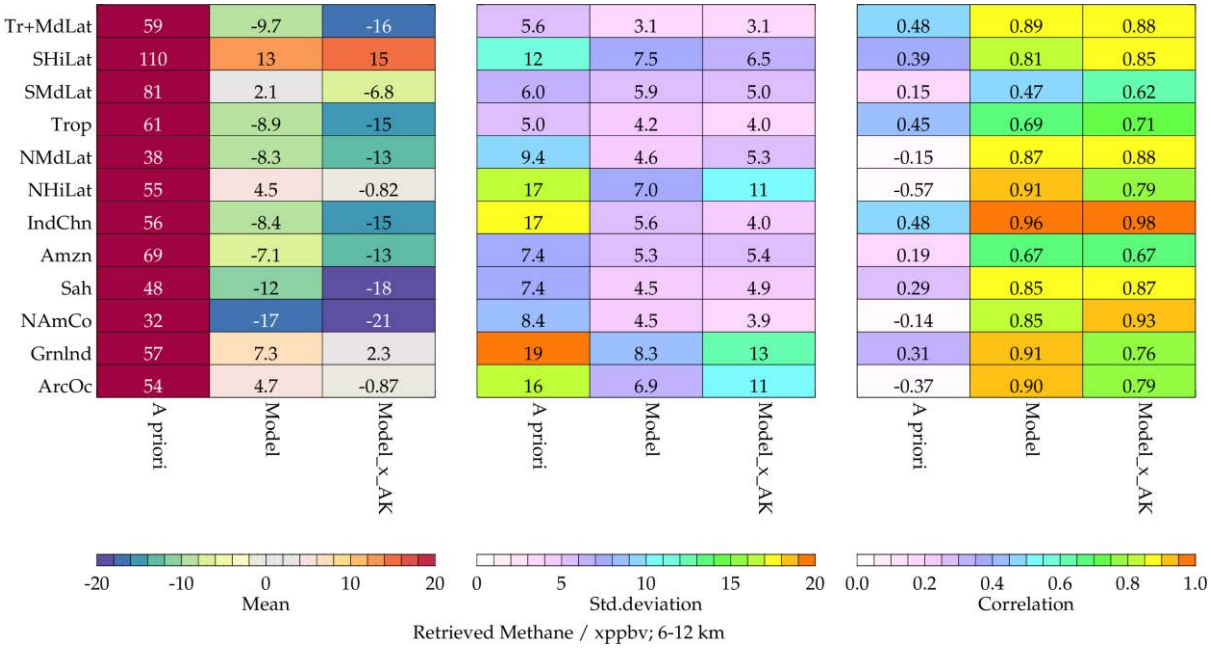

Figure 2-36 : Summary of statistics from monthly time-series comparisons of RAL Methane+ version 1 TIR and CAMS 6-12km sub-column average methane for various regions. Panels from left to right show the mean difference; standard deviation of the monthly mean differences; correlation between IASI and CAMS monthly mean values.

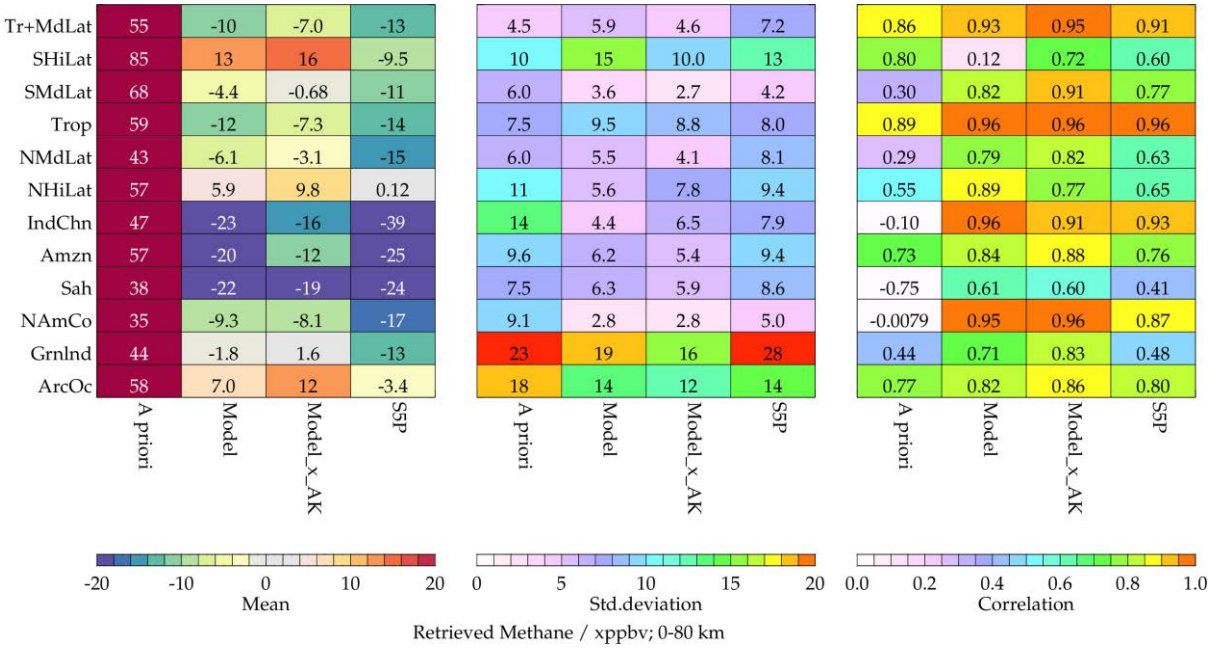

Figure 2-37 : Summary of statistics from monthly time-series comparisons of RAL Methane+ version 1 TIR column averaged methane to S5P (and CAMS sampled to S5P) for various regions. Panels from left to right show the mean difference; standard deviation of the monthly mean differences; correlation between IASI and CAMS monthly mean values.

2.3. Validation from non-satellite sources

2.3.1. Atom-4

The Atmospheric Tomography Mission (ATom) is a series of NASA DC-8 aircraft flight campaigns providing near pole-to-pole sampling of the atmosphere, profiling continuously between 0.2 and 12km altitude ATom (see the Methane+ AUM/DP for further information and links). Methane is measured *in situ* by three instruments: a gas chromatograph, quantum cascade laser (QCL) and a cavity ringdown spectrometer. Here we use the QCL data (for consistency with our analysis of previous HIPPO campaigns). There have been four ATom campaigns covering a similar flight track, each consisting of numerous individual flights between 2016-2018, and spanning each of the four seasons, producing a contiguous dataset. Only the fourth campaign, which occurred between 24th April - 21st May 2018, falls in the analysis window for this project and, therefore, only results from this campaign are shown.

The ATom-4 methane profile data is binned to match the IASI spatial sampling and extended vertically using co-located CAMS v19r1 flux inversion data (in this case *without* using ACE-FTS in the stratosphere). The latter step is necessary in order to apply the IASI averaging kernels which extend higher than the Atom-4 profiles.

All retrieved IASI methane profiles co-located with each ATom-4 profile are combined to produce IASI mean column and layer averages. The co-location criteria allowed IASI IASI profiles within 100km/6hrs of the sampled ATom profile. Further, only IASI methane retrievals with cloud fraction less than 0.2 are included.

Figure 2-38 shows the ATom-4 campaign track, together with the binned (CAMS extended) profiles and the comparison with IASI column and layer averages (with and without application of averaging kernels). Note that the campaign passes over the Atlantic in a region where methane mixing ratios are much larger in the upper troposphere than below (around profile index 57 in the figure), presumably related to outflow from the Amazon. These seems to be well captured by the retrieval of upper and lower tropospheric layers.

Figure 2-39 shows differences between ATom-4 and IASI binned as a function of latitude. The bias is improved by application of averaging kernels, but the standard deviation in the differences is not much changed (indicating that this is dominated by noise on individual retrievals). The latitude dependence and magnitude of the bias is similar to that found for CAMS e.g. in Figure 2-6.

Figure 2-40 shows scatter density plots comparing ATom-4 and IASI retrievals. Each square in each panel is colour coded by the number of binned profiles falling within the area of the square. The retrieval is shown to clearly improve over the prior and agreement is improved by applying averaging kernels to the ATom-4 profile. The 4th

row compares the difference between the 0-6 and 6-12km layer average mixing ratios from IASI and ATom-4, demonstrating that the retrieval has some skill at distinguishing between methane variations in the two layers.

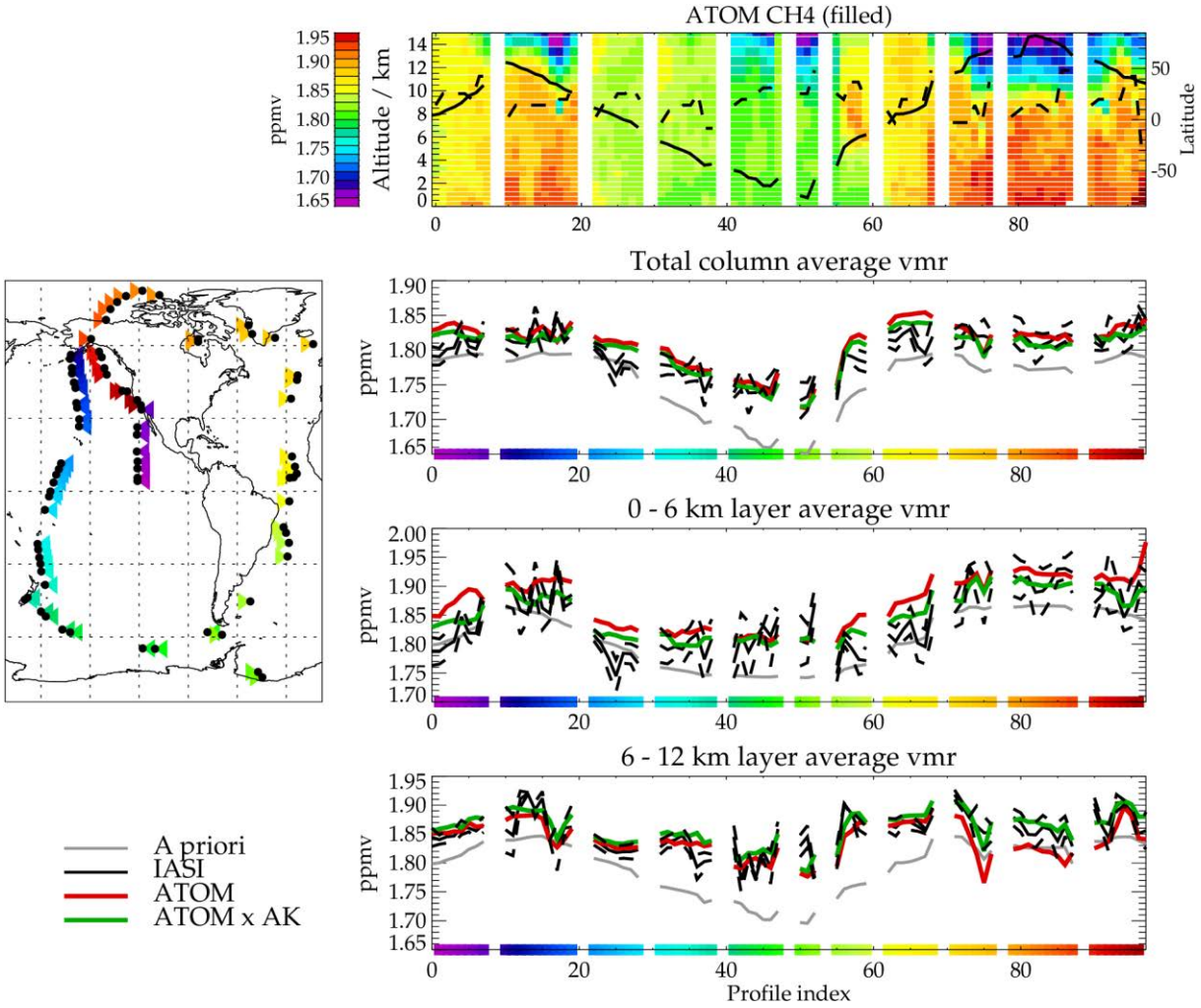

Figure 2-38 : Comparison of RAL Methane+ version 1 TIR and ATom-4 flights (24 April 2018 to 21 May 2018). Map on the left shows the flight track. Actual measurement locations are indicated with black dots; associated coloured triangles indicate the profile index, as shown on the x-axis of panels on the right (colours under the axis correspond to colours used in the map). There are 78 actual profiles in the cross-section. Some null profiles (shown white in the top panel) are inserted to mark gaps between the various flights in each campaign. The top-right panel shows the cross-section along the flight transect as measured by ATom-4, after binning and extending upwards using CAMS v19r1 flux inversion. The solid black line in this plot shows the latitude of each profile (refer to y-axis on the right). The dashed black line shows the maximum (z*) altitude of the ATom-4 measurement, above which profiles are extended with CAMS profiles. Gaps (filled with white) between the coloured regions divide data from different flights (on different days). Panels below compare IASI and ATom-4 column and layer average mixing ratios. The mean of matched IASI retrievals is shown in black. The dashed black lines show +/- the averaged standard deviation of the matched retrievals. Grey shows the IASI a priori. Red shows the ATom-4 result; Green shows ATom-4 after taking into account the IASI averaging kernel.

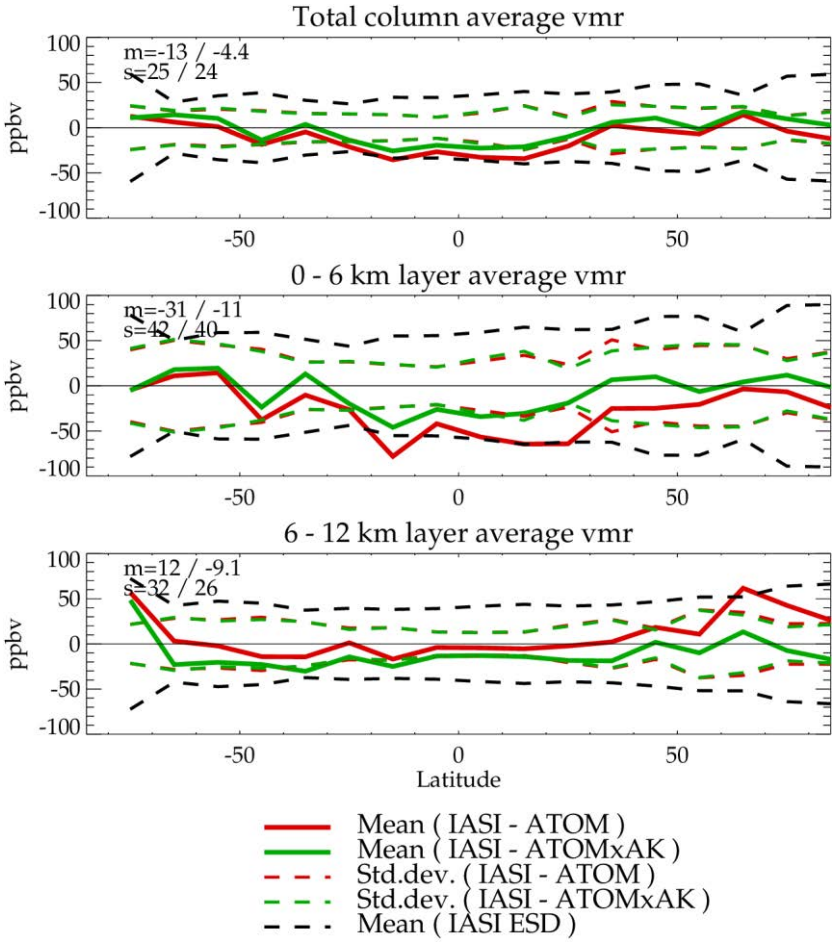

Figure 2-39 : Differences between RAL Methane+ version 1 TIR and ATom-4 binned as a function of latitude. As indicated in the legend, solid lines show the mean difference between IASI and ATom-4 (with (green) and without (red) IASI averaging kernels being applied to ATom-4 data). Corresponding dashed lines show the standard deviation of the individual IASI/ATom-4 matches about the mean difference. Black dashed lines show the mean of the IASI ESD on individual soundings. Figures in the top-left of each panel show the mean difference (m) over all matches and the standard-deviation of the individual matches about the mean without / with application of IASI averaging kernels to ATom-4 data.

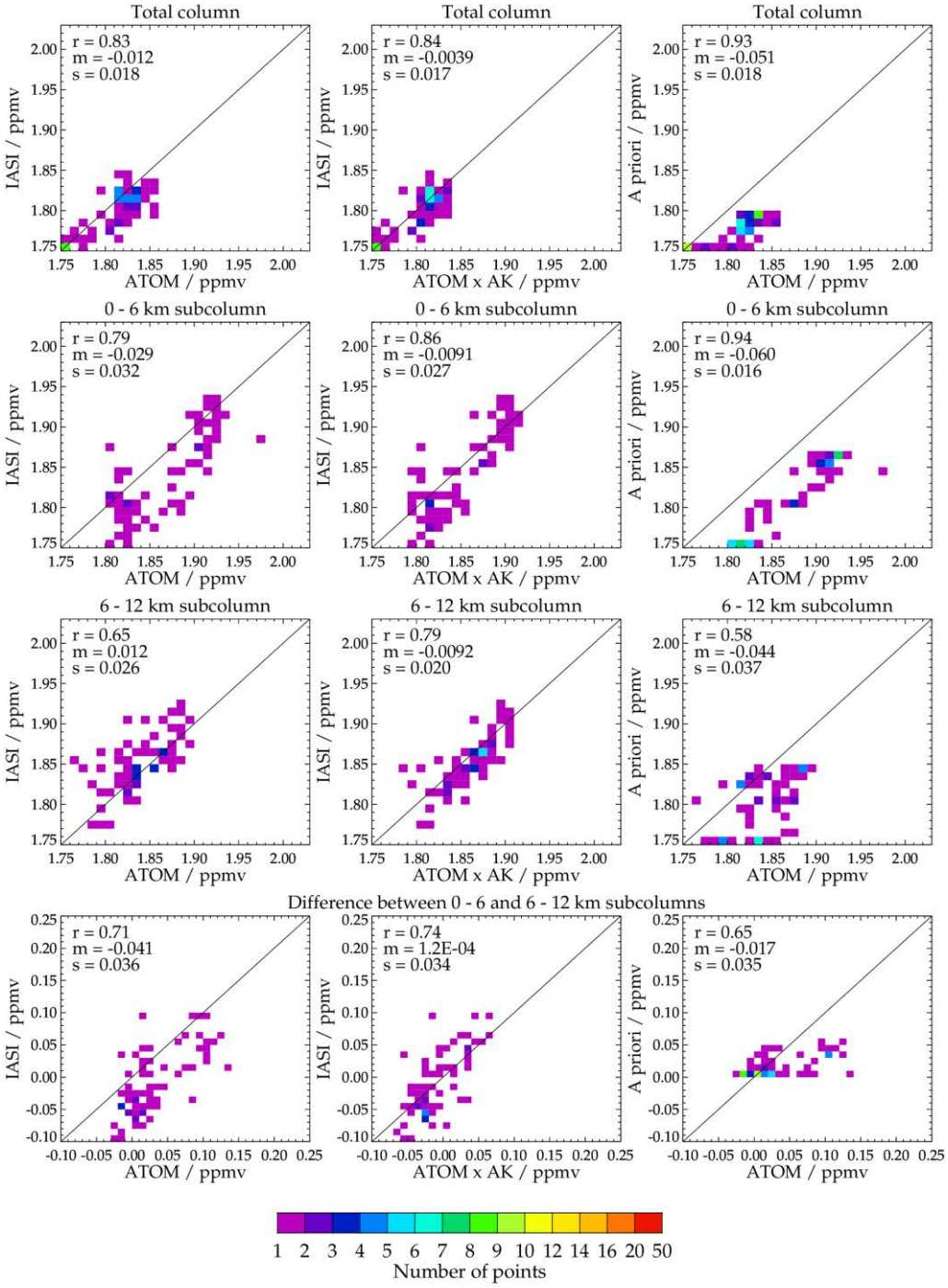

Figure 2-40 : Scatter density plots comparing ATom-4 and RAL Methane+ version 1 TIR. Columns from left to right: IASI vs ATom (left), IASI vs ATom accounting for averaging kernels (centre) and the a priori used in the retrieval vs ATom-4 (right). Rows from top-bottom show the column average, 0-6km layer, 6-12km layer and the difference between the 0-6 and 6-12km layers. The following statistics are shown within each panel: correlation coefficient (r); mean difference (m); standard deviation in the difference (s). The total number of points in each density plot is 78 (one for each profile in the previous figures).

2.3.2. AirCore

The AirCore is an atmospheric sampling system that flies under a meteorological balloon, allowing the measurement of vertical profiles of methane and other gases from the surface up to an altitude of approximately 30km. The original concept was developed at NOAA and has since been implemented across the globe.

Twenty AirCore profiles were identified within this project's analysis period (2018-2019); 16 from the AirCore-Fr program (Membrive, 2017) and 4 from Sodankylä. These profiles were extended vertically using co-located CAMS v19r1 flux inversion profiles and projected onto the CAMS 137 level vertical grid. The LMD team provided RAL with the extended profiles to ensure consistency between comparisons.

The analysis method applied to the AirCore profiles is the same as described above for the ATom-4 data. All retrieved IASI methane profiles co-located with each AirCore profile averaged. The co-location criteria applied allowed for IASI profiles within 100km/6hrs of the sampled AirCore profile. Further, only IASI methane retrievals with cloud fraction less than 0.2 are included.

Figure 2-41 shows the mean difference between IASI and each AirCore profile, for the column average and upper/lower tropospheric layer averages. Figure 2-42 shows the corresponding results after application of the IASI averaging kernels to the AirCore profile. Averaging kernels improve the agreement for the two layers while increasing the bias in the column average.

Figure 2-43 shows scatter plots analogous to those for ATom-4 in Figure 2-40. Note that since there are only nineteen profiles confined to the latitude range 44-65N, the range of methane variability sampled by the AirCore profiles is substantially smaller than that sampled by ATom-4. Retrieval and co-location errors are therefore larger in relation to the range of atmospheric variability sampled and correlation coefficients therefore lower.

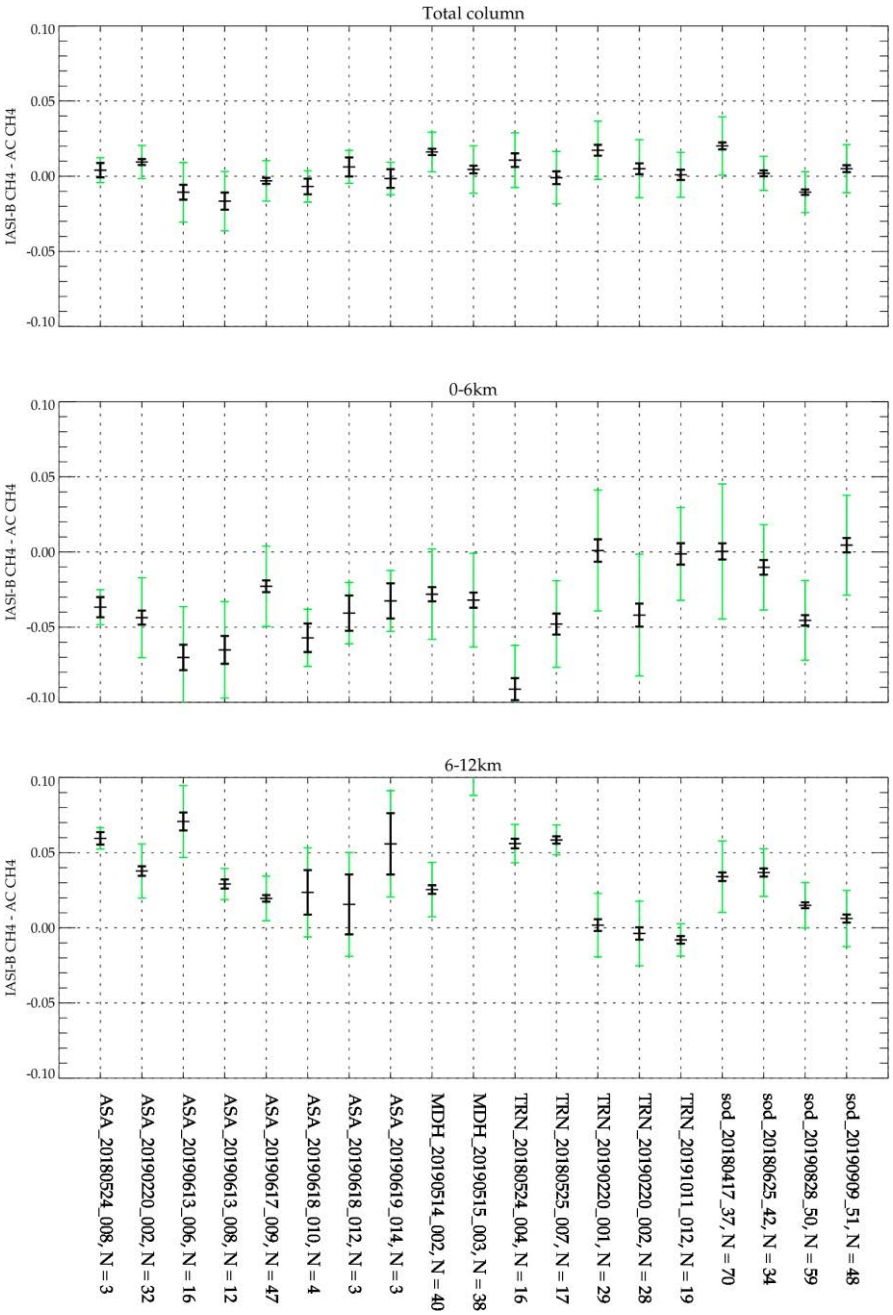

Figure 2-41 : Differences between RAL Methane+ version 1 TIR retrievals and AirCore profile measurements for (a) the column average, 0-80km, (b) the 0-6km layer average, and (c) the 6-12km layer average. The error bars represent the standard errors in the mean (black) and standard deviations (green) of IASI-AirCore differences for the set of IASI soundings co-located with each AirCore profile. Results are shown for all AirCore profiles that passed the quality control criteria.

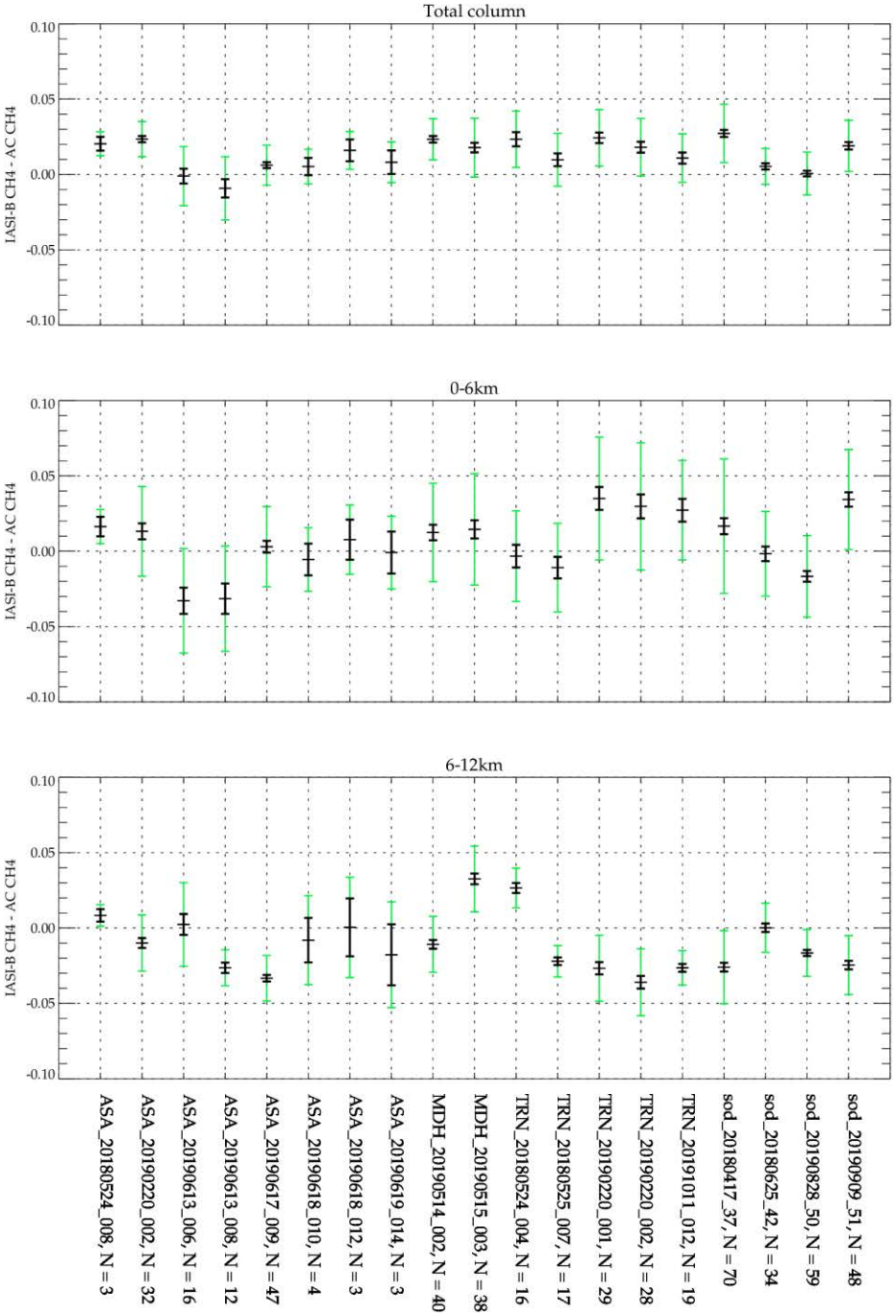

Figure 2-42 : As previous figure but with averaging kernels applied to AirCore profiles

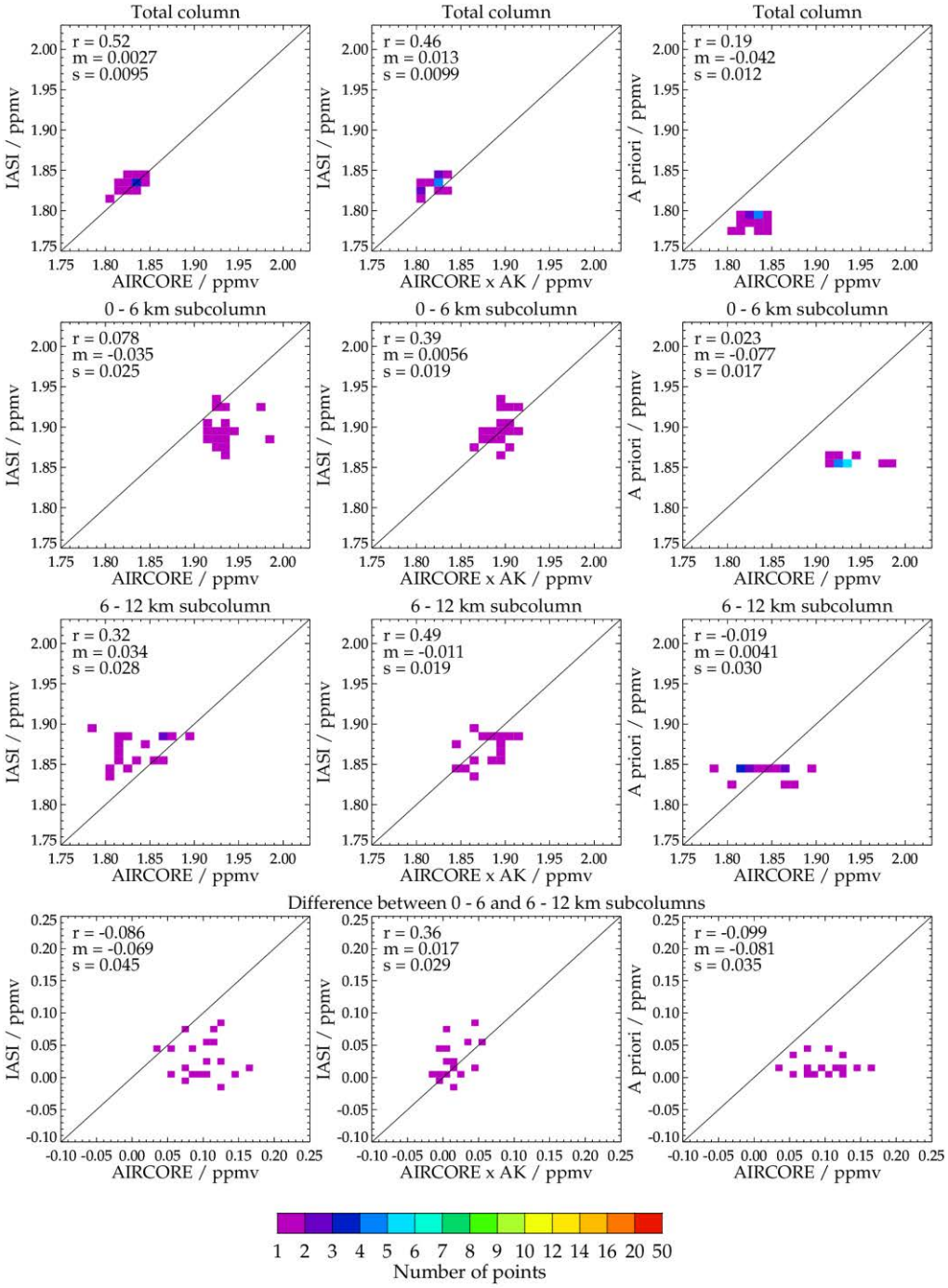

Figure 2-43 : Scatter density plots comparing AirCore and RAL Methane+ version 1 TIR. Columns from left to right: IASI vs AirCore (left), IASI vs AirCore accounting for averaging kernels (centre) and the a priori used in the retrieval vs AirCore (right). Rows from top-bottom show the column average, 0-6km layer, 6-12km layer and the difference between the 0-6 and 6-12km layers. The following statistics are shown within each panel: correlation coefficient (r); mean difference (m); standard deviation in the difference (s).

2.3.3. TCCON

The Total Carbon Column Observing Network (TCCON) is a network of ground-based Fourier Transform Spectrometers taking measurements in the near-infrared (Wunch 20210). TCCON provides a comprehensive set of ground-based column averaged methane measurements.

Here we compare the IASI methane retrievals to all available TCCON data from version “GGG2014“ (downloaded on 21st Jan 2021). Monthly mean column averages are calculated using all IASI retrievals that are co-located with a TCCON measurement, where the IASI profile must lie within 100km of the TCCON station and be within 6 hrs of measurement. When multiple TCCON measurements pass these criteria, the closest spatially to a given IASI sounding is chosen, so an individual IASI sounding is associated with only one TCCON measurement.

Figure 2-44 shows Hovmöller comparing TCCON with IASI in 2018 and 2019. These are obtained by binning co-located IASI and TCCON observations into monthly zonal mean bins.

Figure 2-45 shows scatter plots of monthly mean co-located IASI and TCCON data in specific latitude bands (each point corresponds to an individual cell in the Hovmöller plot).

Figure 2-46 compares co-located IASI and TCCON averaged over regions. Note that some regions have no TCCON station within them (corresponding panels contain no data). Figure 2-47 summarises the statistics from these time-series comparisons.

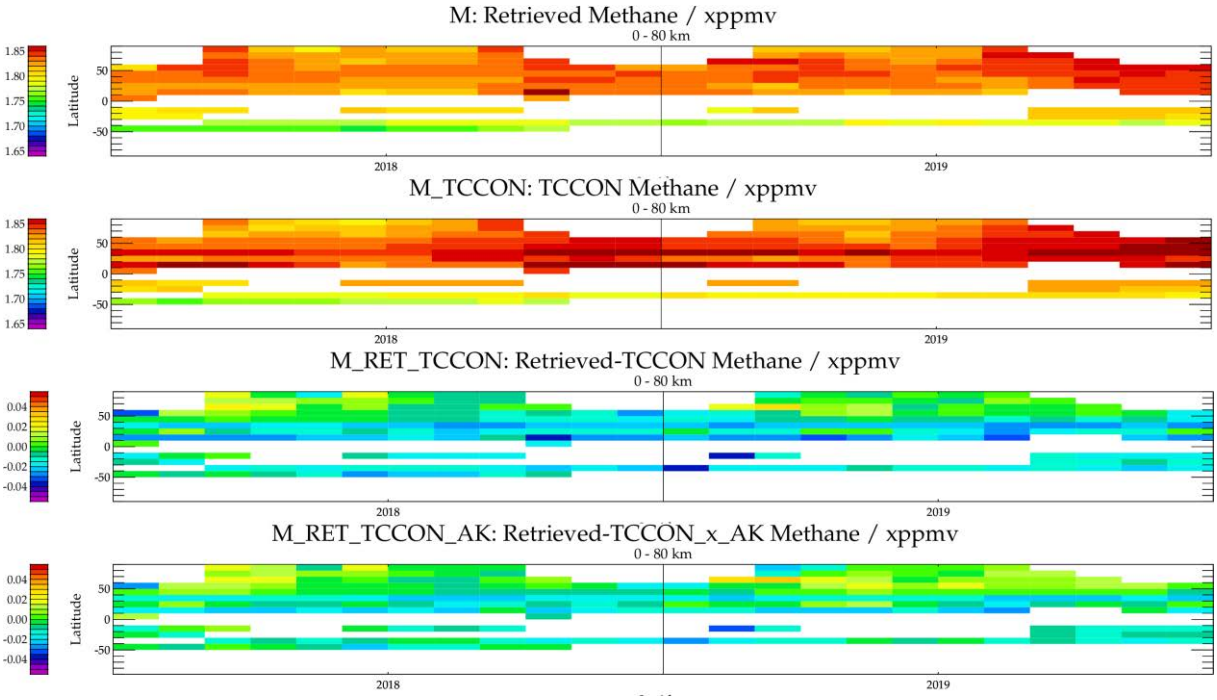

Figure 2-44 : RAL Methane+ version 1 TIR Hovmöller time-series for (a) IASI-B retrieved methane; (b) TCCON methane, measurements; (c) the difference between IASI and TCCON; (d) the difference between IASI and TCCON, adjusted to account for IASI averaging kernels using CAMS. Panels are shown for column average (0-80km) retrievals.

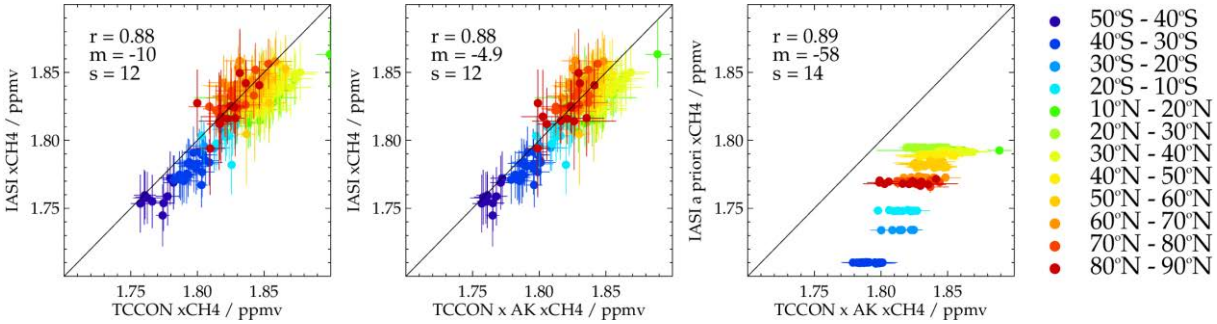

Figure 2-45 : Scatter plots comparing TCCON and RAL Methane+ version 1 TIR column-averaged mixing ratios in 2018/2019. Each point is a monthly mean with colours indicating TCCON stations in the indicated latitude range. Error bars are standard deviations of daily mean values in each average. Panels show (a) IASI retrievals vs TCCON measurements, (b) IASI retrievals vs TCCON measurements adjusted for IASI averaging kernels using CAMS and (c) IASI a priori vs TCCON. Statistics in each panel are the correlation coefficient (r), mean difference (ppbv) and standard deviation (ppbv) for the set of monthly-mean differences.

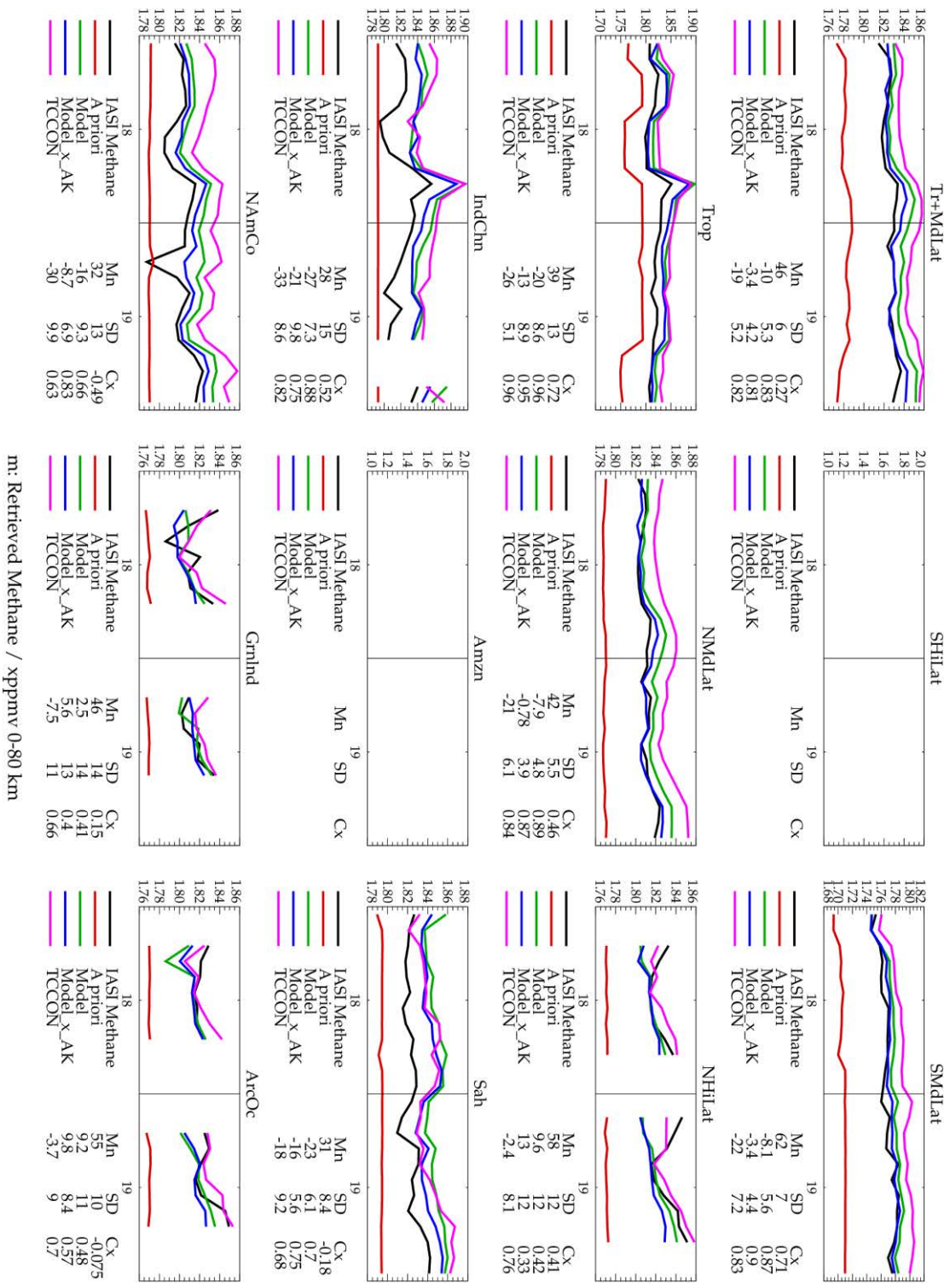

Figure 2-46 : Time series comparing RAL Methane+ version 1 TIR column averages with TCCON and CAMS sampled to TCCON for various regions. Each panel shows a different region as described in section 2.2. Statistics given in the legend under each panel give the mean difference (Mn); standard deviation of the monthly mean differences (SD); correlation between IASI and CAMS monthly mean values

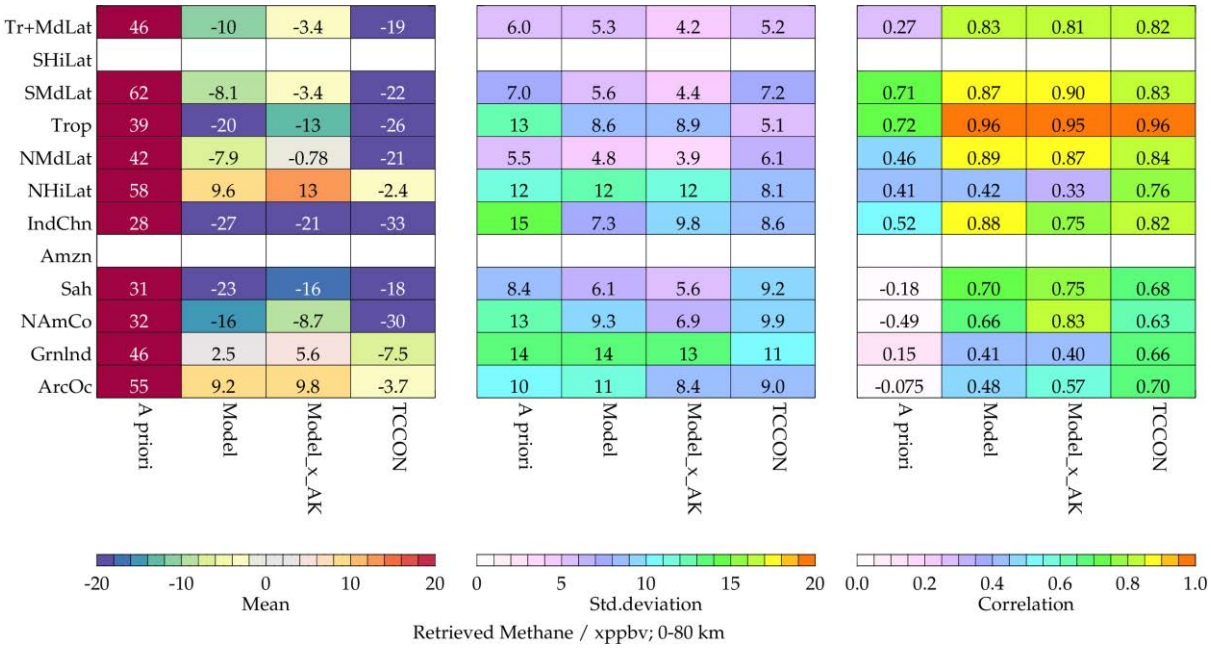

Figure 2-47 : Summary of statistics from monthly time-series comparisons of RAL Methane+ version 1 TIR column averages with TCCON and CAMS sampled to TCCON for various regions. Panels from left to right show the mean difference; standard deviation of the monthly mean differences; correlation between IASI and CAMS monthly mean values.

2.4. Discussion of RAL IASI-B Data (Methane+ Version 1)

In general, the quality of IASI-B data retrieved by the current RAL scheme has been found through the above comparisons to be comparable to that for IASI-A using the same retrieval scheme. Comparison of two-year seasonal average global distributions of column-average methane with those from CAMS GHG flux inversion v19r1 with averaging kernels applied indicates agreement to within +/- 20ppbv, with IASI-B lower by up to 20ppbv in tropical latitudes and higher by up to 20ppbv at high latitudes. Exceptions to this pattern are areas of the Sahara, Arabian peninsula, Greenland and Antarctica where IASI-B values show more spatially structured differences. Hovmoller plots through 2018 and 2019 show how the latitudinal structure seen in seasonal maps varies on a monthly basis in a consistent way in 2018 and 2019.

Maps of two-year seasonal average global differences between IASI-B and S5P column averages over land indicate IASI-B to be lower at most locations except for high northern latitudes (>60N) and a region of central/Easterm Asia in spring and autumn. The IASI-B negative bias is partly explained in some low latitude regions by the respective vertical sensitivties. The corresponding Hovmoller plot, though very sparsely sampled in the southern hemisphere, shows consistency between 2018 & 2019.

Regional maps of IASI-B – CAMS differences with averaging kernels applied reflect the latitudinal variation seen in global maps along with some smaller scale features. Over SE Asia, for example, IASI-B is generally lower by ~20ppbv as elsewhere in the tropics, except over the Himalayas. Over the Indo-Gangetic plain, however, IASI-B is lower by ~40ppbv in summer. In the Amazonian region, IASI-B is similarly lower by ~20ppbv, and by up to ~40ppbv off the west coast in summer. In the mountainous region in southern Venezuela however, there is an area in which IASI-B is persistently high but CAMS shows no feature. This IASI-B feature has subsequently been identified as caused by an errors in the assume surface elevation (from the GTOPO30 DEM) and has been removed in the version 2 scheme (see section 0 below).

Over northern Africa, IASI-B is again generally lower by ~20ppbv, as elsewhere in the tropics. There are persistent spatial patterns in coverage due to the removal of scenes with particularly low emissivity (<0.85) at 1230cm^{-1} which are, in turn related to different soil types. If these scenes are included the corresponding locations show a generally stronger negative bias (~40ppbv). This behaviour is believed to be connected to inadequacies in handling the spectral dependence and possibly also angle dependence of surface emissivity where it is particularly low. Note that emissivity is usually much larger towards the 1290cm^{-1} end of the fitting window, so low emissivity at 1230cm^{-1} also corresponds to scenes with highly spectrally structered emissivity. It also is notable that the number of scenes which pass the retrieval cost criterion over these Sahara areas is low, indicative of difficulty in fitting these spectra.

In the region centred on west coast of USA, IASI-B is again generally lower than CAMS by up to 20ppbv although by up to 30ppbv over ocean west of Baha California. In the Arctic, there is a seasonal variation in the IASI-B – CAMS difference. In summer there is close agreement except for some coastal areas, whereas in spring and autumn, IASI-B is higher than CAMS by up to 20ppbv over the Arctic ocean east of Spizbergen and also over Siberia in spring. Whereas, IASI-B is lower than CAMS over northern Canada in winter and cental Greenland in winter and spring.

Regional difference maps show IASI-B column averages to be systematically lower than S5P by typically ~20-40ppbv over the sampled areas of SE Asia, S.America, north and south of the Sahara and W.USA. Differences tend to be largest in areas of persistent surface methane emissions (eg Indo-Gangetic plain, California central valley, Amazonia), as might be anticipated from the different vertical sensitivities of IASI-B and S5P. In these areas, they also tend to be larger than those for IASI-B – CAMSxAK; supportive of IASI-B – S5P differences in these areas being due in part to vertical sensitivity.

In the Arctic, the picture is mixed, with IASI-B being consistently higher by 20-30ppbv than S5P in autumn but lower by ~40ppbv over Greenland in spring. The agreement is not improved by compensation for the effects of averaging kernels using CAMS.

The ATOM Campaign 4 transect showed IASI-B column average and 0-6km and 6-12km layer averages to track those of the aircaft well. With averaging kernels applied, deviations were consistent with the IASI-B estimated standard deviations and mean IASI-B – ATOM differences over the complete transect were ~ –4ppbv for the column, ~ –11ppbv 0-6km and ~ –9ppbv 6-12km. However, at high latitudes, IASI-B column average was higher by ~10-20ppbv while at equatorial latitudes it is lower by ~20ppbv

Comparison with the nineteen AirCore profiles with averaging kernels applied showed IASI-B column averages to lie within –10 and +30ppbv, with a positive mean bias of 13 ± 10ppbv. The 0-6km and 6-12km layer averages were shown to lie in the range +/- 40ppbv with mean biases, respectively, of 6 ± 20ppbv and –11 ± 19ppbv . Correlation coefficients between IASI-B and the nineteen AirCore profiles for the column, 0-6km, 6-12km and 6-12km - 0-6km (0.46, 0.39, 0.49 and 0.36) were found to be considerably lower than those for the much larger number of ATom profiles (0.85, 0.87, 0.77 and 0.73), which also span a much wider range of values.

The Hovmoller plot generated from comparison of IASI-B with individual TCCON stations in different latitude bands with averaging kernels applied showed a latitude dependence similar to that for CAMS, with IASI-B being lower by up to –20ppbv at low latitudes and higher by up to +20ppbv at northern high latitudes. The similarity with CAMS in the northern hemisphere is notable, although the band of higher IAS-B values around 30S seen in regard to CAMS is not evident for TCCON where the bias is –20ppbv. The scatter plot for monthly data grouped by latitude band shows a correlation of 0.88, comparable to ATOM (0.85).

Taking into consideration the latitude ranges of TCCON measurements together with those of the ATOM transect (85S – 85N) and the nineteen AirCore profiles 44N - 67N, the overall picture is that IASI-B column averages appear to be biassed low by ~−20ppbv at low latitudes and high by ~+20ppbv at high northern latitudes, with a small bias at northern mid-latitudes. This latitude dependence appears to be consistent with the CAMS comparisons in the northern hemisphere and also with S5P comparisons. It therefore seems that a latitude dependent bias correction could be appropriate for inversion of IASI-B column average data in this study.

Global seasonal mean maps and Hovmoller plots of differences between IASI-B and CAMS in the 0-6km (surface-450hPa) layer have a similar latitudinal dependence to the column average, with IASI-B lower in the equatorial region by 20-30ppbv and larger in the Arctic and Antarctic by up to 40ppbv, however, geographical structure is more prominent eg IASI-B lower values over Sahara/Arabian peninsula and off the west coasts of S.America and southern Africa. In the 6-12km (450-170hPa) layer, the latitudinal dependence is somewhat different with IASI-B differing most from CAMS (−30ppbv) in the 30-60N region, still being lower than CAMS at northern high latitudes and only being larger than CAMS 60-90S. Geographical structure in the CAMS difference plots is noticable in the 6-12km layer, with the largest differences (−40ppbv) over northern and southern continents. Latitudinal dependences of differences between IASI-B and ATOM-4 in the 0-6km and 6-12km layers are similar to the IASI-B – CAMS differences. In the 0-6km layer, IASI-B is lower by ~30ppbv in the tropics and slightly higher at northerm high latitudes and in the 6-12km layer IASI-B is lower over a wide latitude range and lowest at northern mid-latitudes.

Regional maps of seasonal mean differences between IASI-B and CAMS in the 0-6km layer indicate IASI-B to be larger over the Himalayas and Andes as well as the southern Venezuelan highlands. Whereas, in the 6-12km layer, differences in these mountainous regions are small and neighboured by areas in which IASI-B is lower than CAMS.

Other than IASI-B artefacts identified over certain areas of the Sahara, Arabian peninsula and southern Venezuelan highlands, geographical structure in both the northern and southern hemisphere, including smaller scale features in the CAMS column average difference maps, could in principle be due to deficiences in either the IASI-B or CAMS fields. Identified features in the CAMS difference maps havel been investigated further through evaluation of IASI-B co-retrieved variables (eg emissivity surface-air temperature contrast, water vapour) and auxiliary data (eg N2O distribution) leading to the definition of the Methane+ version 2 scheme (see below).

3. Validation and comparisons of LMD TIR IASI Metop-B

The following comparisons have been carried out on IASI Metop-B data for 2018/2019 using version 9.1 of the non-linear retrieval scheme (NLIS) of LMD (Crevoisier et al., 2004, 2012, 2018). The retrieved quantity is a mid-tropospheric weighted column of CH_4, denoted MT-CH_4, mostly sensitive to CH_4 in the range 4-12 km. Version 9.1 is the current version of MT-CH_4 from IASI delivered to C3S and has been chosen as the reference IASI L2 product by EUMETSAT.

For any comparison to a profile, the averaging kernels provided by the NLIS algorithm for each retrieval are applied to the profile to derive a mid-tropospheric weighted column that can be directly compared to the one retrieved from IASI.

3.1. Global model comparison

Global maps have been produced from the LMD TIR IASI methane dataset for 2018/2019 based on gridded seasonal averaged data on a 1x1˚grid. CAMS profiles generated from CAMS flux inversions data version 19r1, based on only surface data, have been sampled at the IASI satellite L2 sampling and then gridded in the same manner as the LMD TIR retrievals. IASI averaging kernels have been applied to the CAMS profiles to account for the vertical sensitivity of the retrieval.

Figure 3-1 shows the seasonal averaged gridded maps of IASI MT-CH_4, the corresponding CAMS MT-CH_4 and the difference between the two products.

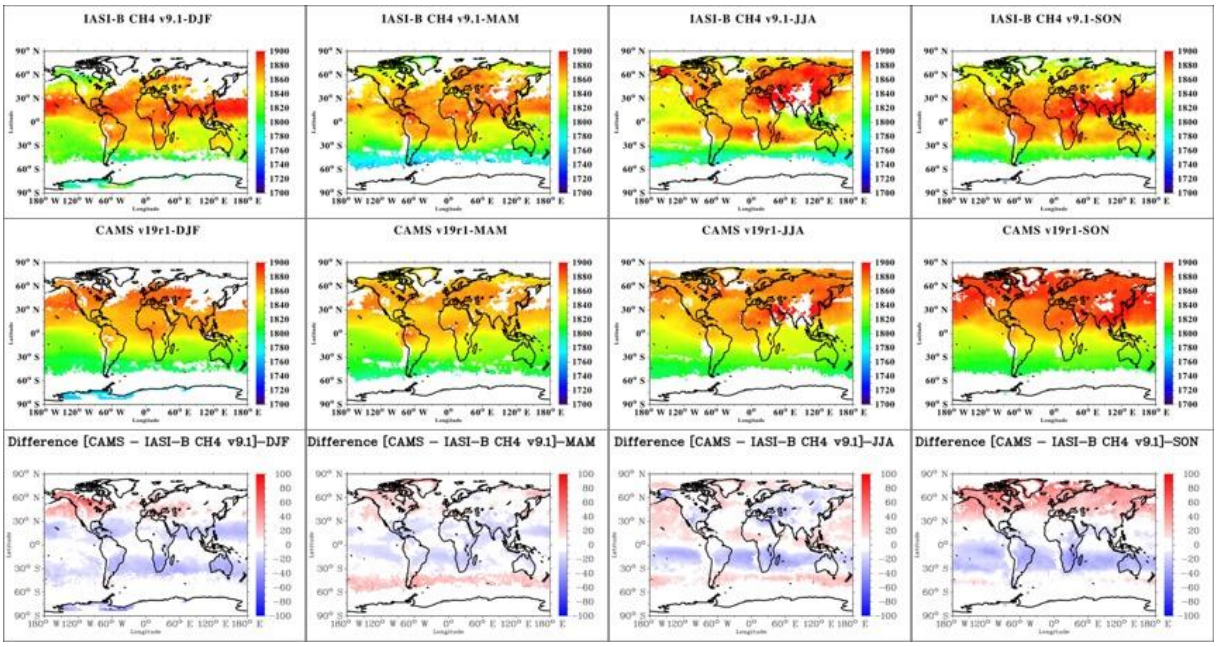

Figure 3-1: Global mid-tropospheric columns of CH_4 retrieved from IASI Metop-B: Each column of the figure shows results for a different season; December, January and February; March, April and May; June, July and August; September, October and November. First and second rows show, respectively, results from IASI retrievals and CAMS v19r profiles with IASI averaging kernels applied. Third row shows differences between CAMS and IASI MT-CH_4.

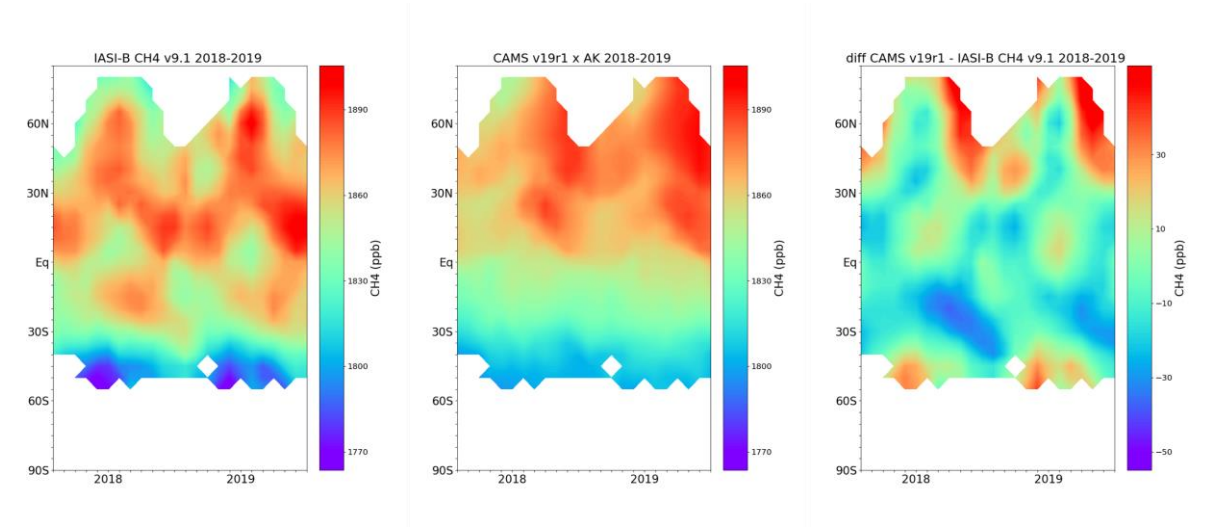

Figure 3-2: Hovmöller time-series for IASI-B v9.1 retrieved methane, CAMS v19r1 methane analyses with IASI averaging kernels applied, and the difference between CAMS and IASI MT-CH_4.

3.2. Model comparisons over target regions

Maps of mid-tropospheric column of methane derived from IASI-B are now presented by focusing on regions of particular interest described in Table 1 of Section 2.2.

3.2.1. Maps

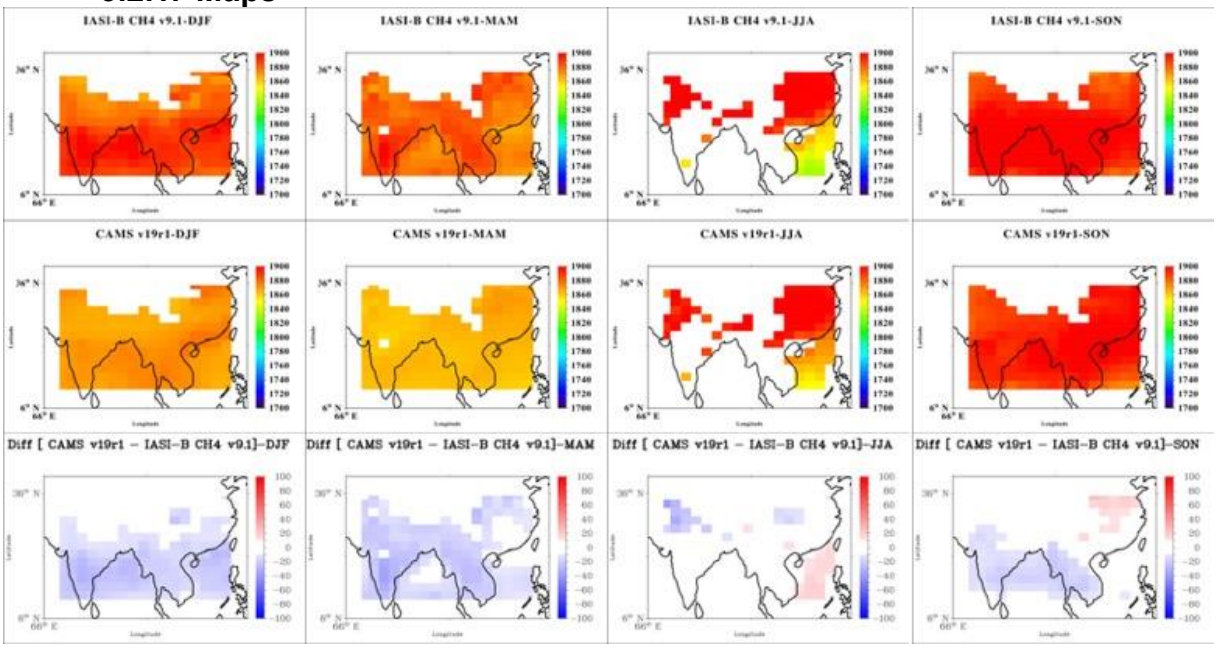

Figure 3-3: Global mid-tropospheric columns of CH_4 retrieved from IASI Metop-B over the target region China-India: Each column of the figure shows results for a different season; December, January and February; March, April and May; June, July and August; September, October and November. First and second rows show, respectively, results from IASI retrievals and CAMS v19r profiles with IASI averaging kernels applied. Third row shows differences between CAMS and IASI MT-CH_4.

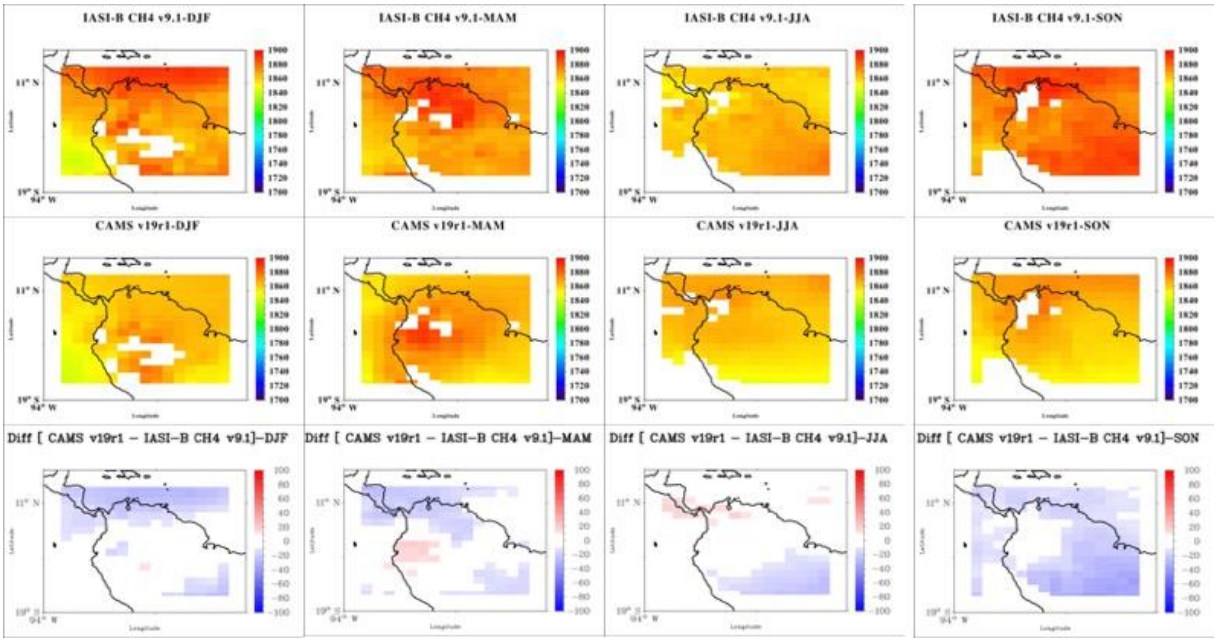

Figure 3-4: Same as Figure 3.3. over the target region Amazon.

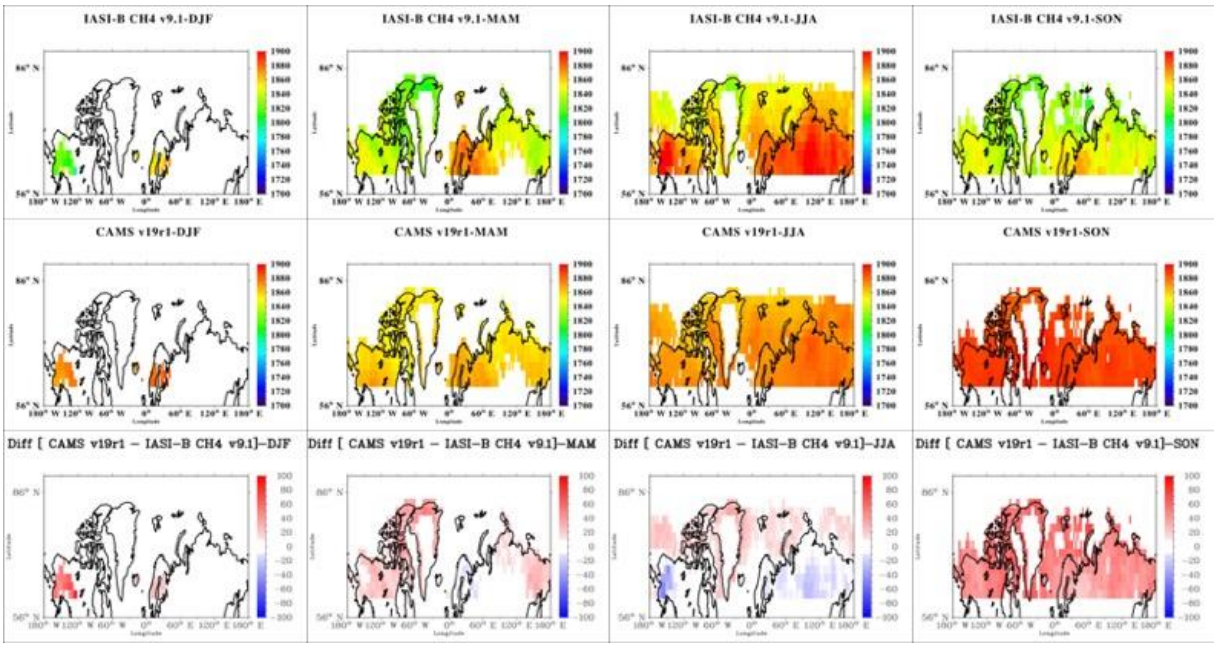

Figure 3-5: Same as Figure 3.3. over the target region High Northern Latitude.

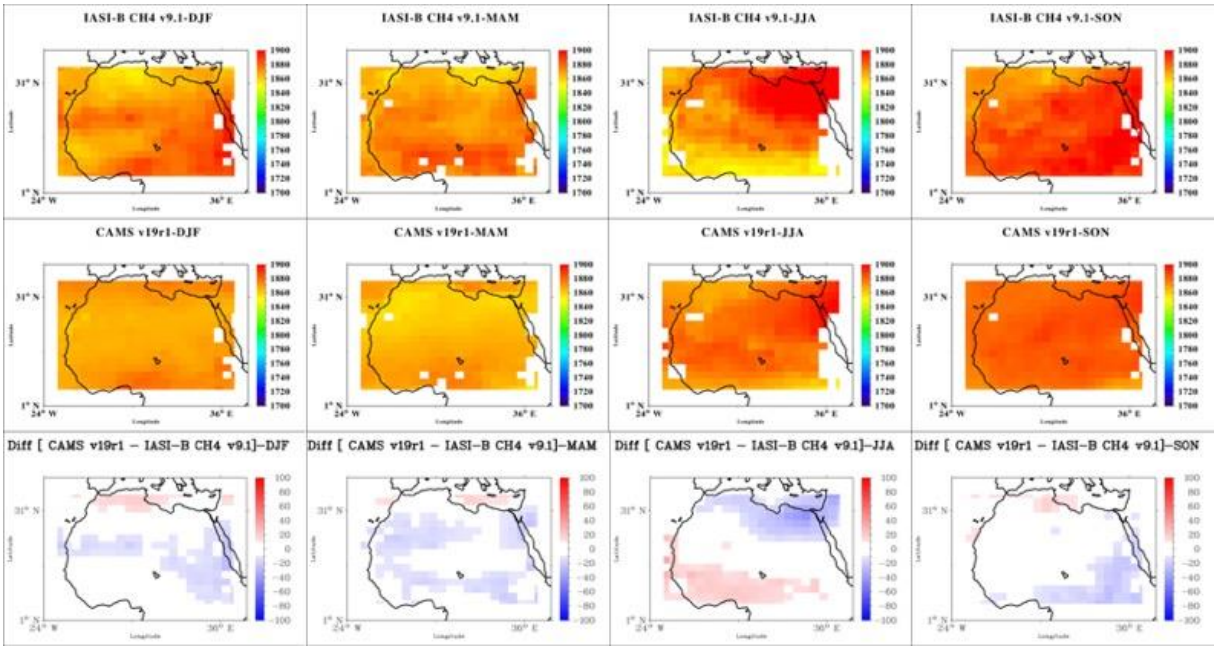

Figure 3-6: Same as Figure 3.3. over the target region Sahara.

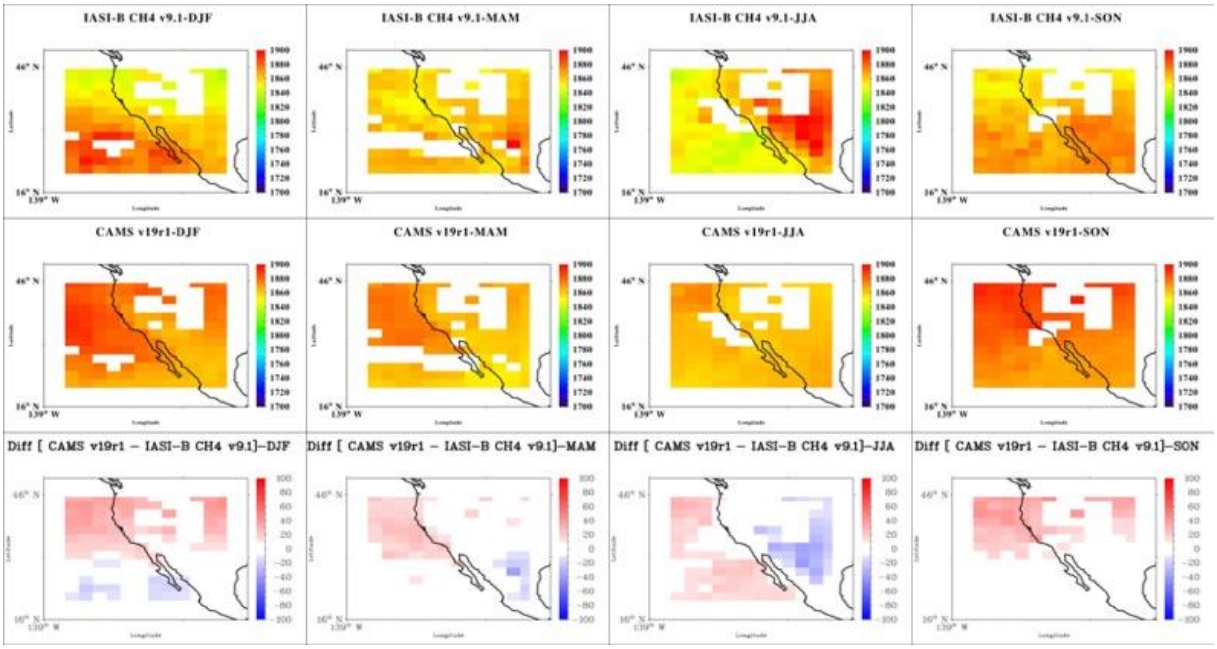

Figure 3-7: Same as Figure 3.3. over the target region North Pacific Coast.

3.2.2. Time series over the target zones

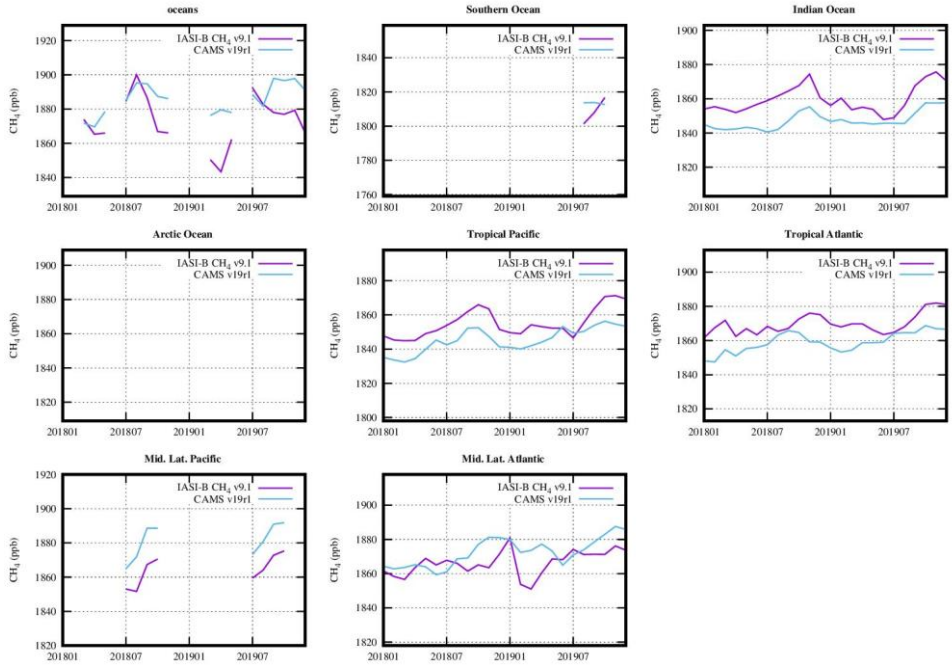

Figure 3-8: Time series comparisons of mid-tropospheric columns of methane derived from IASI v9.1 and CAMS v19r1 for various oceanic regions. Statistics given in the legend under each panel give the mean difference from IASI (Mn); standard deviation of the monthly mean differences (SD); Correlation of the monthly mean values with IASI.

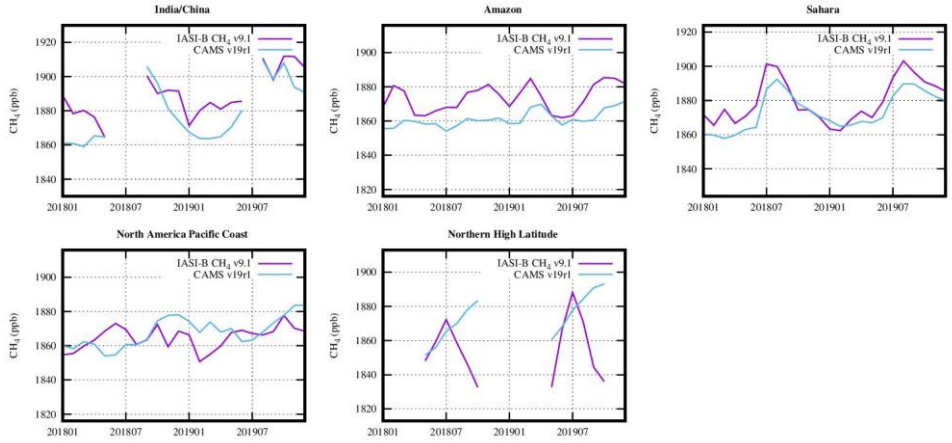

Figure 3-9: Same as Figure 3-8 for the target regions defines in Section 2.2.

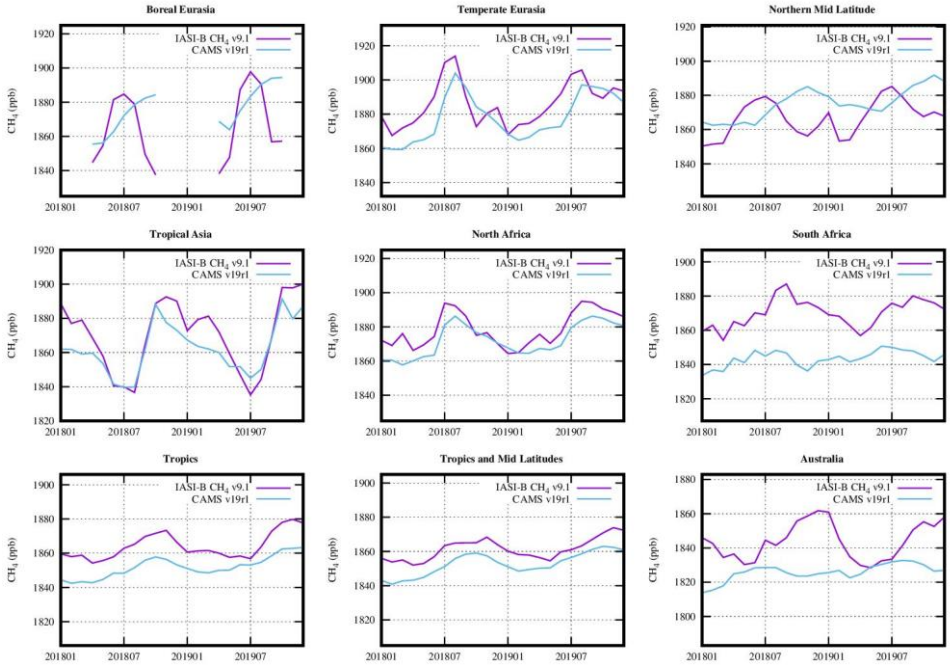

Figure 3-10: Same as Figure 3-8 for the remaining regions.

3.3. Validation from non-satellite sources

3.3.1. Atom

Mid-tropospheric columns of CH4 derived from IASI are now compared to in-itu measurements from the Atmospheric Tomography Mission (ATom), a series of NASA flight campaigns providing global-scale sampling of the atmosphere, profiling continuously between 0.2 and 12km altitude.

The ATom methane profile data is the same as used in Section 2.3. They are binned to match the IASI spatial sampling and extended vertically using co-located CAMS v19r1 data. The latter step is necessary in order to apply the IASI averaging kernels to the ATom profiles.

The co-location criteria applied allowed for IASI profiles within 100km/6hrs of the sampled ATom profile.

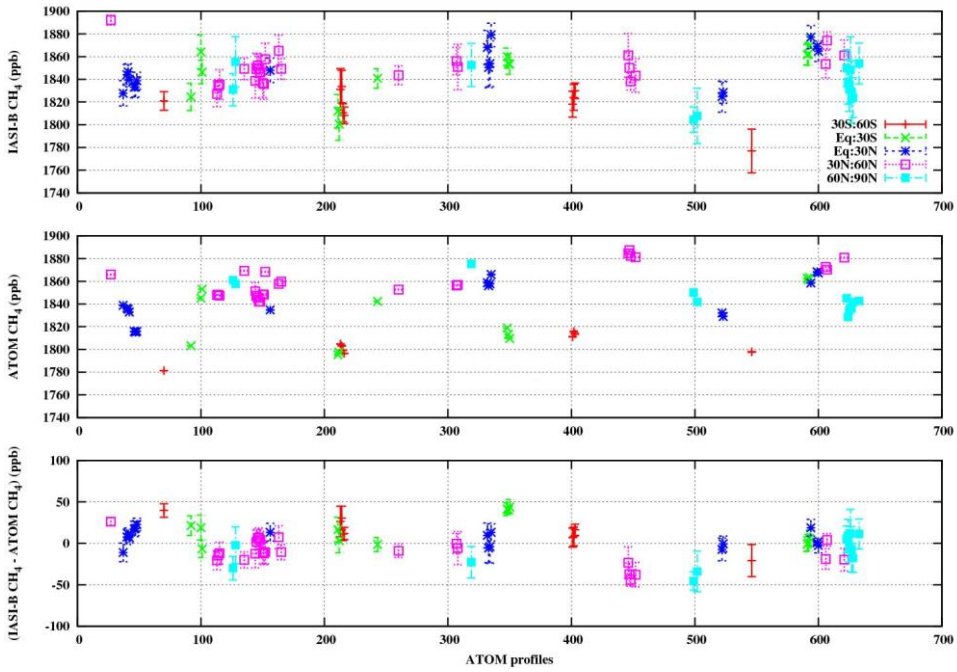

Figure 3-11: Comparison in terms of MT-CH_4 between IASI and Atom extrapolated with CAMS v19r1 profiles. (Top) IASI-B MT-CH4 for all ATOM flights. (Middle) ATOM-CAMS MT-CH4. (Bottom) Difference between collocated IASI-B and ATOM-CAMS data. The colors indicate the latitudinal band where the IASI/Atom matches are located.

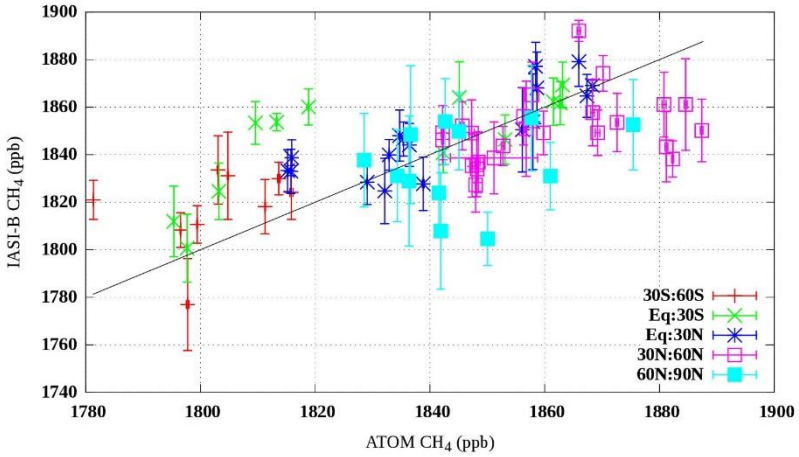

Figure 3-12: Scatter plot showing the agreement between Atom extrapolated with CAMS profiles and IASI mid-tropospheric columns of CH_4. The statistics is: correlation coefficient (r); mean difference (m); standard deviation in the difference (s).

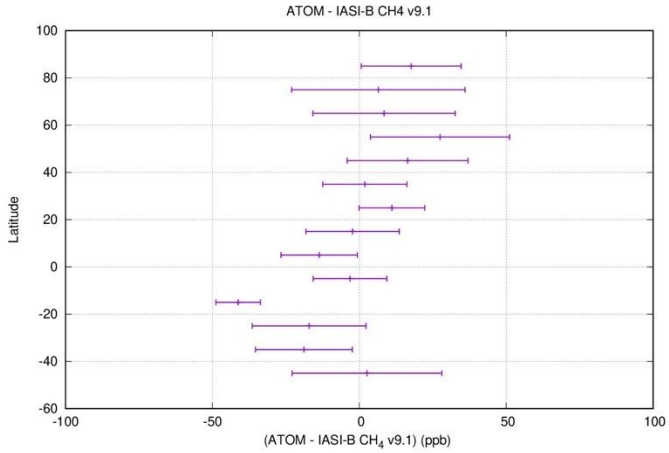

Figure 3-13: Differences between IASI and Atom extrapolated with CAMS v19r1 profiles against the latitude of the IASI/Atom matches. Horizontal lines show the standard deviation of the individual about the mean difference.

3.3.2. AirCore

As described in section 2.3.2, the same analysis method is applied to the AirCore profiles as described for the ATom data. All retrieved IASI methane profiles co-located with each AirCore profile are combined to produce mean mid-tropospheric column. The co- location criteria applied allowed for IASI profiles within 100km/6hrs of the sampled AirCore profile. Results are shown in Figure 3-14.

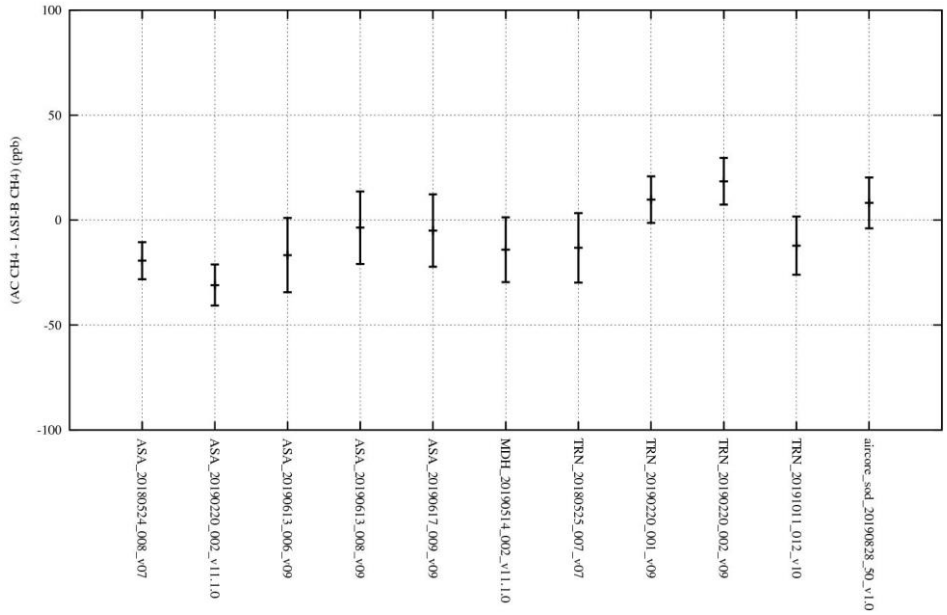

Figure 3-14: Differences in terms of MT-CH_4 between IASI-B v9.1 retrievals and AirCore profile measurements. The error bars represent the standard deviation of the difference. Results are shown for all AirCore profiles that passed the quality control criteria. Overall AirCore-IASI difference is: -0.91 +/- 14.51 ppb

3.4. Discussion of LMD IASI-B Data

The comparison results presented in the previous section are in line with previous validation performed for IASI/Metop-A and the whole series of IASI/Metop-B (see for instance C3S Validation report).

On a global scale (Fig. 3-1), seasonal differences between IASI and CAMS mostly lie within -20 and +20 ppb. CAMS is generally higher than IASI for norther latitude (40-90N), especially in the fall (SON) where the difference reaches 40ppb as seen in Fig. 3-2, whereas CAMS is generally lower than IASI in a band between 20S and 40S, especially during the fall (SON) where the difference is about -30 ppb (Fig. 3-2). Overall, there is no difference between land and sea, except for JJA when CAMS is lower than IASI over northern mid-high-latitude land regions but higher over adjacent ocean basins.

These general characteristics are also seen when looking at specific target regions (Fig. 3-3 to 3-8).

Over China and India (Fig. 3-3), the difference is quite constant over the year, with CAMS lower than IASI by 11 ppb, and a seasonality that matches quite well between both datasets (Fig. 3.9). The difference is higher (about 20 ppb) during the first months of the year. The same result is also obtained over the whole tropical Asia (Fig. 3-10) and Indian Ocean (Fig. 3-8).

Over the Amazon (Fig. 3-4), the difference between CAMS and IASI is about 13 ppb throughout the year with IASI higher than CAMS, with an excellent agreement in terms of seasonal variations (Fig. 3-9) but an amplitude of the seasonal cycle 5 ppb higher for IASI than CAMS.

Over High Norther Latitudes (Fig. 3-5), the difference between CAMS and IASI follows the global behaviour described above. CAMS is generally higher than IASI during winter, spring and fall, but lower than IASI during summer. However, the very low number of situations available for comparison makes it hard to draw conclusions. Nonetheless, this behaviour is also found in over northern mid-latitude regions like Europe (Fig. 3-10) and the North Pacific Coast (Fig. 3-9), with a seasonal variation that differs between both datasets. This is however not the case over adjacent ocean basins (Fig. 3-8 and 3-9), highlighting again the difference in summertime between land and ocean for norther mid-to high-latitudes. This difference, that could come from the upper-troposphere-lower-stratosphere region will be investigated. It is worth noted that, over Eurasia (Fig. 3-10), the seasonality and amplitude of the seasonal cycle are quite close between both datasets, albeit a shift by about 1 month, with CAMS seasonality lagging behind IASI.

Over the Sahara (Fig. 3-6), the difference between CAMS and IASI is low with an average difference of 6 ppb throughout the 2 years (CAMS lower than IASI) and the best agreement over all regions between both datasets in terms of seasonality and amplitude of the seasonal cycle. This result illustrates that the retrieval process is not sensitive to strong emissivity and surface temperature variations, fully validating the approach used in the design of the NLIS algorithm.

Over Australia, strong discrepancies are found between CAMS and IASI, with almost no seasonal variations observed in CAMS while a seasonal cycle displaying similar seasonality than over adjacent regions are observed with IASI. It will be worth investigating the origin of this difference.

Comparisons between ATOM profiles extrapolated with CAMS profiles and IASI retrievals are in line with the comparison between IASI and CAMS. Since the ATOM campaign took place in April-May, ATOM-CAMS MT-CH_4 is generally higher than IASI in the norther mid-to-high latitudes, with an averaged difference between 5 and 15 ppb, except around 50N where the difference is higher, with a very high standard deviation. In the tropics, ATOM-CAMS is generally lower than IASI with a difference close to zero near the equator and around -20 ppb in the southern mid-latitudes.

Finally, comparisons between AirCore (mostly acquired at northern mid-latitudes) and IASI MT-CH_4 shows an average difference of -0.91 +/- 14.51 ppb (over 11 situations only). This result is close to the statistics obtained over the whole period of IASI/Metop-A and IASI/Metop-B with 44 profiles, which come down to an AirCore – IASI average difference of 1.97 ± 12.94 ppb (C3S validation report for LMD IASI v9.1 dataset). This result differs from the one obtained when comparing IASI with CAMS and ATOM extrapolated with CAMS which tends to show higher values for CAMS and ATOM-CAMS profiles than for IASI. As highlighted in Membrive (2016), this might be due to an overestimation of methane in CAMS in the stratosphere, and especially in the upper-troposphere-lower-stratosphere (with a tropopause around 8 km in the mid-to-high latitudes) which has thus an impact on the computation of CH_4 weighted columns. This point is under investigation.

4. Validation and comparisons of RAL TIR IASI Metop-B (Methane+ version 2 data)

Following validation and comparisons of RAL Methane+ V1 data described in Section 2 and their use in inverse modelling trials with TM5 by VU in the Methane+ study, R&D was undertaken with the objective of reducing biases apparent in the V1 data.

An extensive series of tests was undertaken leading to the following modifications to the scheme (for further details see the TIR ATBD [RD-12]):

1. Representation of N_2O was improved: the new SCISAT-ACE v4.1.2 climatology in the stratosphere, merged with CAMS GHG flux inversion in the troposphere (using an approach similar to that described in section 2 to define the reference CAMS+ACE profiles used in comparisons).
2. New RTTOV coefficients were used based on latest Hitran spectroscopy and modelling of line mixing by the LBLRTM line-by-line model.
3. The complete fit window from 1232.25-1290 cm^{-1} is used, without spectral gaps omitted in the V1 scheme to avoid regions affected by line mixing.
4. Variable F14, F22, HNO3 and SO2 were added to the fit.
5. Systematic residual spectra fitted (along with geophysical variables) derived as function of column H2O in addition to view zenith angle
6. A new version of the IMS scheme “IMS-extended” is used to define temperature and surface emissivity. IMS-extended has a more sophisticated approach to model cloud and aerosol compared to the original IMS scheme. This includes fitting sulfuric acid aerosol which is also input and modelled by the CH4 scheme (expected to mitigate the impact of this aerosol on methane in volcanic plumes).
7. The methane scheme fits an offset, with linear spectral dependence, to the IMS-extended spectral emissivity. Surface temperature is no longer retrieved but is defined by the output of IMS-extended.
8. The IMS-extended approach to modelling cloud (as scattering layer rather than black-body), is adopted also in the methane scheme.,
9. The digital elevation model used in the extended IMS scheme and IASI methane module was updated from GTOPO30 to GMTED2010.

The following sub-sets of IASI data have been processed with the V2 scheme, in order to enable sufficient data to effectively repeat the V1 validation:

- The months April, July and October 2018 and January 2019 are fully processed.
- Days 1, 5, 11, 15, 21, 25, 31 of all other months from January 2018 to December 2019 are fully processed.
- In addition, all “granules” of IASI data which contain a V1 retrieval which is co-located with TCCON, Atom-5 or AirCore are processed. (A “granule” refers to 50 scanlines of contiguous IASI data; an orbit comprises 15 or 16 granules.)

This sub-sampling therefore has no impact on the comparisons to Atom-4, Aircore or TCCON, but there are sampling differences which could slightly modify the

comparisons to CAMS and S5P in sections 4.1 and 4.2 (though the differences are not considered significant for the current purposes).

Apart from these subtle sampling differences, comparisons of V2 data have been conducted using the same procedures described in Section 2 for V1.

4.1. Global model and satellite comparisons

The same set of figures are presented as those in section 2:

- Comparisons to CAMS are illustrated in Figure 4-1 for the column average and in Figure 4-2 and Figure 4-3 for the 0-6km and 6-12km layers, respectively.
- The IASI column average is compared to S5P in Figure 4-4.
- Figure 4-5 and Figure 4-6 show the time-series of monthly zonal mean methane column and layer averages as Hovmöller plots.
- Figure 4-7 shows similar plots comparing co-located IASI and S5P column averages.

In all cases, v2 results can be compared to those for the v1 data in the corresponding figure numbers of Section 2.1.

From comparison of global maps with the corresponding figures for V1 data, it is evident that the negative bias at low latitudes with respect to CAMS is substantially reduced in the V2 data, as is also seen in comparison of zonal mean Hovmoller plots for the column average, 0-6 and 6-12km layers. Comparison of global maps and Hovmollers further indicates that a negative bias with respect to the S5P column average at low latitudes is similarly reduced in the V2 data. The reduction in negative bias in the maps is also reflected in reduced view-zenith angle dependence in the bias (bottom panels of Figure 4-1 to Figure 4-3).

Comparison of the same global maps indicates a greater tendency for positive bias in v2 with respect to CAMS at mid to high latitudes, especially in winter. In the winter, the high latitude positive bias is somewhat lower for IASI-S5P than for IASI-CAMS, however the coverage of S5P is limited in high latitude winter. Geographical structure in the IASI – S5P difference is significantly lower for V2 than V1, except at high northern latitudes in SON and DJF.

Hovmoller plots in Figure 4-6 (cf Figure 2-6 for V1) show that the V2 scheme tends to lower standard deviation in the difference compared to CAMS (lower panels in the figures), presumably reflecting reduced spatial structure in the IASI-CAMS differences. However, standard deviations can be larger for V2 at high latitude in winter.

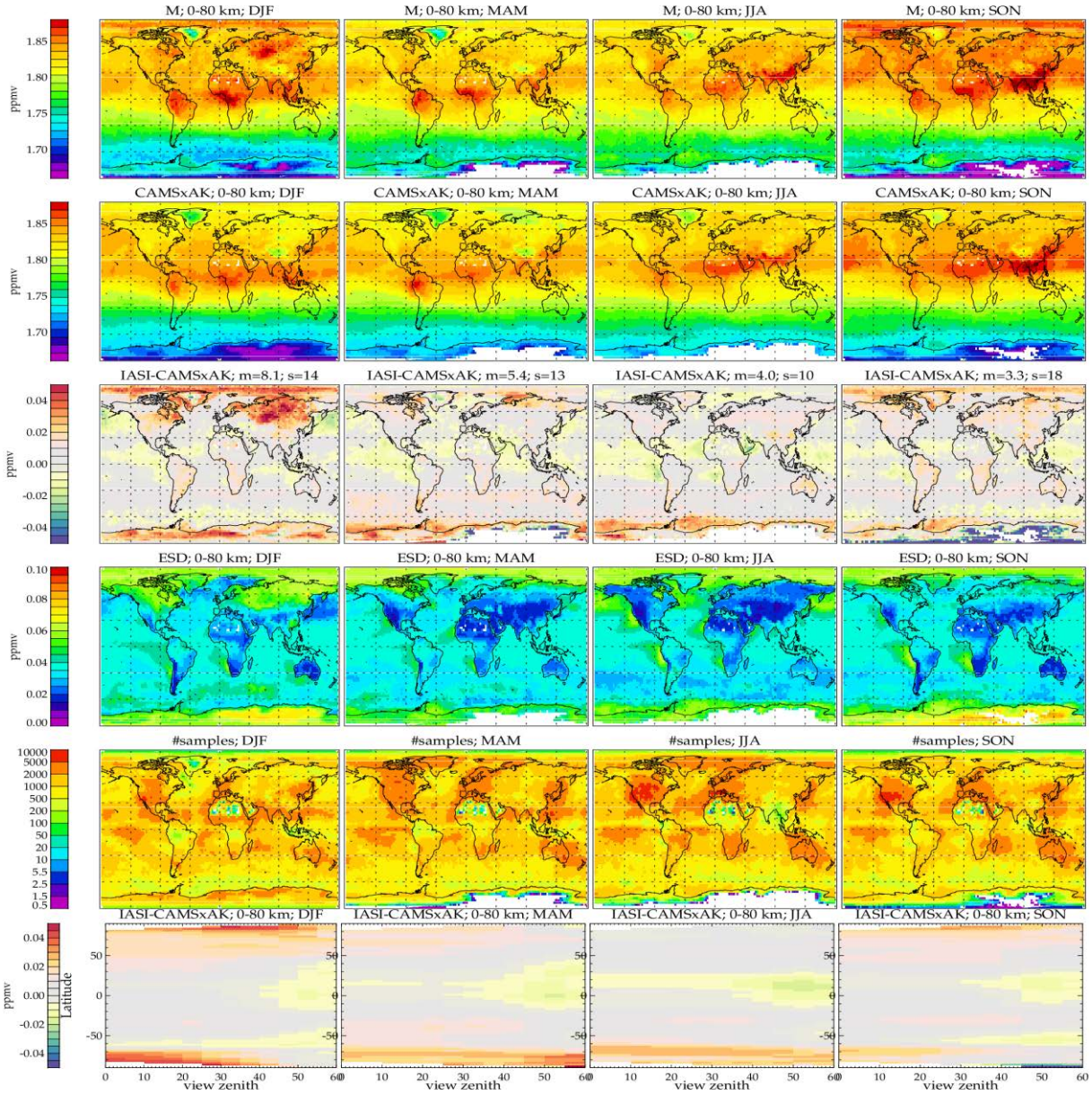

Figure 4-1 : RAL Methane+ version 2 TIR global daytime column average retrievals: columns show results for different seasons (2018 and 2019 combined). Rows from top-bottom show, respectively, results from IASI retrievals; CAMS with averaging kernels applied (CAMSxAK); the difference between IASI and CAMSxAK; the mean of the estimated standard deviation (ESD) on the IASI retrieval; the number of individual IASI retrievals in each of the 2.5x2.5 degree bins. Bottom panels show differences between IASI and CAMSxAK averaged as a function of view zenith angle and latitude.

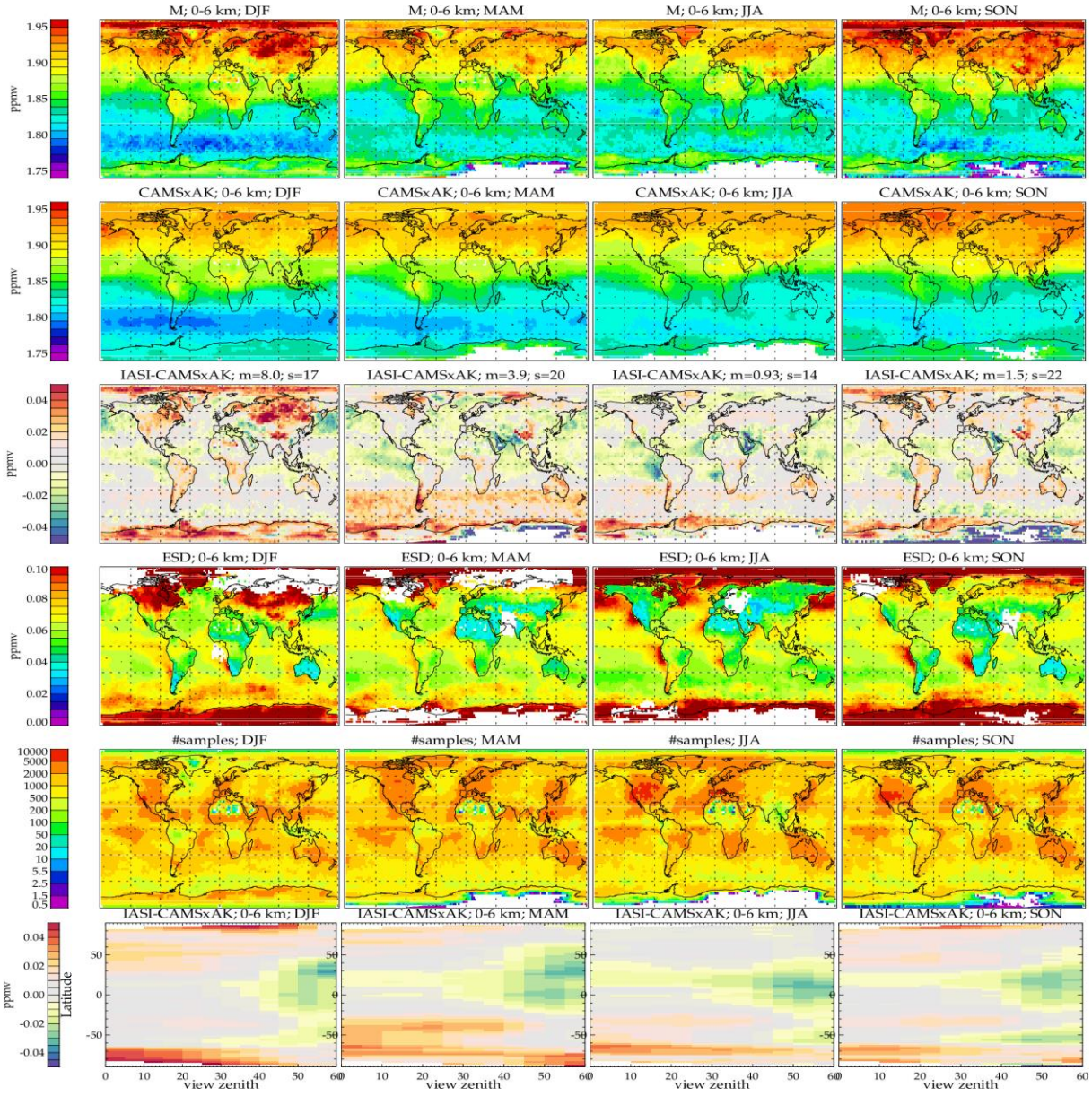

Figure 4-2 : RAL Methane+ version 2 TIR global daytime retrievals for the 0-6km layer average.

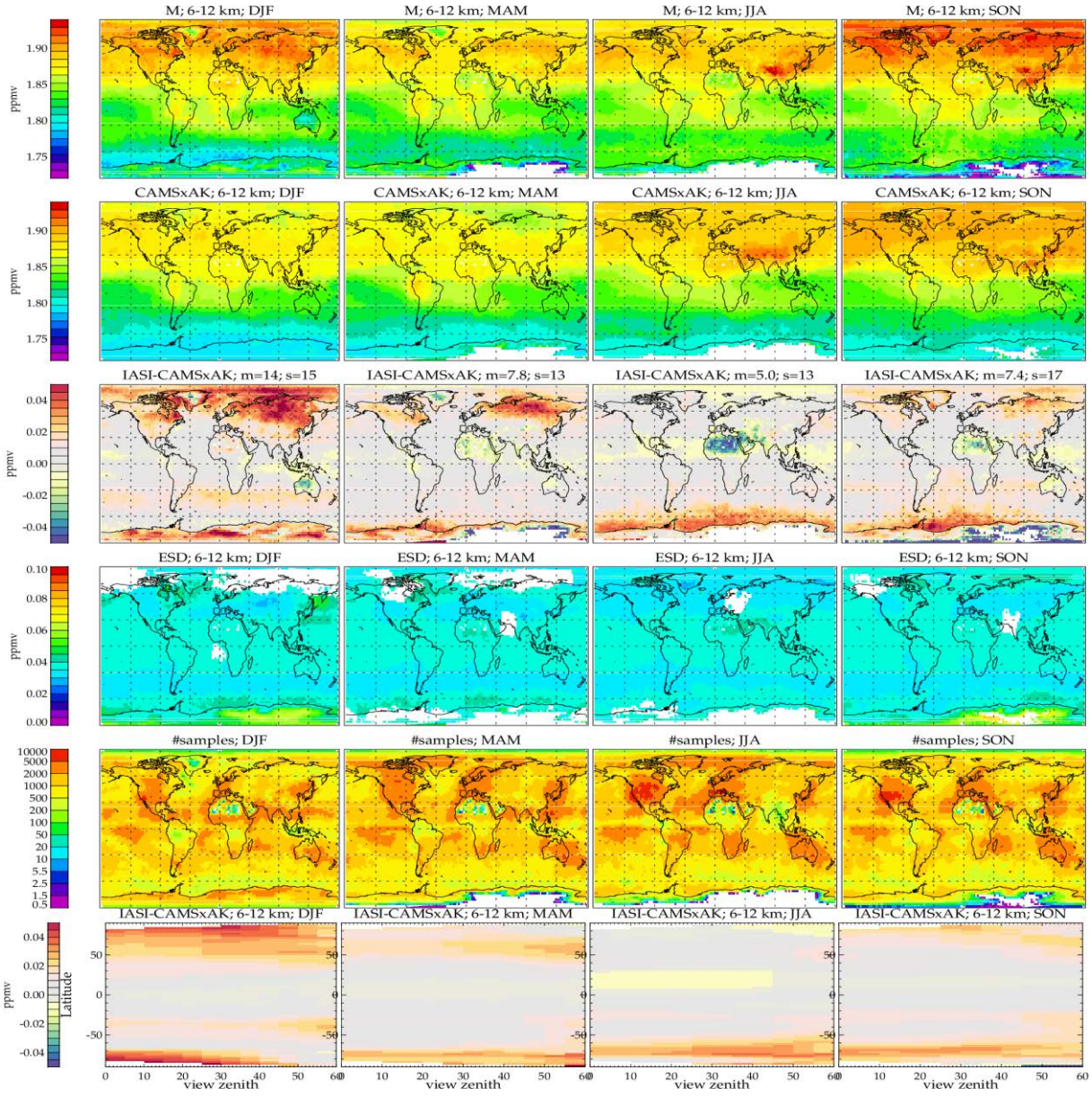

Figure 4-3 : RAL Methane+ version 2 TIR global daytime retrievals for the 6-12km layer average.

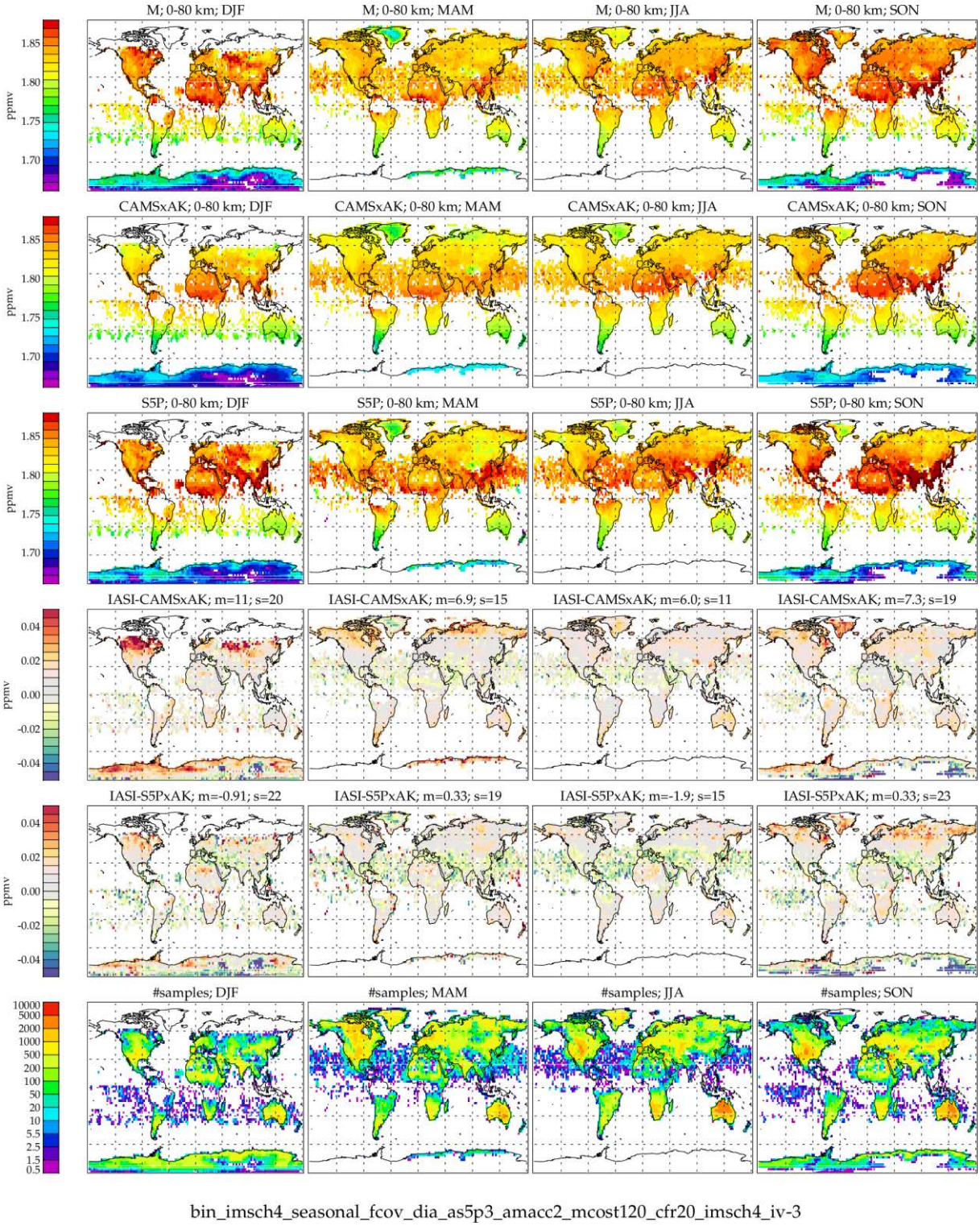

bin_imsch4_seasonal_fcov_dia_as5p3_amacc2_mcost120_cfr20_imsch4_iv-3

Figure 4-4 : RAL Methane+ version 2 TIR global daytime column average retrievals co-located with S5P: Panels as previous figures except that the 2nd row shows S5P results, the 3rd row shows differences between IASI and S5P and the 4th row shows the difference between IASI and S5P after using CAMS to correct for the influence of the IASI averaging kernel.

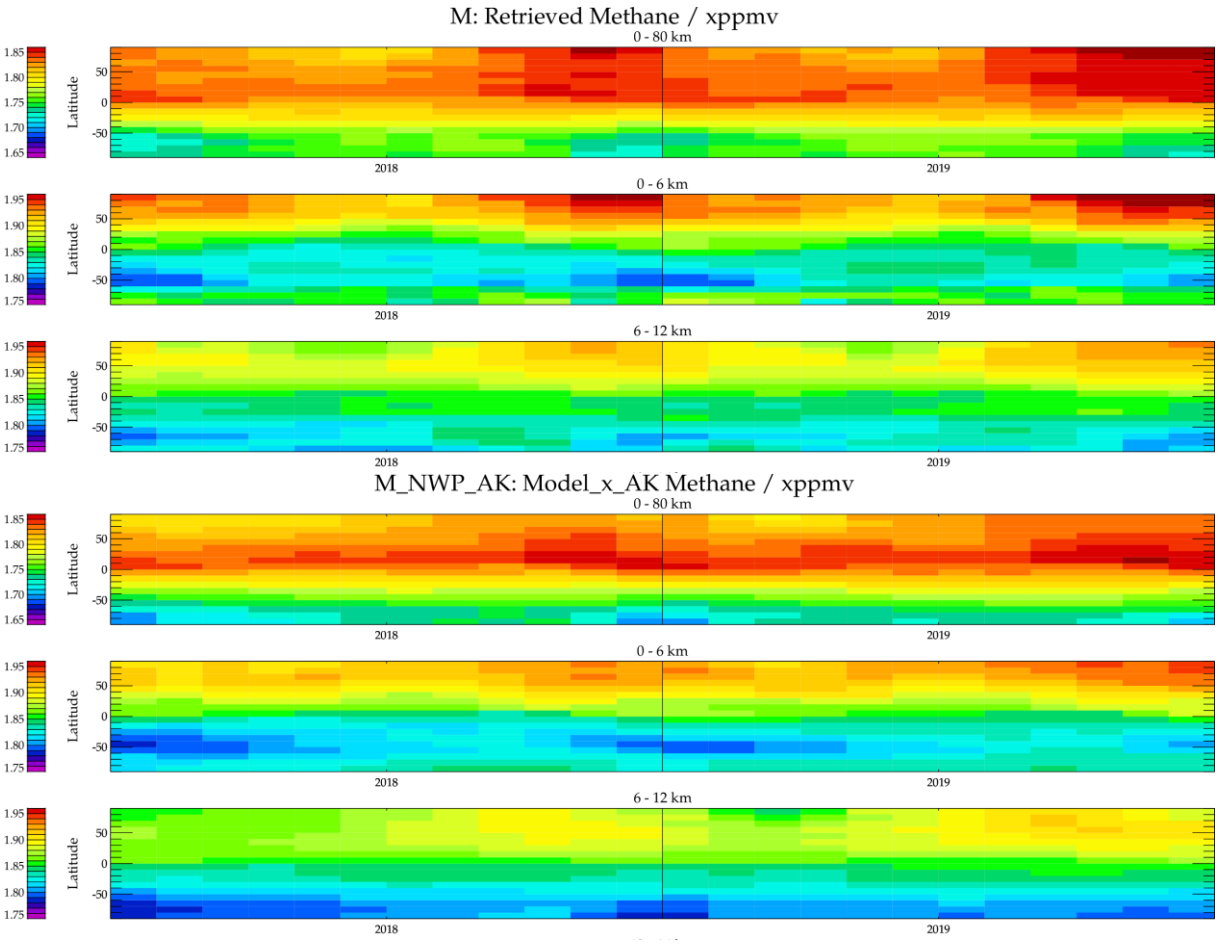

Figure 4-5 : RAL Methane+ version 2 TIR Hovmöller time-series for (a) IASI-B retrieved methane and (b) CAMS v19r1 methane flux inversion with IASI averaging kernels applied. Panels are shown for the column average (0-80km), 0-6km and 6-12km layer averages.

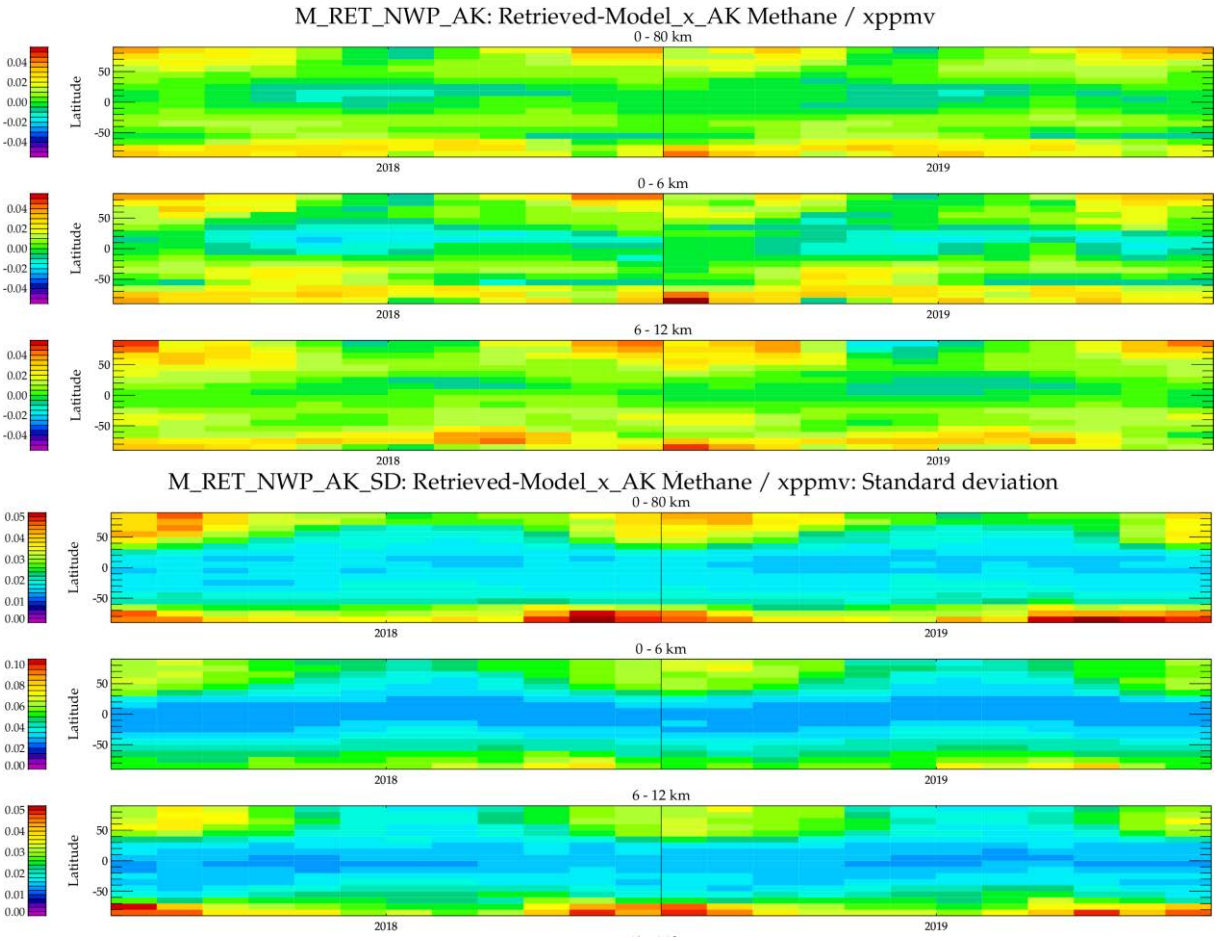

Figure 4-6 : RAL Methane+ version 2 TIR Hovmöller time-series for (a) the mean difference between IASI and CAMS and (b) the standard deviation in the mean difference. Panels are shown for the column average (0-80km), 0-6km and 6-12km layer averages.

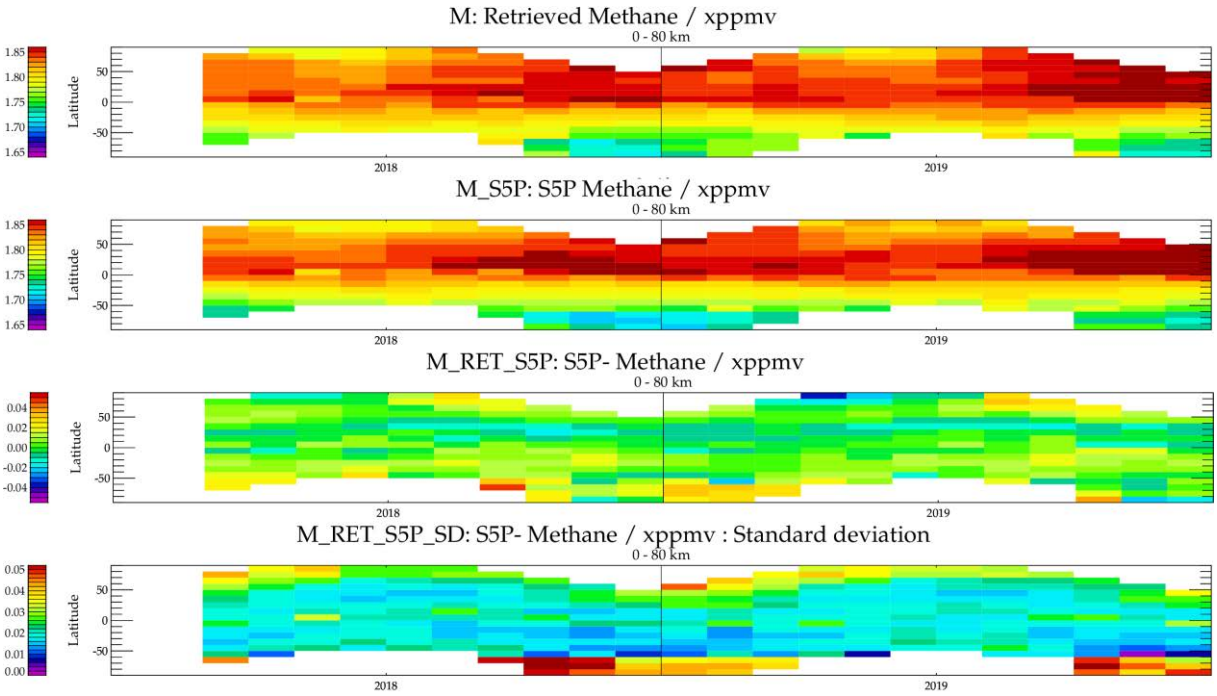

Figure 4-7 : RAL Methane+ version 2 TIR Hovmöller time-series for (a) IASI-B retrieved methane, (b) S5P retrieved methane, and (c) the difference between (a) and (b). Panels are shown for the column averages (0-80km).

4.2. Model and satellite comparisons over target regions

In this section, as in Section 2.2, maps of daytime IASI methane retrievals are presented focusing on regions of particular interest. The same set of figures are shown:

- Comparisons to CAMS are presented as maps (0.5x0.5 degree gridded seasonal averages) in Figure 4-8 to Figure 4-27. For each region (A-E as in the table), figures compare the IASI column averages to CAMS and S5P (in separate figures), and the 0-6km and 6-12km layer averages to CAMS.
- Figure 4-28 and Figure 4-29 summarise the regional differences compared to CAMS and S5P, respectively.
- Time-series comparisons for the 2 years are shown as line plots in Figure 4-30 (column average vs CAMS), Figure 4-31 (0-6km layer average vs CAMS), Figure 4-32 (6-12km layer average vs CAMS) and Figure 4-33 (column average vs S5P).
- Figure 4-34 to Figure 4-38 summarise the time series statistics.

As for the global comparisons, V2 results can be compared to those for the V1 data in the corresponding figure numbers of Section 2.2.

Results generally indicate that changes between V1 and V2 data on a regional scale reflect the latitudinal structure of changes seen in global maps and Hovmoller plots of zonal means outlined in Section 3.1. Some additional features specific to regions are as follows:

- Figure 4-8 to Figure 4-11 (India/China): V2 positive anomaly (with respect to CAMS) over Bangladesh wetlands in SON along with positive bias over Himalayas. V2 negative discrepancies with respect to S5P in column average over regions of emissions in the Indo-Gangetic plain and, in SON, Bangladesh wetlands are consistent with the vertical sensitivities.
- Figure 4-12 to Figure 4-15 (Amazon): The positive artefact found in V1 data over south Venezuelan highlands is eliminated in v2.
- Figure 4-16 to Figure 4-18 (Sahara): In general biases in all layers are reduced. V2 data shows positive anomaly inland around Gulf of Guinea in DJF and MAM.
- Figure 4-20 to Figure 4-22 (North Pacific): V2 positive anomaly introduced off Californian coast in summer. V2 has reduced land sea-contrast compared to V1 around Baha California / Mexico.
- Figure 4-24 to Figure 4-26 (High northern latitude): V2 positive anomaly introduced over Scandinavia and Siberia particularly in DJF. This positive anomaly largely coincides with areas where S5P data is missing, so it is difficult to confirm if this is an IASI retrieval artefact or not. The IASI bias is smaller compared to S5P than it is to CAMS when there is high latitude coverage in spring.

These positive anomalies all merit further investigation. The one off the Californian coast is associated with low-level marine cloud and considered likely to be an artefact, as is the one over the Himalayas. Those in Arctic winter are associated with the lowest surface temperatures and the most extensive snow/ice cover so may also be artefacts. Those over Bangladesh and around the Gulf of Guinea might not be retrieval artefacts, however.

Land-sea discontinuities are evident in regional maps of the difference between IASI V2 and CAMS with vertical sensitivity accounted for by AKs (3rd row of eg Figure 4-28, Figure 4-12, Figure 4-16, Figure 4-20, Figure 4-24). This behaviour also merits further attention.

Summary tables in Figure 4-28 and Figure 4-29 confirm that the V1 bias is generally improved by V2 in all regions, except Arctic autumn/winter. Spatial standard deviations are reduced in some regions (e.g. Sahara) but are larger in Arctic winter.

After allowing for the improved bias at low-mid-latitude of V2, the level of agreement in timeseries (Figure 4-30 - Figure 4-33) is otherwise generally similar to that for V1. The summary tables show that, at low-mid latitudes, the standard deviation and correlation in the monthly values compared to S5P is improved for V2 compared to V1.

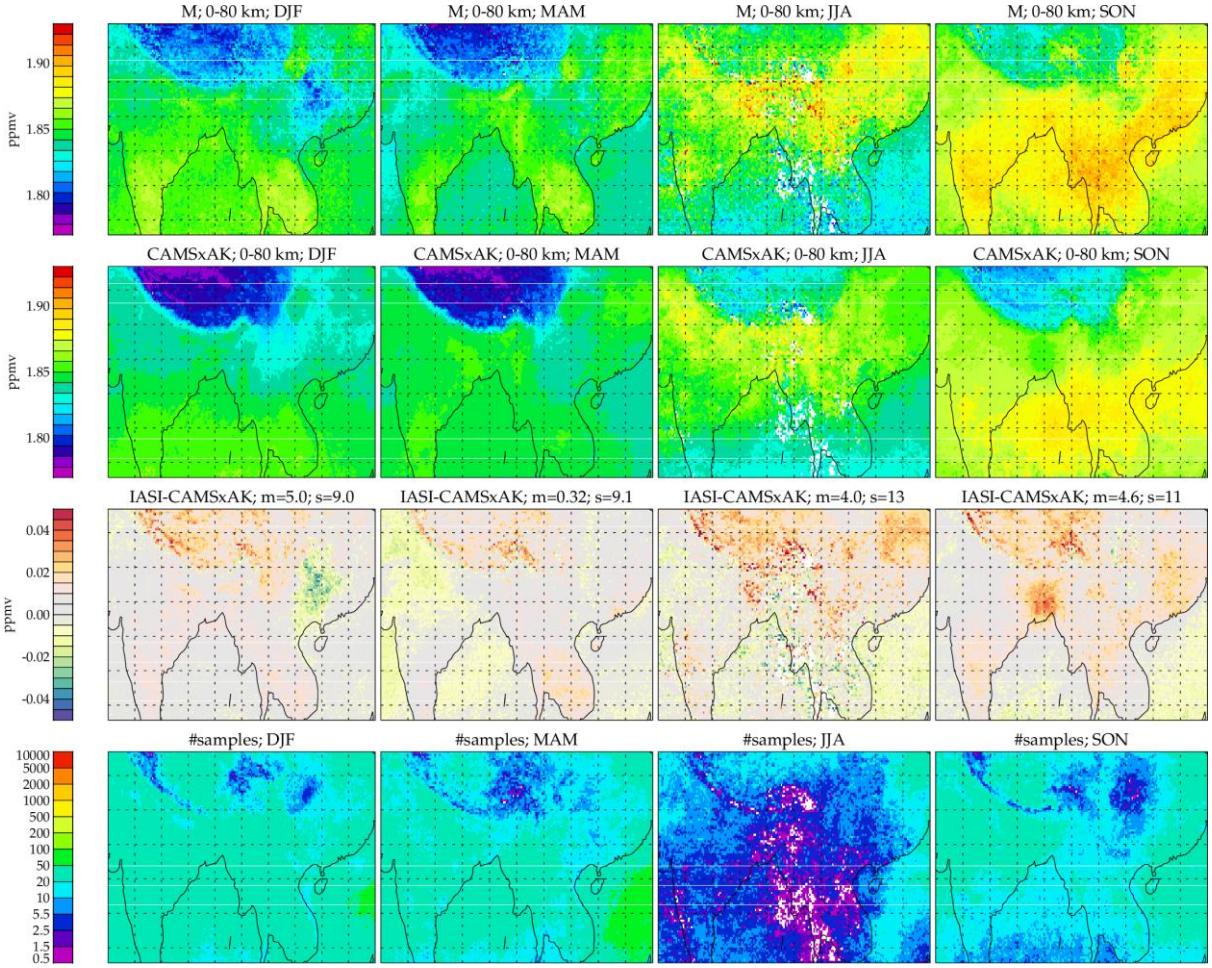

Figure 4-8 : RAL Methane+ version 2 TIR global daytime column average retrievals for region A: Each column of the figure shows results for a different season (2018 and 2019 combined). Rows from top-bottom show, respectively, results from IASI retrievals; CAMS with averaging kernels applied (CAMSxAK); the difference between IASI and CAMSxAK; the number of individual IASI retrievals in each of the 0.5x0.5 degree bins. In panels showing differences, the mean ("m") and standard deviation ("s") of the binned data are given, in ppbv, in the panel title.

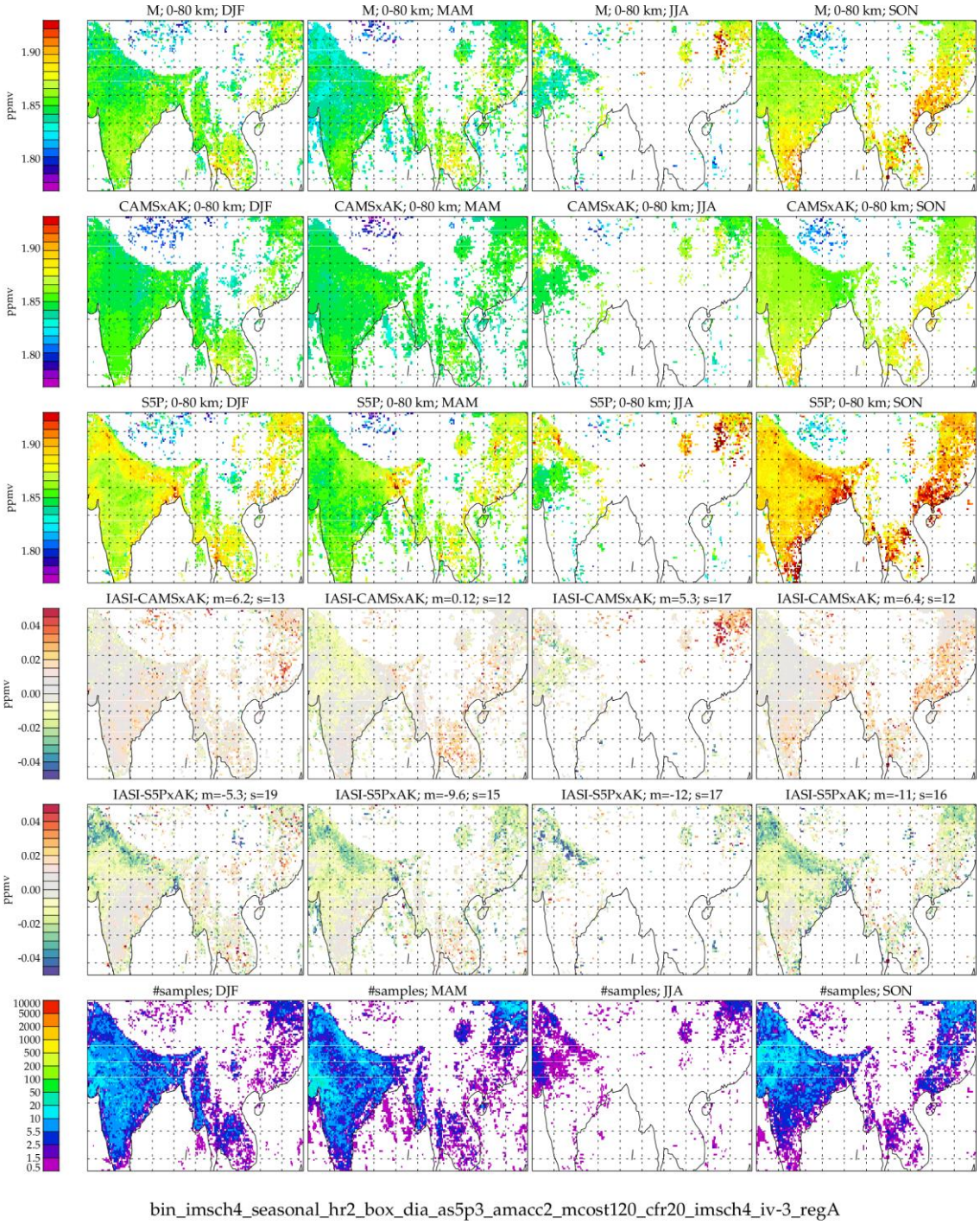

Figure 4-9 : RAL Methane+ version 2 TIR global daytime column average retrievals for region A, collocated with S5P: Each column of the figure shows results for a different season (2018 and 2019 combined). Panels from top-bottom show, respectively, results from IASI retrievals; CAMS; S5P retrievals; Difference between IASI and S5P; Difference between IASI and S5P accounting for the IASI averaging kernel using CAMS; the number of individual IASI retrievals in each of the 0.5x0.5 degree bins. In panels showing differences, the mean ("m") and standard deviation ("s") of the binned data are given, in ppbv, in the panel title.

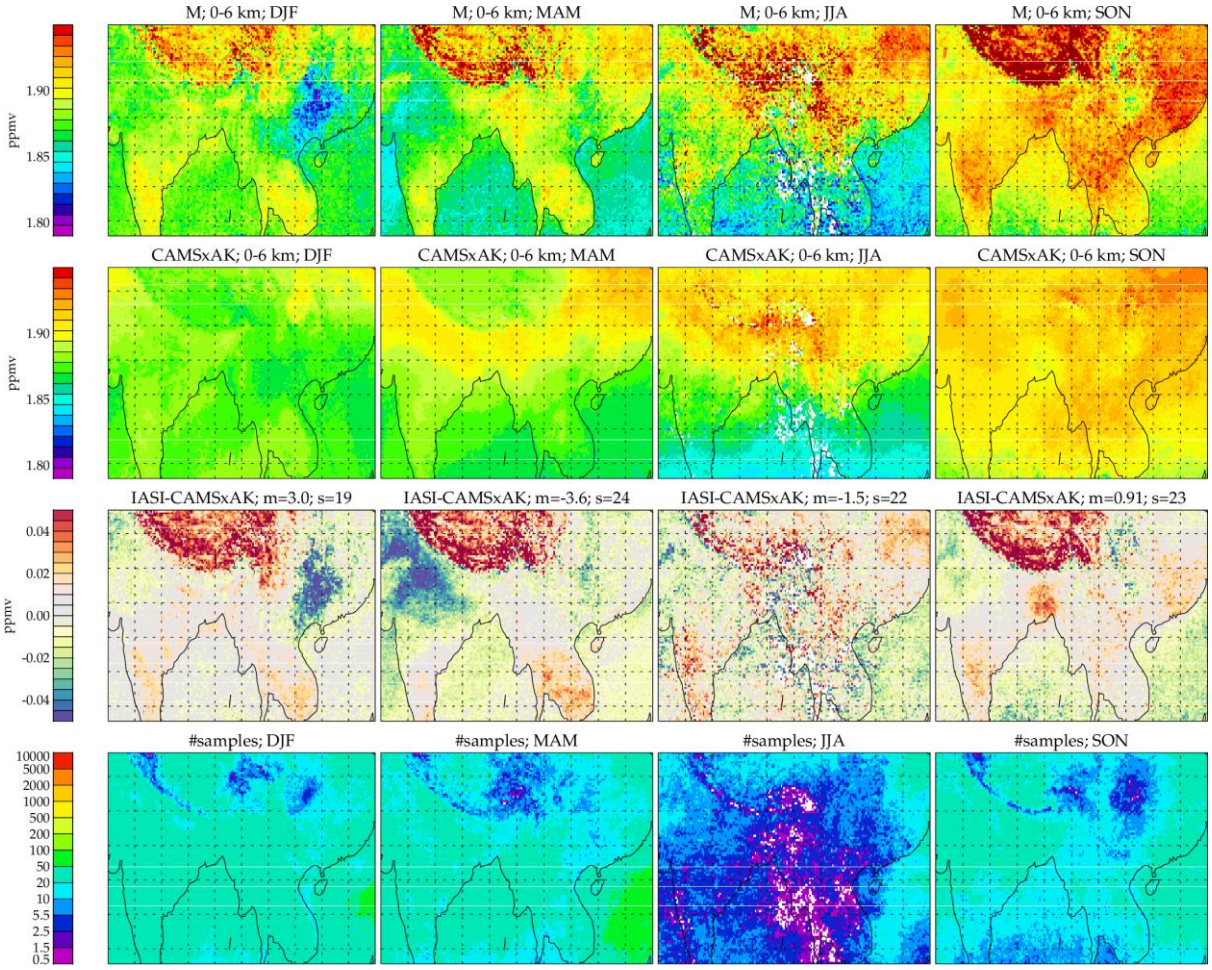

Figure 4-10 : RAL Methane+ version 2 TIR daytime 0-6km layer average retrievals over target region A.

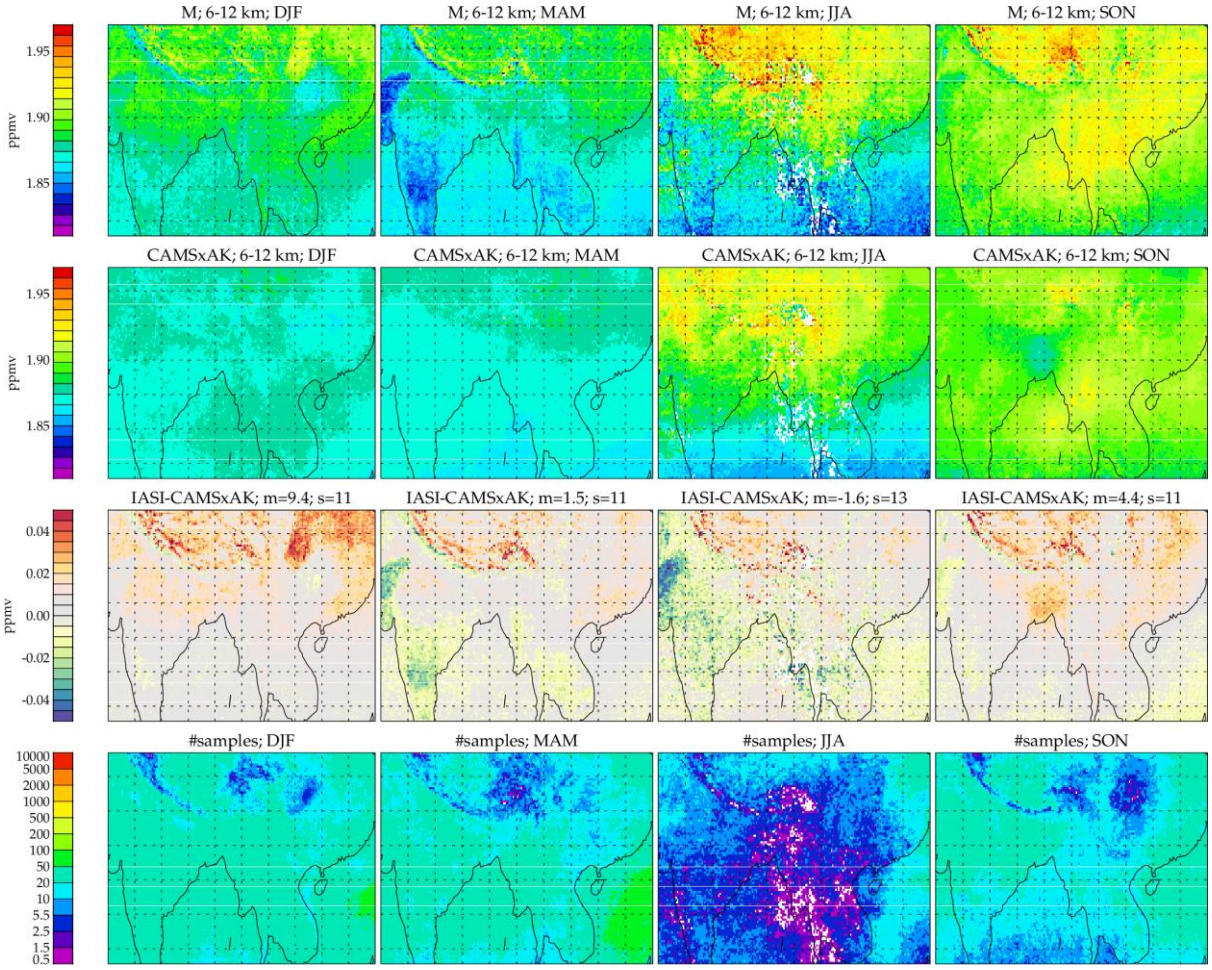

Figure 4-11 : RAL Methane+ version 2 TIR daytime 6-12km layer average retrievals over target region A.

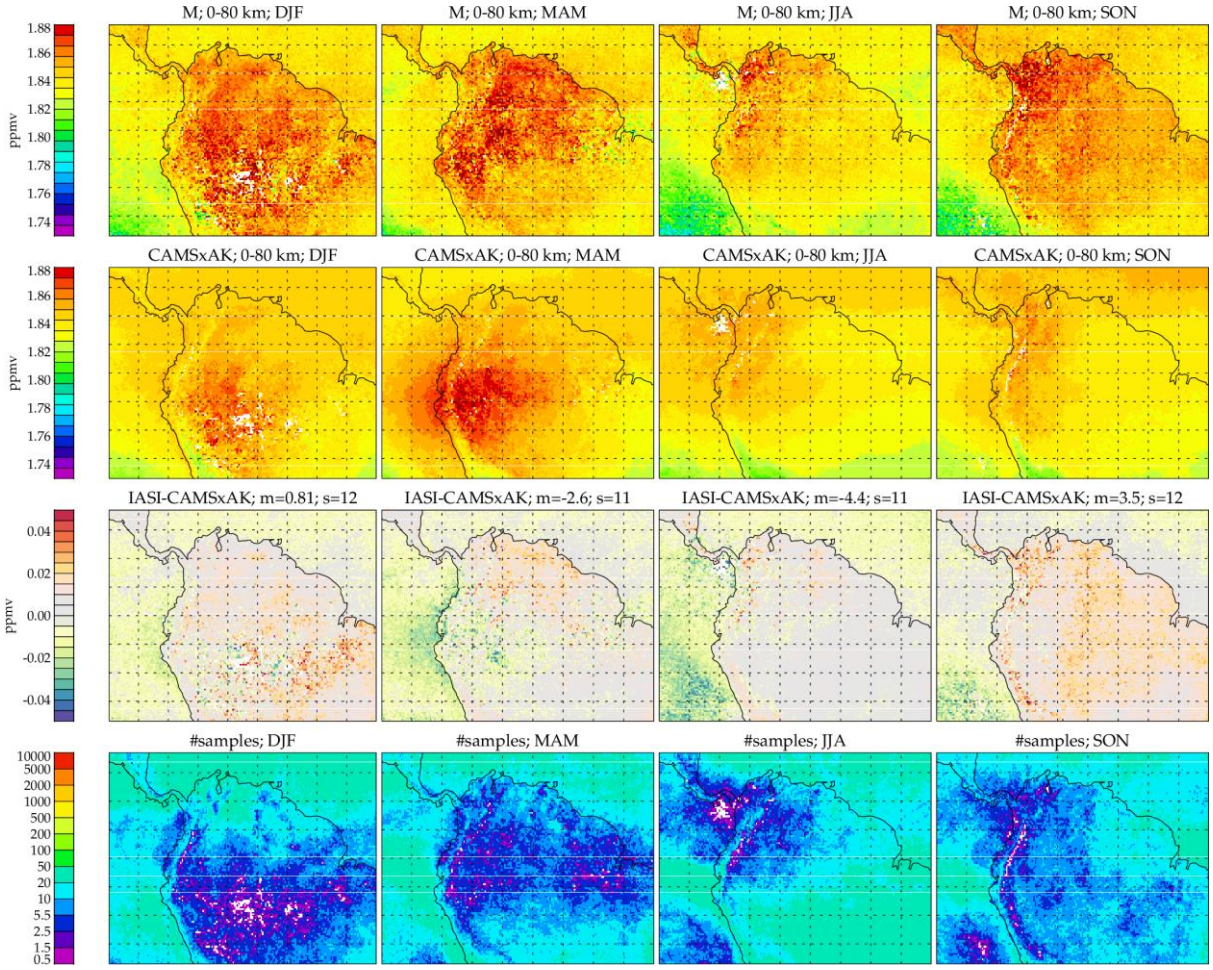

Figure 4-12 : RAL Methane+ version 2 TIR global daytime column average retrievals for region B: Each column of the figure shows results for a different season (2018 and 2019 combined). Rows from top-bottom show, respectively, results from IASI retrievals; CAMS with averaging kernels applied (CAMSxAK); the difference between IASI and CAMSxAK; the number of individual IASI retrievals in each of the 0.5x0.5 degree bins. In panels showing differences, the mean ("m") and standard deviation ("s") of the binned data are given, in ppbv, in the panel title.

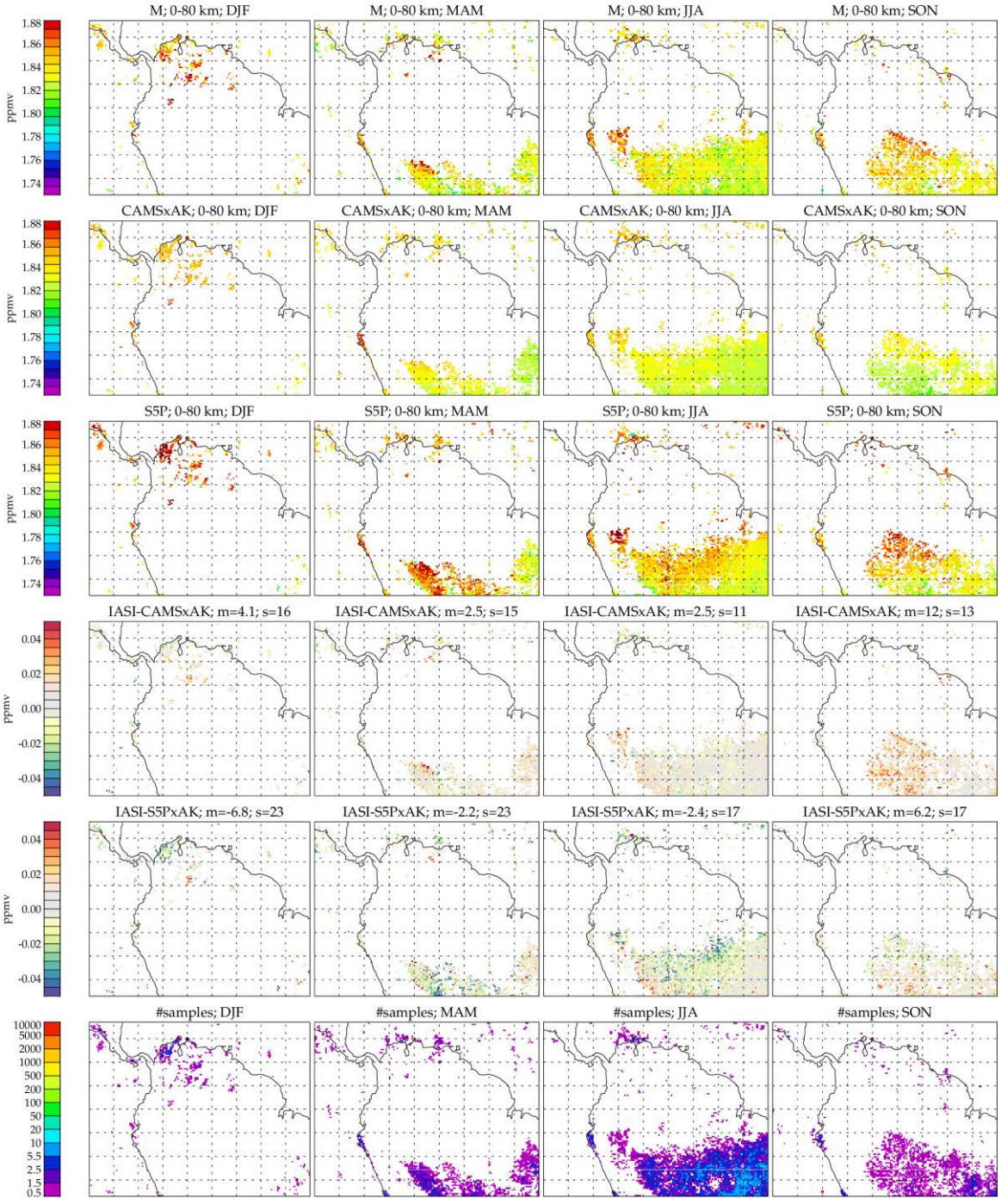

bin_imsch4_seasonal_hr2_box_dia_as5p3_amacc2_mcost120_cfr20_imsch4_iv-3_regB

Figure 4-13 : RAL Methane+ version 2 TIR global daytime column average retrievals for region B, collocated with S5P: Each column of the figure shows results for a different season (2018 and 2019 combined). Panels from top-bottom show, respectively, results from IASI retrievals; CAMS; S5P retrievals; Difference between IASI and S5P; Difference between IASI and S5P accounting for the IASI averaging kernel using CAMS; the number of individual IASI retrievals in each of the 0.5x0.5 degree bins. In panels showing differences, the mean ("m") and standard deviation ("s") of the binned data are given, in ppbv, in the panel title.

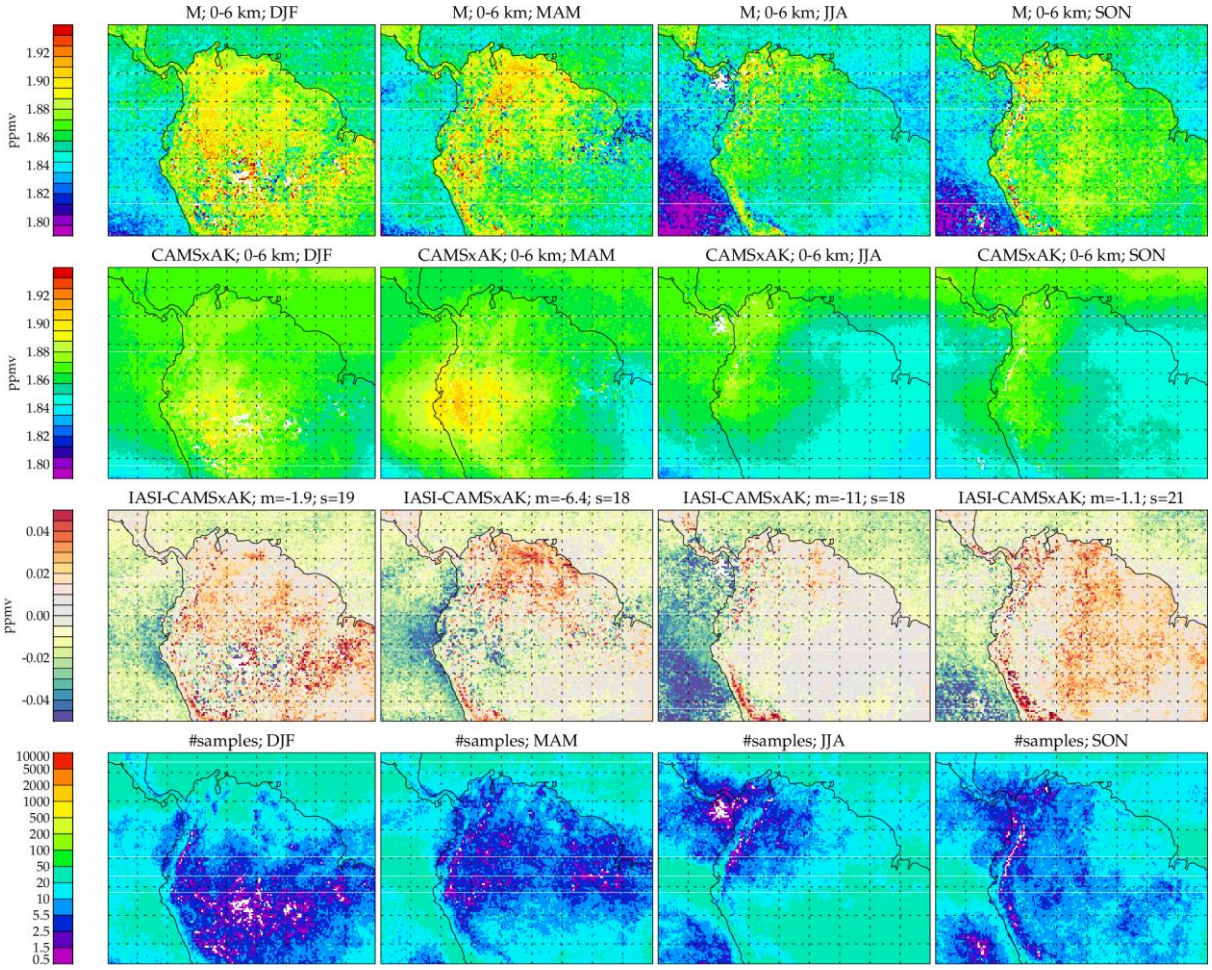

Figure 4-14 : RAL Methane+ version 2 TIR daytime 0-6km layer average retrievals over target region B.

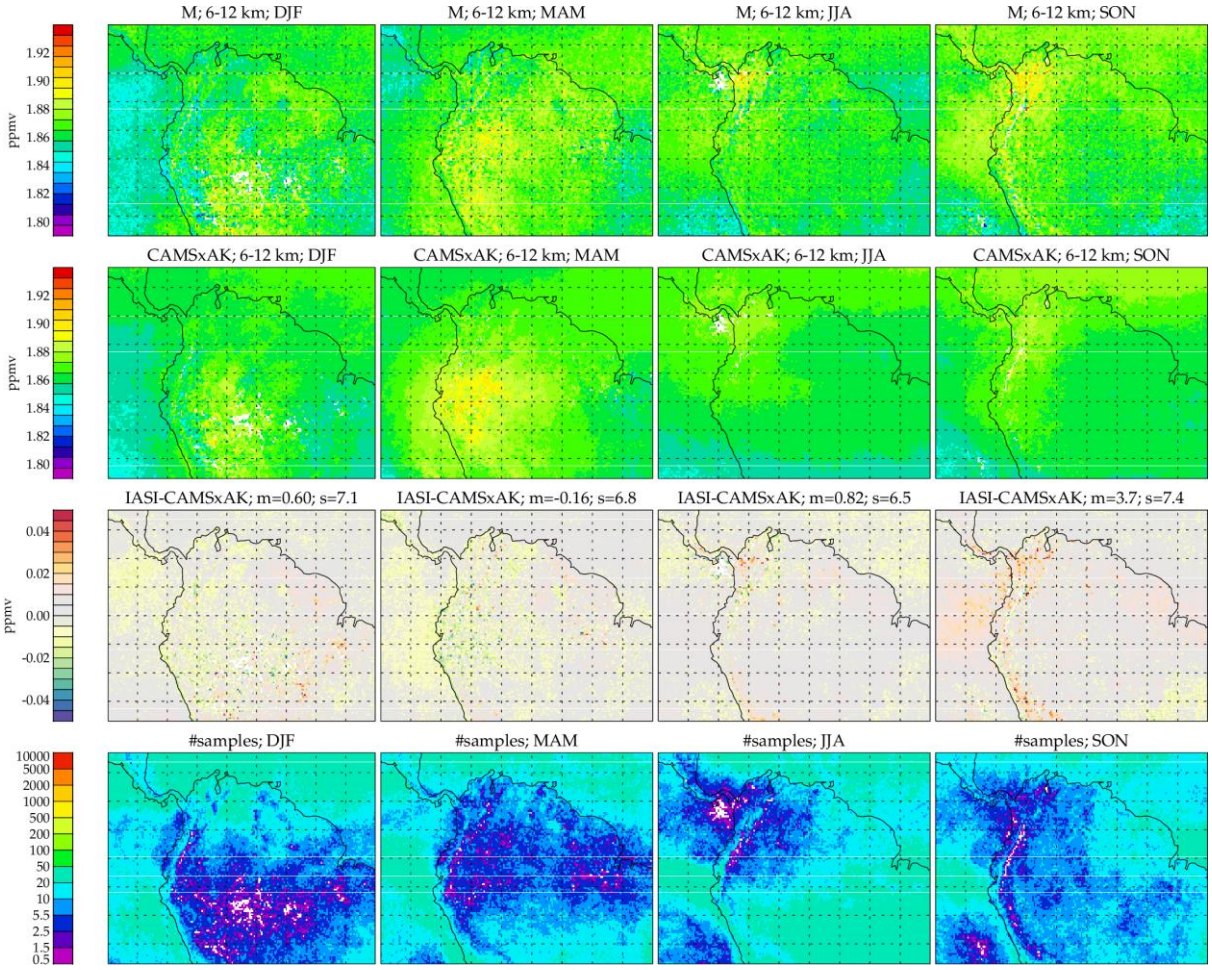

Figure 4-15 : RAL Methane+ version 2 TIR daytime 6-12km layer average retrievals over target region B.

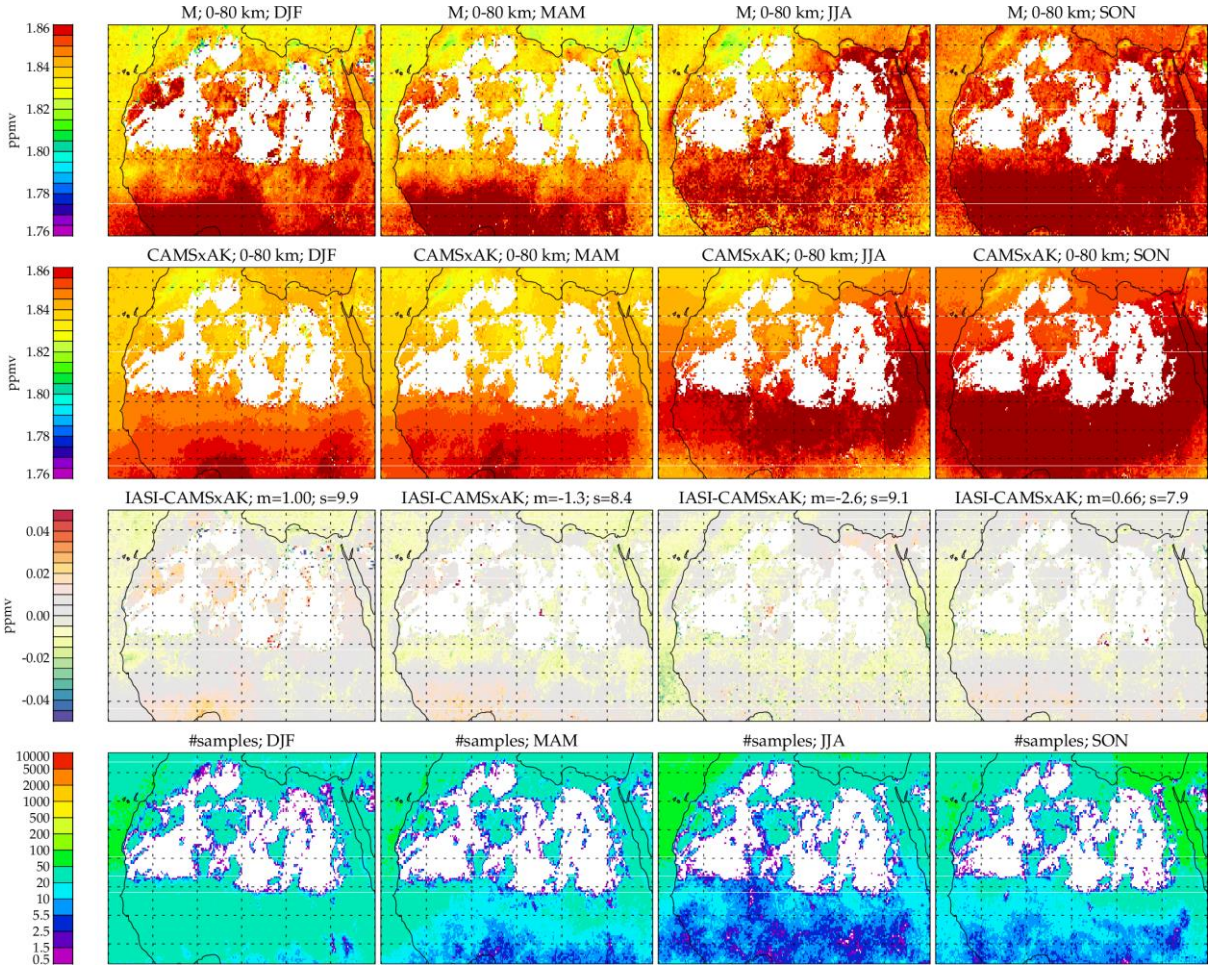

Figure 4-16 : RAL Methane+ version 2 TIR global daytime column average retrievals for region C: Each column of the figure shows results for a different season (2018 and 2019 combined). Rows from top-bottom show, respectively, results from IASI retrievals; CAMS with averaging kernels applied (CAMSxAK); the difference between IASI and CAMSxAK; the number of individual IASI retrievals in each of the 0.5x0.5 degree bins.

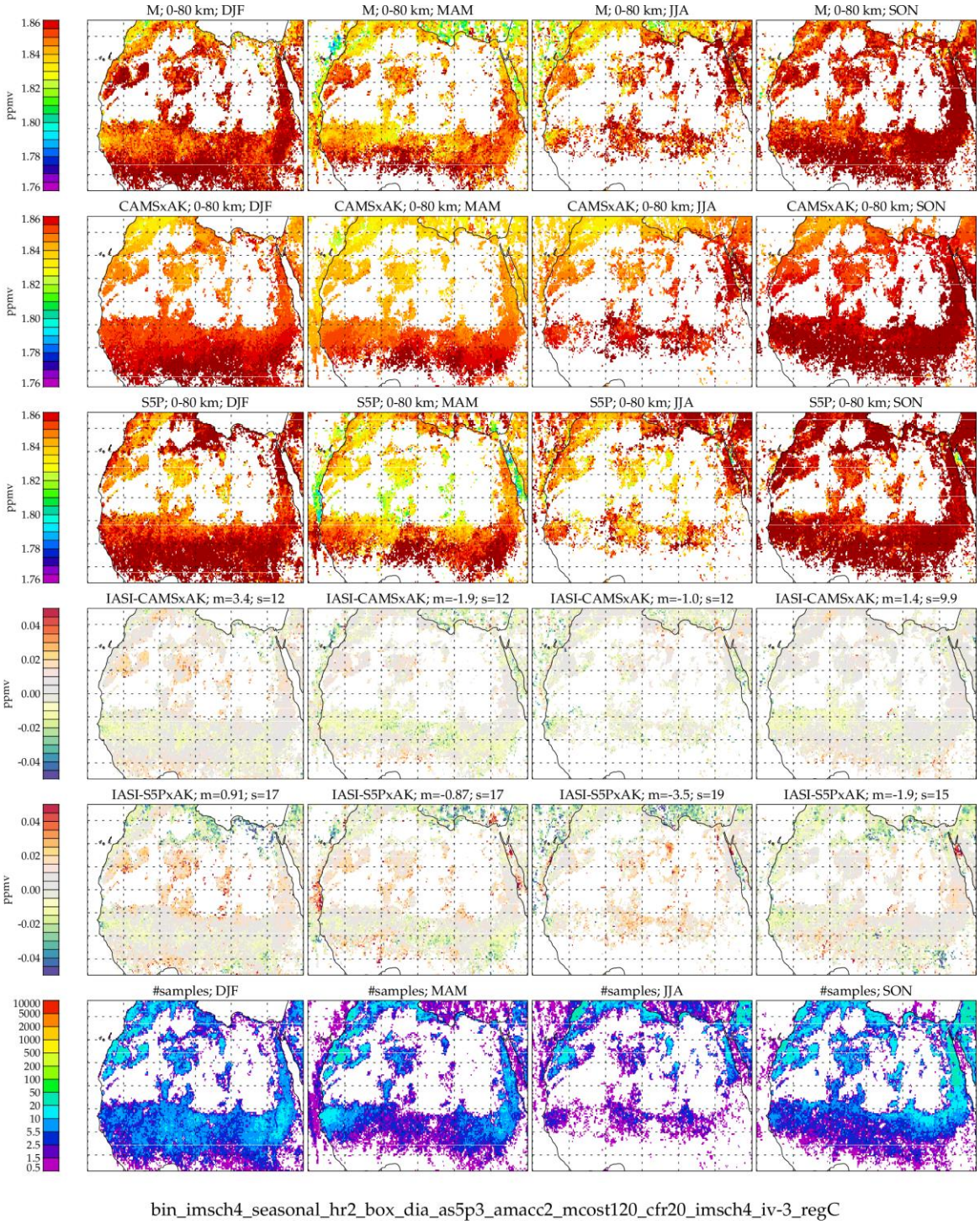

Figure 4-17 : RAL Methane+ version 2 TIR global daytime column average retrievals for region C, collocated with S5P: Each column of the figure shows results for a different season (2018 and 2019 combined). Panels from top-bottom show, respectively, results from IASI retrievals; CAMS; S5P retrievals; Difference between IASI and S5P; Difference between IASI and S5P accounting for the IASI averaging kernel using CAMS; the number of individual IASI retrievals in each of the 0.5x0.5 degree bins. In panels showing differences, the mean ("m") and standard deviation ("s") of the binned data are given, in ppbv, in the panel title.

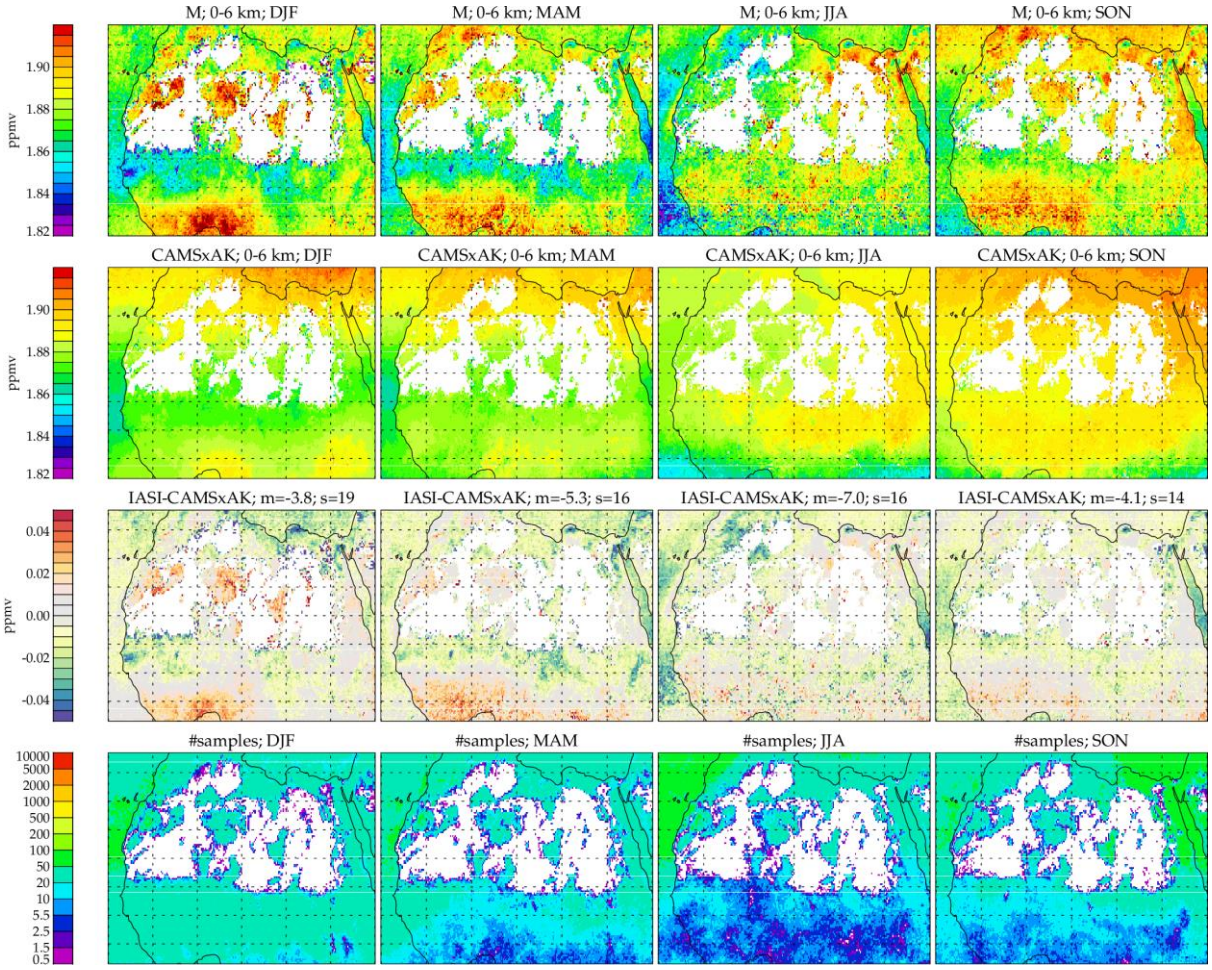

Figure 4-18 : RAL Methane+ version 2 TIR daytime 0-6km layer average retrievals over target region C.

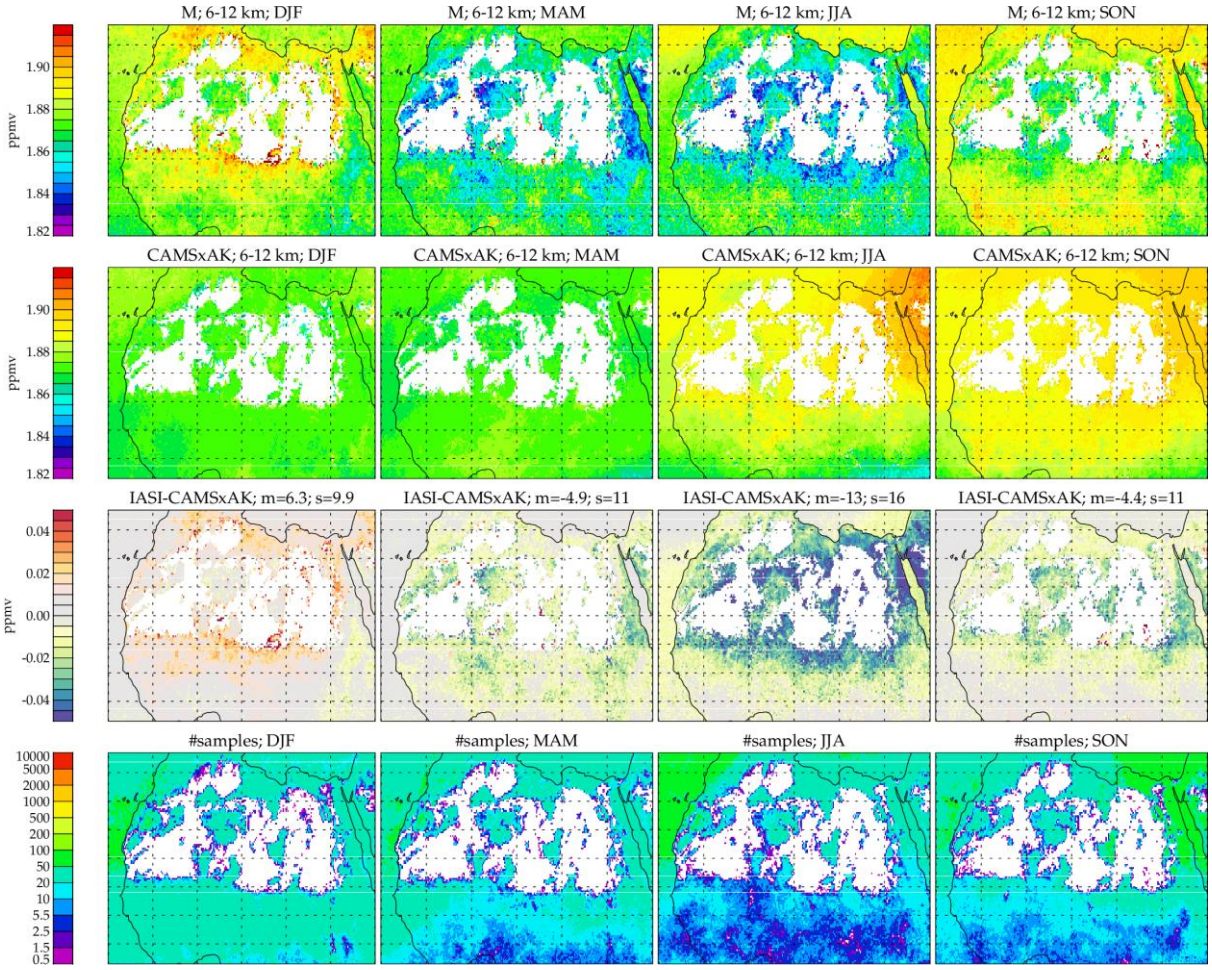

Figure 4-19 : RAL Methane+ version 2 TIR daytime 6-12km layer average retrievals over target region C.

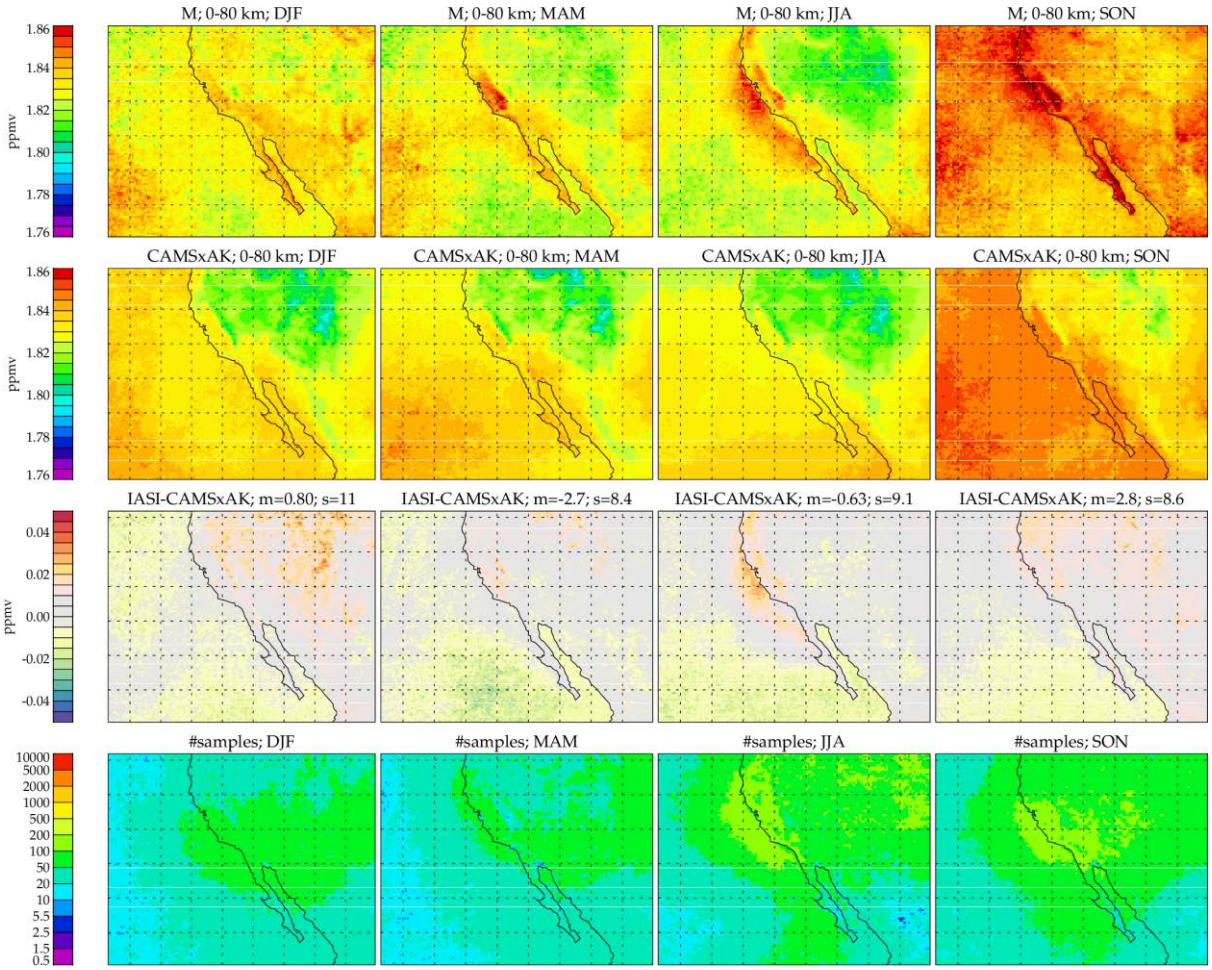

Figure 4-20 : RAL Methane+ version 2 TIR global daytime column average retrievals for region D: Each column of the figure shows results for a different season (2018 and 2019 combined). Rows from top-bottom show, respectively, results from IASI retrievals; CAMS with averaging kernels applied (CAMSxAK); the difference between IASI and CAMSxAK; the number of individual IASI retrievals in each of the 0.5x0.5 degree bins.

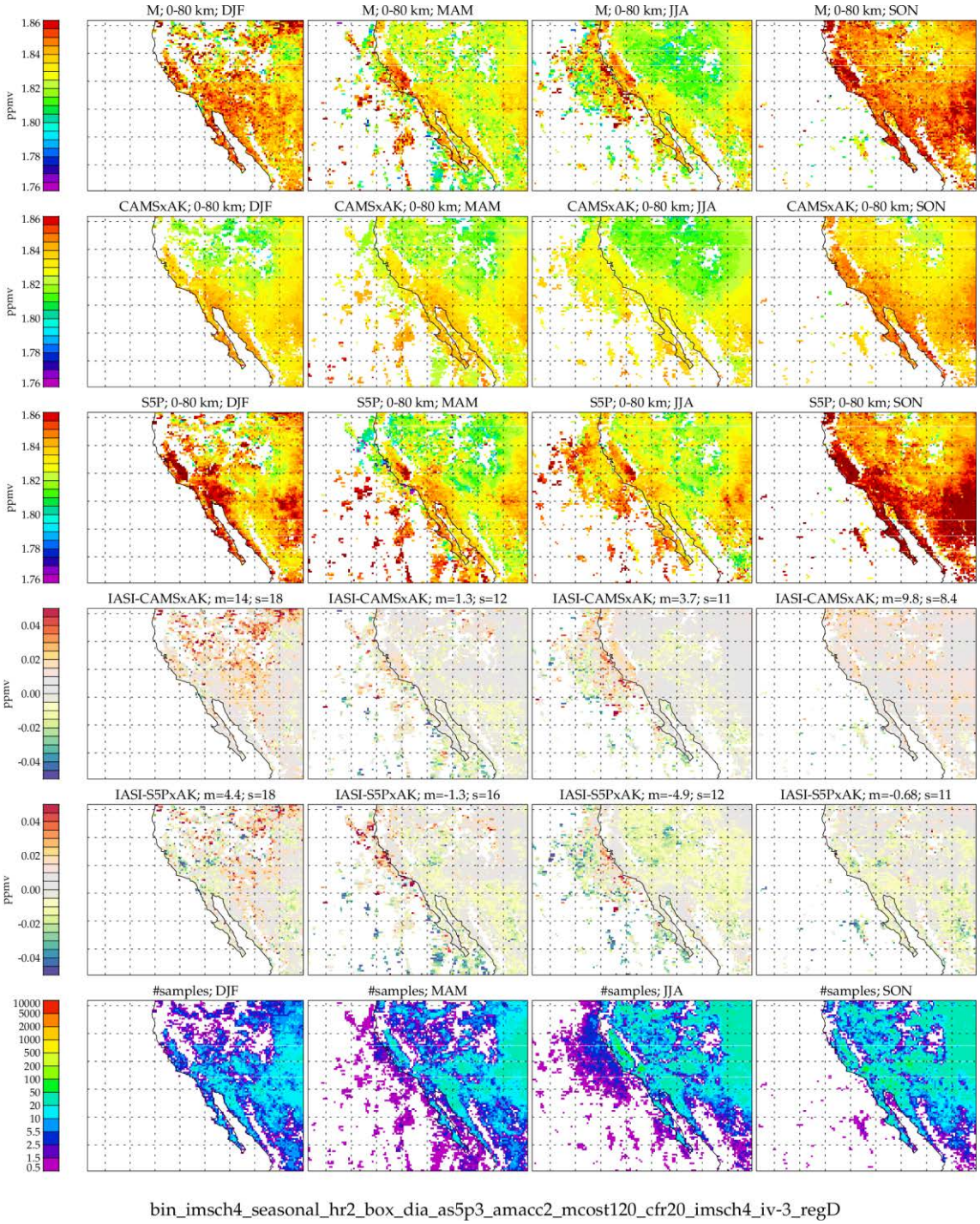

Figure 4-21 : RAL Methane+ version 2 TIR global daytime column average retrievals for region D, collocated with S5P: Each column of the figure shows results for a different season (2018 and 2019 combined). Panels from top-bottom show, respectively, results from IASI retrievals; CAMS; S5P retrievals; Difference between IASI and S5P; Difference between IASI and S5P accounting for the IASI averaging kernel using CAMS; the number of individual IASI retrievals in each of the 0.5x0.5 degree bins. In panels showing differences, the mean ("m") and standard deviation ("s") of the binned data are given, in ppbv, in the panel title.

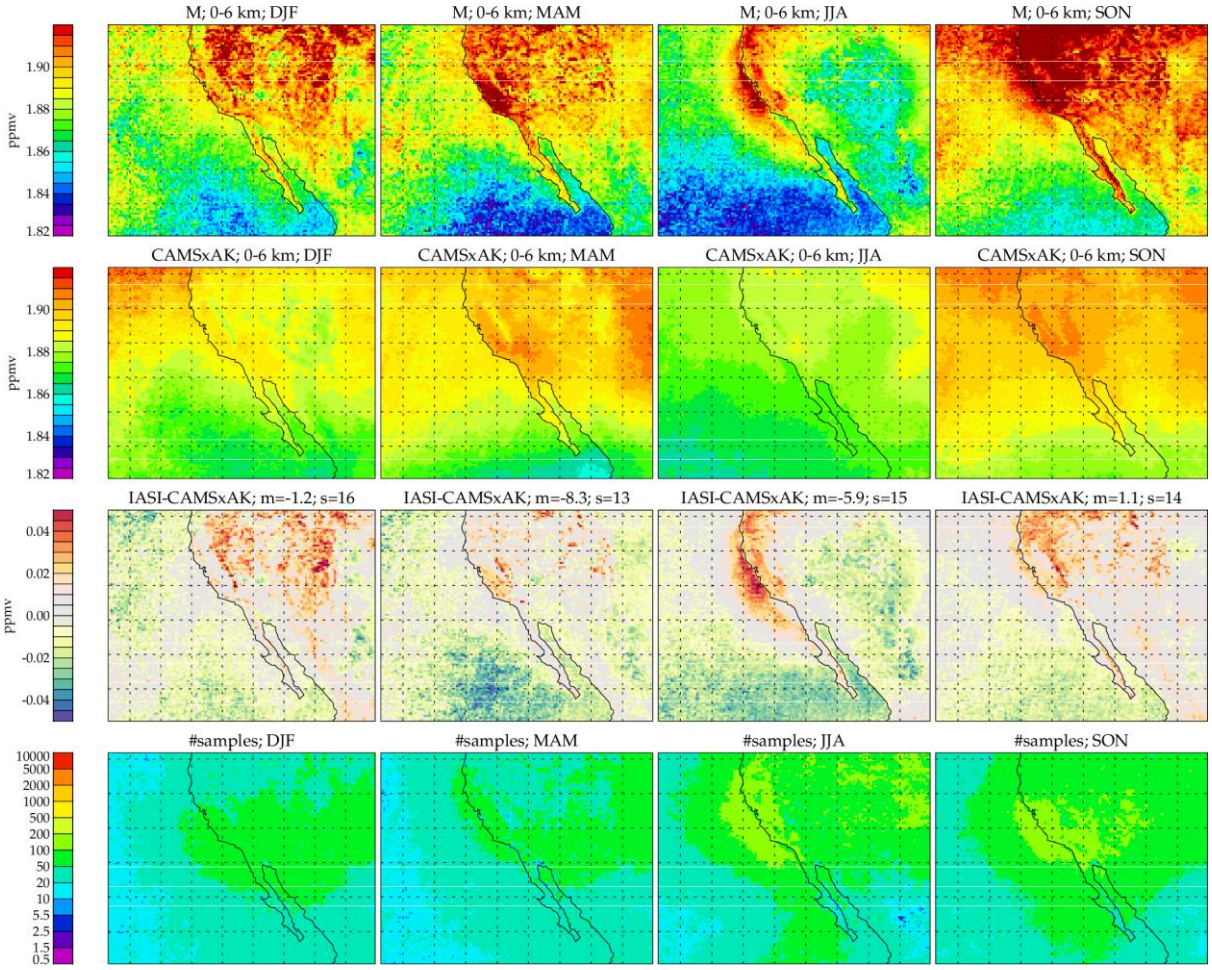

Figure 4-22 : RAL Methane+ version 2 TIR daytime 0-6km layer average retrievals over target region D.

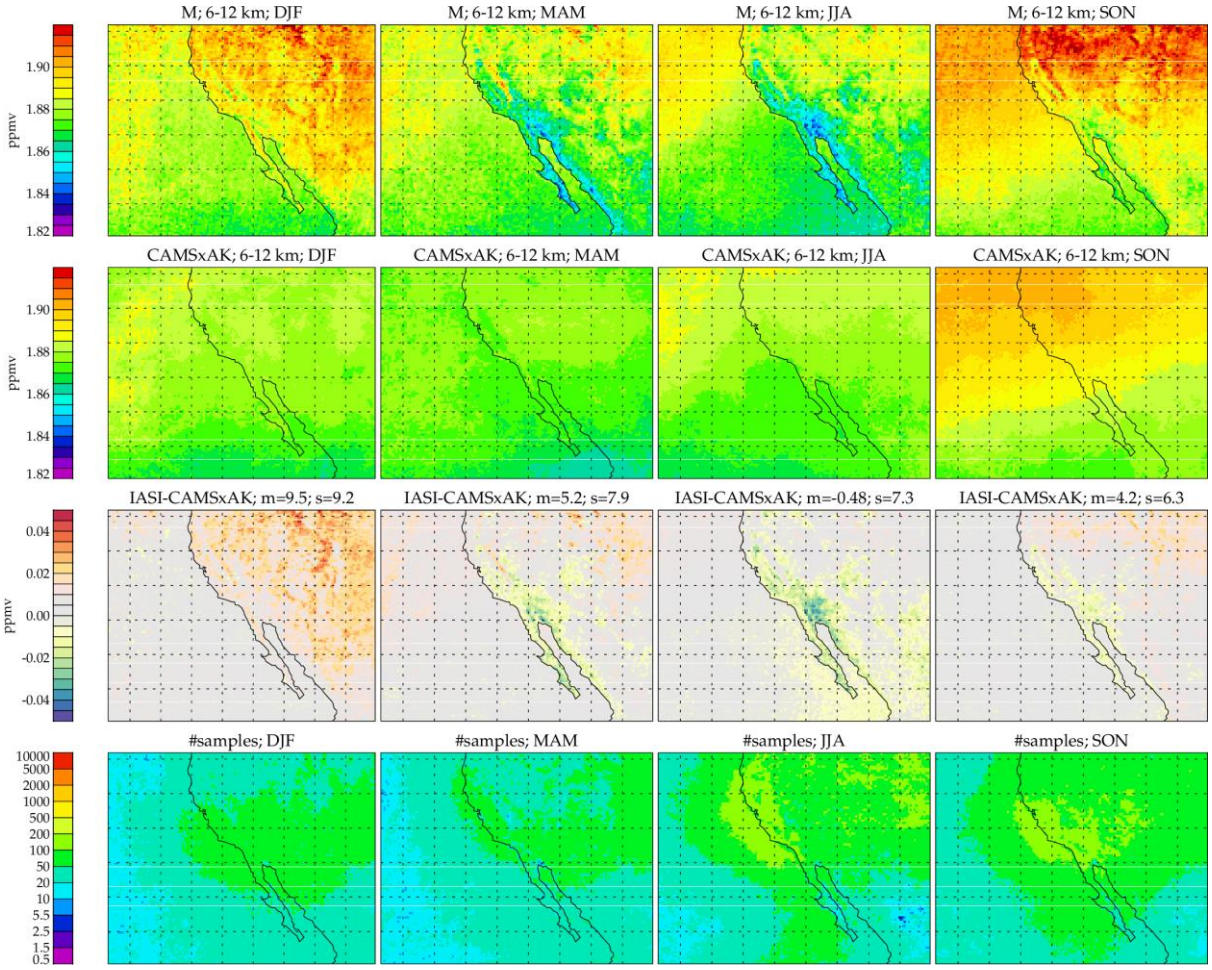

Figure 4-23 : RAL Methane+ version 2 TIR daytime 6-12km layer average retrievals over target region D.

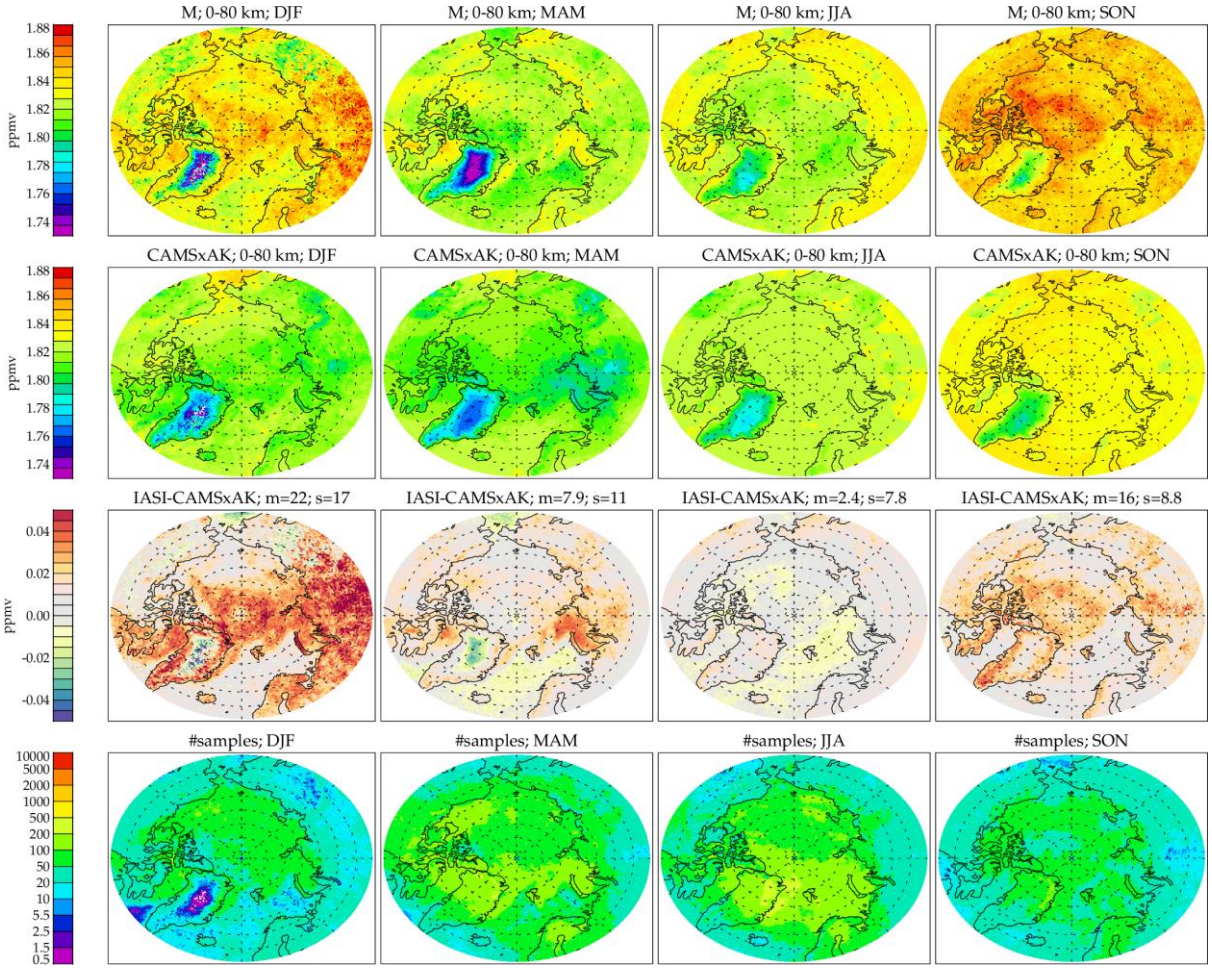

Figure 4-24 : RAL Methane+ version 2 TIR global daytime column average retrievals for region E: Each column of the figure shows results for a different season (2018 and 2019 combined). Rows from top-bottom show, respectively, results from IASI retrievals; CAMS with averaging kernels applied (CAMSxAK); the difference between IASI and CAMSxAK; the number of individual IASI retrievals in each of the 0.5x0.5 degree bins. In panels showing differences, the mean ("m") and standard deviation ("s") of the binned data are given, in ppbv, in the panel title.

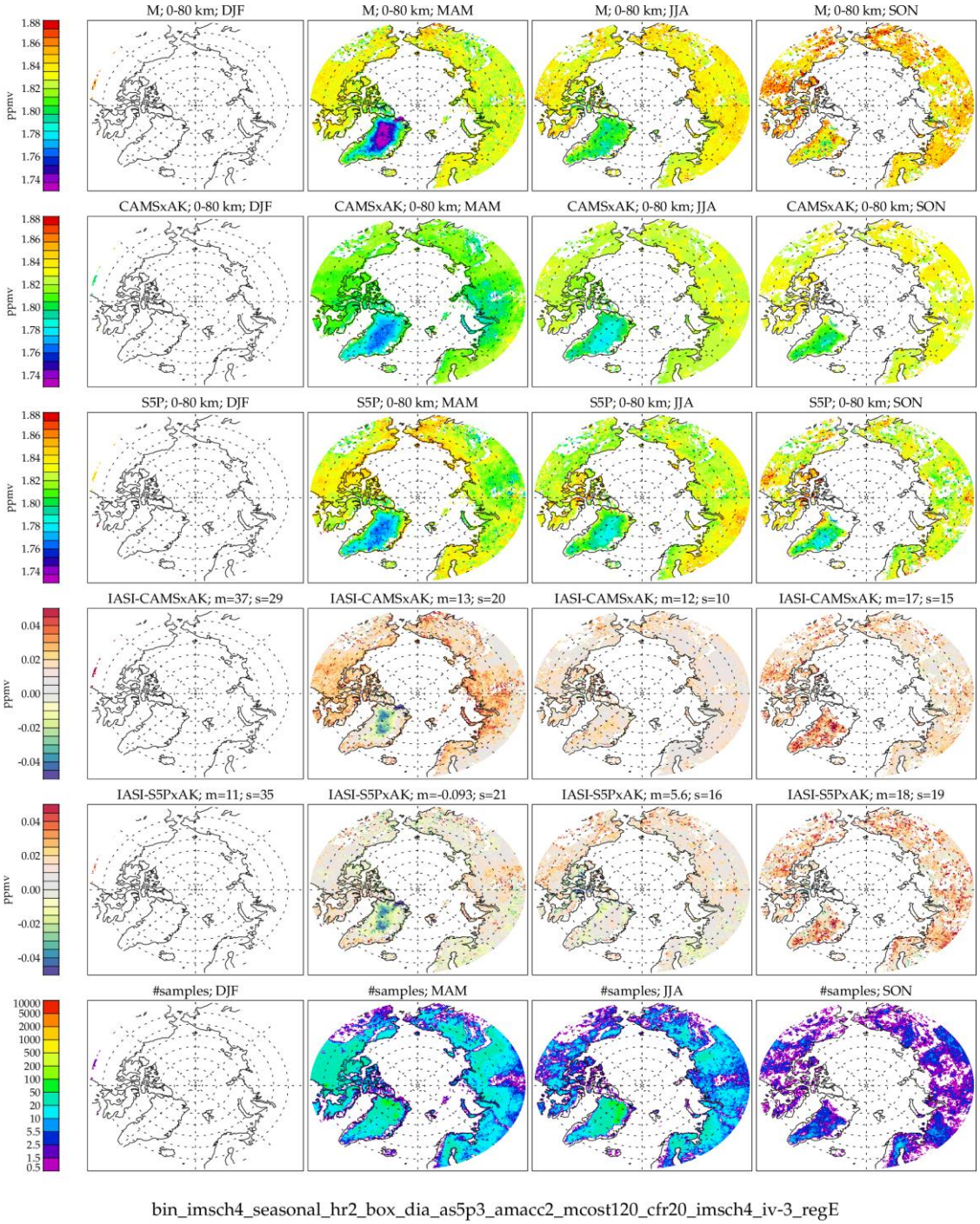

bin_imsch4_seasonal_hr2_box_dia_as5p3_amacc2_mcost120_cfr20_imsch4_iv-3_regE

Figure 4-25 : RAL Methane+ version 2 TIR global daytime column average retrievals for region E, collocated with S5P: Each column of the figure shows results for a different season (2018 and 2019 combined). Panels from top-bottom show, respectively, results from IASI retrievals; CAMS; S5P retrievals; Difference between IASI and S5P; Difference between IASI and S5P accounting for the IASI averaging kernel using CAMS; the number of individual IASI retrievals in each of the 0.5x0.5 degree bins. In panels showing differences, the mean ("m") and standard deviation ("s") of the binned data are given, in ppbv, in the panel title.

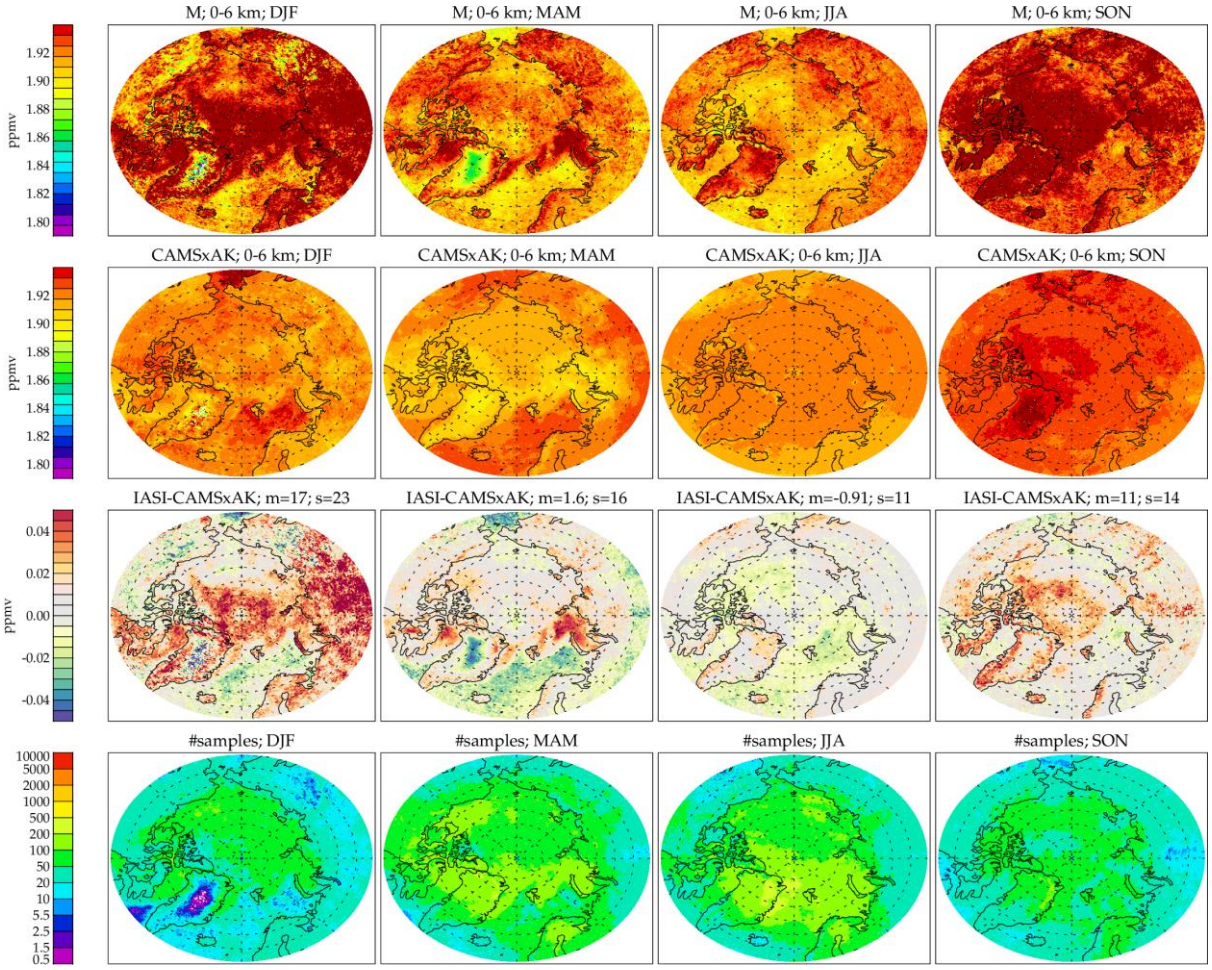

Figure 4-26 : RAL Methane+ version 2 TIR daytime 0-6km layer average retrievals over target region E.

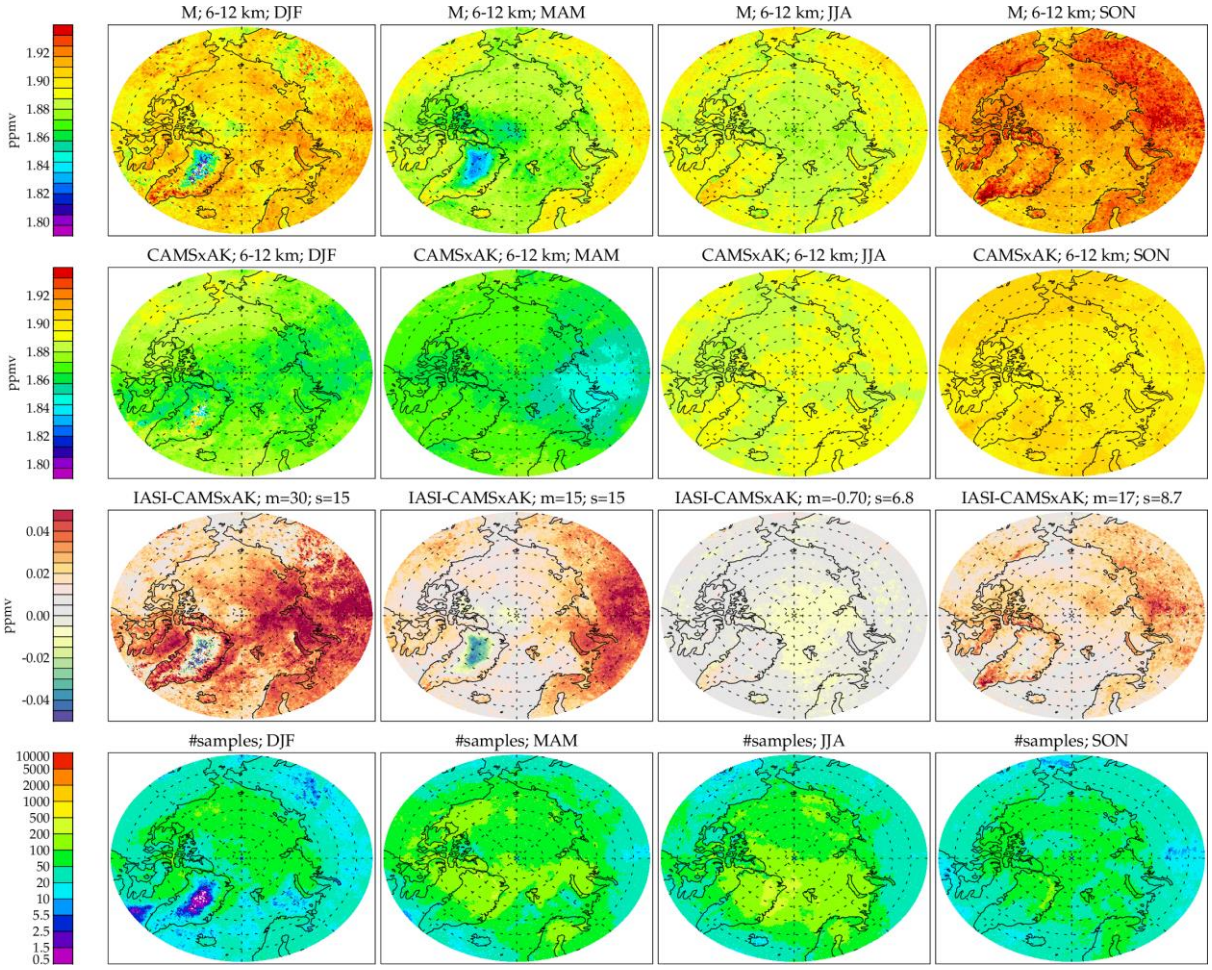

Figure 4-27 : RAL Methane+ version 2 TIR daytime 6-12km layer average retrievals over target region E.

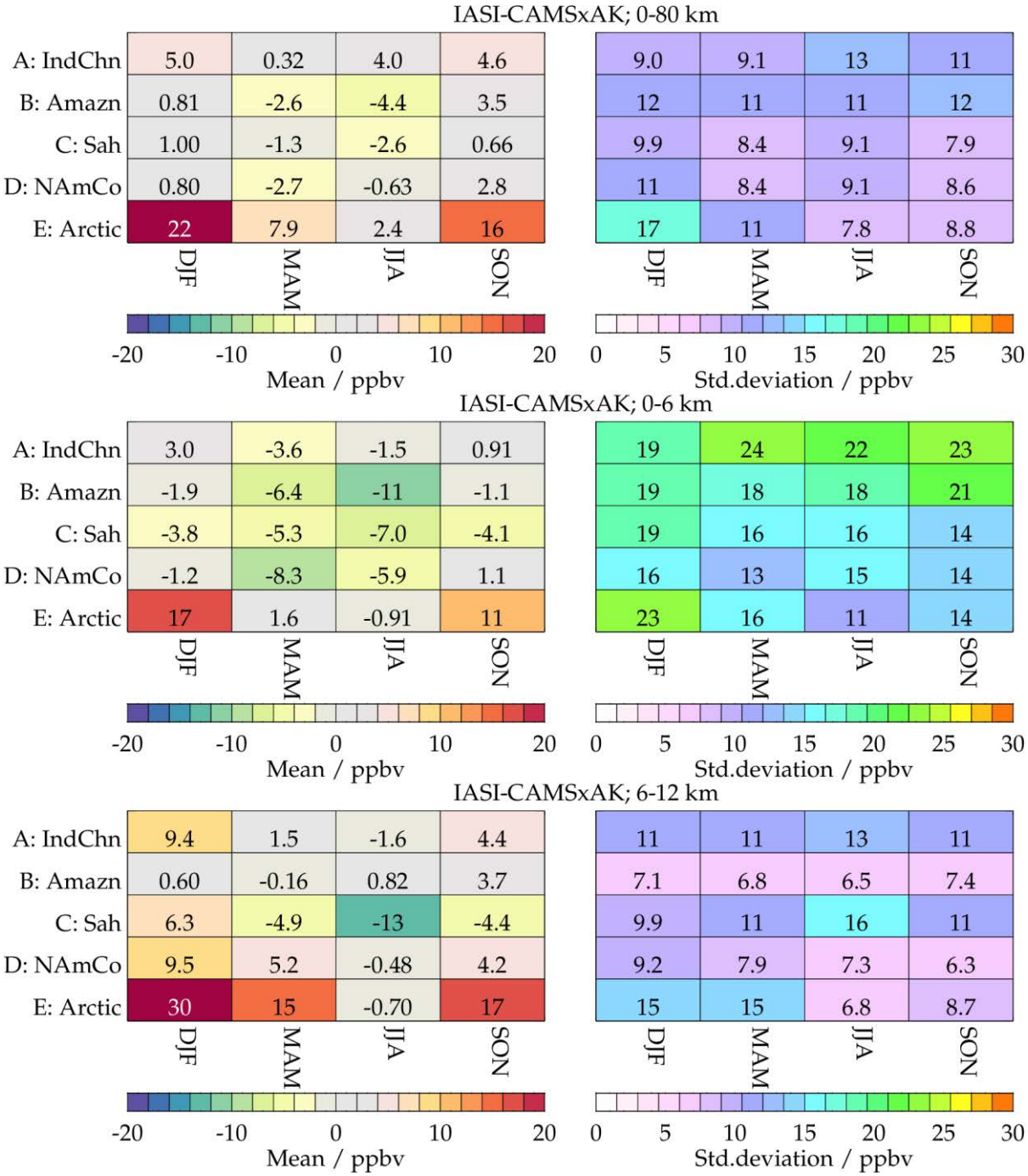

Figure 4-28 : Summary of seasonally averaged differences between RAL Methane+ version 2 TIR retrievals and CAMS for each region. Left-hand panel shows the mean difference in each region/season; Right-hand panel shows the standard deviation in the mean (considering the spatial variation of the difference for each of the 0.5x0.5 degree bins). Panels from top-bottom show results for total, 0-6 and 6-12km layer averages.

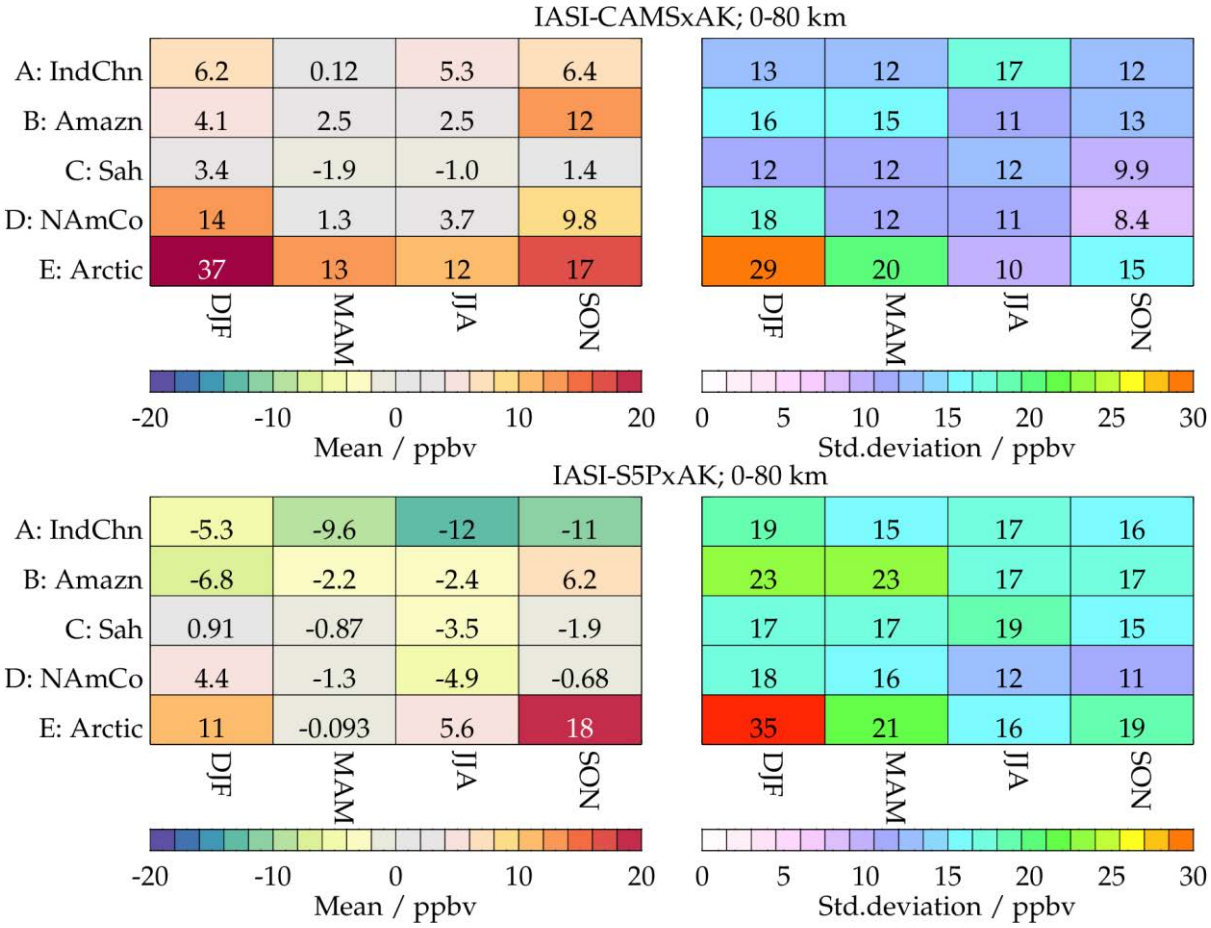

Figure 4-29 : Summary of seasonally averaged total column differences between RAL Methane+ version 2 TIR retrievals, CAMS and S5P for each region. Left-hand panel shows the mean difference in each region/season; Right-hand panel shows the standard deviation in the mean (considering the spatial variation of the mean difference for each of the 0.5x0.5 degree bins). Upper panels show the difference between IASI and CAMS (with averaging kernels); lower panels show the difference between IASI and S5P. Note that, in this figure, the comparisons to CAMS in upper panels are for the same sub-set of scenes for which there are S5P co-locations.

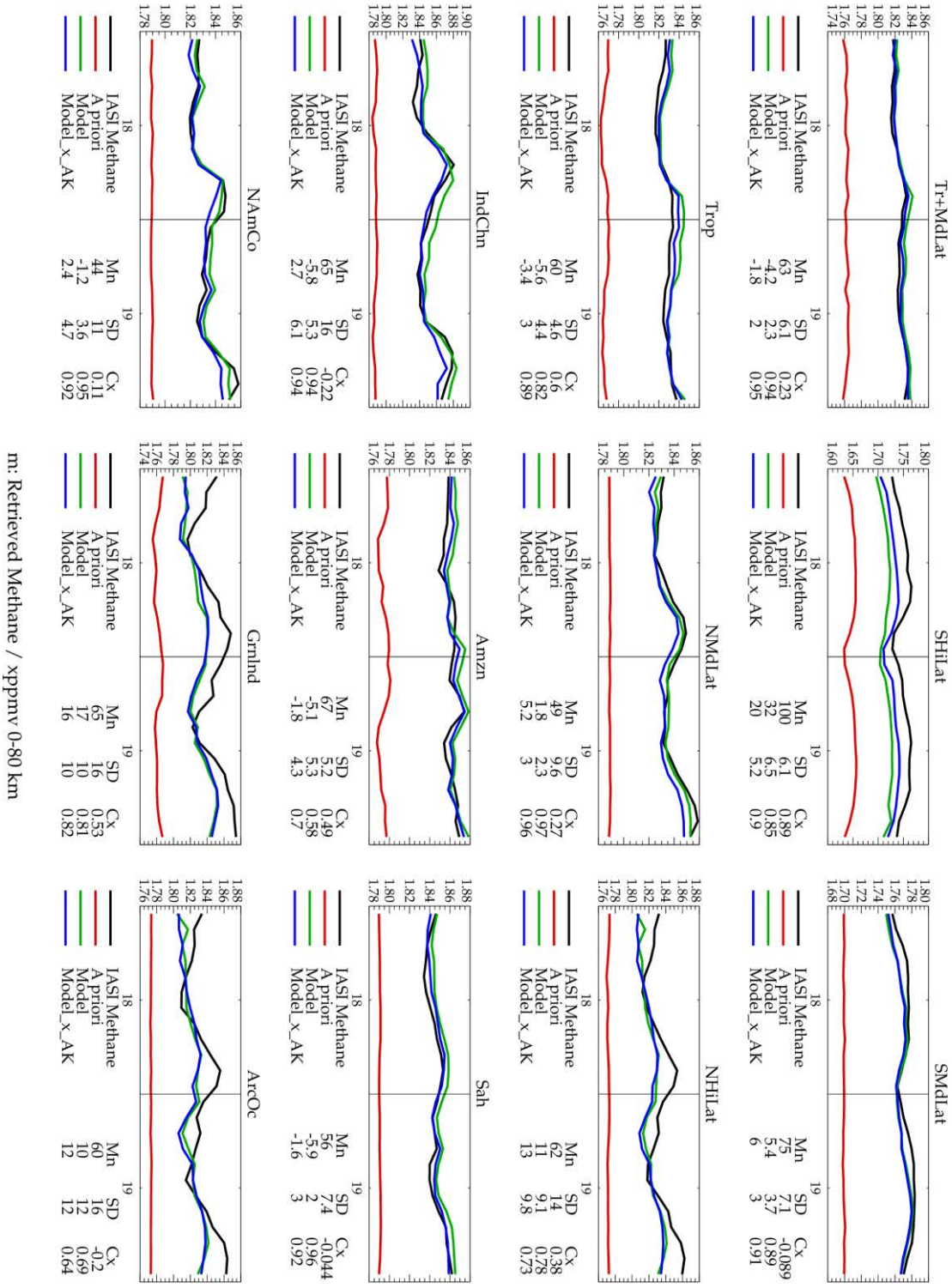

Figure 4-30 : Time series comparisons of RAL Methane+ version 2 TIR and CAMS column average methane for various regions. Each panel shows a different region as described in section 2.2. Statistics given in the legend under each panel give the mean difference (Mn); standard deviation of the monthly mean differences (SD); correlation between IASI and CAMS monthly mean values.

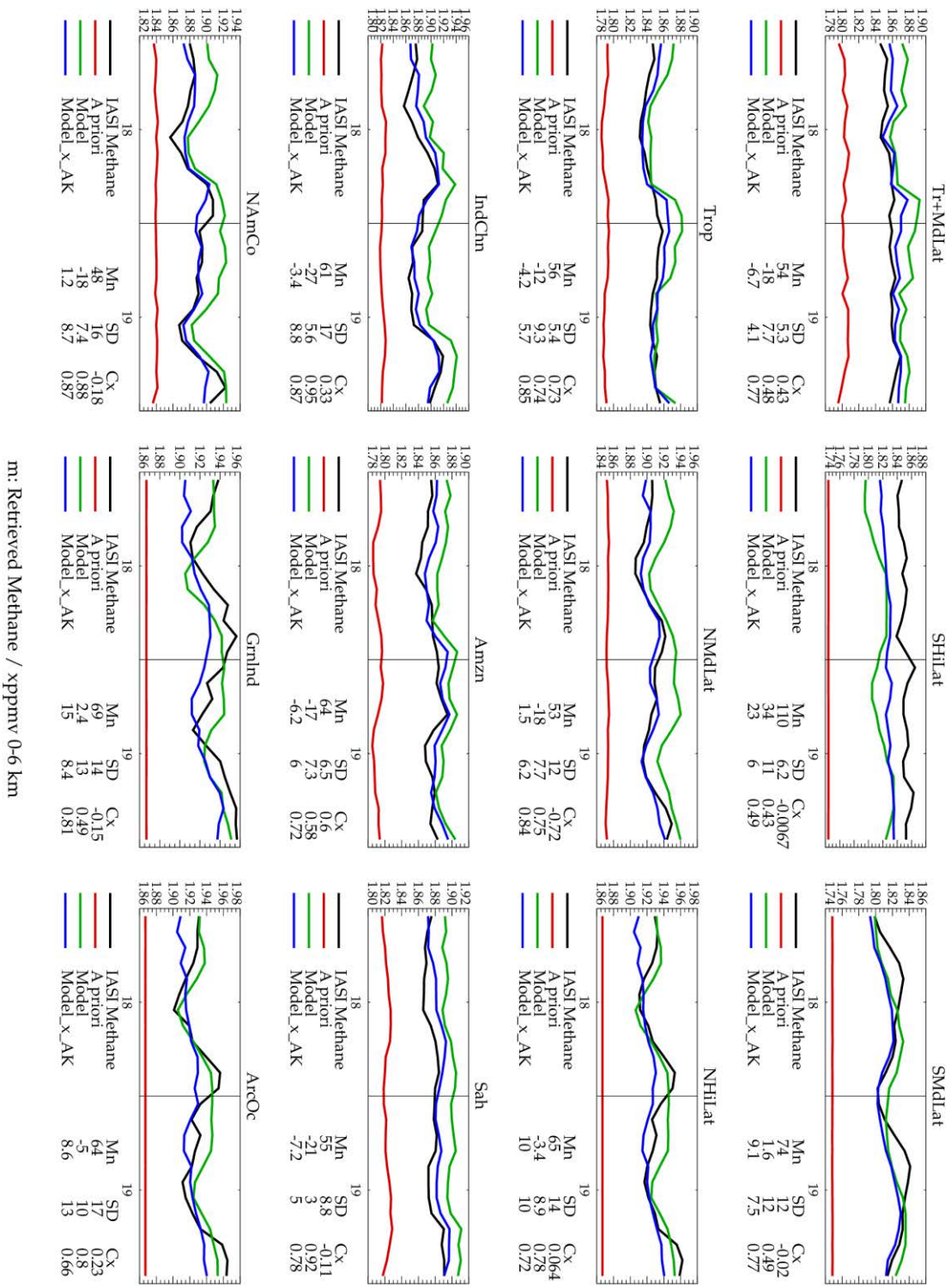

Figure 4-31 : Time series comparisons of RAL Methane+ version 2 TIR and CAMS 0-6km sub-column average methane for various regions. Each panel shows a different region as described in section 2.2. Statistics given in the legend under each panel give the mean difference (Mn); standard deviation of the monthly mean differences (SD); correlation between IASI and CAMS monthly mean values.

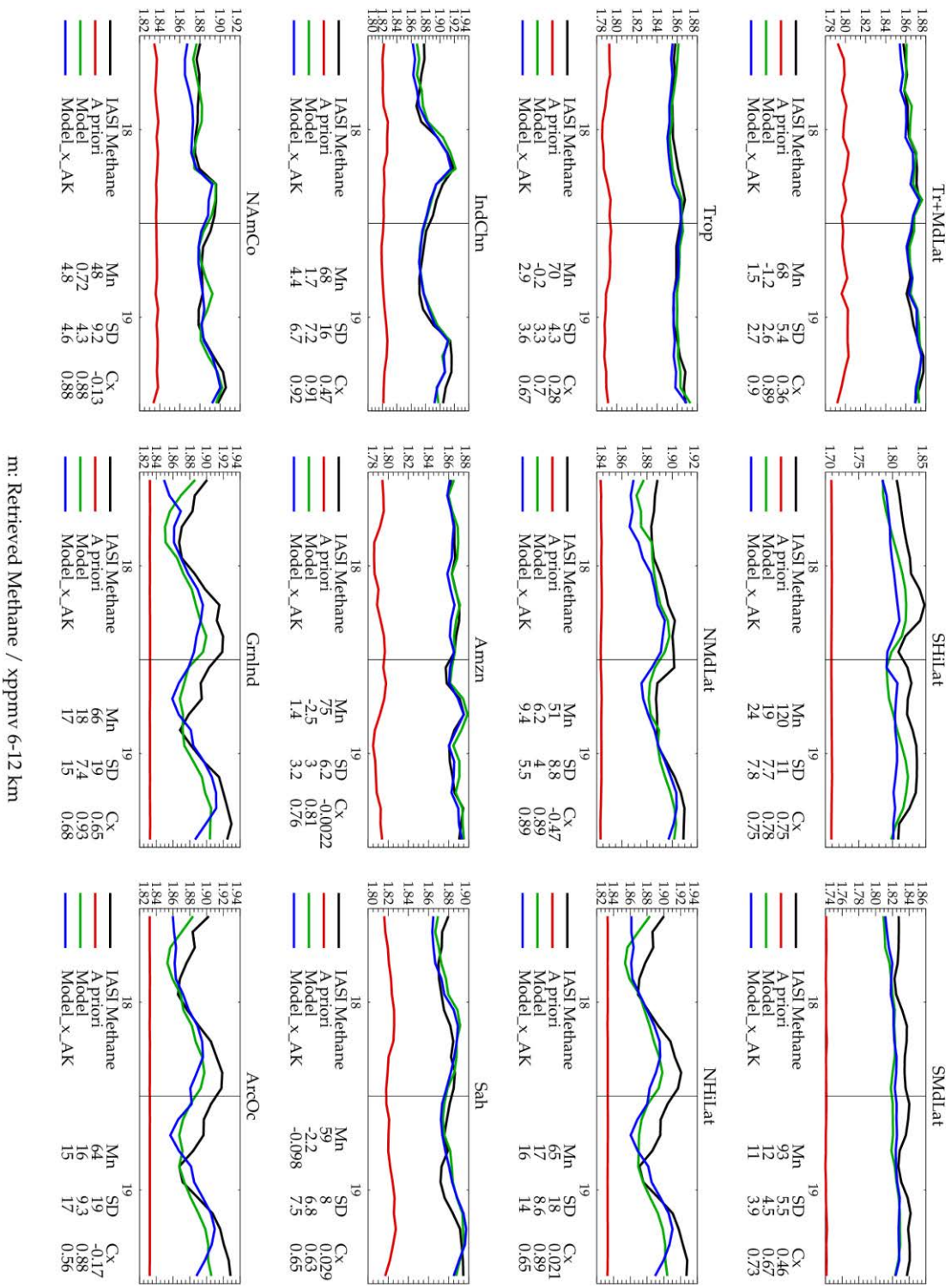

Figure 4-32 : Time series comparisons of RAL Methane+ version 2 TIR and CAMS 6-12km sub-column average methane for various regions. Each panel shows a different region as described in section 2.2. Statistics given in the legend under each panel give the mean difference (Mn); standard deviation of the monthly mean differences (SD); correlation between IASI and CAMS monthly mean values.

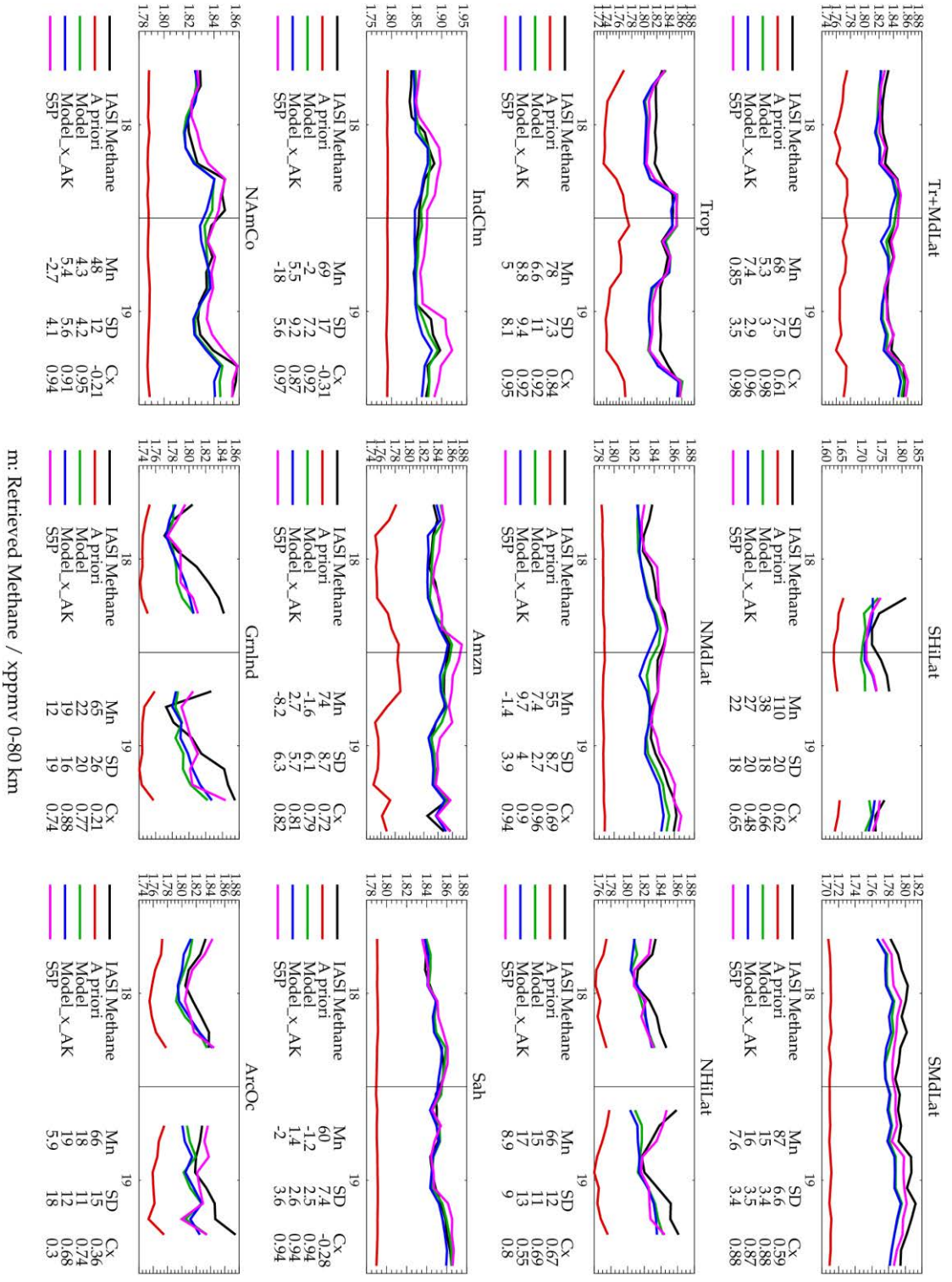

Figure 4-33 : Time series comparisons of RAL Methane+ version 2 TIR column average averaged methane to S5P (and CAMS sampled to S5P) for various regions. Each panel shows a different region as described in section 2.2. Statistics given in the legend under each panel give the mean difference from IASI (Mn); standard deviation of the monthly mean difference (SD); Correlation of the monthly mean values with IASI.

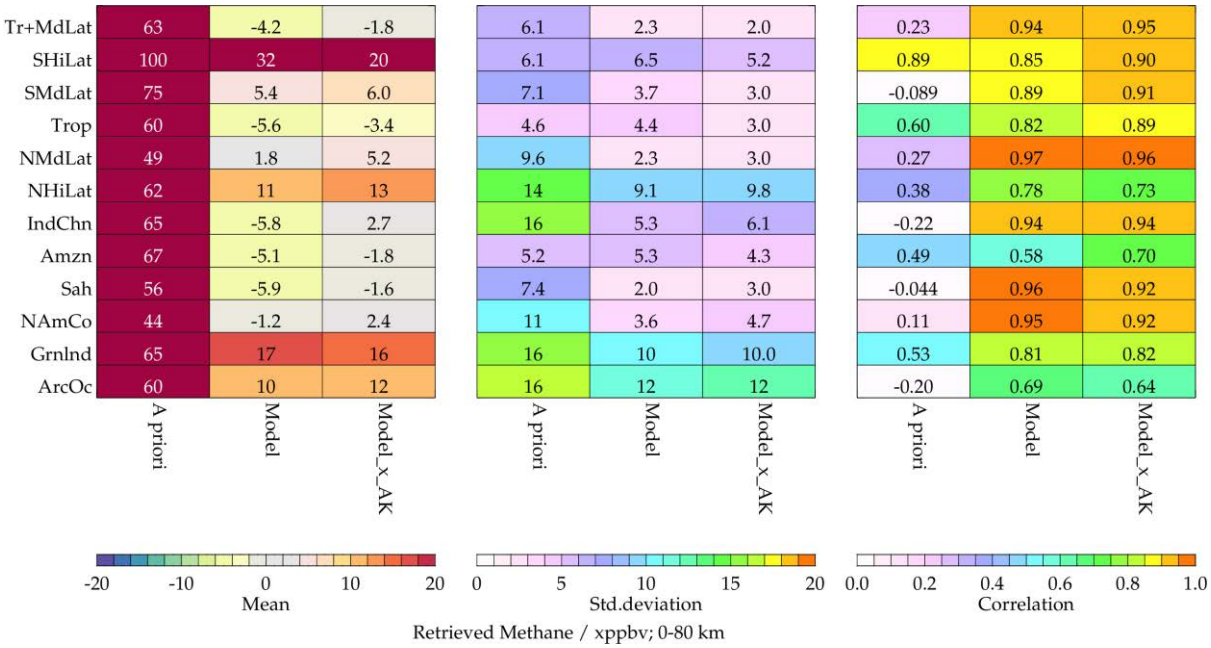

Figure 4-34 : Summary of statistics from monthly time-series comparisons of RAL Methane+ version 2 TIR and CAMS column average methane for various regions. Panels from left to right show the mean difference; standard deviation of the monthly mean differences; correlation between IASI and CAMS monthly mean values.

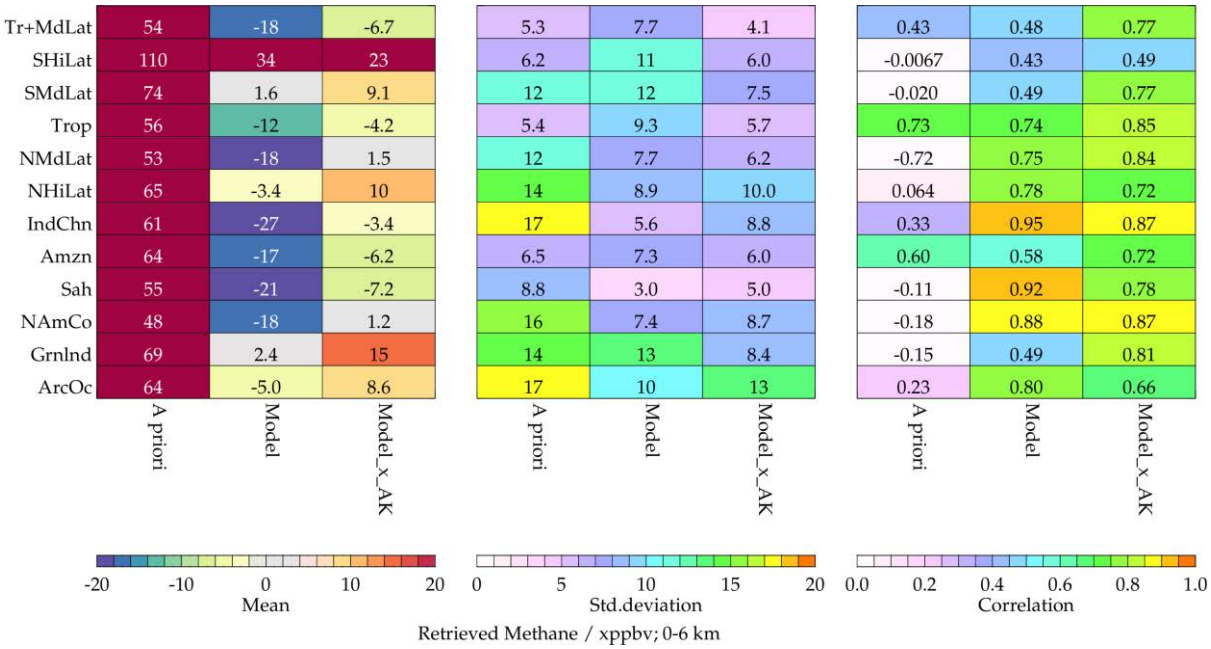

Figure 4-35 : Summary of statistics from monthly time-series comparisons of RAL Methane+ version 2 TIR and CAMS 0-6km sub-column average methane for various regions. Panels from left to right show the mean difference; standard deviation of the monthly mean differences; correlation between IASI and CAMS monthly mean values.

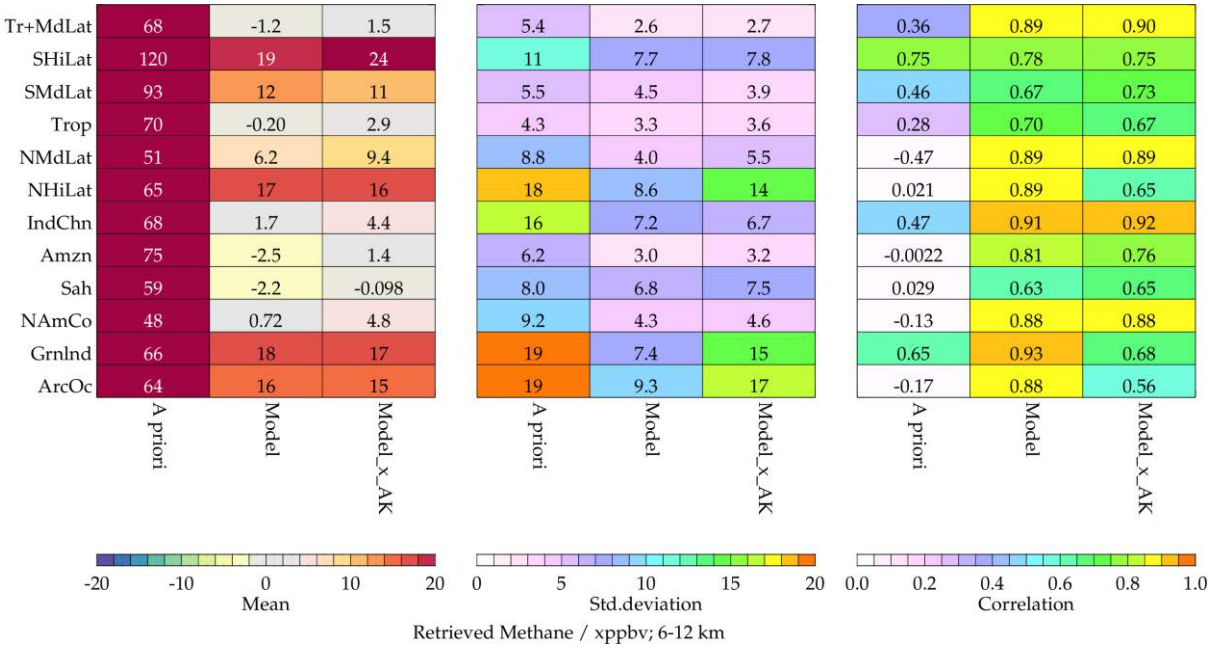

Figure 4-36 : Summary of statistics from monthly time-series comparisons of RAL Methane+ version 2 TIR and CAMS 6-12km sub-column average methane for various regions. Panels from left to right show the mean difference; standard deviation of the monthly mean differences; correlation between IASI and CAMS monthly mean values.

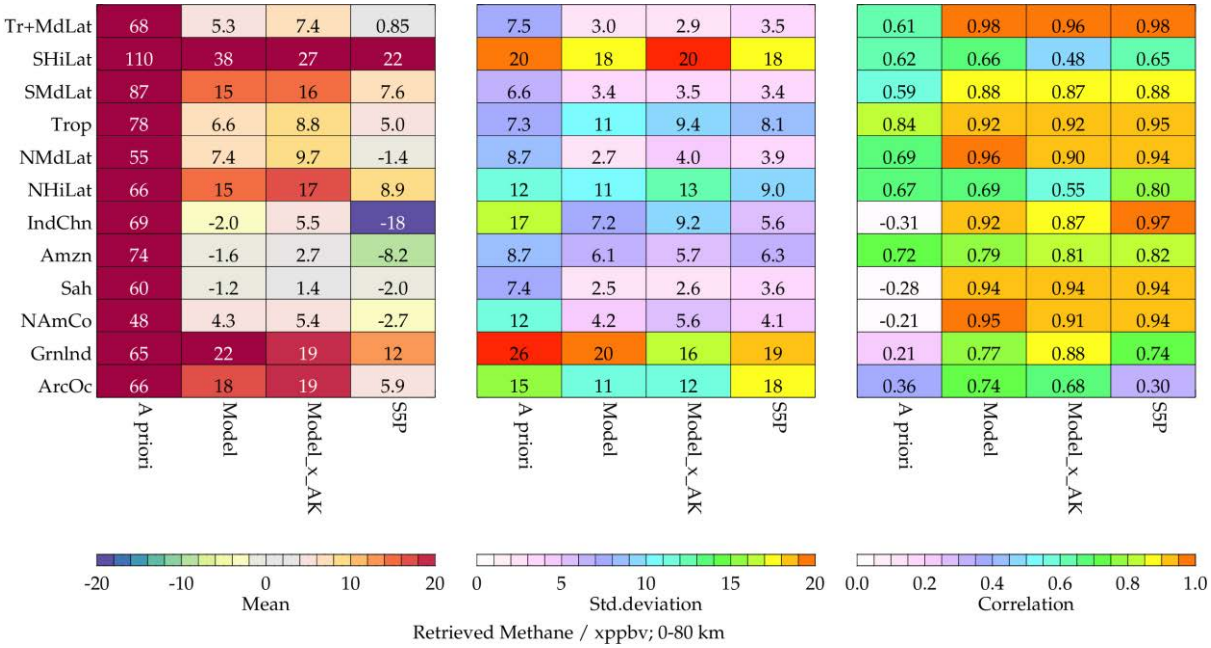

Figure 4-37 : Summary of statistics from monthly time-series comparisons of RAL Methane+ version 2 TIR column averaged methane to S5P (and CAMS sampled to S5P) for various regions. Panels from left to right show the mean difference; standard deviation of the monthly mean differences; correlation between IASI and CAMS monthly mean values.

4.3. Validation from non-satellite sources

4.3.1. Atom-4

As in section 2.3.1, the following figures are presented:

- Figure 4-38 shows the ATom-4 campaign track, together with the binned (CAMS extended) profiles and the comparison with IASI column and layer averages (with and without application of averaging kernels).
- Figure 4-39 shows differences between ATom-4 and IASI binned as a function of latitude.
- Figure 4-40 shows scatter density plots comparing ATom-4 and IASI retrievals.

These show the latitude-dependent change from V1 and V2 data in comparison to ATom-4 measurements to be consistent with that for CAMS: the mean bias moves in a positive direction for the column and layer averages, with negative bias at low latitudes being reduced. Some positive bias is introduced at higher southern latitudes in the column and layer averages, however, positive bias at high northern latitudes is introduced only in the 0-6km layer.

The scatter density plots show similar agreement (apart from bias) between V1 and V2, though most statistics (e.g. correlation) are slightly worse for V2. It should be noted however that more co-located profiles are found for V2 (reflecting changes of coverage connected to the different treatment of cloud) and the additional profiles are in more challenging retrieval conditions (e.g. high southern latitudes).

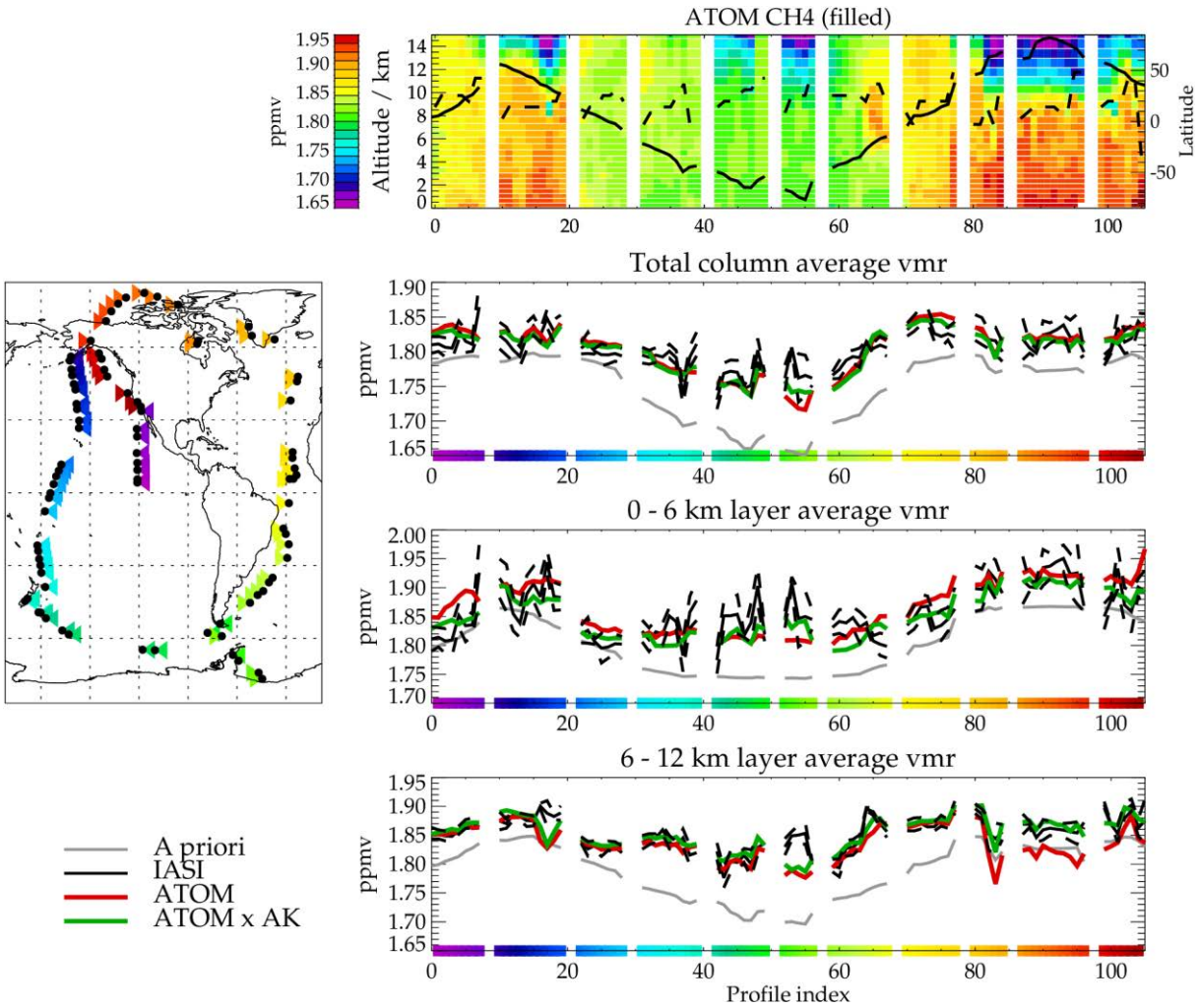

Figure 4-38 : Comparison of RAL Methane+ version 2 TIR and ATom-4 flights (24 April 2018 to 21 May 2018). Map on the left shows the flight track. Actual measurement locations are indicated with black dots; associated coloured triangles indicate the profile index, as shown on the x-axis of panels on the right (colours under the axis correspond to colours used in the map). There are 78 actual profiles in the cross-section. Some null profiles (shown white in the top panel) are inserted to mark gaps between the various flights in each campaign. The top-right panel shows the cross-section along the flight transect as measured by ATom-4, after binning and extending upwards using CAMS v19r1 flux inversion. The solid black line in this plot shows the latitude of each profile (refer to y-axis on the right). The dashed black line shows the maximum (z*) altitude of the ATom-4 measurement, above which profiles are extended with CAMS profiles. Gaps (filled with white) between the coloured regions divide data from different flights (on different days). Panels below compare IASI and ATom-4 column and layer average mixing ratios. The mean of matched IASI retrievals is shown in black. The dashed black lines show +/- the averaged standard deviation of the matched retrievals. Grey shows the IASI a priori. Red shows the ATom-4 result; Green shows ATom-4 after taking into account the IASI averaging kernel.

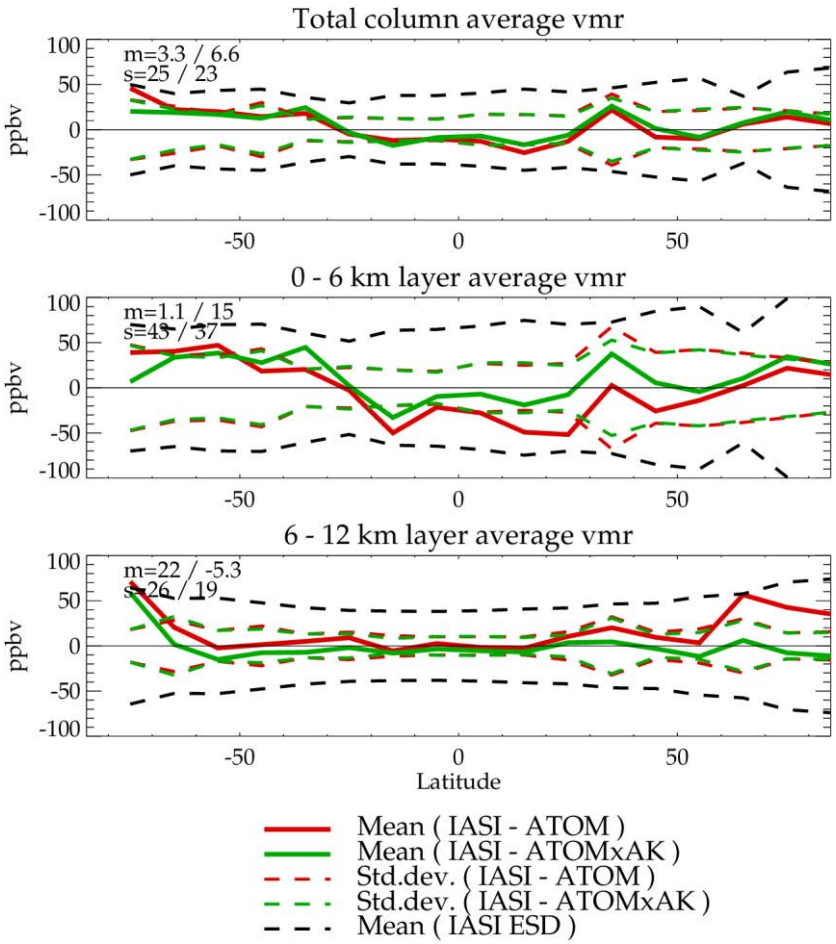

Figure 4-39 : Differences between RAL Methane+ version 2 TIR and ATom-4 binned as a function of latitude. As indicated in the legend, solid lines show the mean difference between IASI and ATom-4 (with (green) and without (red) IASI averaging kernels being applied to ATom-4 data). Corresponding dashed lines show the standard deviation of the individual IASI/ATom-4 matches about the mean difference. Black dashed lines show the mean of the IASI ESD on individual soundings. Figures in the top-left of each panel show the mean difference (m) over all matches and the standard-deviation of the individual matches about the mean without / with application of IASI averaging kernels to ATom-4 data.

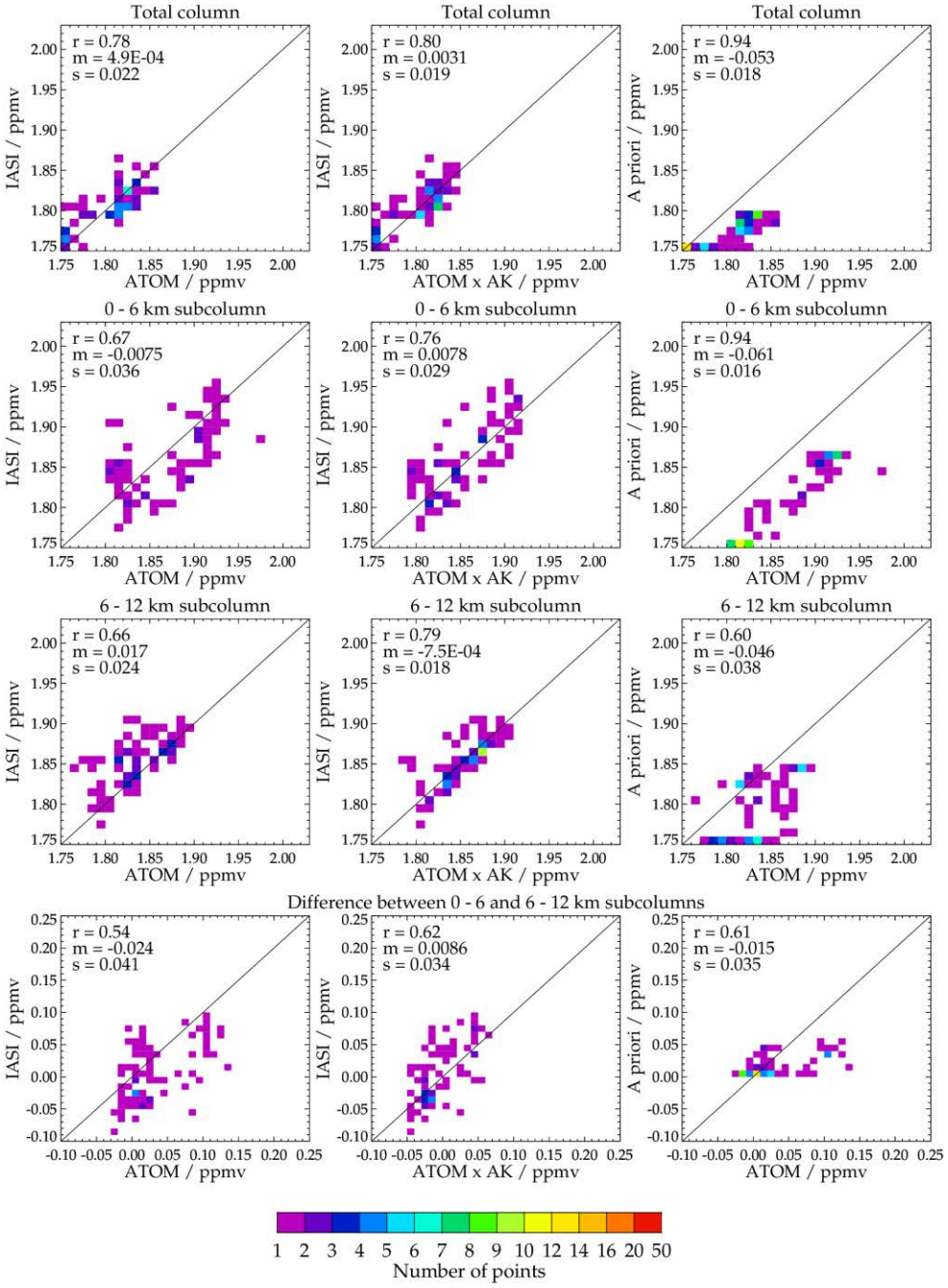

Figure 4-40 : Scatter density plots comparing ATom-4 and RAL Methane+ version 2 TIR. Columns from left to right: IASI vs ATom (left), IASI vs ATom accounting for averaging kernels (centre) and the a priori used in the retrieval vs ATom-4 (right). Rows from top-bottom show the column average, 0-6km layer, 6-12km layer and the difference between the 0-6 and 6-12km layers. The following statistics are shown within each panel: correlation coefficient (r); mean difference (m); standard deviation in the difference (s). The total number of points in each density plot is 78 (one for each profile in the previous figures).

4.3.2. AirCore

As in section 2.3.2, the following figures are presented:

- Figure 4-41 shows the mean difference between IASI and each AirCore profile, for the column average and upper/lower tropospheric layer averages.
- Figure 4-42 shows the corresponding results after application of the IASI averaging kernels to the AirCore profile.
- Figure 4-43 shows scatter plots analogous to those for ATom-4 in Figure 2-40.

Figure 4-42 and Figure 2-42 show the change in comparison with AirCore profiles between v1 and v2 data to be consistent with results for comparisons with Atom-4 and CAMS at northern mid to high latitudes. The tendency is for positive bias with respect to AirCore to increase in the column and 0-6km layer averages and negative bias in the 6-12km layer average to decrease. Correlation values in the scatter plots are slightly higher for the V2 scheme. It is also noted that the standard deviation in the mean differences for the individual air-core profiles (error bars in Figure 4-42) are mostly reduced for V2, indicating more consistent IASI retrievals in the vicinity of the AirCore profile.

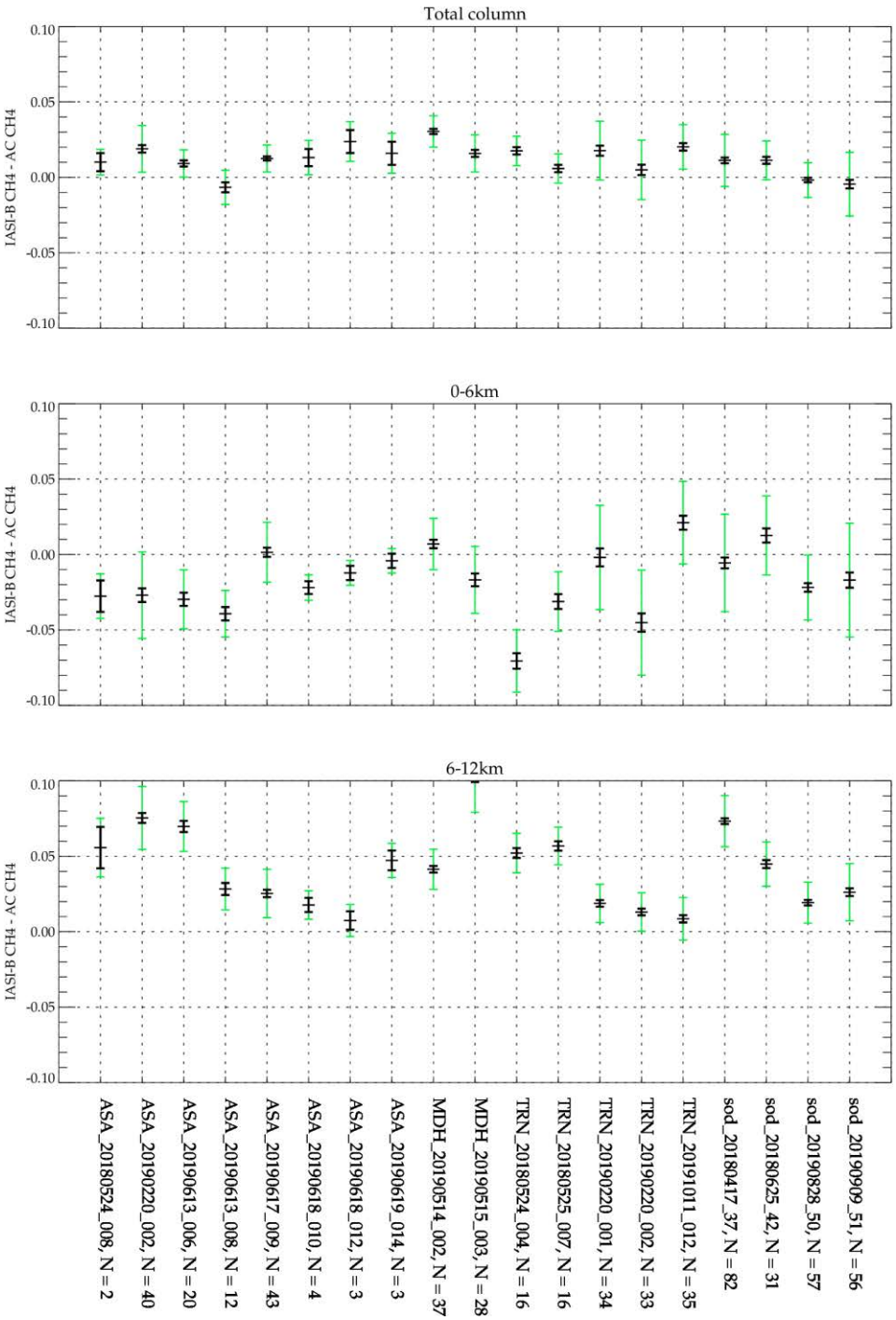

Figure 4-41 : Differences between RAL Methane+ version 2 TIR retrievals and AirCore profile measurements for (a) the column average, 0-80km, (b) the 0-6km layer average, and (c) the 6-12km layer average. The error bars represent the standard errors in the mean (black) and standard deviations (green) of IASI-AirCore differences for the set of IASI soundings co-located with each AirCore profile. Results are shown for all AirCore profiles that passed the quality control criteria.

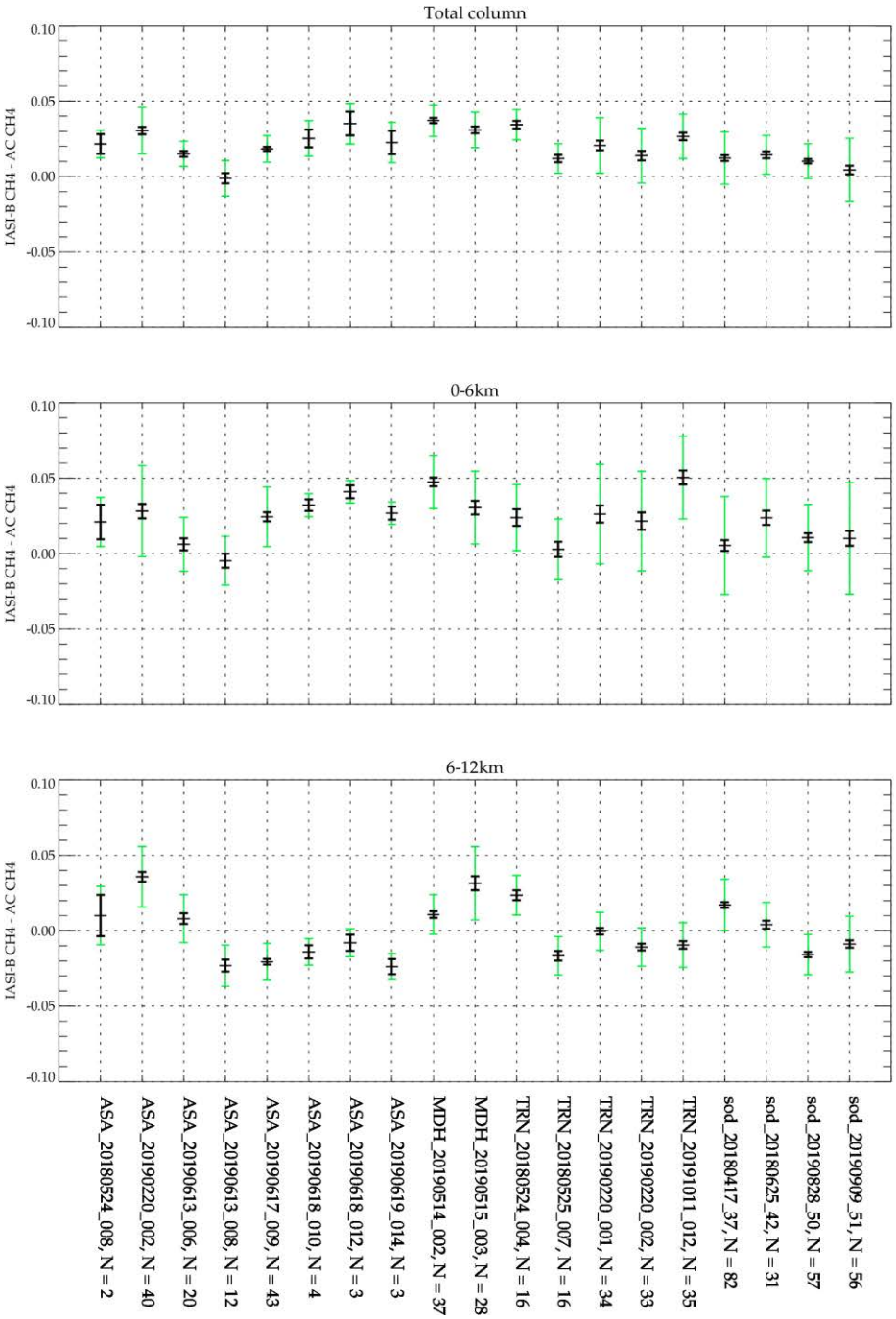

Figure 4-42 : As previous figure but with averaging kernels applied to AirCore profiles

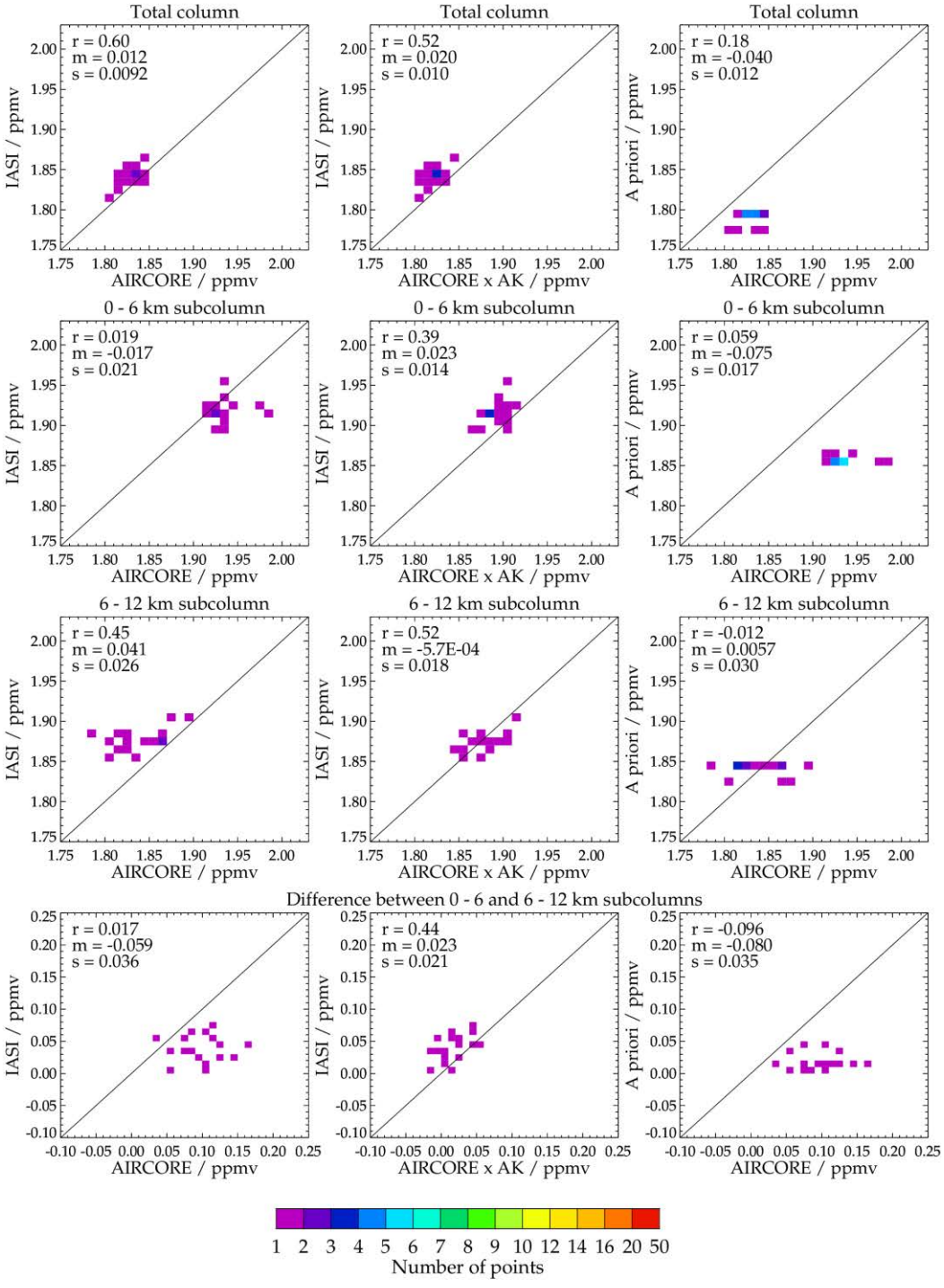

Figure 4-43 : Scatter density plots comparing AirCore and RAL Methane+ version 2 TIR. Columns from left to right: IASI vs AirCore (left), IASI vs AirCore accounting for averaging kernels (centre) and the a priori used in the retrieval vs AirCore (right). Rows from top-bottom show the column average, 0-6km layer, 6-12km layer and the difference between the 0-6 and 6-12km layers. The following statistics are shown within each panel: correlation coefficient (r); mean difference (m); standard deviation in the difference (s).

4.3.3. TCCON

As in section2.3.3, the following figures are presented:

- Figure 4-44 shows Hovmöller comparing TCCON with IASI in 2018 and 2019. These are obtained by binning co-located IASI and TCCON observations into monthly zonal mean bins.
- Figure 4-45 shows scatter plots of monthly mean co-located IASI and TCCON data collected into latitude bands (as in the Hovmoller plots).
- Figure 4-46 compares time series of co-located IASI and TCCON averaged over regions.
- Figure 4-47 summarises the statistics from the time-series.

Figures 3-38 and 2-38 show that the change between V1 and V2 data in comparison of column average with TCCON measurements is consistent at low latitudes with the changes seen for CAMS, and ATOM-4 ie the V1 negative bias is substantially reduced. However, this is not accompanied by a positive bias emerging at higher latitudes in V2 data as it does in other comparisons; particularly CAMS. This discrepancy could be related to the specific sampling of the high Northern latitudes by TCCON observations. It remains the case that the statistics for V2 are only clearly improved compared to V1 in low/mid latitude regions. The overall TCCON bias, standard deviation and correlation shown in Figure 4-45 are better for V2 than V1.

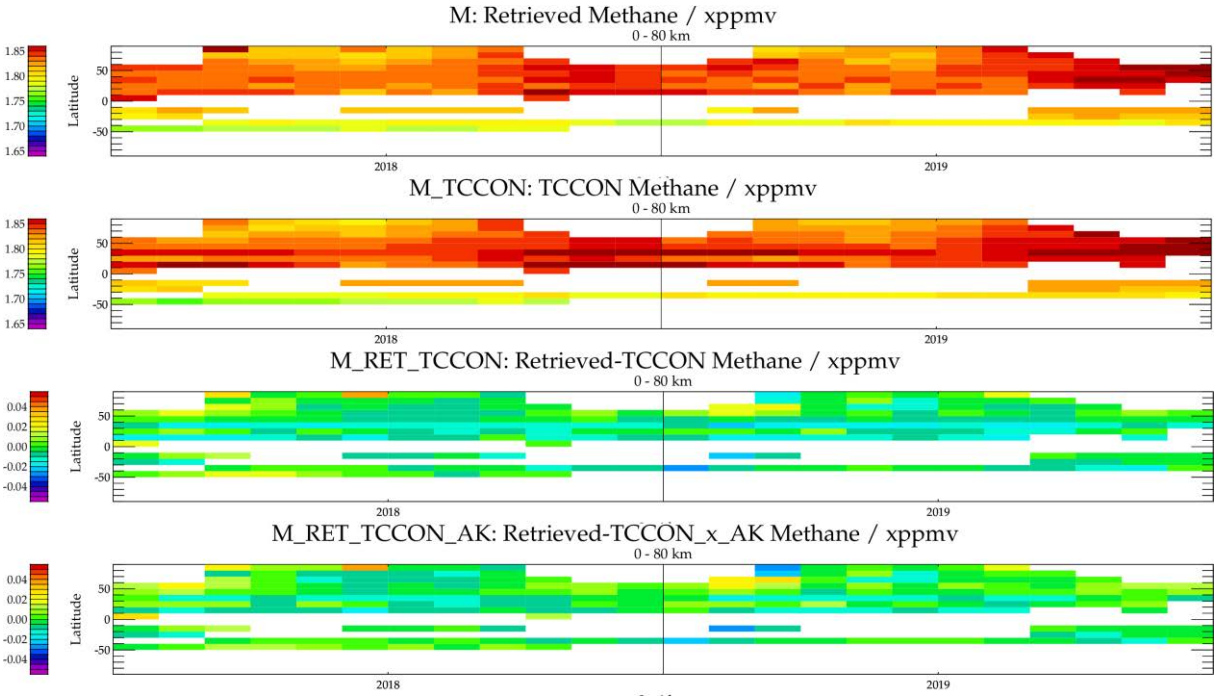

Figure 4-44 : RAL Methane+ version 2 TIR Hovmöller time-series for (a) IASI-B retrieved methane; (b) TCCON methane, measurements; (c) the difference between IASI and TCCON; (d) the difference between IASI and TCCON, adjusted to account for IASI averaging kernels using CAMS. Panels are shown for column average (0-80km) retrievals.

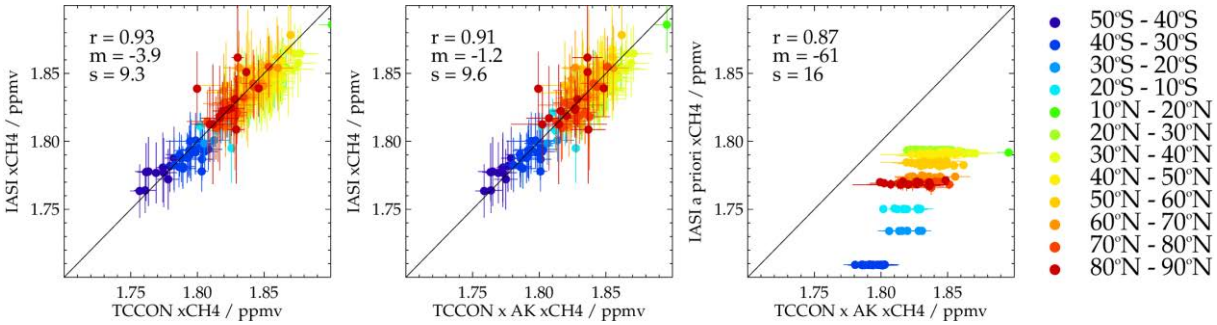

Figure 4-45 : Scatter plots comparing TCCON and RAL Methane+ version 2 TIR column-averaged mixing ratios in 2018/2019. Each point is a monthly mean with colours indicating TCCON stations in the indicated latitude range. Error bars are standard deviations of daily mean values in each average. Panels show (a) IASI retrievals vs TCCON measurements, (b) IASI retrievals vs TCCON measurements adjusted for IASI averaging kernels using CAMS and (c) IASI a priori vs TCCON. Statistics in each panel are the correlation coefficient (r), mean difference (ppbv) and standard deviation (ppbv) for the set of monthly-mean differences.

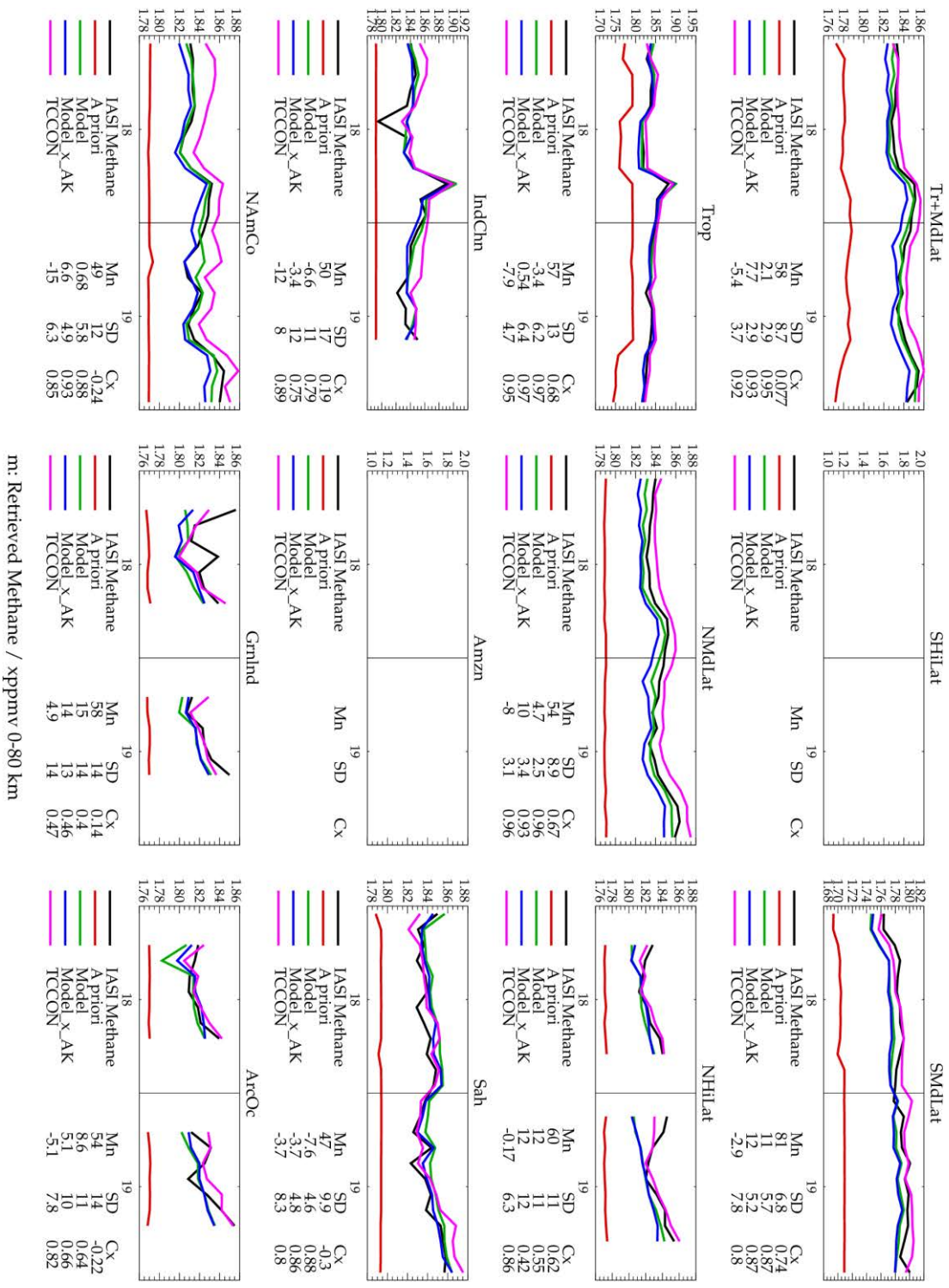

Figure 4-46 : Time series comparing RAL Methane+ version 2 TIR column averages with TCCON and CAMS sampled to TCCON for various regions. Each panel shows a different region as described in section 2.2. Statistics given in the legend under each panel give the mean difference (Mn); standard deviation of the monthly mean differences (SD); correlation between IASI and CAMS monthly mean values

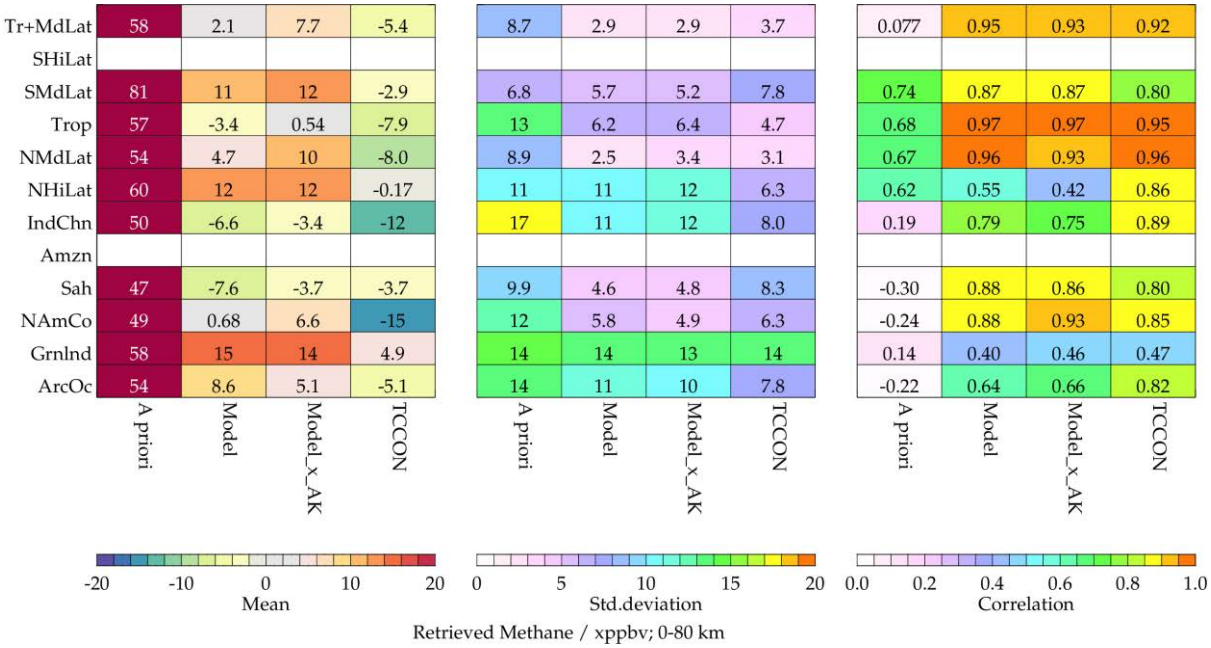

Figure 4-47 : Summary of statistics from monthly time-series comparisons of RAL Methane+ version 2 TIR column averages with TCCON and CAMS sampled to TCCON for various regions. Panels from left to right show the mean difference; standard deviation of the monthly mean differences; correlation between IASI and CAMS monthly mean values.

4.4. Discussion of RAL IASI-B Data (Methane+ Version 2)

On the basis of zonal mean biases seen in Hovmoller plots comparing with CAMS, S5P and TCCON, agreement is better for V2 than V1 data at lower latitudes and is comparable at higher latitudes. I.e. there is a generally smaller bias, with weaker latitude dependence in the V2 data, together with reduced standard deviation in zonal mean differences. Importantly, the V2 bias is also less dependent on view zenith angle. However, the V2 improvement appears less clear-cut for the ATom-4 transect and for global and regional maps comparing with CAMS. In these it seems to be confined to lower latitudes with a positive bias being introduced at higher latitudes (together with increased variability in the differences). Comparisons with AirCore, which are limited to northern mid-high latitudes, show a significant positive bias (23ppbv) to be introduced in V2 data in the 0-6km layer and column averages (compensated by a smaller bias than V1 in the 6-12km layer). AirCore correlations are slightly improved in V2, as is the spread of the individual observations compared to each AirCore profile.

It needs to be borne in mind that global and regional comparisons of V2 data with CAMS described in Section 3.1 were based on sub-sampling of IASI-B soundings (as described in the introduction). On the basis of analyses of other RAL IASI methane data, this sub-sampling is not expected to affect results significantly though.

On the basis of comparisons and validation described in Sections 3.1-3.3, the potential benefit of re-processing IASI-B to produce a fully-sampled V2 data set is somewhat dependent on the intended application. To repeat the inverse modelling trials performed by VU with the TM5 model in this Methane+ study, for example, it would be expected that the latitude v month bias corrections to be applied to IASI-B column averages would be significantly smaller for V2 at low latitudes. Another rationale to produce a full V2 data set with the current version of the RAL scheme would be that the level of consistency in column average with S5P is higher for V2, except northern high latitudes in SON and DJF. To leverage lower troposphere information through the combination of SWIR and TIR in the retrieval domain depends critically on the level of consistency between SWIR and TIR so the quality of a TIR-SWIR lower troposphere (0-6km) product would be expected to be higher if V2 data were used instead of V1.

However, comparisons and validation of V2 data reported in Section 3 point to the need for further R&D to improve the RAL TIR retrieval scheme and reduce biases beyond what has been possible in the Methane+ study, with particular consideration of the apparently degraded performance at higher latitudes. Topics identified for attention include:

- Implementation of improved spectroscopic line data which is expected to be produced by an ongoing ESA study. Improved accuracy of CH4 line parameters including line mixing is expected to: improve spectral fitting accuracy; reduce

the need to fit systematic spectral residual spectra and enable spectral coverage to be extended to strong CH4 lines to improve resolution of lower and upper troposphere and UTLS retrieval accuracy.

- Further diagnosis of specific conditions giving rise to apparent positive bias between V2 TIR retrievals and correlative data.
- Handling of marine low cloud / temperature inversions, which can lead to artefacts in continental outflow regions e.g. off Californian coast.
- Assess remaining issues leading to land-sea discontinuities which are not explained by vertical sensitivity.
- Handling of cold surfaces to improve accuracy in the Arctic, Antartica and over sea ice where photometric precision is low due to cold surface temperatures.
- Inverstigate further parameterisation of mean residual patterns (beyond dependence on view zenith and water vapour), including as a function of surface temperature or air/surface temperature contrast.

5. Validation and comparisons of SWIR-TIR data.

The scheme used to combine SWIR column averages with co-located TIR height-resolved retrievals is described in the joint scheme ATBD (RD-13). It has been applied in the Methane+ study using SRON S5P Version 18_17 data and RAL IASI-B V1 data, whose validation is detailed in Section 2. As described in the ATBD, the combination uses the total column measurement from S5P, combined with IASI sub-columns 0-6km, 6-12km 12-16km and 16km to top-of-atmosphere. Latitude and time dependent bias corrections, relative to CAMS, are applied to both S5P and the IASI products before the combination is performed. The combination is performed for S5P scenes, using the nearest co-located IASI retrieval (provided one is found within the co-location criteria defined in the ATBD). This generally results in spatial coverage similar to that of S5P, slightly reduced where no co-located IASI retrieval is found within 30km of the S5P pixel centre.

The same approaches as those used in Sections 2 and 4 have been adopted to compare SWIR-TIR outputs on column and layer averages with global and regional CAMS distributions and with correlative TCCON and AirCore measurements. Comparisons to Atom-4 are not performed as there are too few co-located measurements because Atom measurements are mainly over sea and the S5P coverage over sea is limited to scenes with sun-glint.

5.1. Global model and satellite comparisons

Comparisons to CAMS are presented in Figure 5-1 for the column average and in Figure 5-2, Figure 5-3 and Figure 5-4 for the 0-2km, 0-6km and 6-12km layer averages, respectively. The figures show the SWIR-TIR combined retrieval, CAMS+ACE (with the joint AK applied) and the difference of the joint retrieval with respect to CAMS+ACE (5^{th} row of panels). Differences with respect to CAMS+ACE are also shown for "joint" retrievals based on applying the scheme to S5P data only (4^{th} row labelled "oS5P") and to IASI data only (3d row, labelled "oIASI"). The following points should be noted:

- IASI-only or S5P-only "joint" retrievals will differ from the corresponding input data because (a) bias corrections have been applied to the input retrievals (b) the combination scheme uses a different prior constraint (though this latter effect is small); (c) the definition of the TIR-SWIR sub-columns is modified by surface pressure (see below).
- Spatial structures in the S5P-only ("oS5P") in all sub-columns will generally follow spatial structures in the S5P total column: in this case the joint retrieval will mainly scale its prior methane profile to match the total column, resulting in positively correlated spatial structure in all layers.
- For the SWIR-TIR retrieval, which is expected to have some specific near-surface information, we also examine the quality of the 0-2km layeras well as 0-

6 and 6-12km sub-columns. (Because of this there is not a one-to-one correspondence to figures in sections 2 and 4.)

- Column averages from the joint scheme are not compared directly with those from S5P since these are inputs to the scheme.
- The precise definition of the sub-columns is changed compared to those used in the validation of the TIR product. As described in the introduction to section 2, for TIR-only the sub-columns are defined in terms of surface pressure and fixed pressure levels corresponding approximately to 6 and 12 km (above sea level). However, the SWIR-TIR retrieval uses a hybrid-sigma vertical grid (which adapts to the surface pressure). Sub-columns for SWIR-TIR are fixed in hybrid-sigma levels such that they are the same as TIR-only for a surface pressure of 1000hPa, but track the actual surface pressure / altitude. This means that the "0-2km" sub-column is defined relative to the surface and is meaningful even over areas of high surface elevation.
- The co-location approach used to compare IASI retrievals to S5P in earlier sections is based on identifying a valid S5P retrieval within the IASI footprint. This is different from the approach used to co-locate retrievals in the combination scheme (which is based on the S5P spatial sampling). This can lead to some (usually minor) differences in coverage of the plots in this section compared to plots comparing IASI and S5P in sections 2 and 4.

Comparing panels showing differences from CAMS with averaging kernels applied in the 3rd row of Figure 2-1 with the corresponding panels of Figure 2-4 and Figure 5-1, it can be seen that global distributions of column averages from IASI-B when propagated through the SWIR-TIR scheme differ significantly from the IASI-B v1 data themselves and from IASI-B v1 sampled as S5P. This is mainly a consequence of the bias correction which has been applied (indeed the amplitude of a simple latitude dependent component to the differences is reduced).

An important point to note from Figure 5-1 and Figure 5-4 is that output from the combined scheme when inputting both IASI-B and S5P information follows that from inputting S5P only in the column average and that from IASI-B only in the 6-12km layer average, reflecting their respective vertical sensitivities and therefore as expected. Figure 5-3, on the other hand, shows that output from the combined scheme in the 0-6km layer does not simply follow that from either S5P only or IASI-B only so is affected by both.

The 0-2km layer from the SWIR-TIR combination is shown in Figure 5-2. This vertical layer is important as it is situated closest to surface emission sources but constitutes only a small fraction (~20%) of the total atmospheric column. The estimated standard deviations on individual soundings seen for the 0-2km layer (5th row) are seen to be correspondingly larger than those for the column average and 0-6km layer; typically around 80-100ppbv compared to <10ppbv for the column average and 20-35ppbv for the 0-6km layer. Deviations from CAMS with averaging kernels applied are seen in the 4th row of Figure 5-2 to fall within the ±100 ppbv range. Geographical variation in

the CAMS 0-2km is in the range ~1800-2000 ppbv, so there is consistency at the ~5% level in this first application of the SWIR-TIR scheme.

Figure 5-5 and Figure 5-6 show the time-series of monthly zonal mean methane column and layer averages as Hovmöller plots. Comparison of Hovmoller plots with those for V1 shows latitudinal structure in the deviation from CAMS with averaging kernels applied to be less pronounced for SWIR-TIR than TIR v1, as expected. For the 0-6km layer average, latitudinal structure in the deviation is also flatter at low and mid-latitudes for SWIR-TIR than for TIR v1.

The 0-2km layer in Figure 5-6 shows zonal mean deviations from CAMS with averaging kernels applied to be in the ± 50ppbv range and there to be some coherence in structure between the two years, with peak positive deviations occurring around 40N and 40S in spring. The zonal mean standard deviation indicates variability which is comparable to that predicted by the ESD, however it is clear from the maps that deviations are not only related to random noise, but occur also in coherent regions, particularly over land, to some extent where enhancements from emissions are also seen in CAMS. However, these enhancements are generally much larger in the joint retrieval for 0-2km than in CAMS. The magnitudes of these enhancements are much more comparable with CAMS in the 0-6km layer average.

.

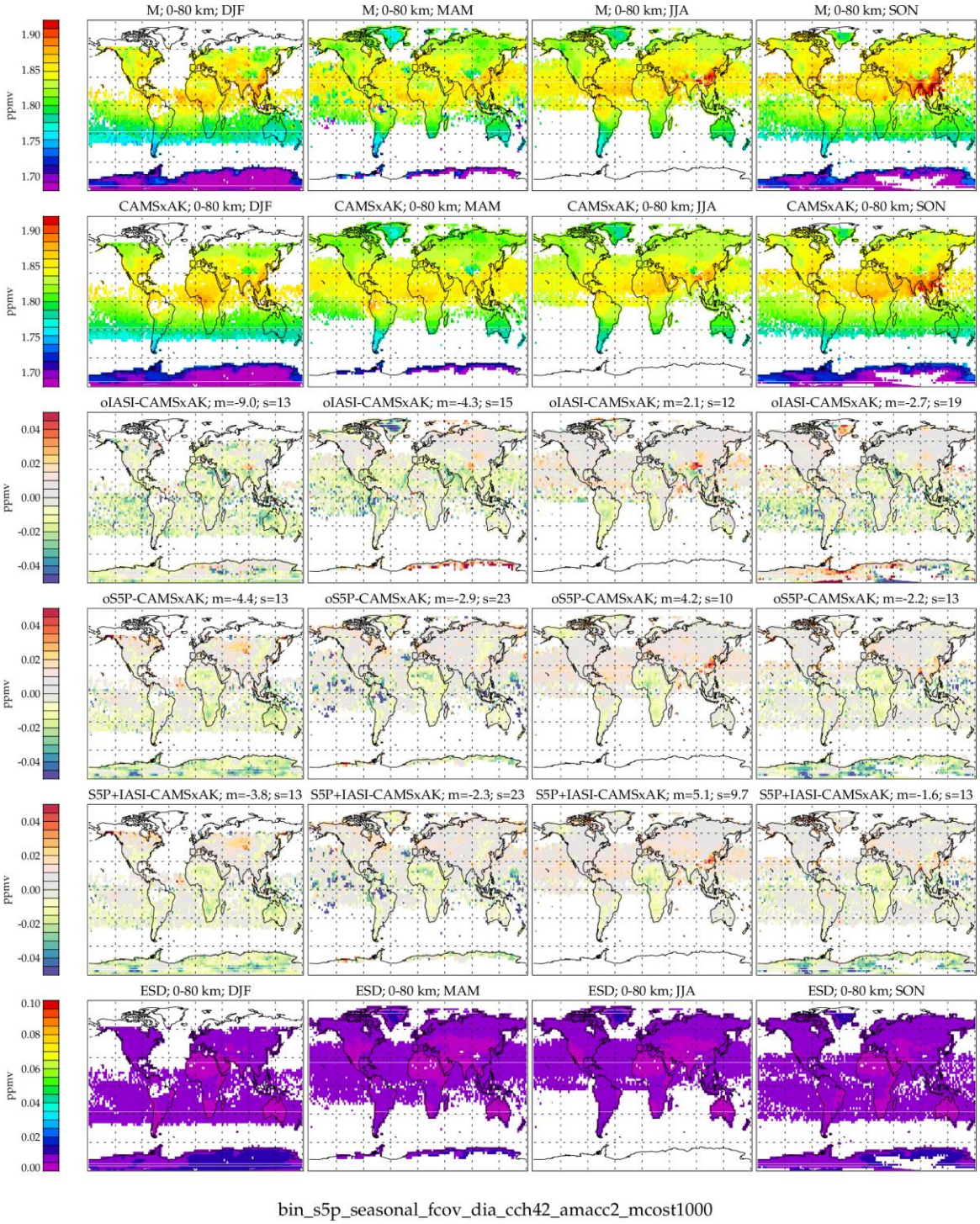

Figure 5-1 : SWIR+TIR global daytime column average retrievals: columns show results for different seasons (2018 and 2019 combined). Rows from top-bottom show, respectively, results from IASI retrievals; Combined retrieval; CAMS with averaging kernels applied (CAMSxAK); the difference between IASI and CAMSxAK; the mean of the estimated standard deviation (ESD) on the IASI retrieval; In panels showing differences, the mean ("m") and standard deviation ("s") of the binned data are given, in ppbv, in the panel title.

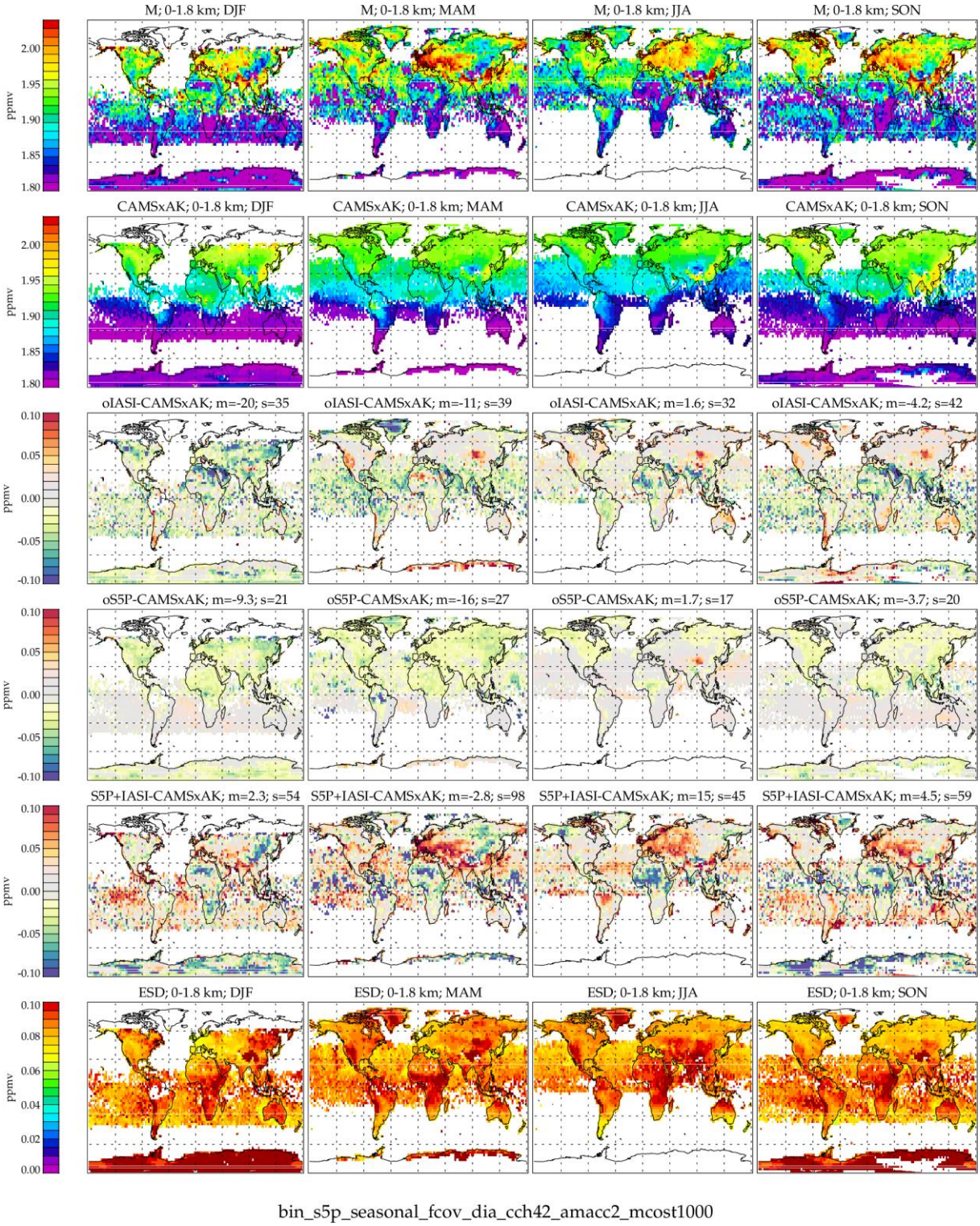

Figure 5-2 : SWIR+TIR global daytime retrievals for the 0-2km layer average.

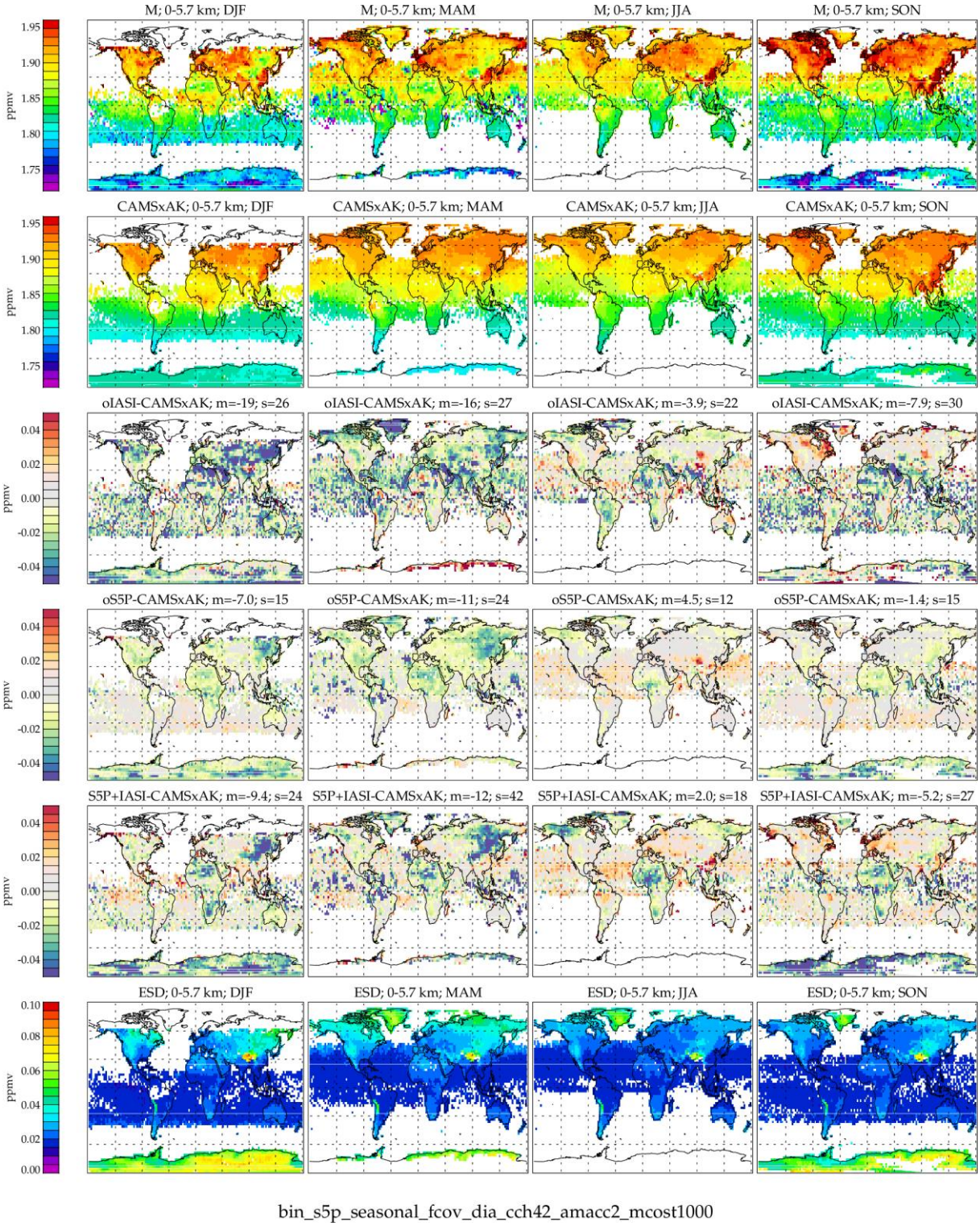

Figure 5-3 : SWIR+TIR global daytime retrievals for the 0-6km layer average.

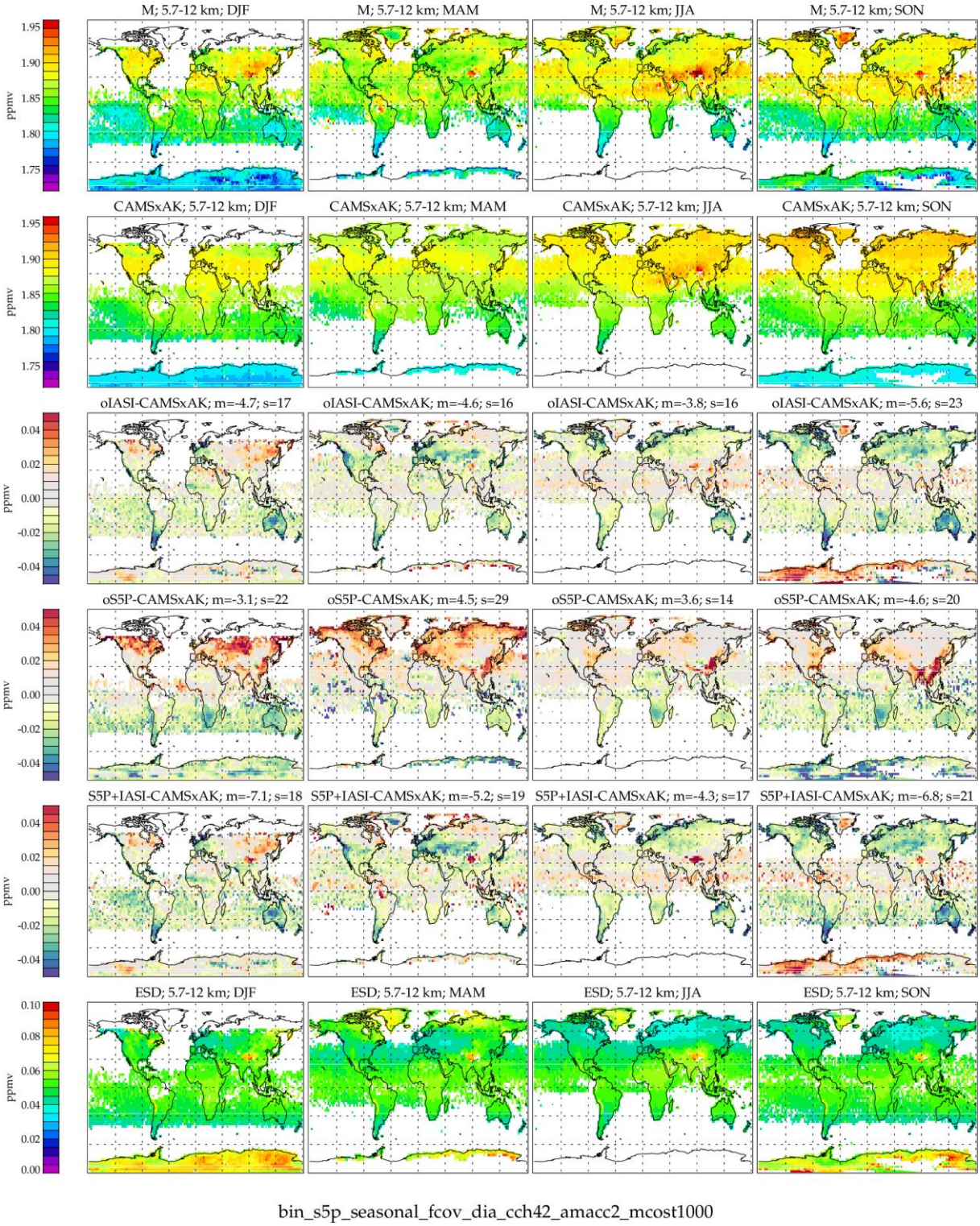

Figure 5-4 : SWIR+TIR global daytime retrievals for the 6-12km layer average.

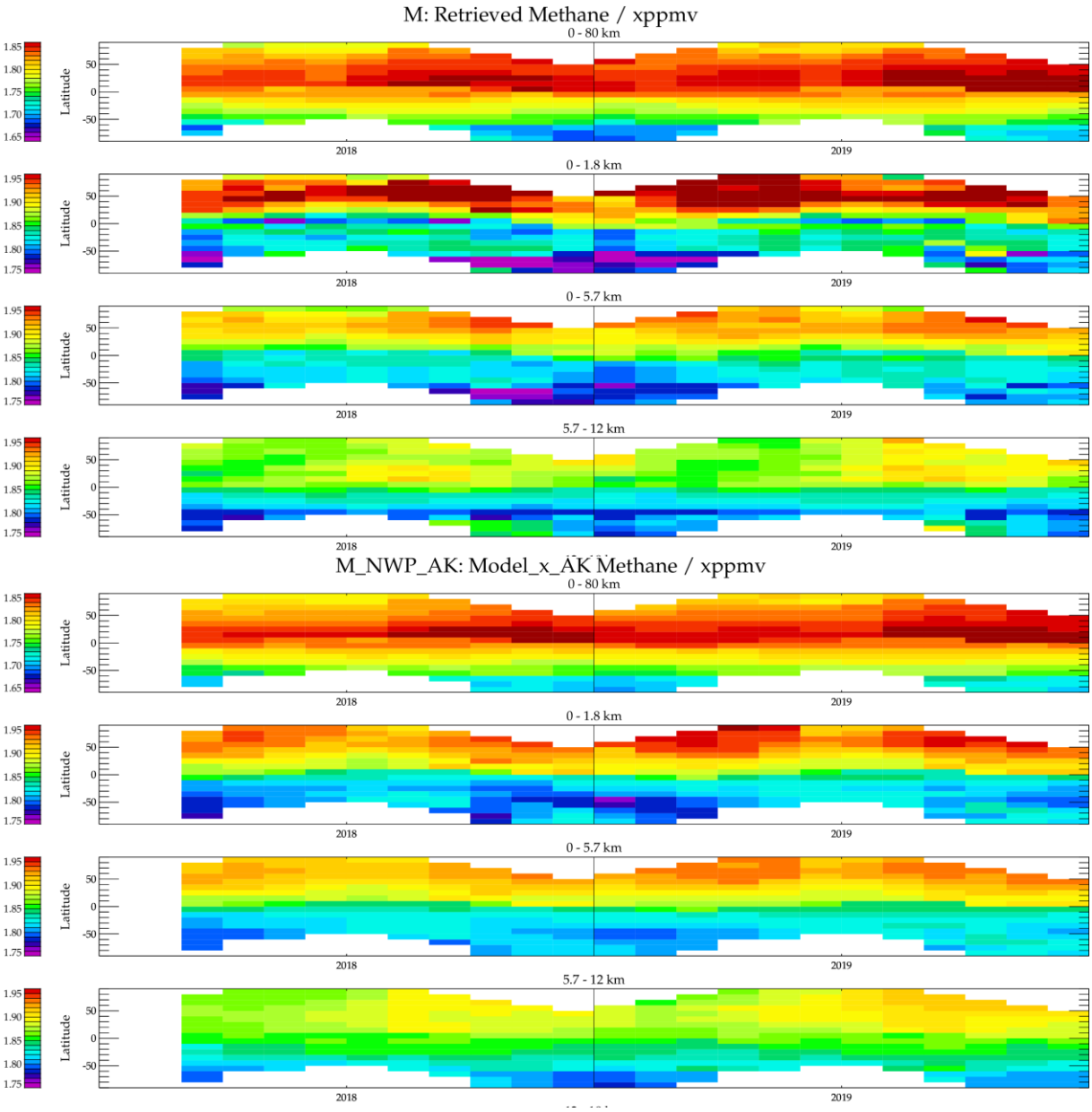

Figure 5-5 : SWIR+TIR Hovmöller time-series for (a) IASI-B retrieved methane and (b) CAMS v19r1 methane flux inversion with IASI averaging kernels applied. Panels are shown for the column average (0-80km), 0-2km, 0-6km and 6-12km layer averages.

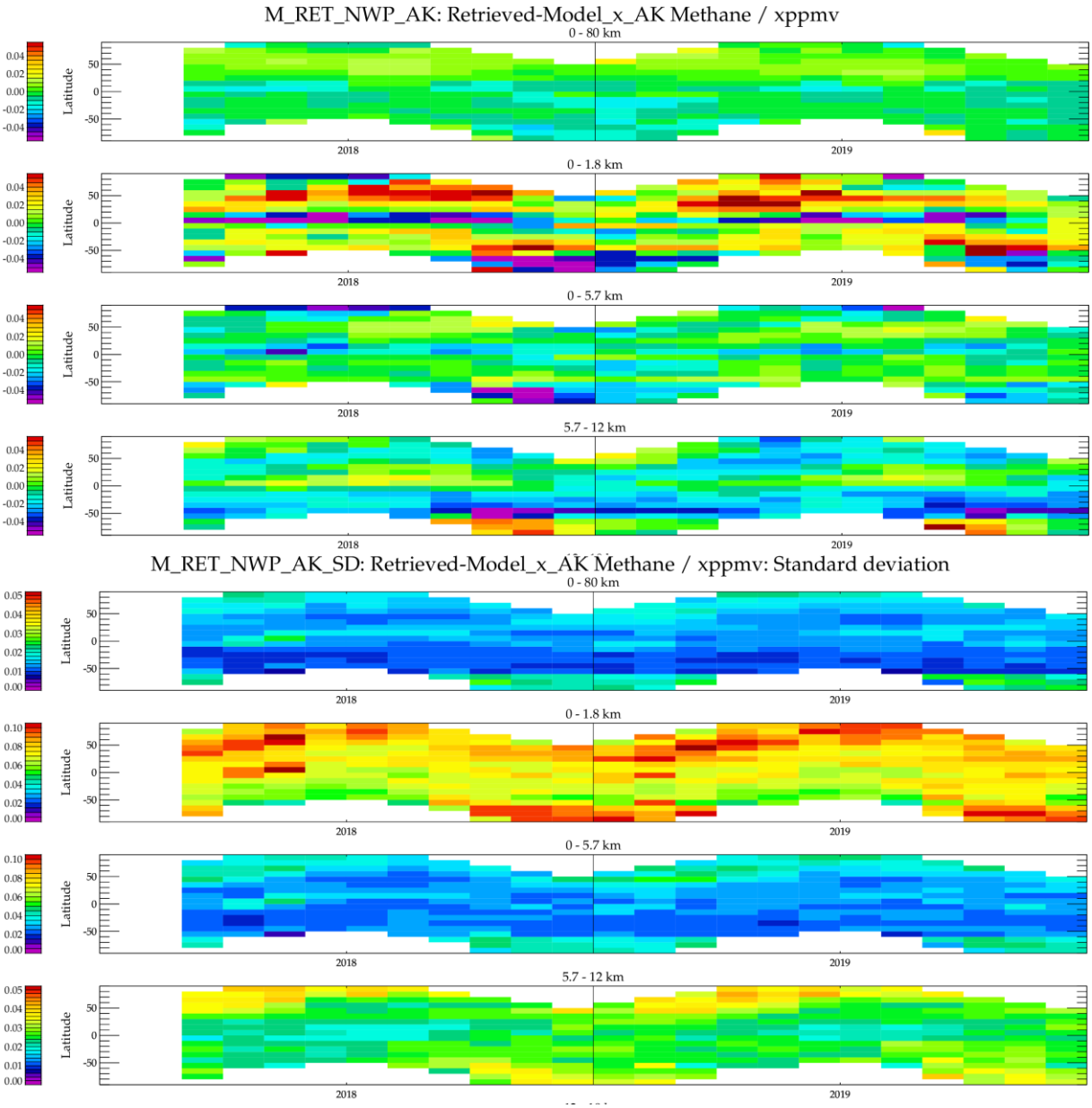

Figure 5-6 : SWIR+TIR Hovmöller time-series for (a) the mean difference between IASI and CAMS and (b) the standard deviation in the mean difference. Panels are shown for the column average (0-80km), 0-2km, 0-6km and 6-12km layer averages.

5.2. Model and satellite comparisons over target regions

In this section maps of the SWIR-TIR retrievals are presented focusing on regions of particular interest. A similar set of figures to those in sections 2.2 and 4.2 are shown:

- Comparisons to CAMS are presented as maps (0.5x0.5 degree gridded seasonal averages) in Figure 5-7 to Figure 5-26. For each region (A-E as in the table), figures compare the combined scheme (sub-)column averages to CAMS.
- Figure 5-27 contains a summary of the statistics derived from the previous figures for each region.
- Time-series comparisons for the 2 years are shown as line plots in Figure 5-28 (column average vs CAMS), Figure 5-29 (0-2km layer average vs CAMS), Figure 5-30 (0-6km layer average vs CAMS) and Figure 5-31 (6-12km layer average vs CAMS).
- Figure 5-32 to Figure 5-35 summarise statistics derived from the time-series plots.

In these regional plots, as in global plots, column average distributions from the SWIR-TIR combination can be seen to closely resemble those from S5P-only being input to the SWIR-TIR scheme whereas 6-12km layer distributions resemble those from IASI-B-only being input.

Comparing the summary statistics for total column in Figure 5-27 with those for the IASI V1 compared to CAMS at S5P sampling (in Figure 2-29), there is a strong improvement in bias and slight general improvement in standard deviation (except in spring) for the joint retrieval, presumably reflecting better agreement of S5P total column with CAMS. Bias is also improved in the 0-6 and 6-12km layers compared to the IASI/CAMS comparison in Figure 2-28, however standard deviations are mostly increased, particularly in spring. The increase in these spatial standard deviations in the seasonal mean could be caused by the more sparse sampling of the joint retrieval compared to IASI (i.e. the spatial standard deviations are reduced by averaging over many more samples in Figure 2-28). These standard deviations could also be increased by real spatially structured differences detected by S5P (filtered by the IASI averaging kernel in Figure 2-28). The spatial standard deviations are generally small compared to the estimated standard deviation.

Figure 5-7 to Figure 5-10 (SE Asia) shows that the joint retrieval produces particularly high mixing ratios in the 0-2km layer where positive anomalies, likely related to surface emission, are found in the S5P total column. These are generally not reflected in the 6-12km layer, and are seen with reduced amplitude in the 0-6km layer. This is qualitatively consistent with near-surface emissions being distributed vertically, however the amplitudes of the positive anomalies are much larger than CAMS in the 0-2km layer. The 6-12km layer shows a positive bias over the Himalayan plateau

(reflecting a similar bias in IASI), though should be noted that this coincides with particularly large ESD.

Figure 5-11 to Figure 5-14 (South America) shows sparse sampling over the Amazon caused by cloud screening of S5P observations. The joint retrieval emphases a positive anomaly in S5P compared to CAMS in the southern part of the region, leading to stronger positive anomalies in the 0-2 and 0-6km layers.

Figure 5-15 to Figure 5-18 (Sahara) shows structure over the desert which is probably mainly driven by artefacts in the IASI retrieval. (It can be anticipated that these features would be considerably reduced if the V2 IASI data was used for the joint retrieval.) In the South-East of the domain there is a strong positive anomaly in S5P data, over the Sudd wetlands. This is realistically reflected in large mixing ratios in the 0-2 and 0-6km layers, and is not apparent in the 6-12km layer.

Figure 5-19 to Figure 5-22 (West coast America) show a near-surface feature over Central Valley California, stronger in the joint retrieval than predicted by CAMS. Structure over the sea is somewhat incoherent due to sampling limitations.

Figure 5-23 to Figure 5-26 (Northern high latitudes) show weak positive anomalies (up to 20ppb) in S5P total column compared to CAMS are reflected in much stronger anomalies in the 0-2km layer (~80ppb). Anomalies with respect to CAMS have quite different spatial distributions in the 0-6km layer. There is relatively little spatial variation in the 6-12km layer, except over Greenland (where ESD is relatively large and retrieval artefacts related to ice / cold surface / surface altitude are plausible).

Time-series comparisons for the 2 years and derived statistics (Figure 5-32) show general improvements in total column bias, standard deviation and correlation compared to CAMS (reflecting the good agreement of S5P total column with CAMS). Bias is improved in other layer (as might be expected following bias correction). Standard deviations in the 0-6 (Figure 5-34 cf Figure 2-35) and 6-12km (Figure 5-35 cf Figure 2-36) layers are in the range 4-20 ppb, comparable to those of TIR V1 (worse in some regions, better in others) though a direct comparison is difficult due to the reduced sampling of the joint retrieval compared to the v1 TIR data. Standard deviations are substantially larger in the 0-2km layer (10-30ppb excluding Greenland).

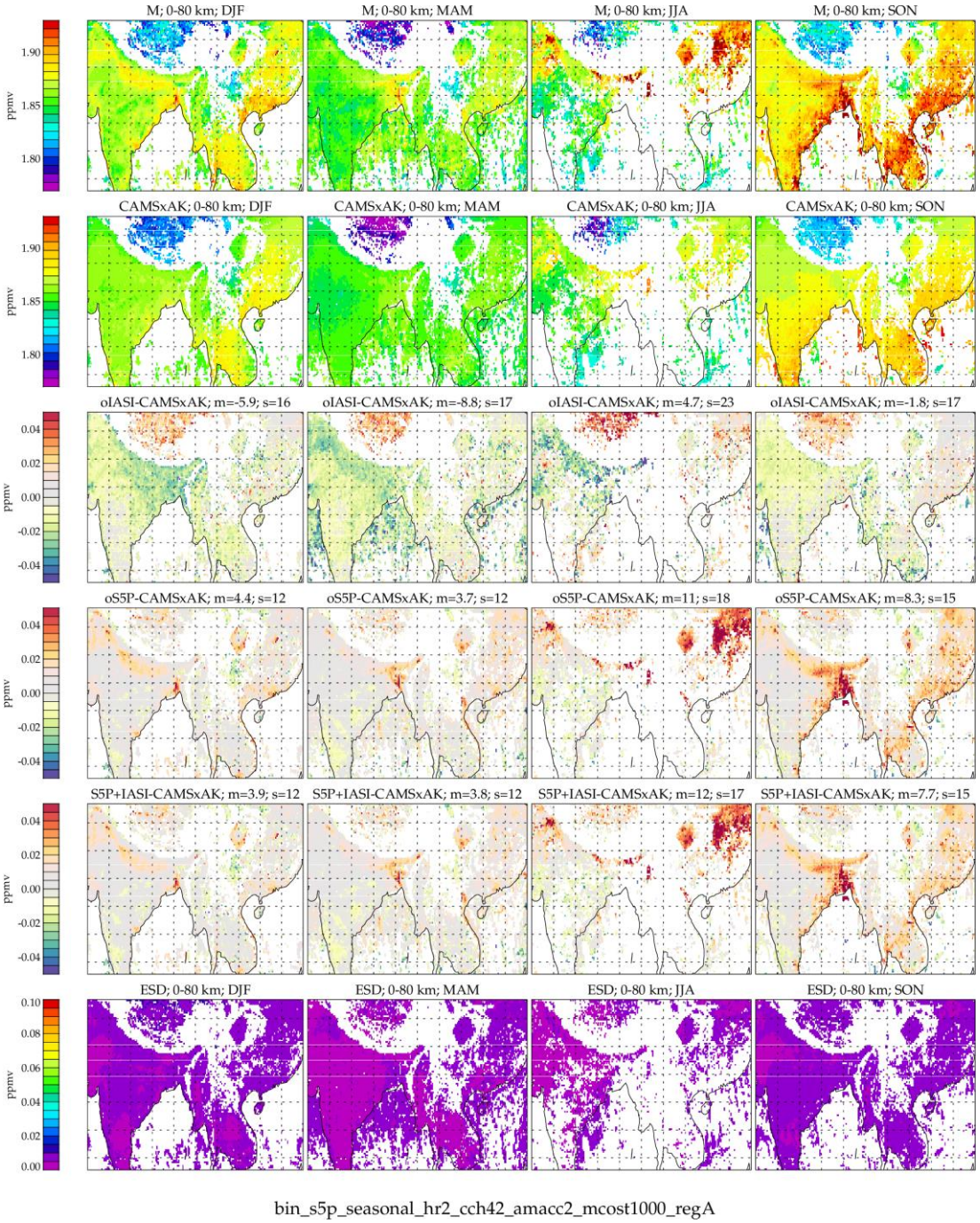

Figure 5-7 : SWIR+TIR global daytime column average retrievals for region A: Each column of the figure shows results for a different season (2018 and 2019 combined). Rows from top-bottom show, respectively, the combined retrieval; CAMS with averaging kernels applied (CAMSxAK); difference from CAMSxAK of "joint" results when only IASI is used; differences from CAMSxAK of "joint" results when only S5P is used; differences from CAMSxAK of joint IASI+S5P results; estimated standard deviation (ESD) of the joint IASI+S5P retrieval. In panels showing differences, the mean ("m") and standard deviation ("s") of the binned data are given, in ppbv, in the panel title.

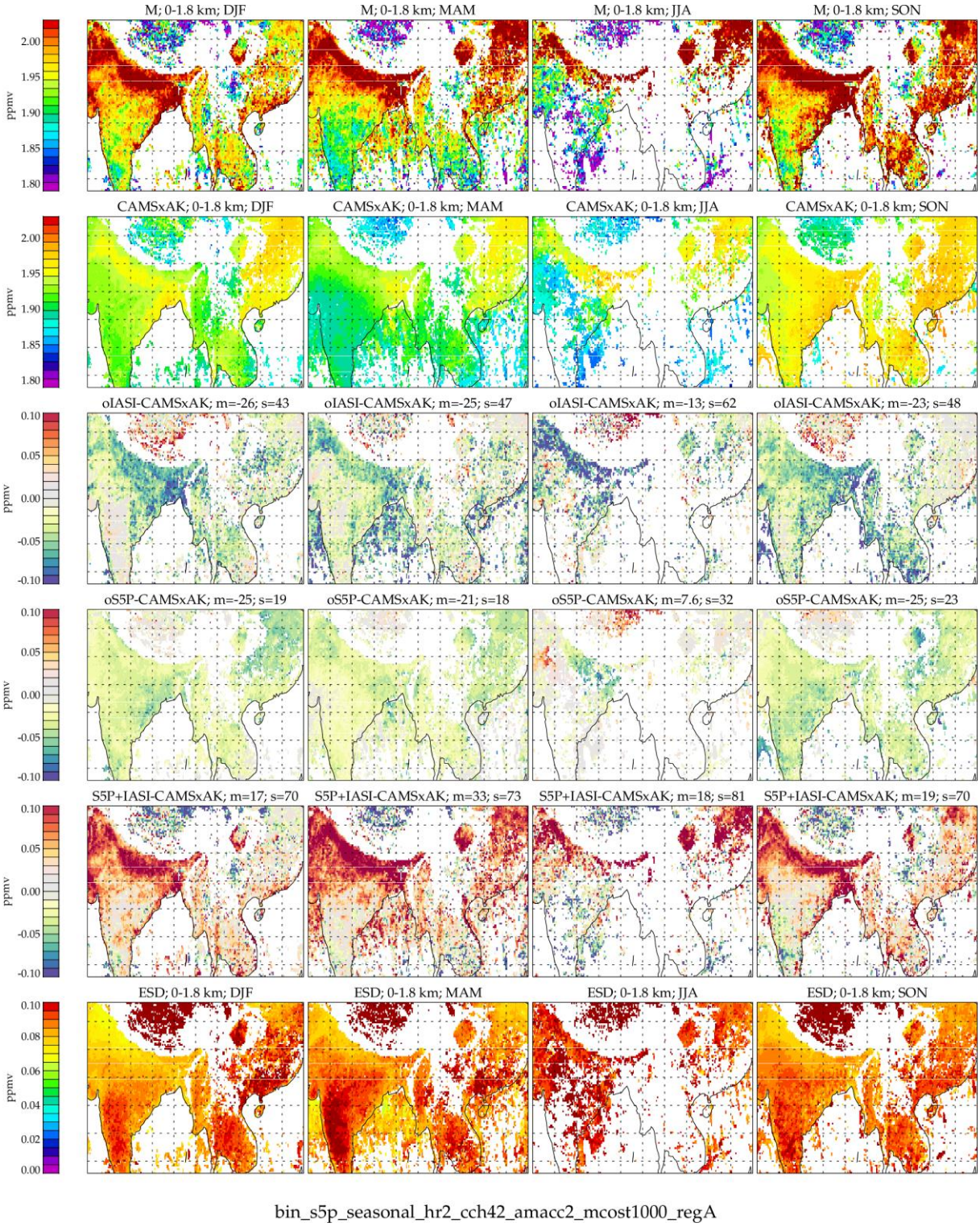

Figure 5-8 : SWIR+TIR daytime 0-2km layer average retrievals over target region A.

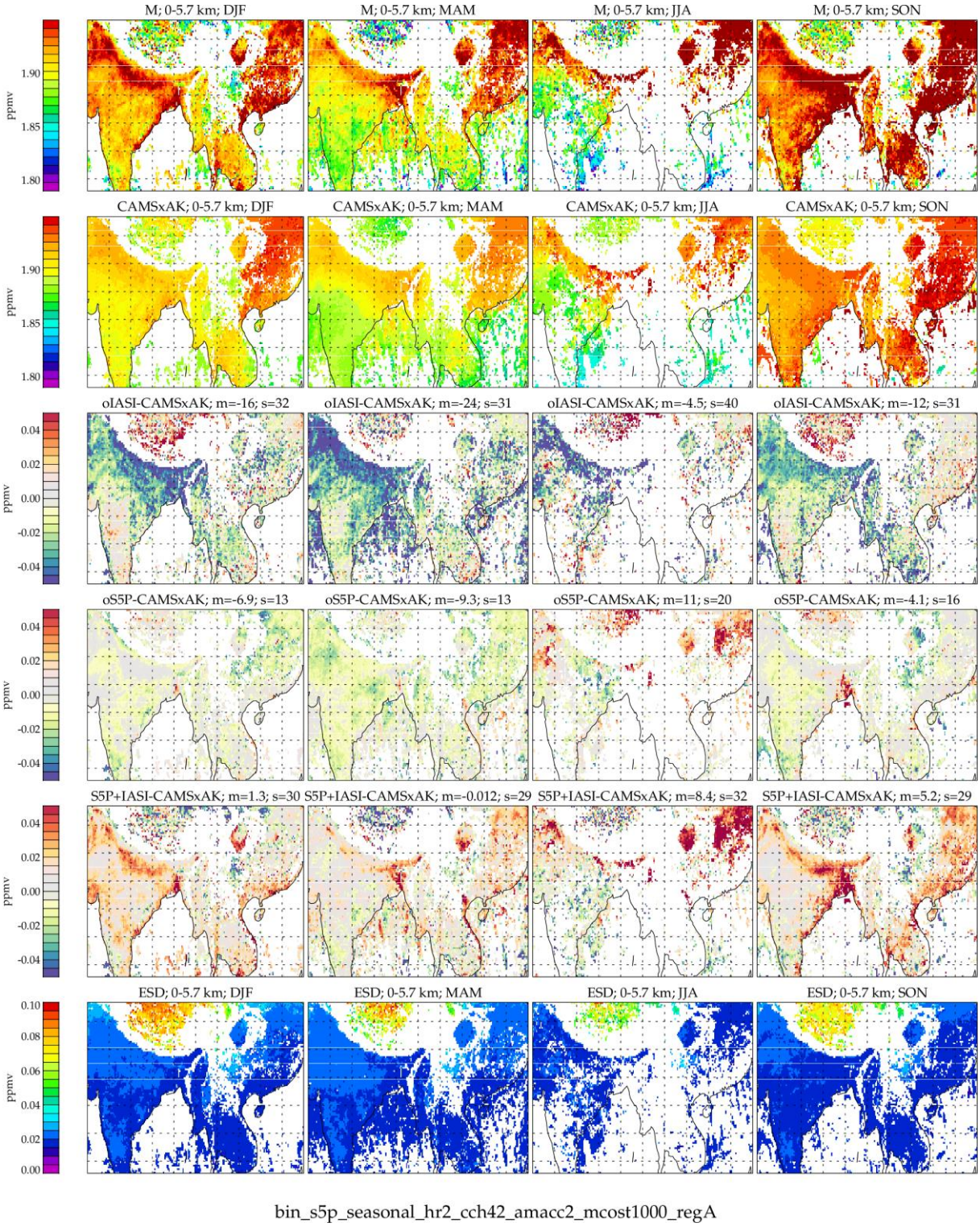

Figure 5-9 : SWIR+TIR daytime 0-6km layer average retrievals over target region A.

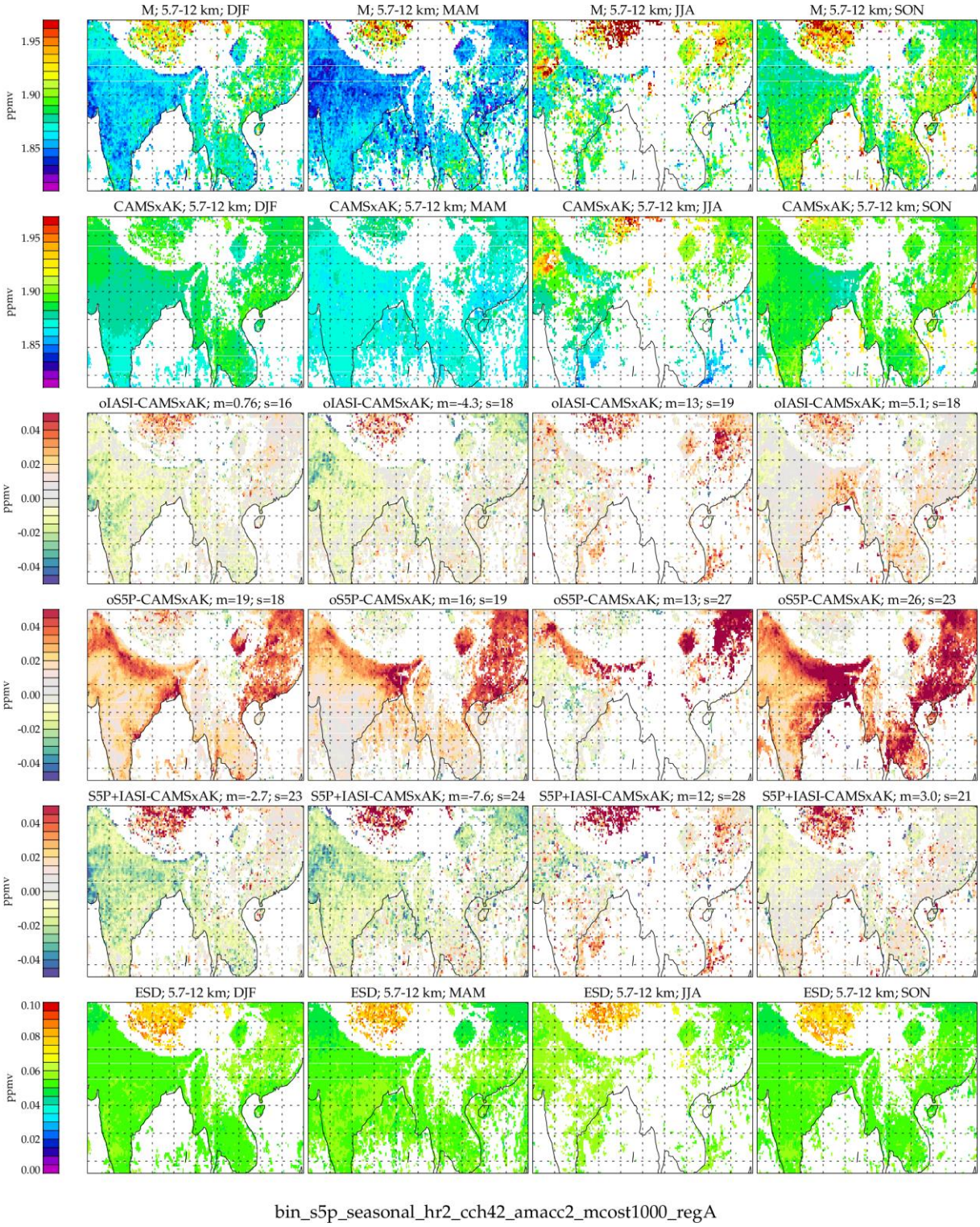

Figure 5-10 : SWIR+TIR daytime 6-12km layer average retrievals over target region A.

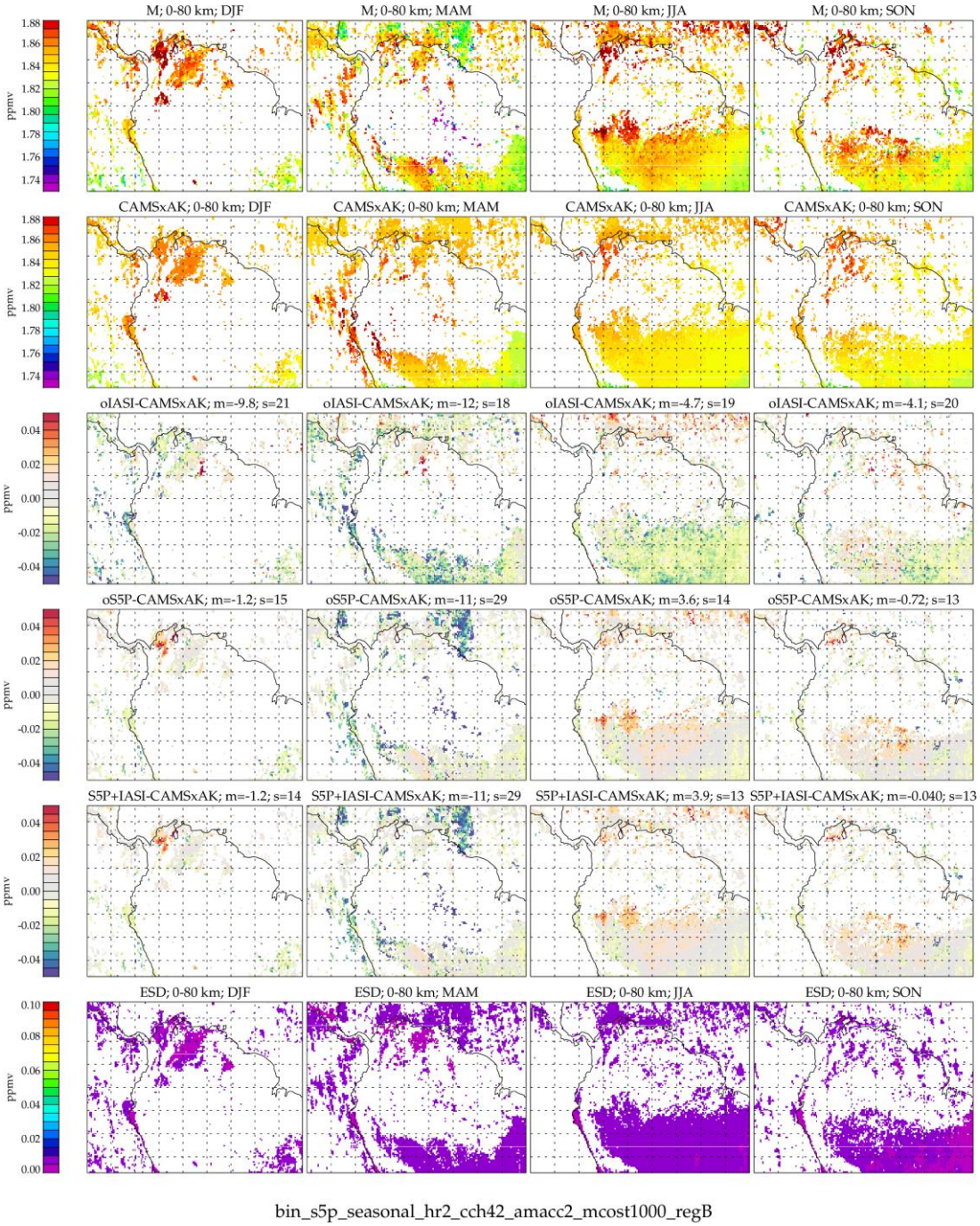

Figure 5-11 : SWIR+TIR global daytime column average retrievals for region B: Each column of the figure shows results for a different season (2018 and 2019 combined). Rows from top-bottom show, respectively, the combined retrieval, CAMS with averaging kernels applied (CAMSxAK); difference from CAMSxAK of "joint" results when only IASI is used; differences from CAMSxAK of "joint" results when only S5P is used; differences from CAMSxAK of joint IASI+S5P results; estimated standard deviation (ESD) of the joint IASI+S5P retrieval. In panels showing differences, the mean ("m") and standard deviation ("s") of the binned data are given, in ppbv, in the panel title.

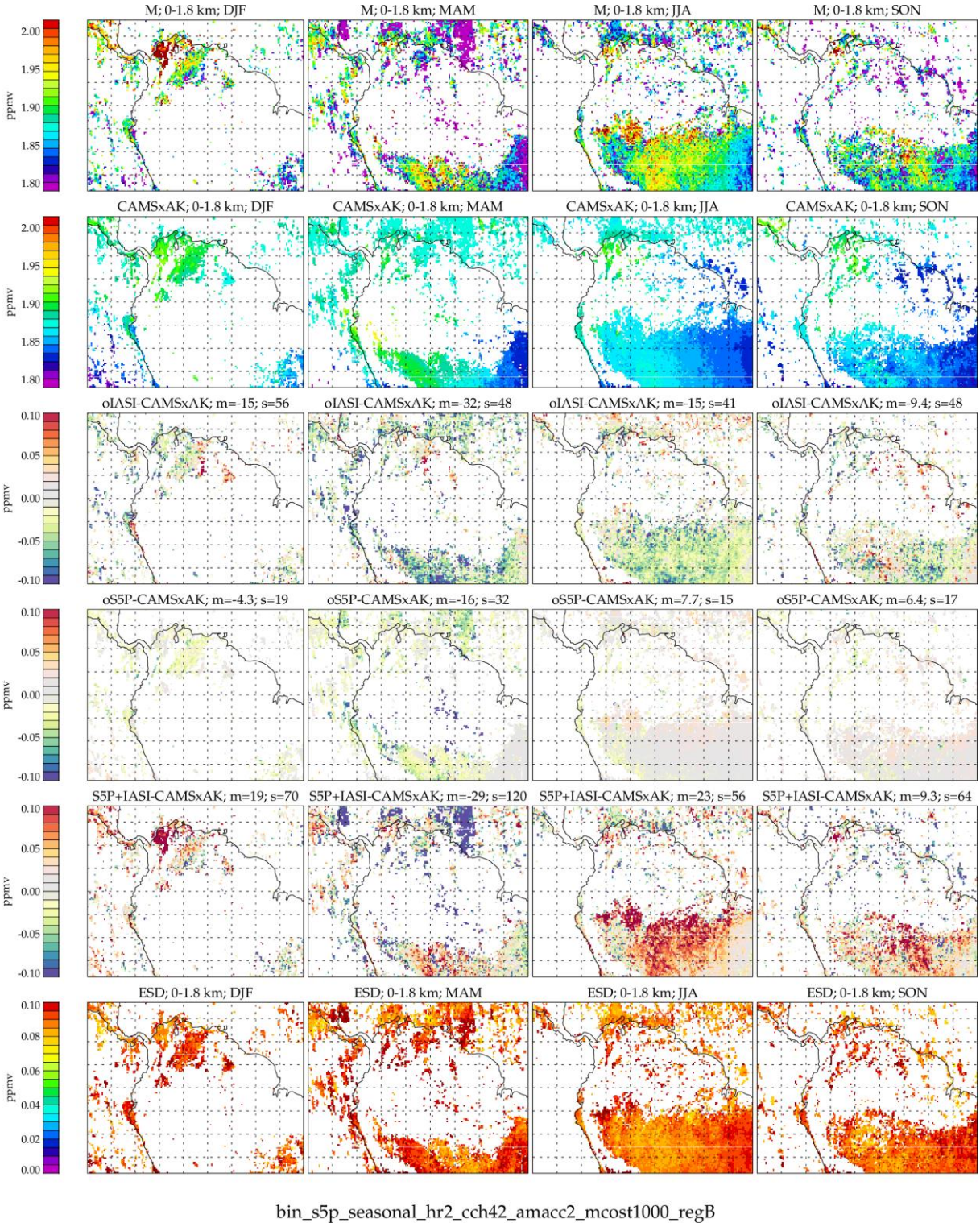

Figure 5-12 : SWIR+TIR daytime 0-2km layer average retrievals over target region B.

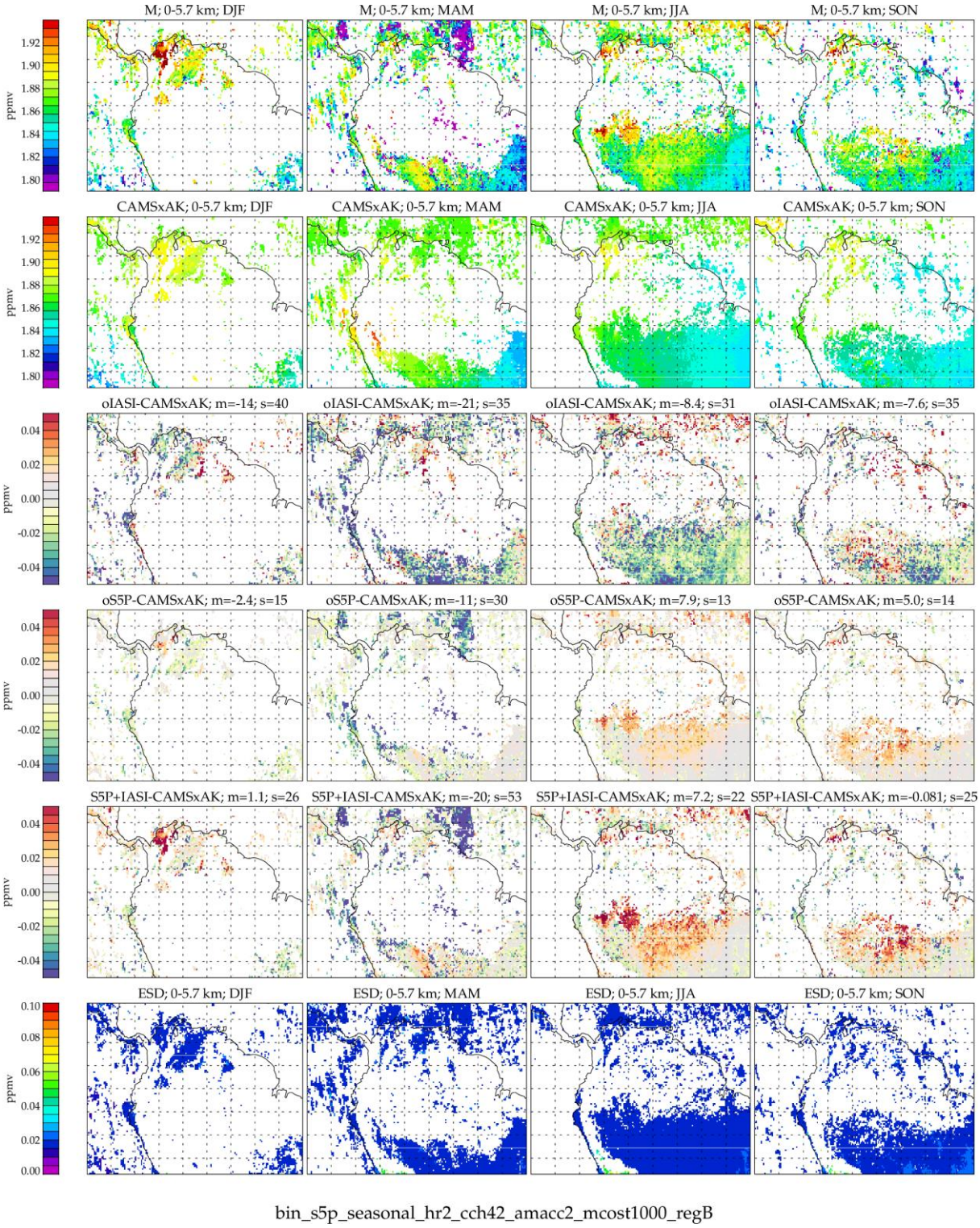

Figure 5-13 : SWIR+TIR daytime 0-6km layer average retrievals over target region B.

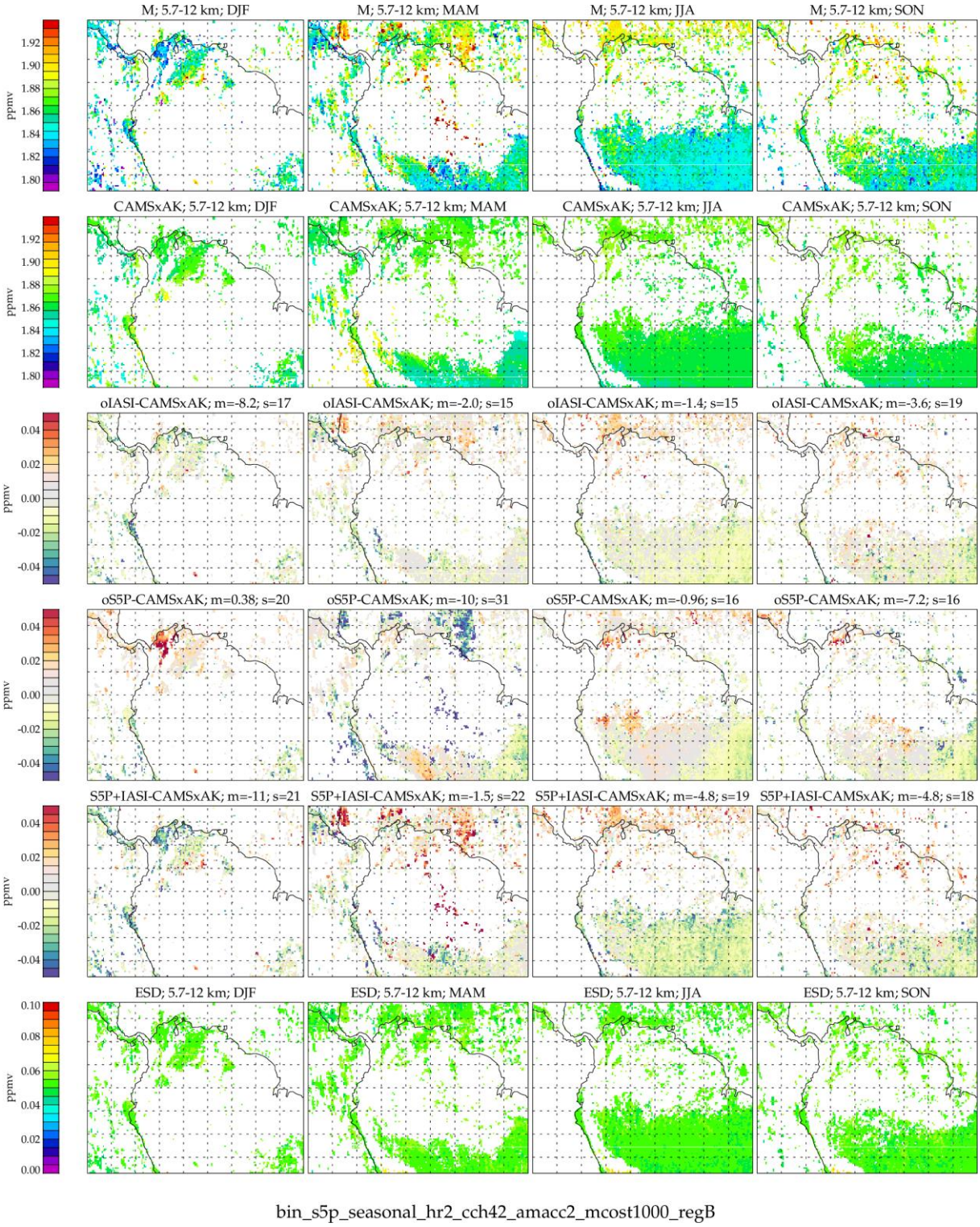

Figure 5-14 : SWIR+TIR daytime 6-12km layer average retrievals over target region B.

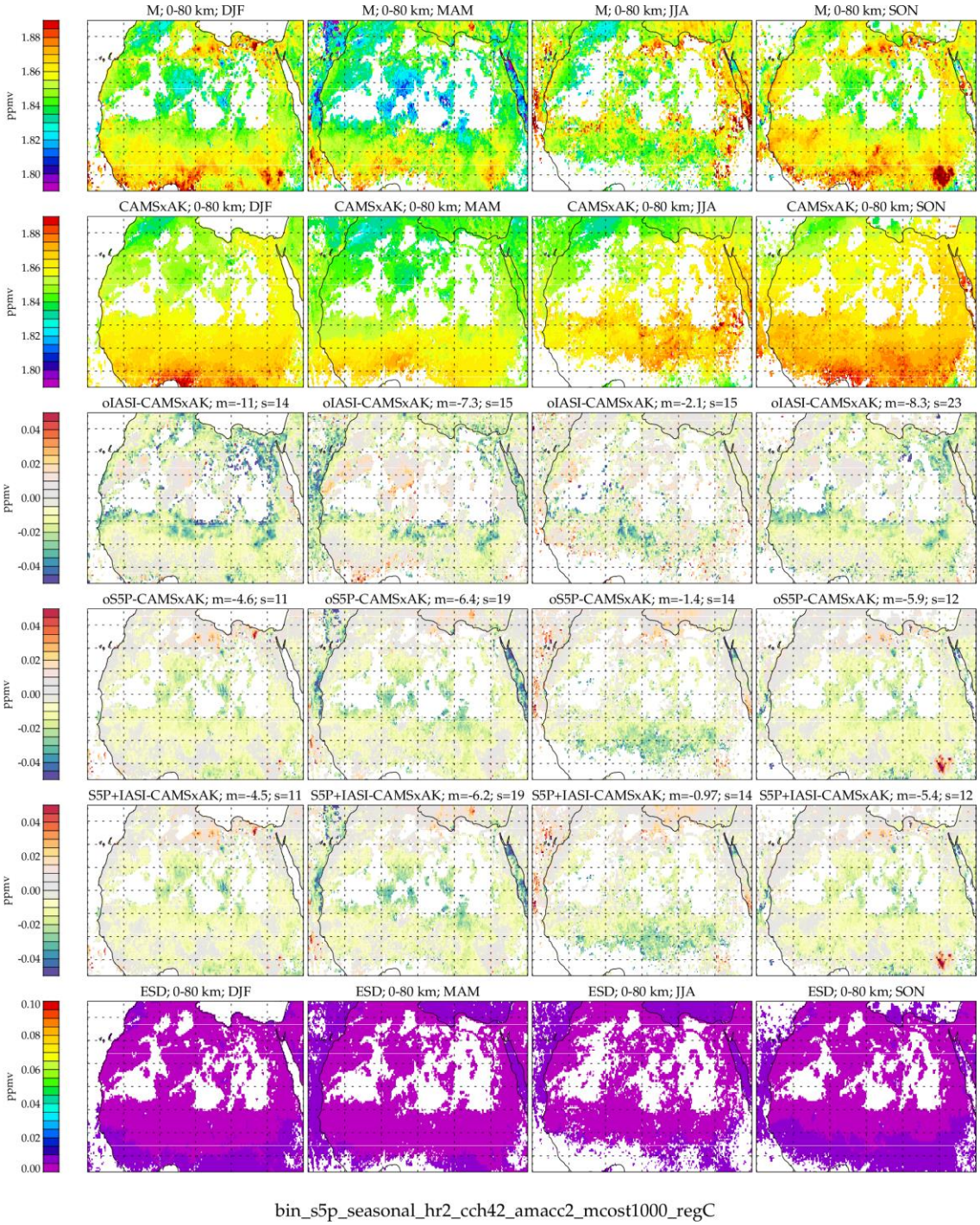

Figure 5-15 : SWIR+TIR global daytime column average retrievals for region C: Each column of the figure shows results for a different season (2018 and 2019 combined). Rows from top-bottom show, respectively, the combined retrieval, CAMS with averaging kernels applied (CAMSxAK); difference from CAMSxAK of "joint" results when only IASI is used; differences from CAMSxAK of "joint" results when only S5P is used; differences from CAMSxAK of joint IASI+S5P results; estimated standard deviation (ESD) of the joint IASI+S5P retrieval. In panels showing differences, the mean ("m") and standard deviation ("s") of the binned data are given, in ppbv, in the panel title.

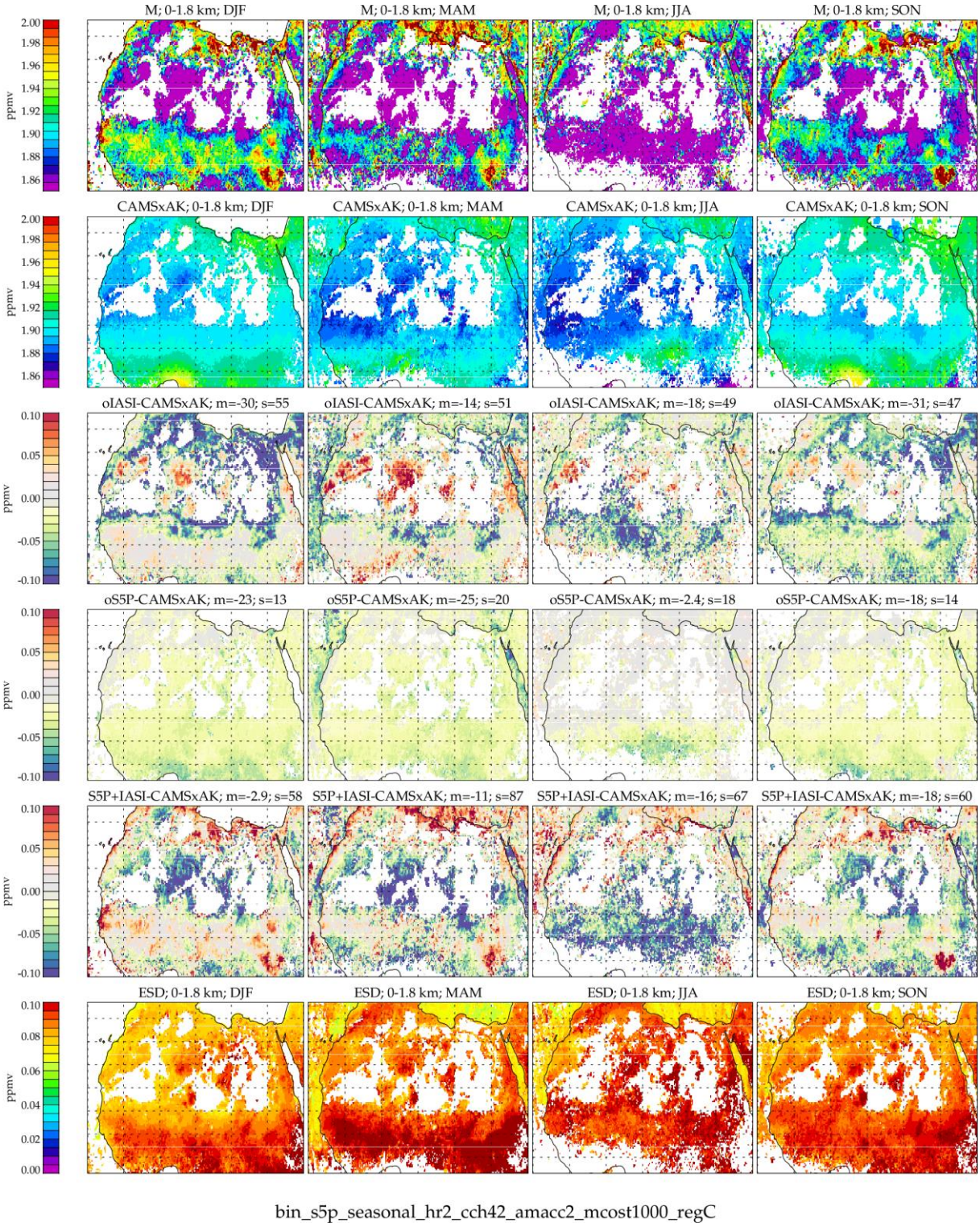

Figure 5-16 : SWIR+TIR daytime 0-2km layer average retrievals over target region C.

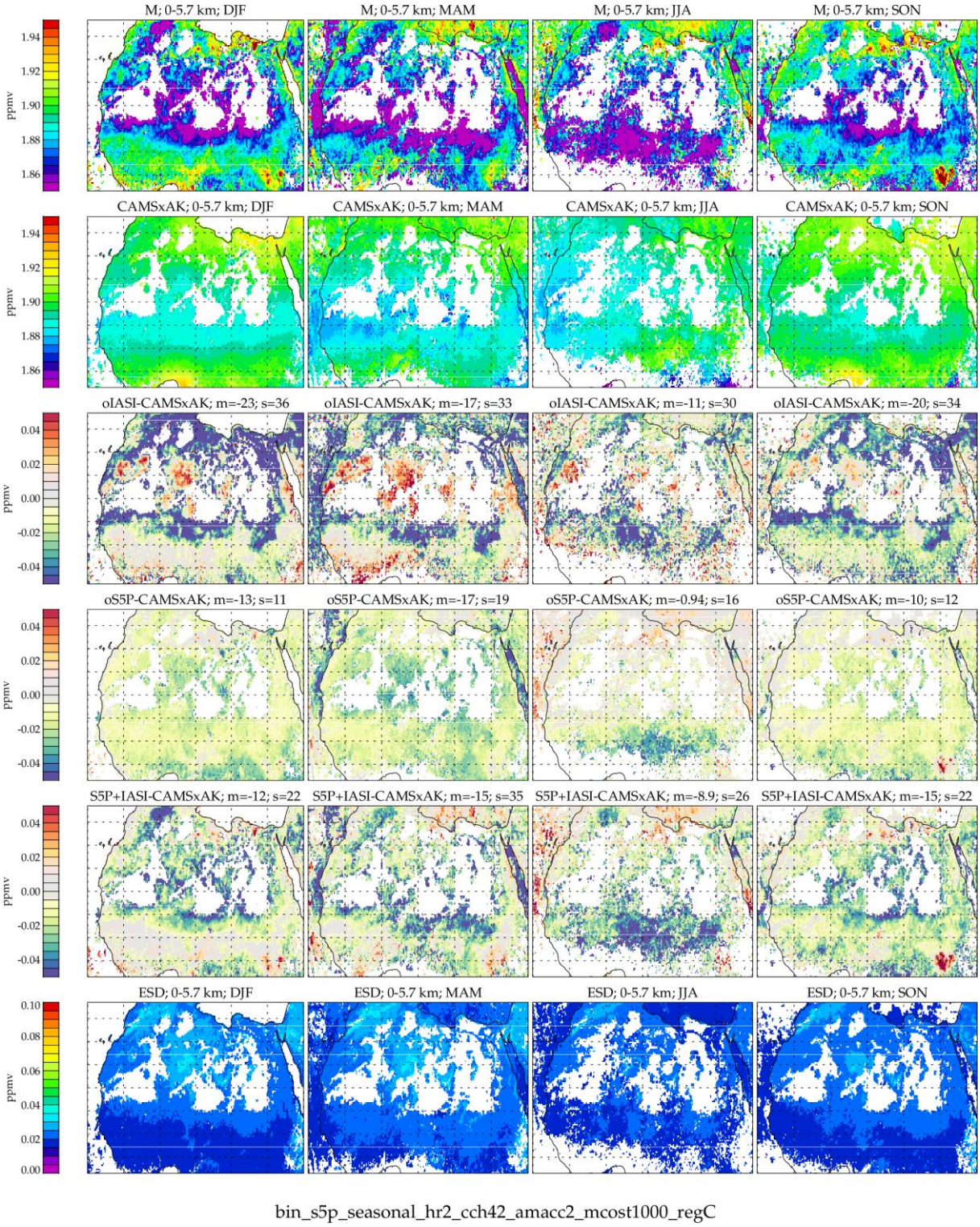

Figure 5-17 : SWIR+TIR daytime 0-6km layer average retrievals over target region C.

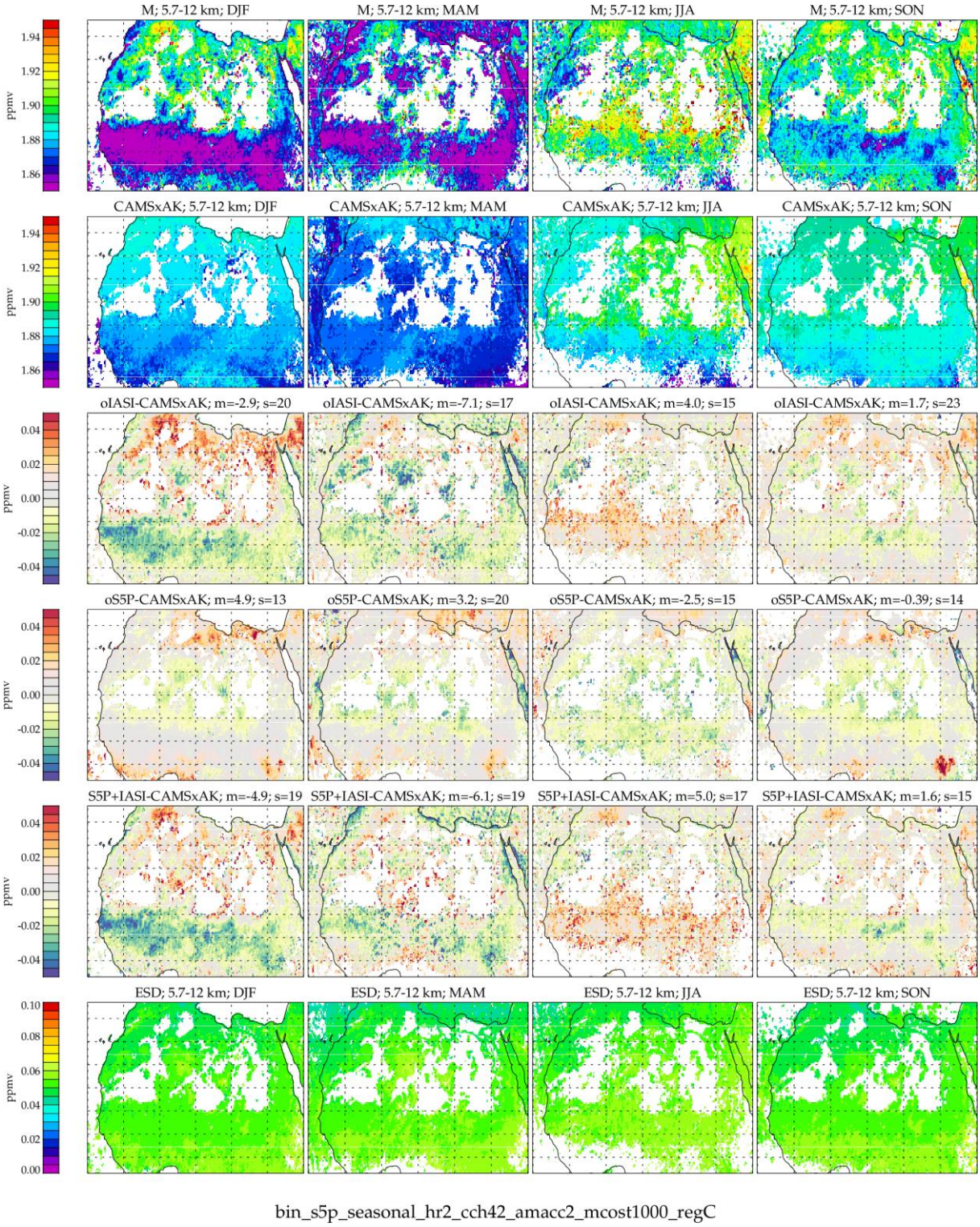

Figure 5-18 : SWIR+TIR daytime 6-12km layer average retrievals over target region C.

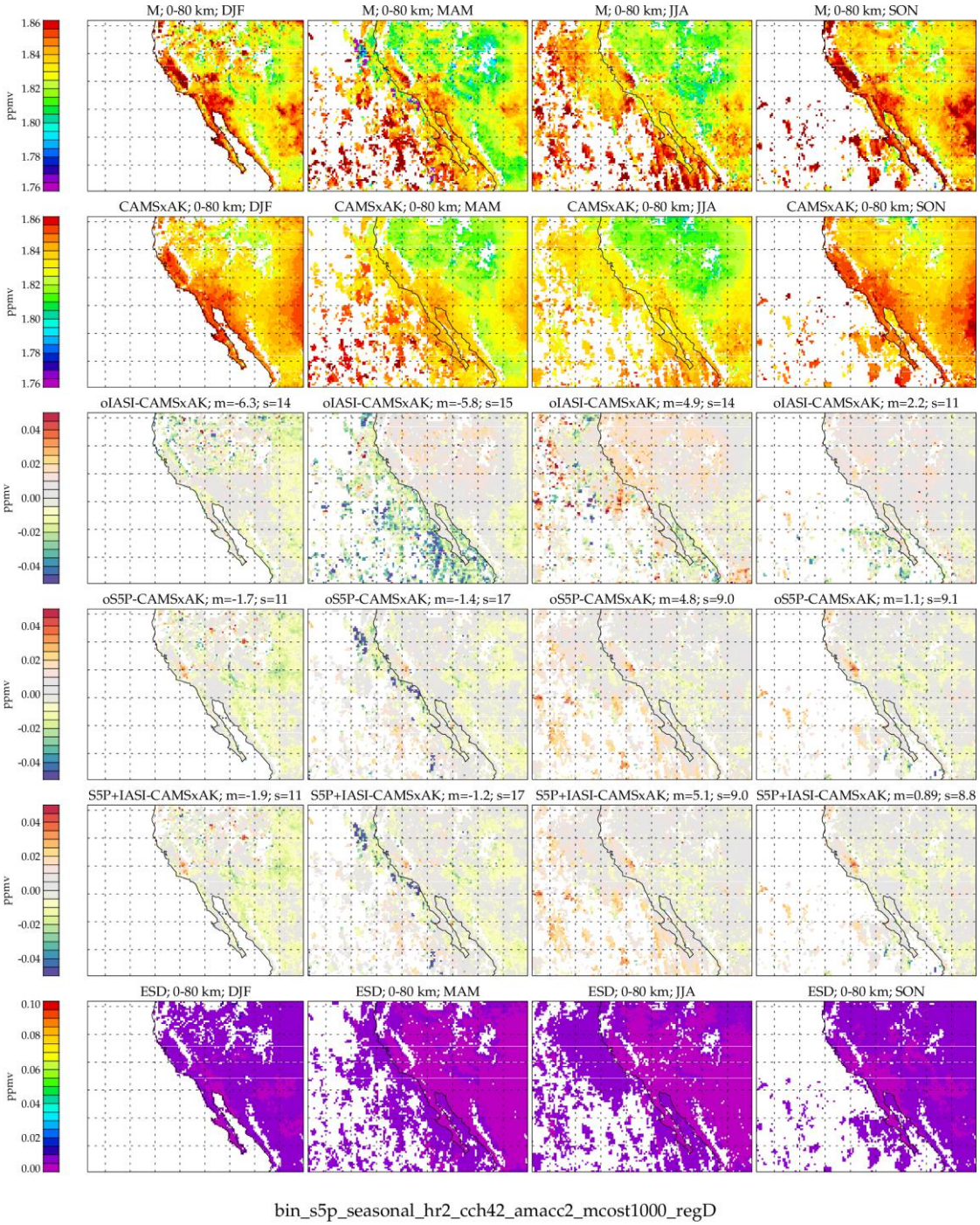

Figure 5-19 : SWIR+TIR global daytime column average retrievals for region D: Each column of the figure shows results for a different season (2018 and 2019 combined). Rows from top-bottom show, respectively, the combined retrieval, CAMS with averaging kernels applied (CAMSxAK); difference from CAMSxAK of "joint" results when only IASI is used; differences from CAMSxAK of "joint" results when only S5P is used; differences from CAMSxAK of joint IASI+S5P results; estimated standard deviation (ESD) of the joint IASI+S5P retrieval. In panels showing differences, the mean ("m") and standard deviation ("s") of the binned data are given, in ppbv, in the panel title.

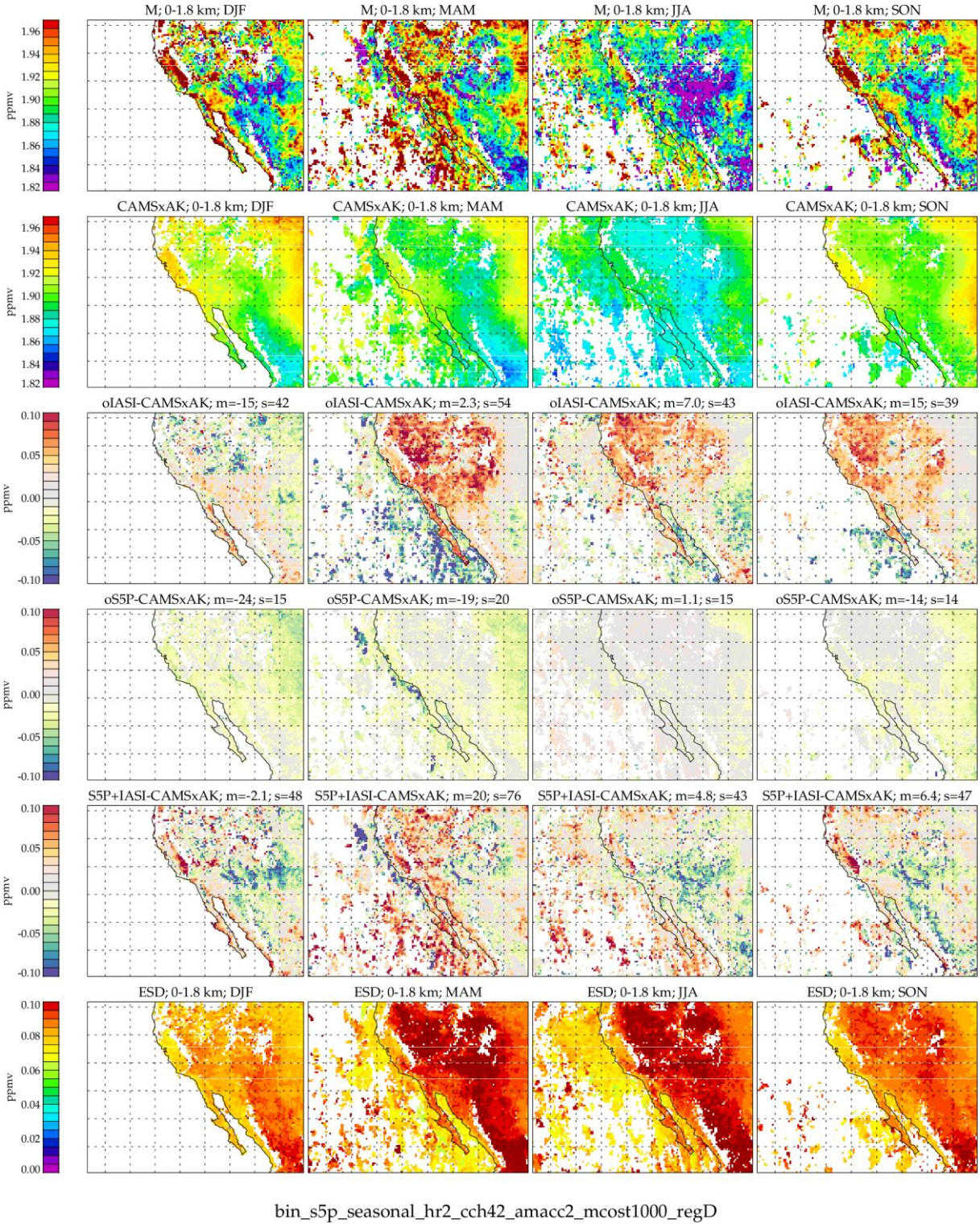

Figure 5-20 : SWIR+TIR daytime 0-2km layer average retrievals over target region D.

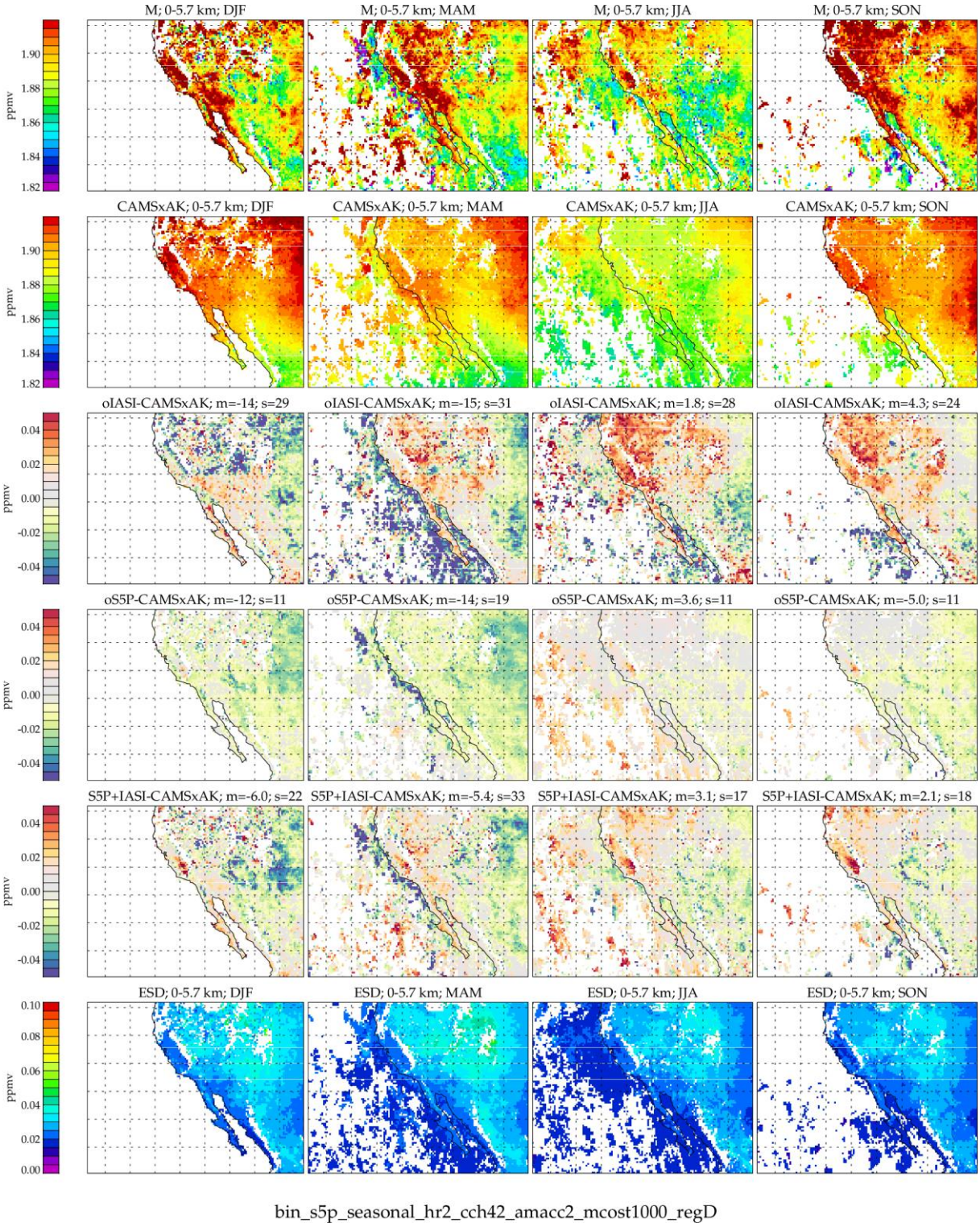

Figure 5-21 : SWIR+TIR daytime 0-6km layer average retrievals over target region D.

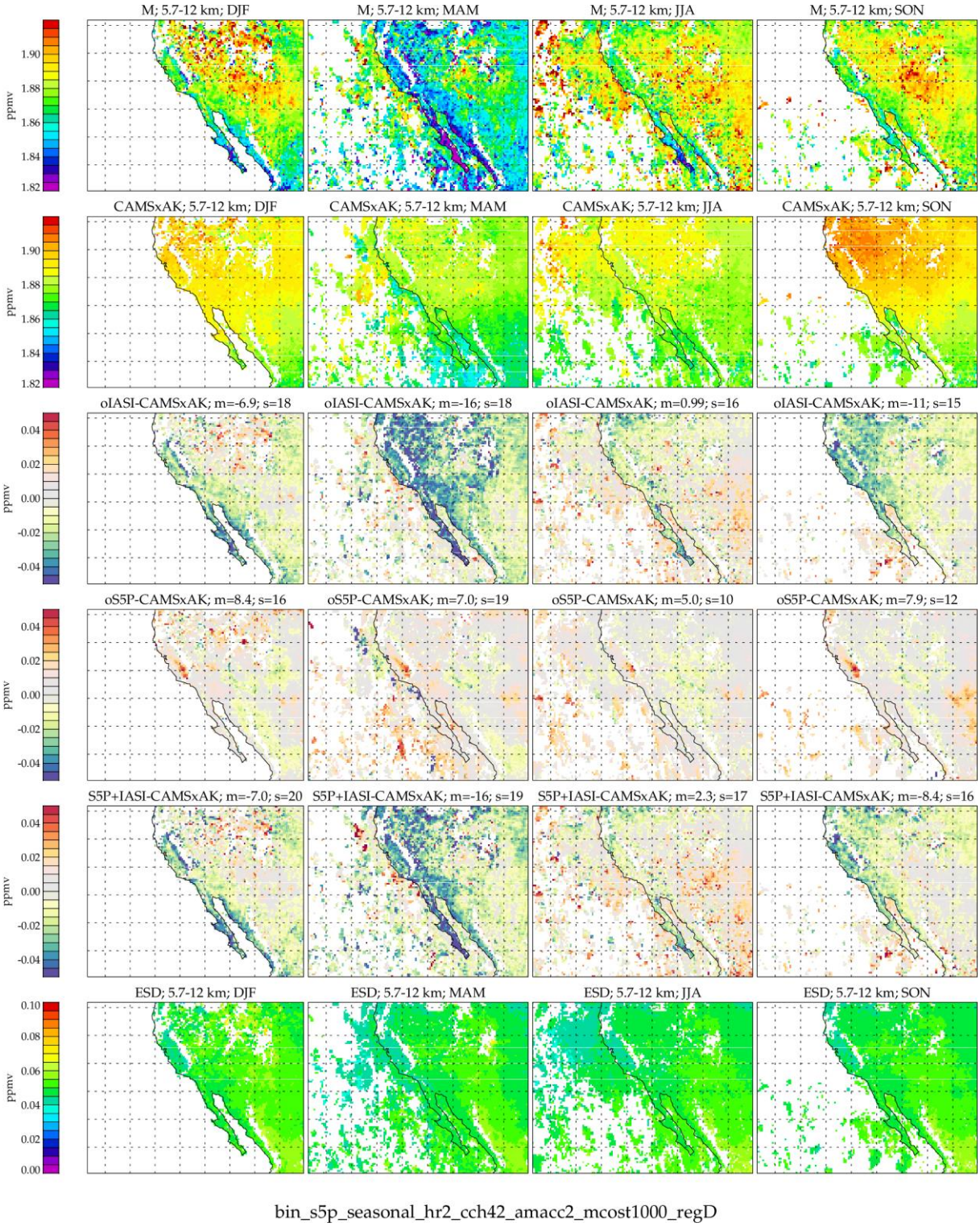

Figure 5-22 : SWIR+TIR daytime 6-12km layer average retrievals over target region D.

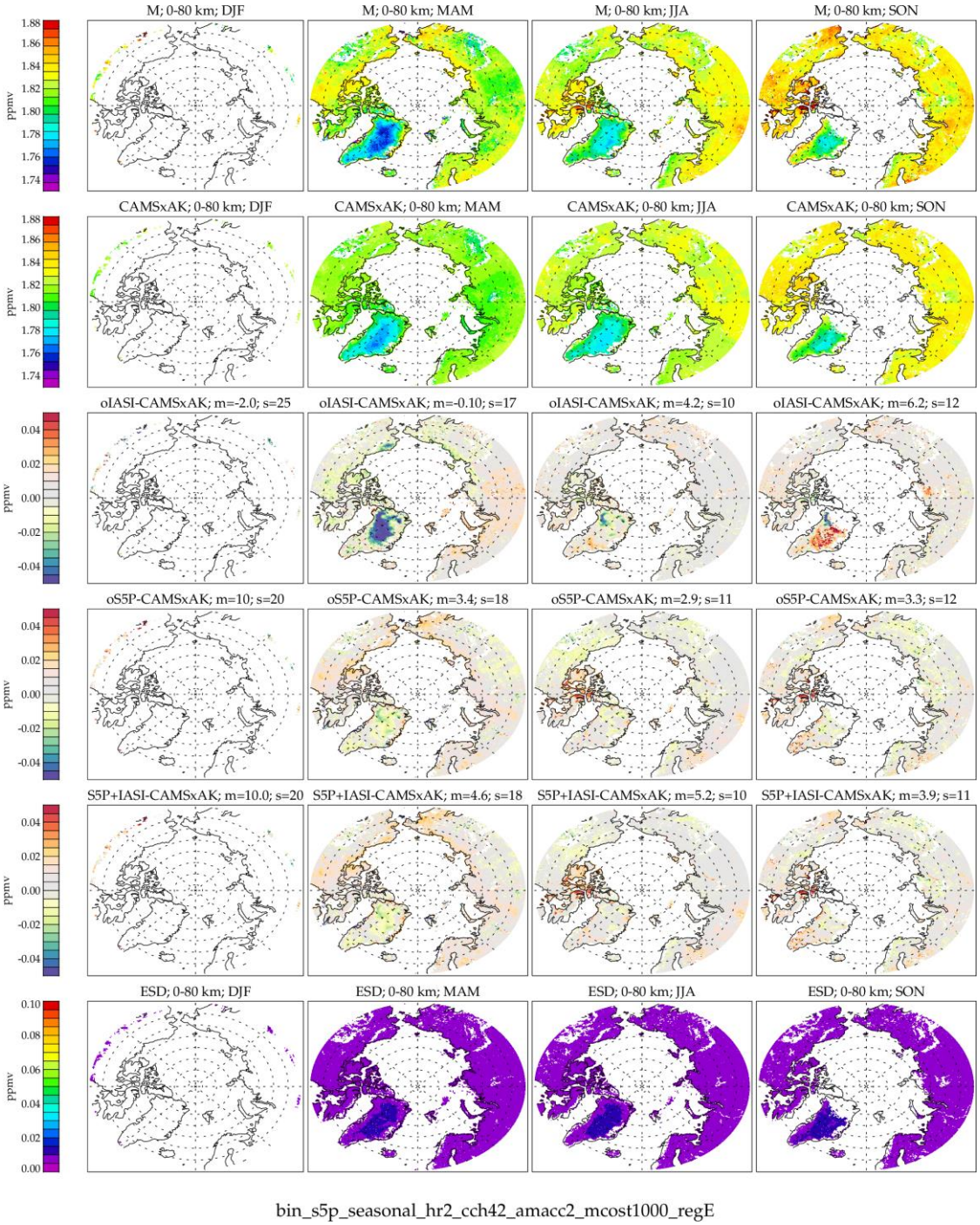

Figure 5-23 : SWIR+TIR global daytime column average retrievals for region E: Each column of the figure shows results for a different season (2018 and 2019 combined). Rows from top-bottom show, respectively, the combined retrieval, CAMS with averaging kernels applied (CAMSxAK); difference from CAMSxAK of "joint" results when only IASI is used; differences from CAMSxAK of "joint" results when only S5P is used; differences from CAMSxAK of joint IASI+S5P results; estimated standard deviation (ESD) of the joint IASI+S5P retrieval. In panels showing differences, the mean ("m") and standard deviation ("s") of the binned data are given, in ppbv, in the panel title.

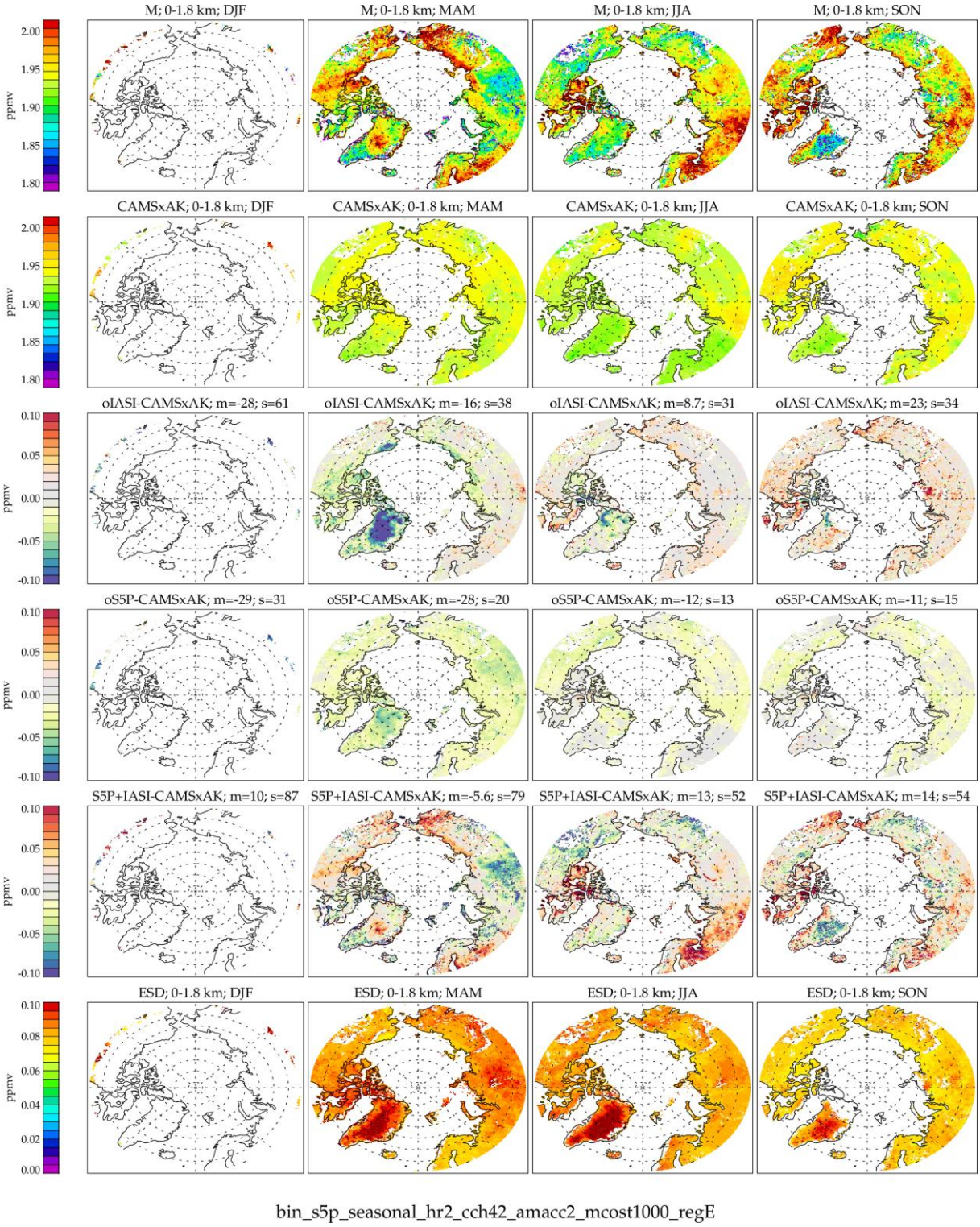

Figure 5-24 : SWIR+TIR daytime 0-2km layer average retrievals over target region E.

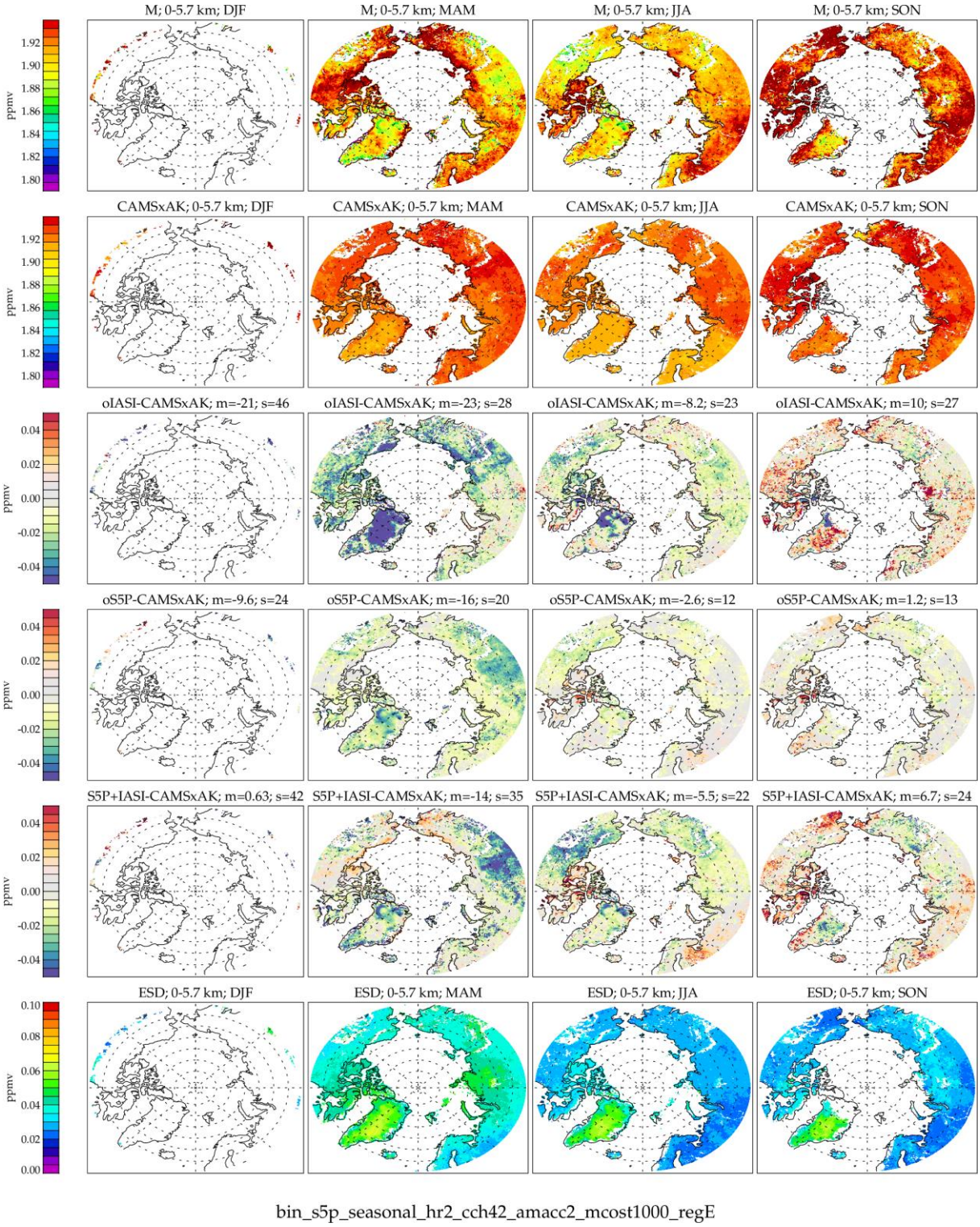

Figure 5-25 : SWIR+TIR daytime 0-6km layer average retrievals over target region E.

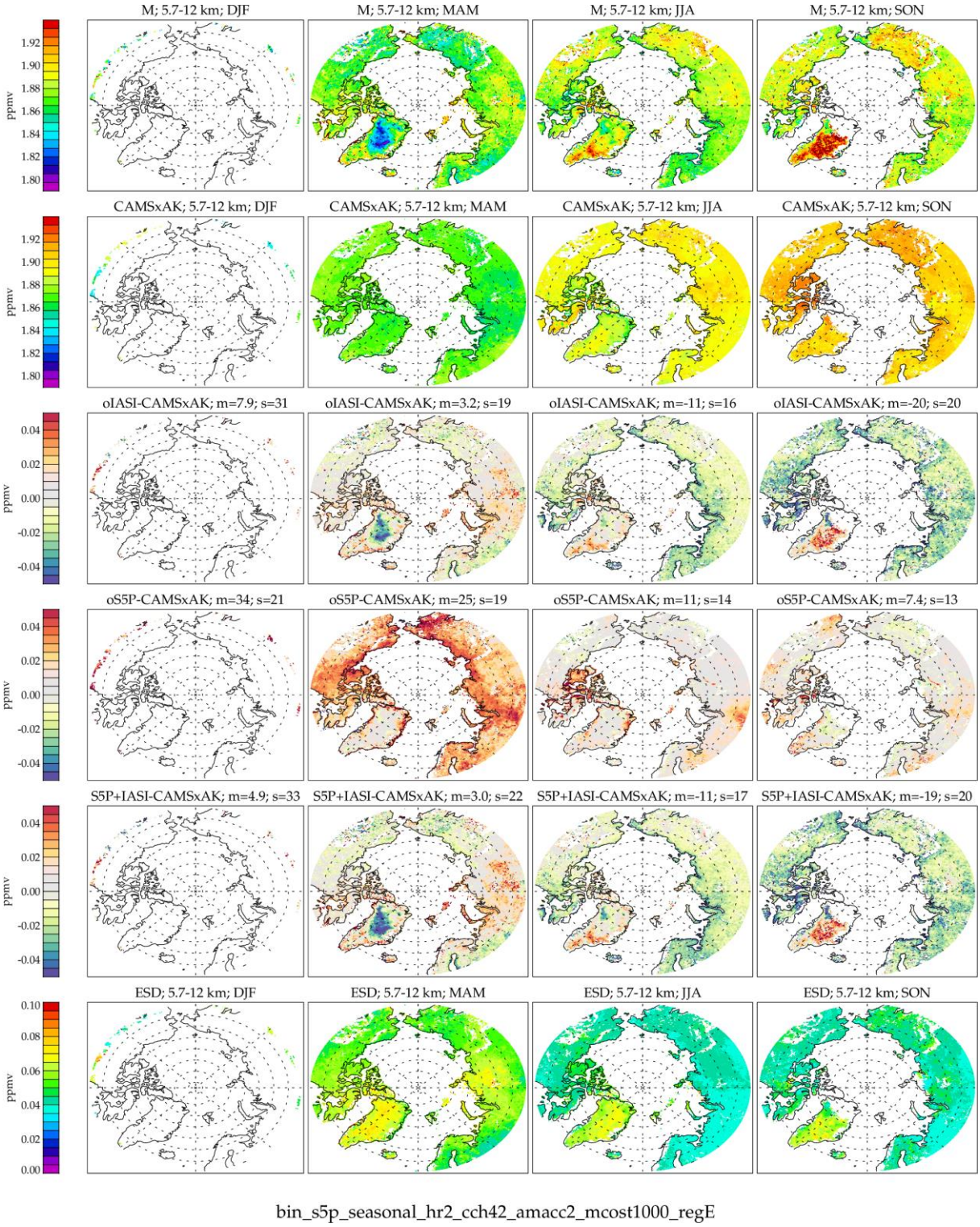

Figure 5-26 : SWIR+TIR daytime 6-12km layer average retrievals over target region E.

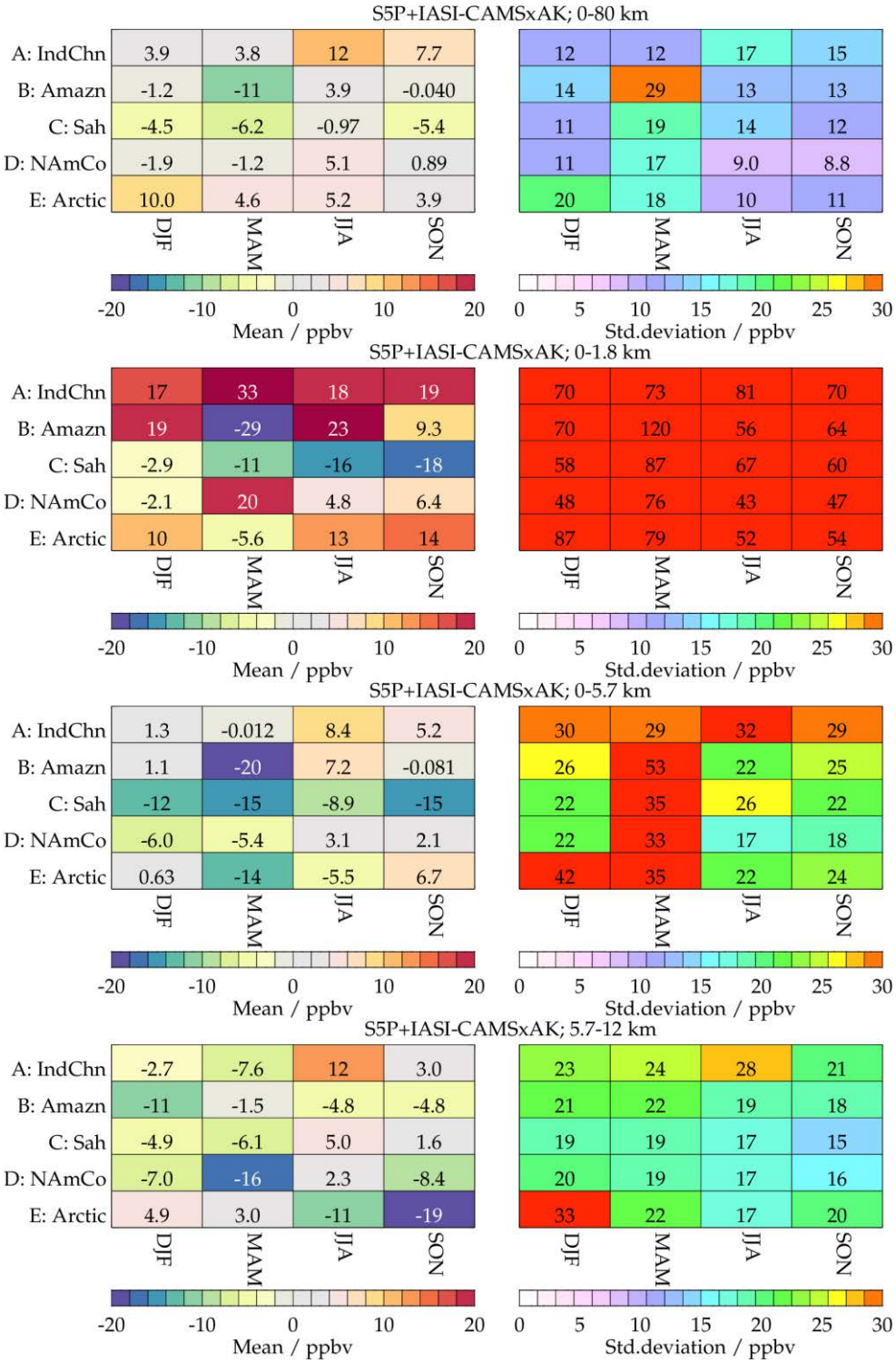

Figure 5-27 : Summary of seasonally averaged differences between SWIR+TIR retrievals and CAMS for each region. Left-hand panel shows the mean difference in each region/season; Right-hand panel shows the standard deviation in the mean (considering the spatial variation of the difference for each of the 0.5x0.5 degree bins). Panels from top-bottom show results for total, 0-2km, 0-6 and 6-12km layer averages.

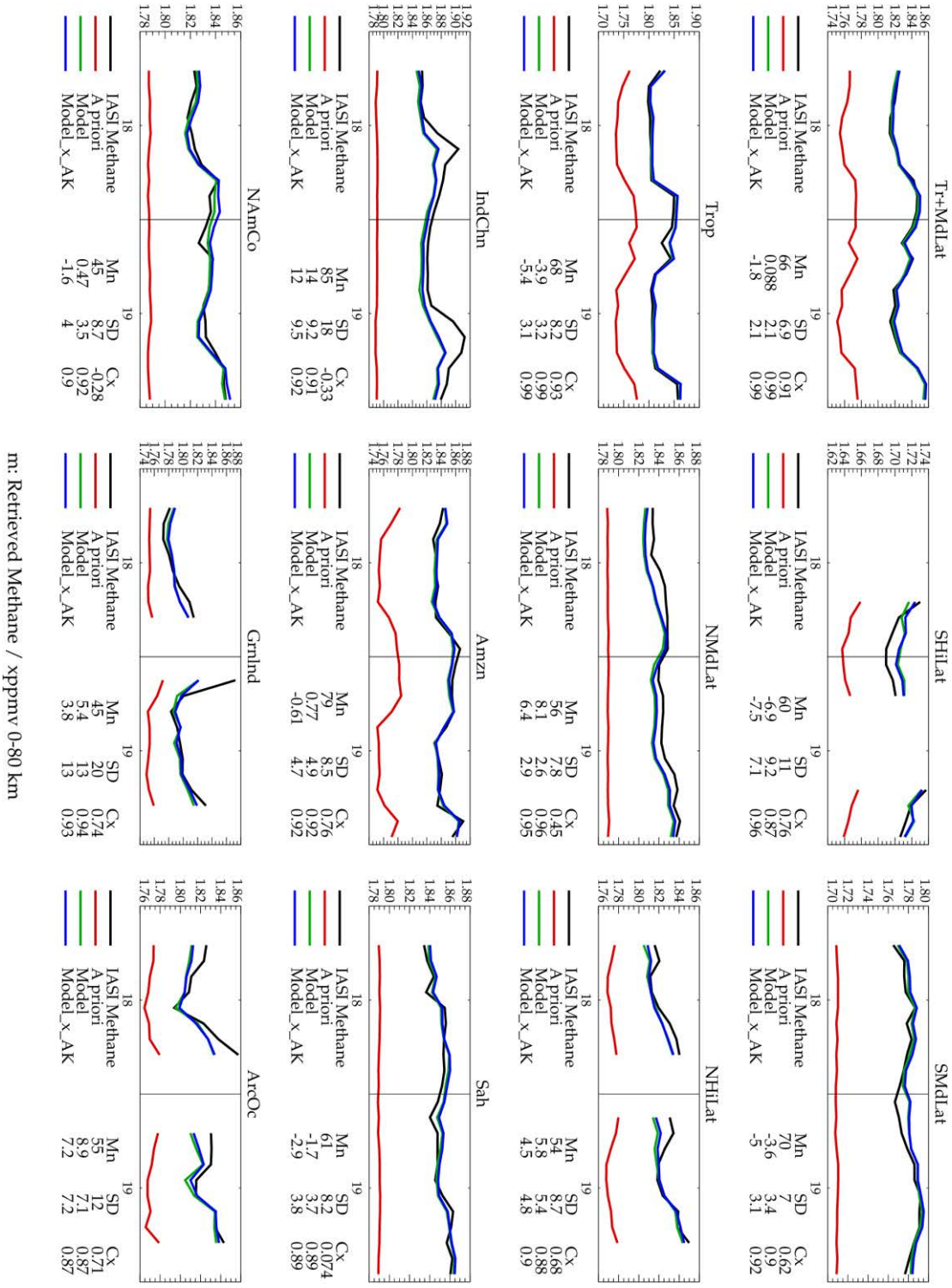

Figure 5-28 : Time series comparisons of SWIR+TIR and CAMS column average methane for various regions. Each panel shows a different region as described in section 2.2. Statistics given in the legend under each panel give the mean difference (Mn); standard deviation of the monthly mean differences (SD); correlation between IASI and CAMS monthly mean values.

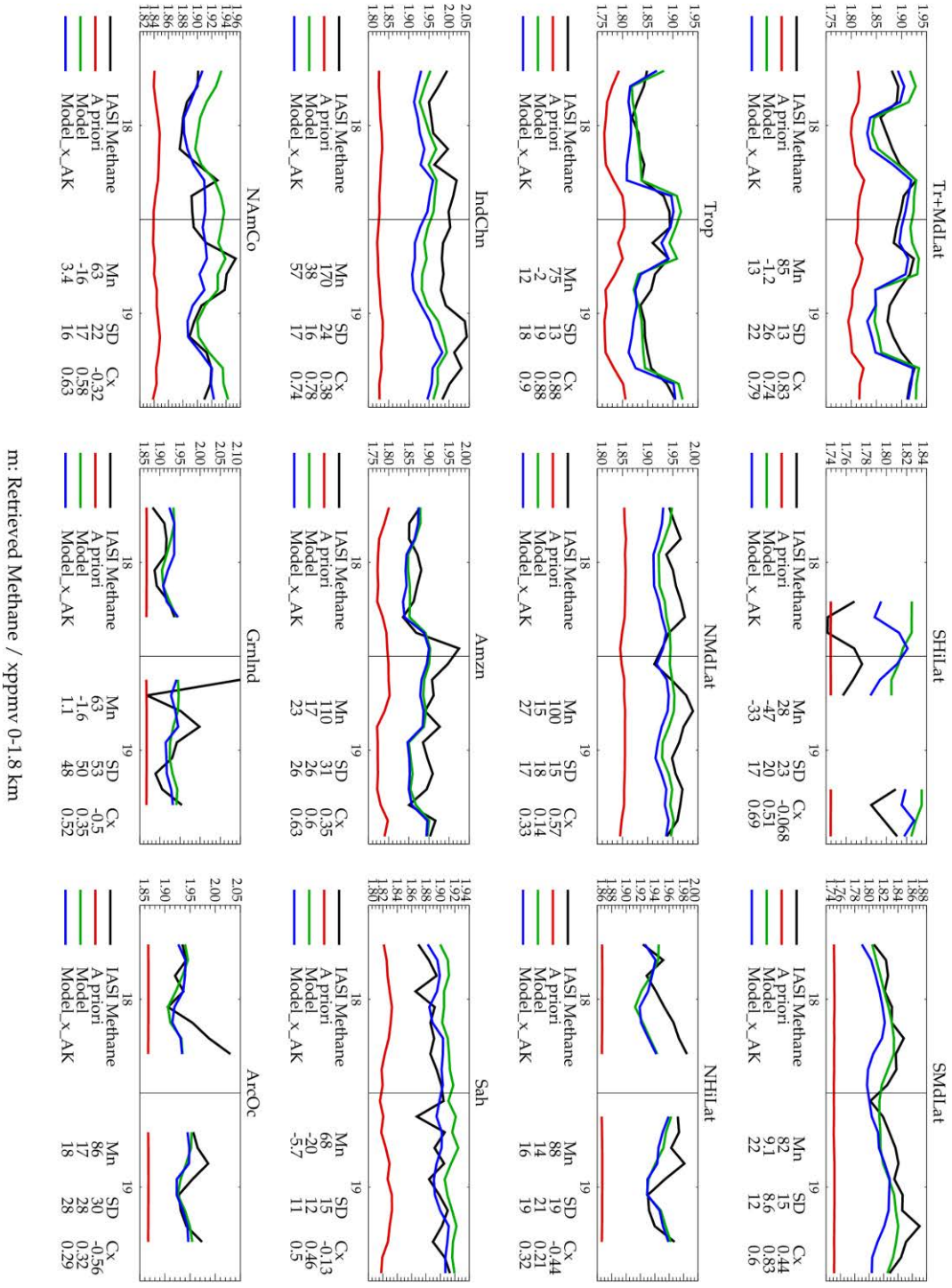

Figure 5-29 : Time series comparisons of SWIR+TIR and CAMS 0-2km sub-column average methane for various regions. Each panel shows a different region as described in section 2.2. Statistics given in the legend under each panel give the mean difference (Mn); standard deviation of the monthly mean differences (SD); correlation between IASI and CAMS monthly mean values.

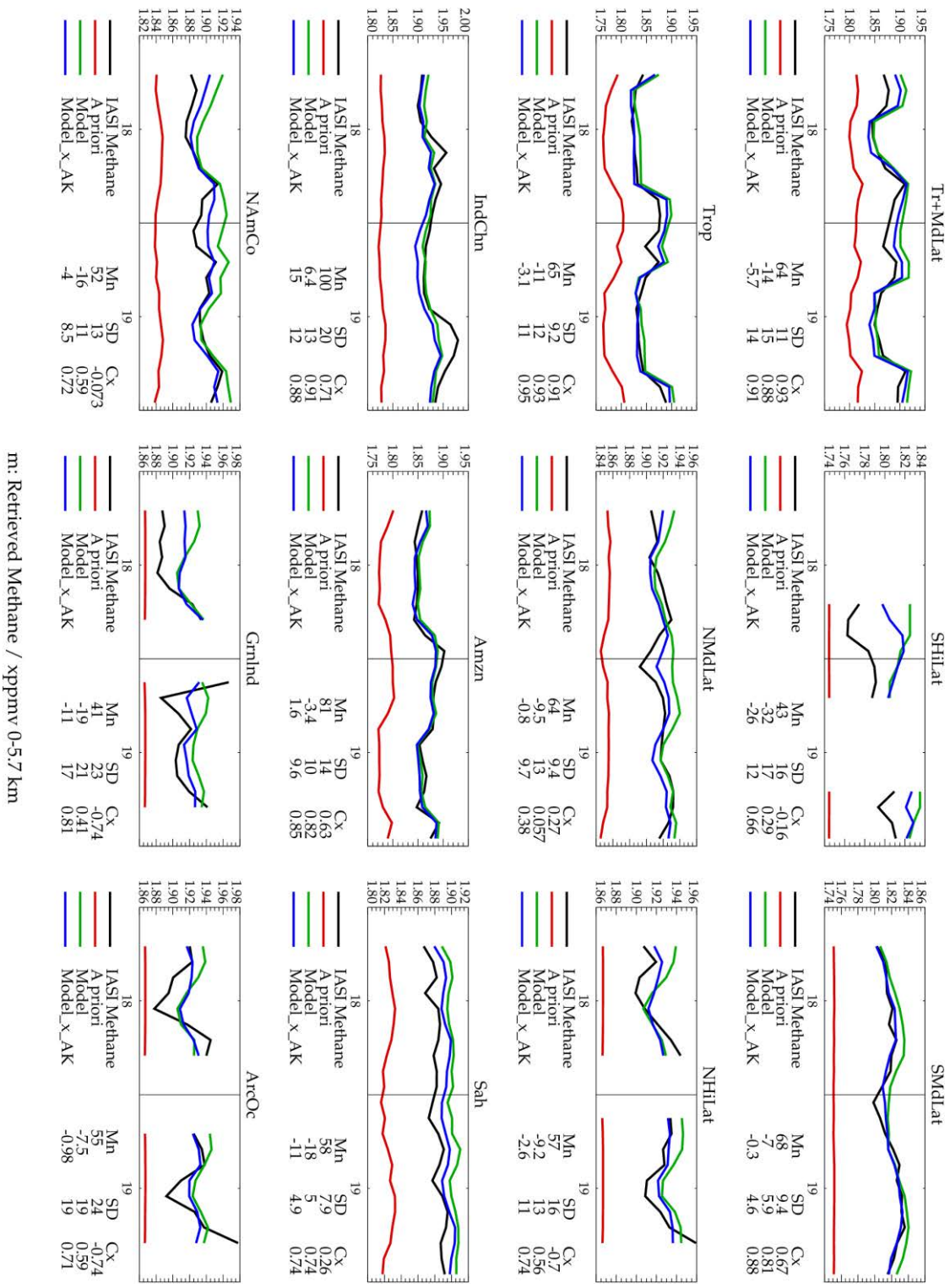

Figure 5-30 : Time series comparisons of SWIR+TIR and CAMS 0-6km sub-column average methane for various regions. Each panel shows a different region as described in section 2.2. Statistics given in the legend under each panel give the mean difference (Mn); standard deviation of the monthly mean differences (SD); correlation between IASI and CAMS monthly mean values.

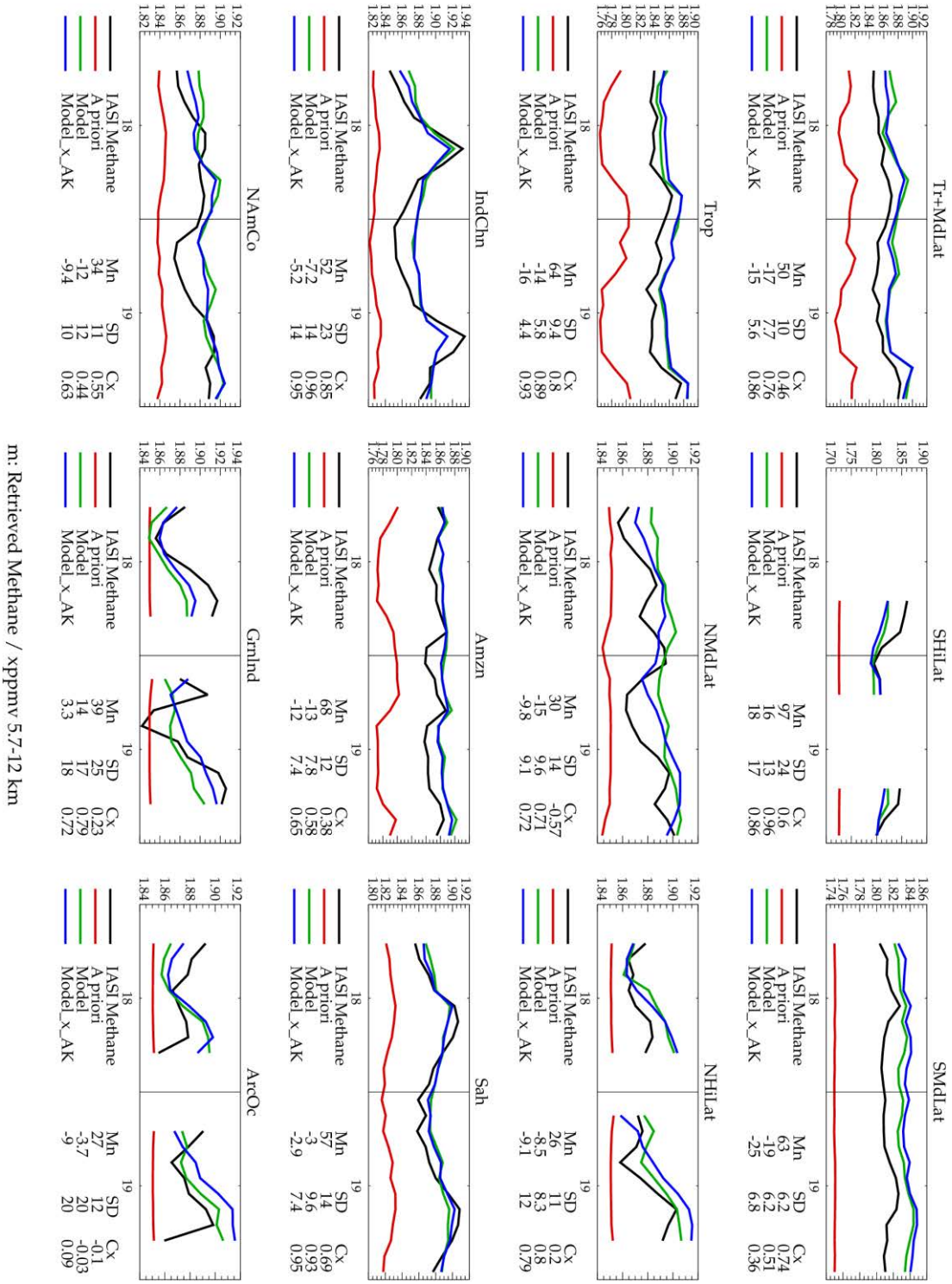

Figure 5-31 : Time series comparisons of SWIR+TIR and CAMS 6-12km sub-column average methane for various regions. Each panel shows a different region as described in section 2.2. Statistics given in the legend under each panel give the mean difference (Mn); standard deviation of the monthly mean differences (SD); correlation between IASI and CAMS monthly mean values.

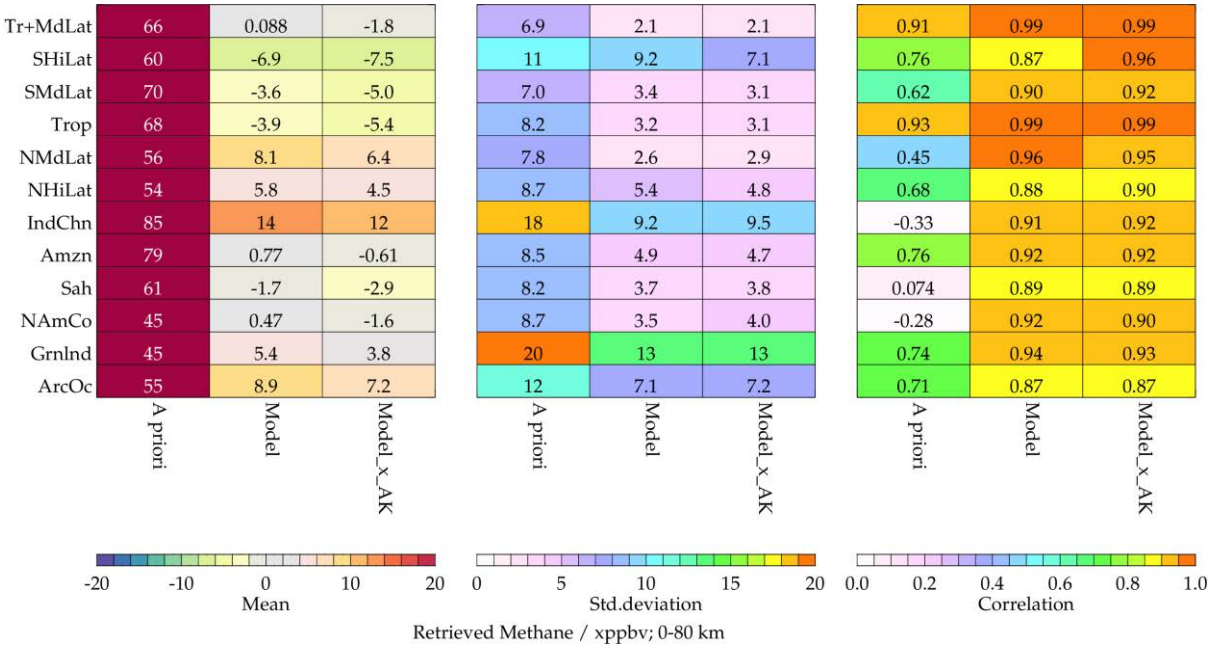

Figure 5-32 : Summary of statistics from monthly time-series comparisons of SWIR+TIR and CAMS column average methane for various regions. Panels from left to right show the mean difference; standard deviation of the monthly mean differences; correlation between IASI and CAMS monthly mean values.

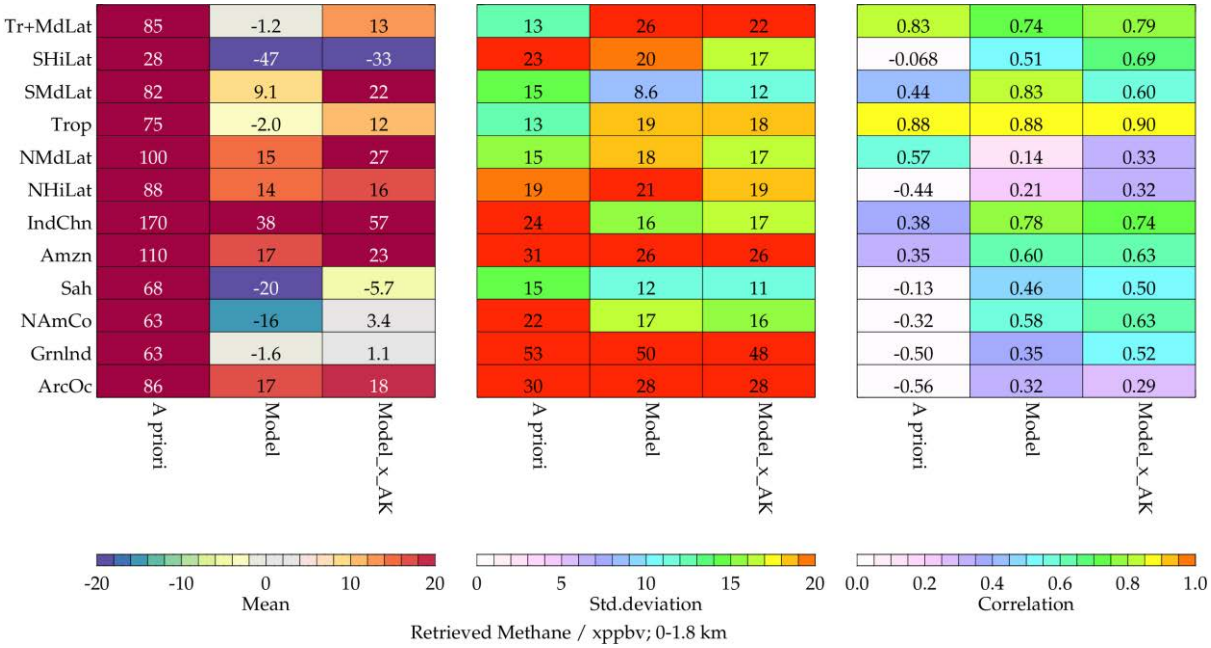

Figure 5-33 : Summary of statistics from monthly time-series comparisons of SWIR+TIR and CAMS 0-2km sub-column average methane for various regions. Panels from left to right show the mean difference; standard deviation of the monthly mean differences; correlation between IASI and CAMS monthly mean values.

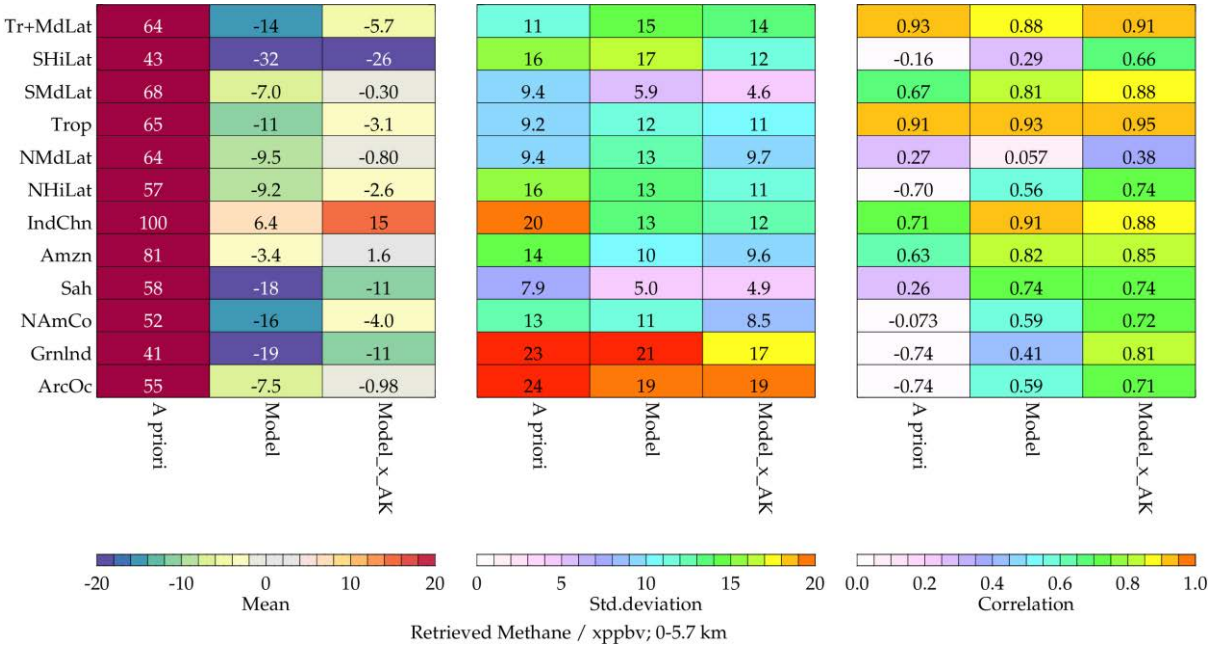

Figure 5-34 : Summary of statistics from monthly time-series comparisons of SWIR+TIR and CAMS 0-6km sub-column average methane for various regions. Panels from left to right show the mean difference; standard deviation of the monthly mean differences; correlation between IASI and CAMS monthly mean values.

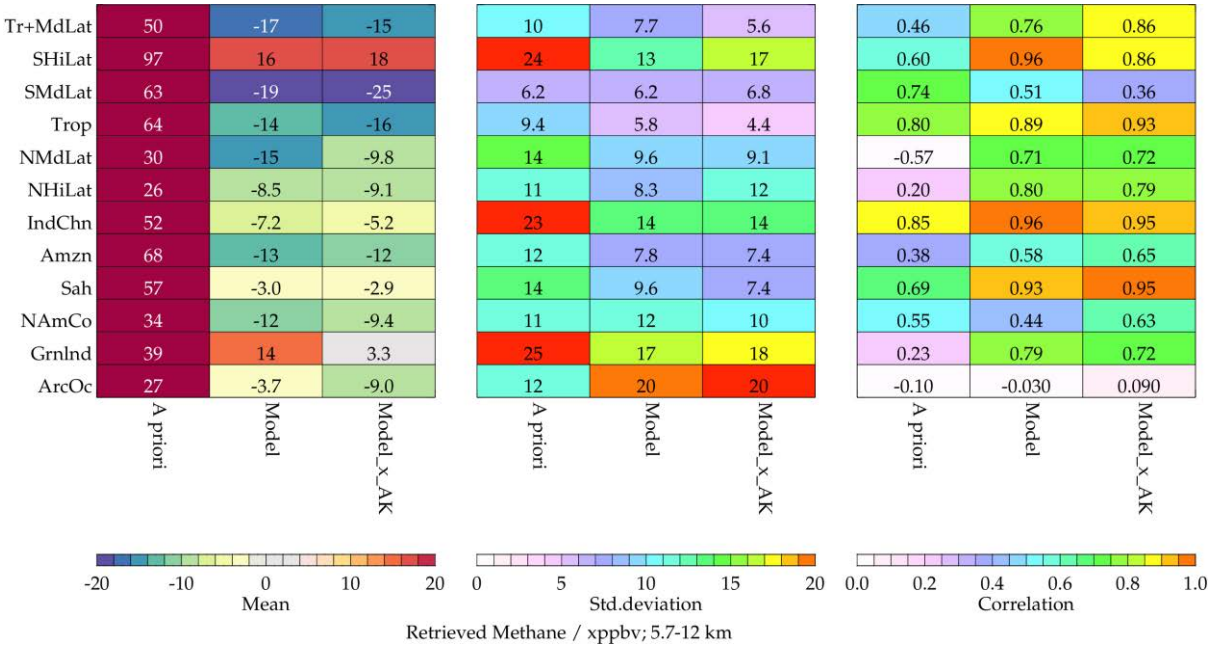

Figure 5-35 : Summary of statistics from monthly time-series comparisons of SWIR+TIR and CAMS 6-12km sub-column average methane for various regions. Panels from left to right show the mean difference; standard deviation of the monthly mean differences; correlation between IASI and CAMS monthly mean values.

5.3. Validation from non-satellite sources

5.3.1. Atom-4

Comparisons with Atom-4 are not shown for the SWIR-TIR retrieval because there are too few co-locations (Atom flights are mainly over the sea where coverage of S5P data is limited to sun-glint conditions).

5.3.2. AirCore

Figure 5-36 shows the mean difference between outputs from the SWIR-TIR scheme and each AirCore profile, for the column average and three tropospheric layer averages. Figure 5-37 shows the corresponding results after application of the IASI averaging kernels to the AirCore profile. Figure 5-38 shows scatter plots.

Comparison with Figure 2-41 to Figure 2-43 shows little substantive difference between IASI-B v1 and the combined SWIR-TIR (which uses v1 TIR) in their agreement with AirCore (there are fewer co-located profiles so a direct quantitative comparison is not straightforward). Departures are relatively large in the 0-2km layer compared to the other layers, consistent with the behaviour of the larger scale comparisons with CAMS.

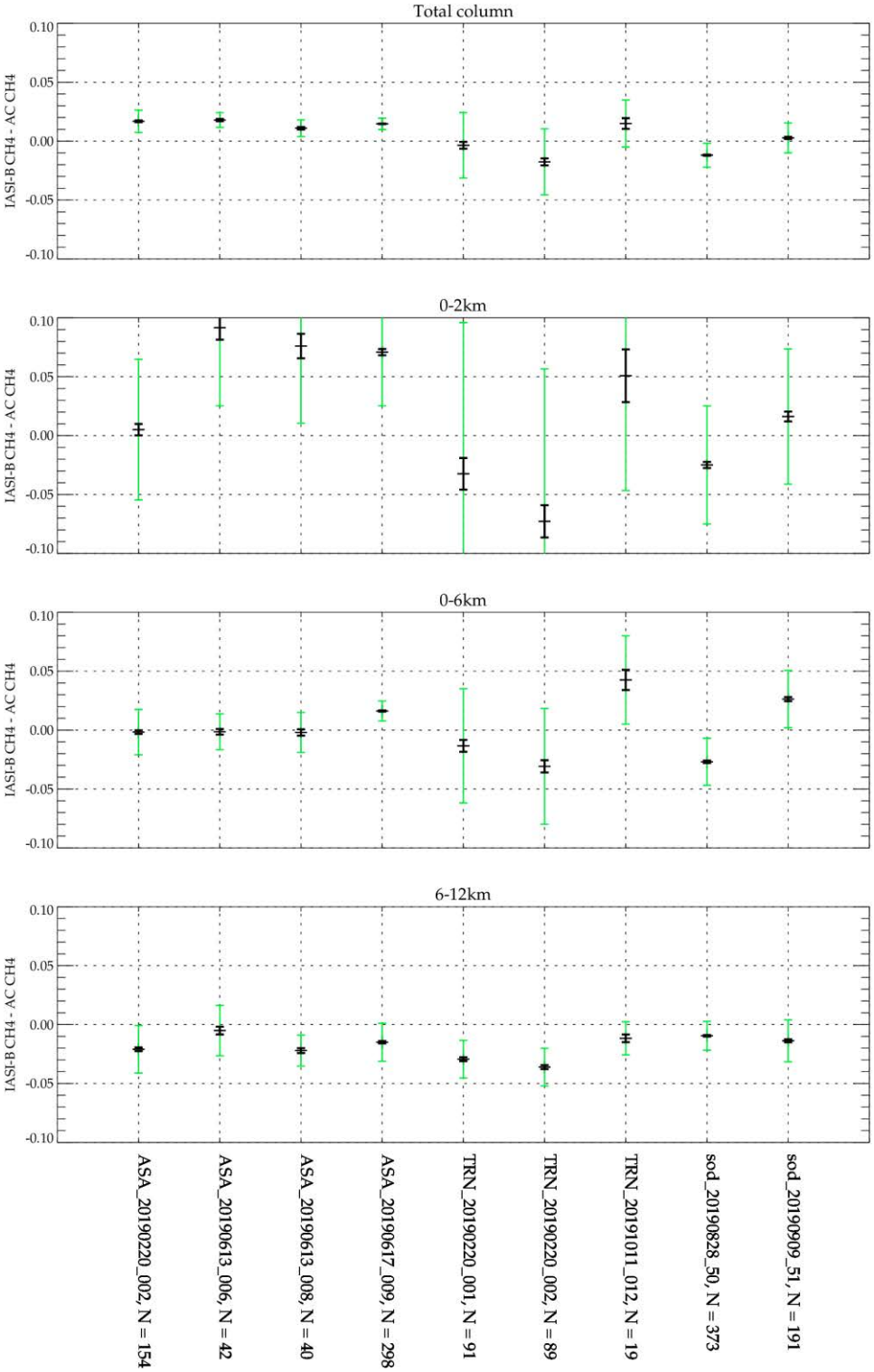

Figure 5-36 : Differences between SWIR+TIR retrievals and AirCore profile measurements for (a) the column average, 0-80km, (b) the 0-6km layer average, and (c) the 6-12km layer average. The error bars represent the standard errors in the mean (black) and standard deviations (green) of IASI-AirCore differences for the set of IASI soundings co-located with each AirCore profile. Results are shown for all AirCore profiles that passed the quality control criteria.

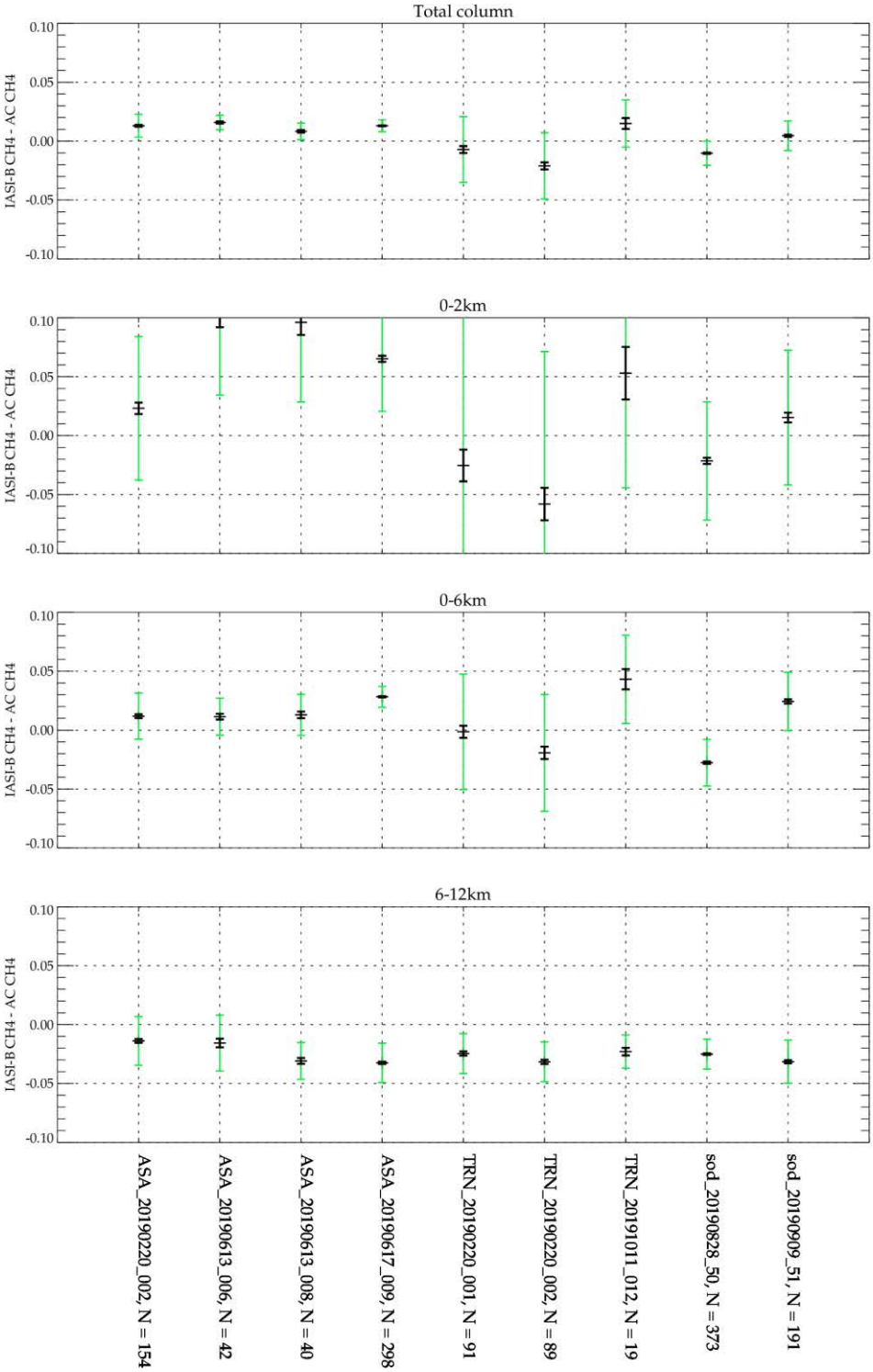

Figure 5-37 : As previous figure but with averaging kernels applied to AirCore profiles

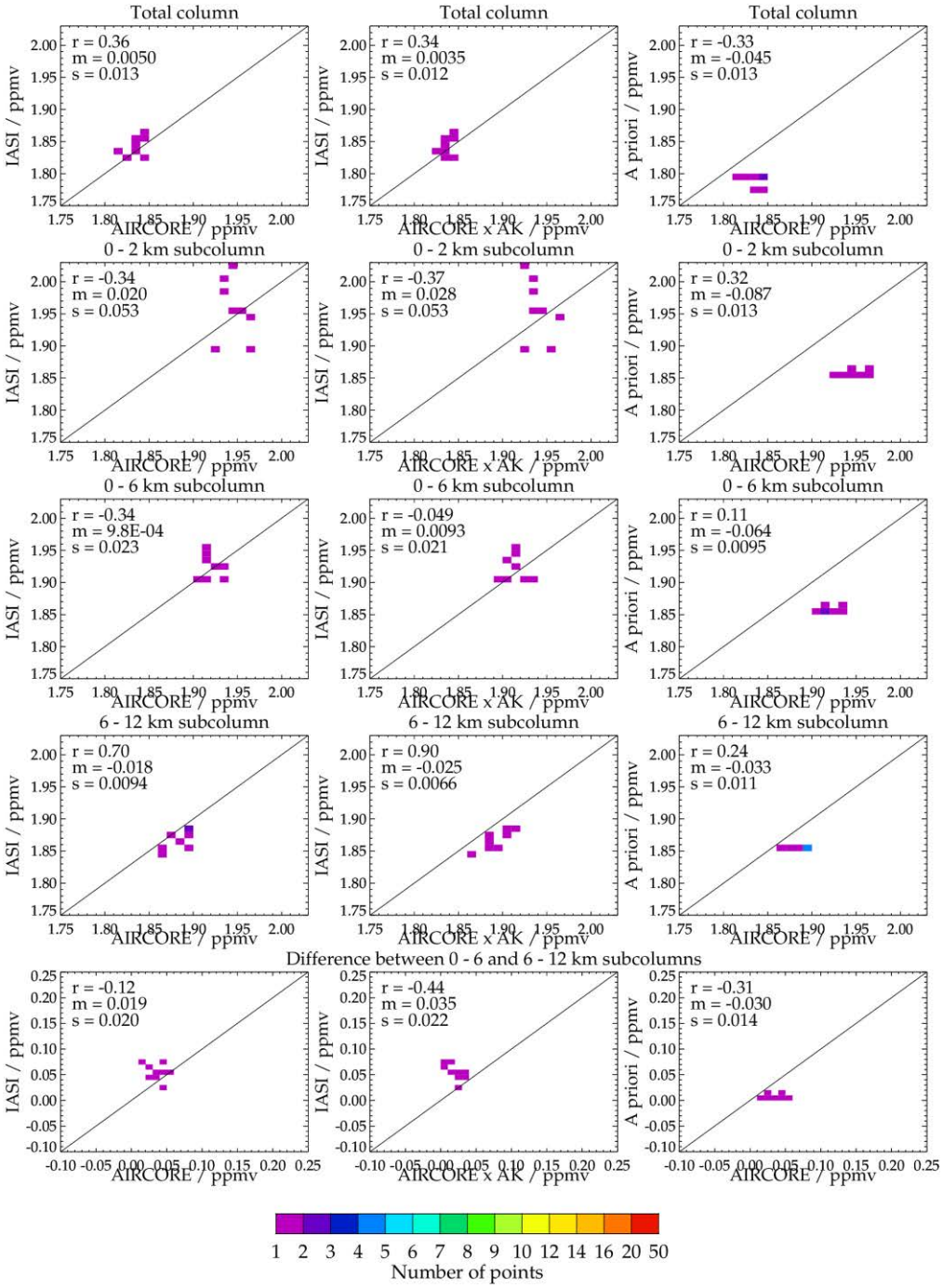

Figure 5-38 : Scatter density plots comparing AirCore and SWIR+TIR. Columns from left to right: IASI vs AirCore (left), IASI vs AirCore accounting for averaging kernels (centre) and the a priori used in the retrieval vs AirCore (right). Rows from top-bottom show the column average, 0-6km layer, 6-12km layer and the difference between the 0-6 and 6-12km layers. The following statistics are shown within each panel: correlation coefficient (r); mean difference (m); standard deviation in the difference (s).

5.3.3. TCCON

As in section2.3.3, the following figures are presented:

- Figure 5-39 shows Hovmöller comparing TCCON with the SWIR-TIR retrieval.
- Figure 5-40 shows scatter plots of monthly mean co-located IASI and TCCON data collected into latitude bands (as in the Hovmoller plots).
- Figure 5-41 compares time series of co-located IASI and TCCON averaged over regions.
- Figure 5-42 summarises the statistics from the time-series.

Only the total column from the joint scheme can be compared to TCCON. Compared to the corresponding figures in section 2.3.3, agreement with CAMS is generally improved reflecting mainly the better agreement with CAMS of the input (bias-corrected) S5P data, faithfully propagated by the joint retrieval scheme. Standard deviations in the monthly mean differences summarised in Figure 5-42 are generally comparable to those of the V1 TIR data, however the correlations are reduced in some regions. This is mainly caused by sampling differences (there are many more TCCON co-locations with the TIR only dataset). E.g. there is very sparse sampling of the India-China region by the SWIR-TIR retrieval,

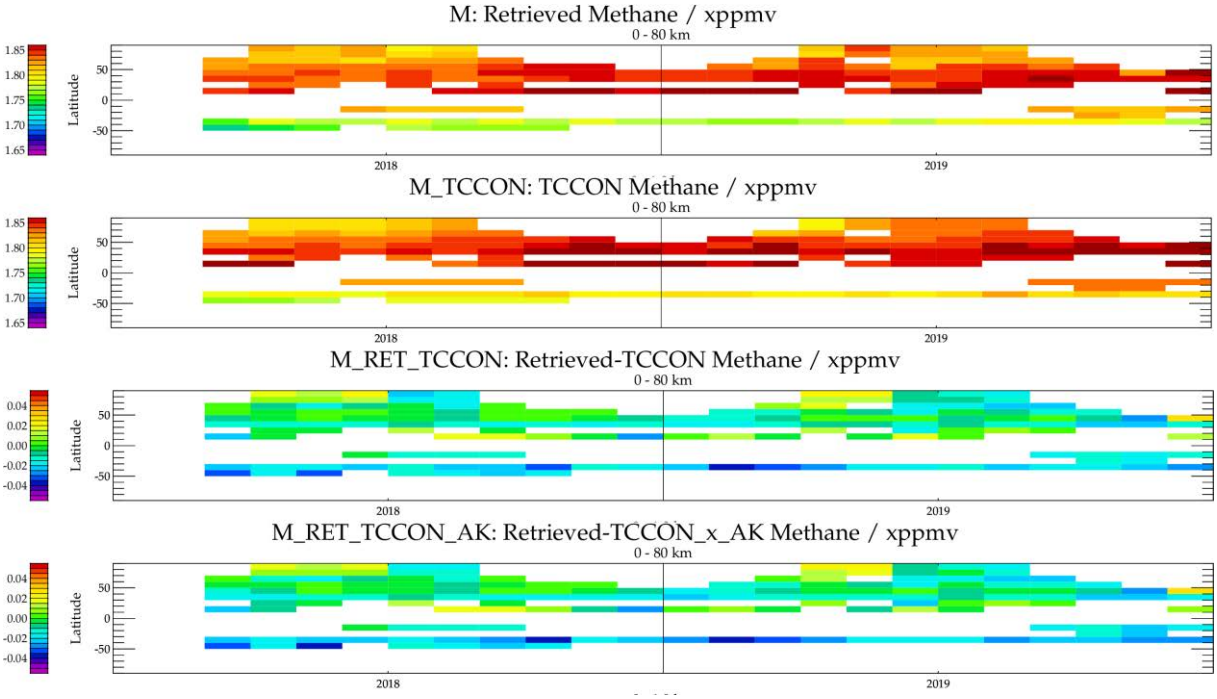

Figure 5-39 : SWIR+TIR Hovmöller time-series for (a) IASI-B retrieved methane; (b) TCCON methane, measurements; (c) the difference between IASI and TCCON; (d) the difference between IASI and TCCON, adjusted to account for IASI averaging kernels using CAMS. Panels are shown for column average (0-80km) retrievals.

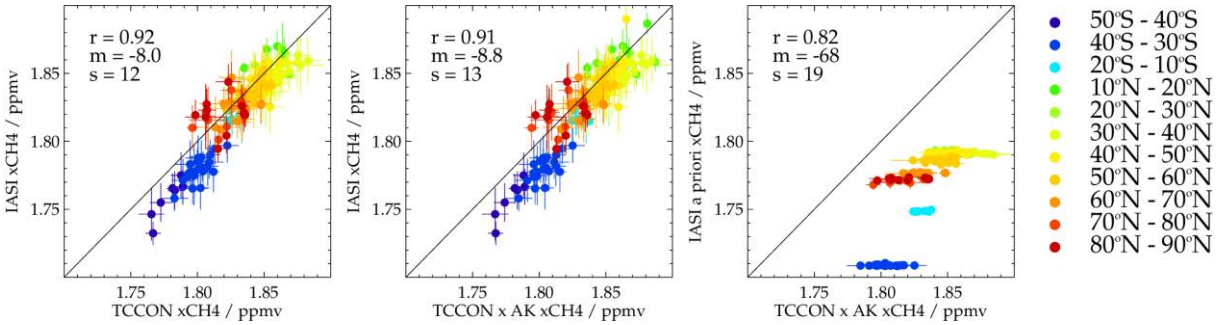

Figure 5-40 : Scatter plots comparing TCCON and SWIR+TIR column-averaged mixing ratios in 2018/2019. Each point is a monthly mean with colours indicating TCCON stations in the indicated latitude range. Error bars are standard deviations of daily mean values in each average. Panels show (a) IASI retrievals vs TCCON measurements, (b) IASI retrievals vs TCCON measurements adjusted for IASI averaging kernels using CAMS and (c) IASI a priori vs TCCON. Statistics in each panel are the correlation coefficient (r), mean difference (ppbv) and standard deviation (ppbv) for the set of monthly-mean differences.

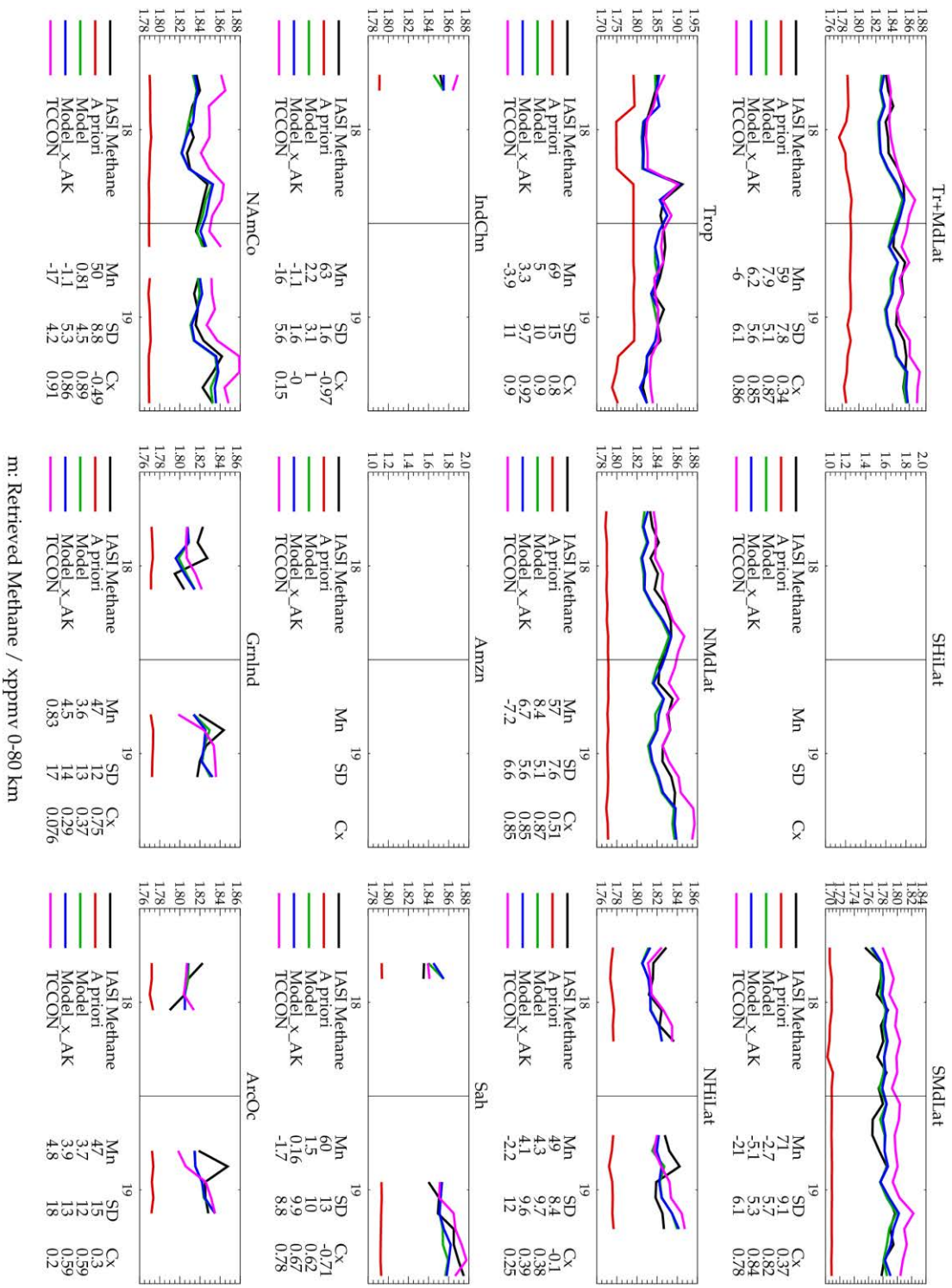

Figure 5-41 : Time series comparing SWIR+TIR column averages with TCCON and CAMS sampled to TCCON for various regions. Each panel shows a different region as described in section 2.2. Statistics given in the legend under each panel give the mean difference (Mn); standard deviation of the monthly mean differences (SD); correlation between IASI and CAMS monthly mean values

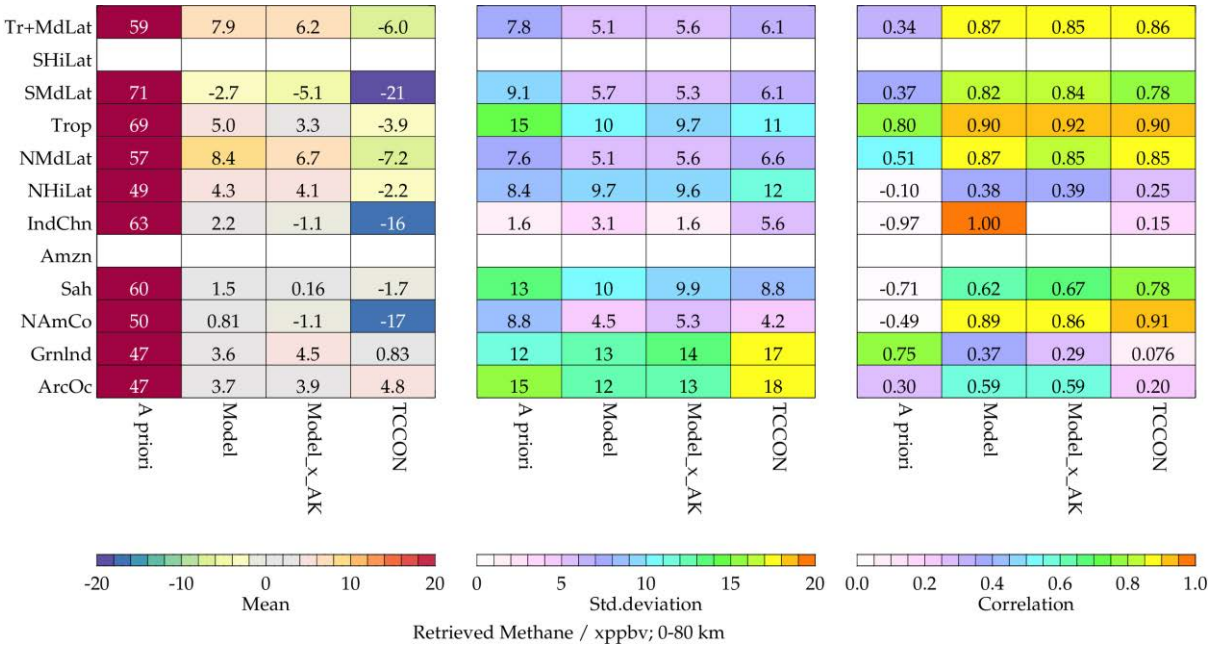

Figure 5-42 : Summary of statistics from monthly time-series comparisons of SWIR+TIR column averages with TCCON and CAMS sampled to TCCON for various regions. Panels from left to right show the mean difference; standard deviation of the monthly mean differences; correlation between IASI and CAMS monthly mean values.

5.4. Discussion of combined SWIR-TIR Data

The comparisons and validation presented in Sections 5.1 to 5.3 demonstrate that the machinery of the SWIR-TIR scheme is functioning as intended in this first application to methane: the column average output from the combination closely tracks that from S5P whereas the 6-12km layer (and higher layers) track those from IASI-B v1. Results for the 0-6km layer reflect information from both sensors, often emphasising localised enhancements in S5P to be consistent with surface emissions.

Estimated precision on the 0-2km layer (which constitutes only ~20% of the total column) is around 80-100ppbv, which in principle should be sufficient to provide information on large local enhancements in the vicinity of strong emission sources. It is notable that prominent positive anomalies with respect to CAMS seen in regional maps are located over methane source regions.

On the basis of this exercise, our finding is therefore that the SWIR-TIR combination does have potential to provide added value to SWIR column averages and TIR height resolved data. To exploit this potential, however, greater accuracy is needed on the S5P and IASI-B retrievals individually. On the basis of Section 3 of this report, use of IASI-B v2 data in place of v1 will provide greater accuracy at lower latitudes. Further R&D to the TIR scheme, as outlined in section 4.4, would improve accuracy more generally at higher as well as lower latitudes. In addition, the SWIR-TIR scheme is itself amenable to improvement eg through modification of the prior constraint..

Looking ahead, co-located SWIR and TIR measurements to be made by S5 and IASI-NG on MetOp-SG offer an ideal opportunity to exploit the potential of the SWIR-TIR approach to monitor methane in the lower troposphere from the mid-2020s onwards.

6. Summary

In the first phase of this study, data from the V1 RAL optimal estimation scheme and LMD non-linear inference scheme applied to Metop-B IASI through 2018 and 19 were compared on a common basis, applying vertical averaging kernels (AKs), with co-located profiles from the ATOM-4 campaign and AirCore launches over France and Sodankylä. For both ATOM-4 and AirCore, profiles were extrapolated with the CAMS v19 r1 GHG flux inversion re-analysis. Data were also compared with global and regional seasonal maps and Hovmoller plots from the same CAMS re-analysis. Column averages from the RAL scheme were compared in addition with those from TCCON and Sentinel-5P. Results for the RAL (V1) and LMD schemes from these analyses for Metop-B were found to be similar to those from earlier analyses for Metop-A.

LMD coverage is generally limited to latitudes 60S – 60N except in northern summer due to strict quality filters. Fundamental differences in retrieval methodology and spectral sampling mean that the vertical sensitivity of the LMD mid-troposphere column (MT-CH_4) differs from that of the RAL column average, surface-450hPa (0-6km) and 450-170hPa (6-12km) layers. This in turn means that global and regional maps and Hovmoller plots would not generally be expected to show a consistent structure and nor would their comparisons with CAMS. This was evident from CAMS global and regional maps with respective averaging kernels applied for the LMD MT-CH_4 and RAL (v1) column and layer averages. Global and regional maps for the different layers retrieved by the RAL scheme, and their deviation from CAMS, exhibited significantly different structure. The RAL (V1) column average (CA) was generally within +/-20ppbv of CAMS and the LMD MT-CH_4 within +/-40ppbv, with the highest deviations at high-latitude. In cases where CAMSxAK maps were similar for RAL CA and LMD MT-CH_4, there is an indication that latitude dependent biases with respect to CAMS were different: negative at low latitudes and positive at high latitudes for RAL and vice versa for LMD MT-CH_4, as evident in the India/SE Asian and S. America regional maps as well as the global maps.

Overall, RAL CA and LMD MT-CH_4 retrievals both exhibited small positive biases with respect to ATOM-4 profiles extrapolated with those from the CAMS v19 r1 GHG flux inversion re-analysis: 4±23 ppbv and 0.05 +/- 22.08 ppbv, respectively. In the case of both RAL CA and LMD MT-CH_4, latitude dependences of discrepancies with respect to ATOM-4 were similar to those with respect to CAMS in spring. For the selected AirCore profiles, biases for LMD MT-CH_4 (11 profiles) and RAL CA (19 profiles) were again found to be small: -0.91 +/- 14.51 ppbv and 13±10 ppbv, respectively.

Stratospheric influence on retrievals increases with latitude and representation of stratospheric methane in CAMS has an increasing importance on comparisons at high latitudes. In northern mid-latitudes the RAL V1 6-12km layer was lower than CAMS, as

was the LMD MT-CH_4. However, the discrepancy was not higher in the Arctic for the RAL 6-12km layer and was largest and of opposite sign over the Antarctic.

Given the different vertical sensitivities and comparable levels of agreement with ATOM-4 and AirCore profiles found for RAL column and layer averages and LMD MT-CH_4, the RAL V1 data would be expected to add value to LMD data in the CAMS assimilation system once a bias correction has been applied. Comparisons of RAL V1 column averages with TCCON, ATOM-4- (extrapolated with CAMS) and CAMS pointed towards a latitude dependent bias which varied from -20ppbv at low latitudes to +20pbbv high latitudes. Comparison of RAL V1 column averages with those of S5P further indicated latitude dependent bias correction(s) of similar magnitude to be necessary to assimilate the two data sets consistently for surface flux estimation in this study.

On the basis of this analysis and further investigation of artefacts eg low emissivity areas of Sahara and a topographic feature in southern Venezuela, improvements were made to the RAL scheme, resulting in a “candidate” V2 dataset which was subsequently validated in a similar way.. The negative bias found at lower latitudes for V1 data is substantially reduced in the V2 data but results at higher latitudes are mixed, with a larger positive bias particular in winter/spring. It was therefore decided not to proceed with a full scale reprocessing with the new V2 candidate scheme, until further work is conducted to address the remaining issues (outside the scope of the current study).

Joint SWIR-TIR retrievals (based on S5P and RAL V1 TIR data) have also been assessed here. This first attempt at the SWIR-TIR combination shows considerable promise. Features detected in the column average by SWIR in areas of prominent methane sources are located in the lower troposphere by the combination, while upper layers follow structures from the TIR retrieval. Results from this first application are limited by the quality of both S5P and MetOp-B retrievals and it is expected that the improvements on the TIR V1 data, including those demonstrated by this project for the candidate V2 and those expected from future work, along with improvements implemented for the next processing for S5P, will lead to a higher quality combination in the next version.

.

7. Acronyms and abbreviations

Acronym	Meaning
ATBD	Algorithm Theoretical Baseline Document
ACE / ACE-FTS	Atmospheric Chemistry Experiment Fourier Transform Spectrometer
ATom	Atmospheric Tomography Mission
CAMS	Copernicus Atmospheric Monitoring System
IASI	Infrared Atmospheric Sounding Interferometer
IMS	Infrared and Microwave Sounder
LMD	Laboratoire de Météorologie Dynamique
NOAA	National Oceanic and Atmospheric Administration
RAL	Rutherford Appleton Laboratory
S5P	Sentinel-5 Precursor
SRON	Space Research Organisation of the Netherlands
SWIR	Short wave Infrared
TCCON	Total Carbon Column Observing Network
TIR	Thermal Infrared
TROPOMI	Tropospheric Monitoring Instrument

8. References

RD-1. ESA project METHANE+, Deliverables 4 and 5 (D4 & 5)Version: Draft 0.9, Data Pool (DP) description / Auxiliary dataset User Manual (AUM); Doc ID:TN-D4and5-CH4PLUS; Date: 3 June 2020

RD-2. Crevoisier, C., Chédin, A., Matsueda, H., et al., First year of upper tropospheric integrated content of CO2 from IASI hyperspectral infrared observations, Atmos. Chem. Phys., 9, 4797-4810, 2009.

RD-3. Crevoisier, C., Nobileau, D., Fiore, A., Armante, R., Chédin, A., and Scott, N. A.: Tropospheric methane in the tropics – first year from IASI hyperspectral infrared observations, Atmos. Chem. Phys., 9, 6337–6350, doi:10.5194/acp-9-6337-2009, 2009b.

RD-4. Crevoisier, C., Nobileau, D., Armante, R., et al., The 2007–2011 evolution of tropical methane in the mid-troposphere as seen from space by MetOp-A/IASI, Atmos. Chem. Phys., 13, 4279-4289, 2013.

RD-5. Houweling, S., Bergamaschi, P., Chevallier, F., Heimann, M., Kaminski, T., Krol, M., Michalak, A. M., and Patra, P.: Global inverse modeling of CH4 sources and sinks: an overview of methods, Atmos. Chem. Phys., 17, 235–256, https://doi.org/10.5194/acp-17-235-2017, 2017.

RD-6. Jones, A., Technical Note: A trace gas climatology derived from the Atmospheric Chemistry Experiment Fourier Transform Spectrometer dataset, Atmos. Chem. Phys., 12, 5207-5220, doi:10.5194/acp-12-5207-2012

RD-7. Karion, Anna, Colm Sweeney, Pieter Tans and Timothy Newberger, AirCore: An Innovative Atmospheric Sampling System, Journal of Atmospheric and Oceanic Technology, Nov 2010, https://doi.org/10.1175/2010JTECHA1448.1

RD-8. Membrive O., Crevoisier C., Sweeney C., Danis F., Hertzog A., Engel A., Bönisch H. and Picon L., AirCore-HR: A high resolution column sampling to enhance the vertical description of CH4 and CO2, Atmos. Meas. Tech., 10, 2163-2181, 2017, https://doi.org/10.5194/amt-10-2163-2017

RD-9. Segers, A. and S. Houweling, 2020, Description of the CH4 Inversion Production Chain, Copernicus Atmosphere Monitoring Service, https://atmosphere.copernicus.eu/sites/default/files/2020-01/CAMS73_2018SC1_D73.5.2.2-2019_202001_production_chain_v1.pdf

RD-10. Siddans, R., Knappett, D., Kerridge, B., Waterfall, A., Hurley, J., Latter, B., Boesch, H., and Parker, R.: Global height-resolved methane retrievals from the Infrared Atmospheric Sounding Interferometer (IASI) on MetOp, Atmos. Meas. Tech., 10, 4135–4164, https://doi.org/10.5194/amt-10-4135-2017, 2017

RD-11. Siddans, R. (2020). Water Vapour Climate Change Initiative – Phase One: ATBD Part 2 – IMS L2 Product.

RD-12. Siddans, R. (2022), IASI Methane CH4 Operational Retrieval ATBD. version 2p-, 2022-05-02

RD-13. Siddans, R. (2022), Joint SWIR/TIR Retrieval Scheme ATBD. version 1.0, 2022-05-27

RD-14. Wofsy, S.C.et al 2018. ATom: Merged Atmospheric Chemistry, Trace Gases, and Aerosols. ORNL DAAC, Oak Ridge, Tennessee, USA. https://doi.org/10.3334/ORNLDAAC/1581

RD-15. Wunch, D., G.C. Toon, J.-F.L. Blavier, R.A. Washenfelder, J. Notholt, B.J. Connor, D.W.T. Griffith, V. Sherlock, P.O. Wennberg. The Total Carbon Column Observing Network. Phil. Trans. R. Soc. A (2011) 369, doi:10.1098/rsta.2010.0240